

# Biochemistry of human peroxidasin 1

Doctoral thesis submitted by:  
Dipl.-Ing Benjamin Sevcnikar



In Partial Fulfillment of the Requirements for the Degree Doctor of  
Philosophy (PhD)

Supervisor:  
Univ. Prof. Dr. Christian Obinger

BOKU - University of Natural Resources and Life Sciences, Vienna  
Department of Chemistry  
Muthgasse 18, 1190 Vienna, Austria

August, 2020

# Table of content

Acknowledgements	II
Declaration	III
Abstract	IV
Zusammenfassung	V
Introduction	1
Aim of the thesis	21
Publications	
Pre-steady-state kinetics reveal the substrate specificity and mechanism of halide oxidation of truncated human peroxidasin 1	23
Reaction of human peroxidasin 1 compound I and compound II with one-electron donors	35
The leucine-rich repeat domain of human peroxidasin 1 promotes binding to laminin in basement membranes	43
Conclusion	51
References	55
Appendices	67
Curriculum Vitae	127

## Acknowledgements

First, I want to express my gratitude towards Christian Obinger for giving me the opportunity to work in his Protein Biochemistry group. With his supervision and scientific guidance, I was able to overcome all challenges that I faced during my thesis. Many thanks also go to Paul Furtmüller for his amazing scientific input and advice that was incredibly valuable over the last four years.

Second, I want to thank Michael Jonathan Davies for giving me the chance to work in his lab in Copenhagen. Special thanks go to Christine, Luke, Michele, Line, Sandra and Lisa for all the fun moments in- and outside of the lab during my six months abroad.

Special thanks go to my students Georg, Mara and Michael for their commitment and support for my work. In addition, I want to thank the whole BioToP family and the rest of the BioB working group for providing a supportive and cheerful atmosphere every single day.

Moreover, I would like to thank my friends Benji, Clemens, Dominik, Jenny, Sophie, Stella and all the others for always having an open ear and a shoulder to cry on when my sailboat was passing through rough seas. Thank you, Christina, for your love and understanding during the good and bad times.

Finally, I want to thank my whole family for giving me the support and encouragement throughout all stages of my life. I owe you everything.

## Declaration

All biochemical, spectroscopic and kinetic work presented in this thesis was carried out in the lab of Christian Obinger (University of Natural Resources and Life Sciences, Department of Chemistry, Division of Biochemistry, Muthgasse 18, 1190 Vienna, Austria) supported by the bachelor students Georg Fröhlich, Mara Mitstorfer and Michael Laichmann.

Immunoprecipitation experiments and identification of laminin via western blot analysis was performed with the help of Christine Chuang in the laboratory of Michael Jonathan Davies (University of Copenhagen, Department of Biomedical Sciences, Blegdamsvej 3, 2200 København N, Denmark).

Surface plasmon resonance (SPR) experiments were performed with the help of Irene Schaffner, on the SPR equipment kindly provided by the EQ-BOKU VIBT GmbH and the BOKU Core Facility Biomolecular & Cellular Analysis (University of Natural Resources and Life Sciences, Muthgasse 11, 1190 Vienna, Austria).

This work was supported by the Austrian Science Fund, FWF [Doctoral Program BioToP-Biomolecular Technology of Proteins (W1224) and the stand-alone project P25538]. Additional financial support from the Novo Nordisk Foundation and Danmarks Frie Forskningsfond (grants NNF13OC0004294 and DFF-7014-00047, respectively, to MJD) is gratefully acknowledged.

## Abstract

Human peroxidasin 1 (hsPxd01) is a homotrimeric multidomain heme peroxidase that is closely related to other mammalian heme peroxidases (e.g. myeloperoxidase or lactoperoxidase) and secreted into the extracellular space. It catalyzes the hypobromous acid-mediated formation of a biologically unique sulfilimine crosslink (S=N) at the interface of two collagen IV chains in the basement membrane, which is essential for tissue development and basement membrane integrity. However, it is yet unclear if and how peroxidasin interacts with the complex composition of the extracellular matrix (ECM) and how these interactions mediate the formation of this specific link without causing damage to the ECM.

This thesis provides pre-steady-state kinetic analysis that sheds light on the substrate specificity and the reaction mechanism of peroxidasin. It shows that peroxidasin is able to react with two-electron donors like thiocyanate, iodide and bromide while being unable to react with chloride. Furthermore, it is demonstrated that peroxidasin is able to follow the peroxidase cycle by reacting with one-electron donors like urate and nitrite that additionally modulate the halogenation activity. Laminin, a key player in basement membrane assembly, is identified as the first known interaction partner of peroxidasin in the extracellular matrix. Analysis of the interaction with surface plasmon resonance revealed the dissociation constant of 1  $\mu\text{M}$  and necessity of the leucine-rich repeat domain for proper binding of peroxidasin towards laminin. The obtained data is discussed in respect to other mammalian peroxidases and to the recently published in-solution structures of the peroxidasin constructs and the proposed biological role of peroxidasin.

## Zusammenfassung

Humanes Peroxidasin 1 (hsPxd01) ist eine homotrimere Hämperoxidase, die aus mehreren Proteindomänen besteht, nah verwandt zu anderen Hämperoxidasen wie Myeloperoxidase oder Lactoperoxidase ist und in den extrazellulären Raum sekretiert wird. Durch die Bereitstellung von hypobromiger Säure katalysiert es die Bildung von einer in der Natur einzigartigen Sulfiliminbindung (S=N) an der Schnittstelle von zwei Collagen IV Fasern in der Basalmembran. Diese Sulfiliminbindung ist essentiell für die Entwicklung von Geweben und der Integrität von Basalmembranen. Es ist jedoch unklar, ob und wie Peroxidasin mit der großen Anzahl an Proteinen und Zuckern in der Basalmembran interagiert und wie diese Interaktion die Entstehung der Sulfiliminbindung beeinflusst, ohne dabei Schaden an der extrazellulären Matrix anzurichten.

Diese Arbeit umfasst umfangreiche Multimixing-Stopped-Flow-Untersuchungen zur Aufklärung des Reaktionsmechanismus und der Substratspezifität von humanem Peroxidasin. Es wird gezeigt, dass Peroxidasin mit Zwei-Elektron Donoren wie Thiocyanat, Iodid und Bromid reagiert, jedoch nicht mit Chlorid. Weiters wird gezeigt, dass Peroxidasin dem Peroxidase-Zyklus durch die Reaktion mit Ein-Elektron Donoren wie Urat und Nitrit folgen kann. Diese Ein-Elektron Donoren können auch die Halogenierungsaktivität von Peroxidasin beeinflussen. Zudem wurde Laminin, ein wichtiges Protein in der Basalmembran, als erster bekannter Bindungspartner in der extrazellulären Matrix von Peroxidasin identifiziert. Durch die Analyse der Interaktion zwischen Laminin und Peroxidasin mit Hilfe von Oberflächen-Plasmon-Resonanz Spektroskopie konnte die Dissoziationskonstante mit  $1 \mu\text{M}$  bestimmen. Weiters stellte sich heraus, dass die „Leucine-rich-repeat“ Domäne von Peroxidasin für eine starke Bindung essentiell ist. Die im Zuge dieser Arbeit erhaltenen Daten, werden im Vergleich mit anderen Peroxidasen, der unlängst aufgeklärten Struktur von diversen Peroxidasinkonstrukten in Lösung und der biologischen Funktion von Peroxidasin diskutiert.

# 1. Introduction

## 1.1 Heme peroxidases

Heme peroxidases are proteins with heme *b* or post-translationally modified heme as co-factor. They use hydrogen peroxide as an electron acceptor to catalyze one- and two-electron oxidation reactions of numerous organic and inorganic compounds or proteins (1, 2). Heme peroxidases can be found in all kingdoms of life and in the course of evolution four different superfamilies emerged independently. However, they differ greatly in their overall fold, enzymatic activity and active site architecture. Three superfamilies, namely the peroxidase-catalase, dye decolorizing peroxidases and peroxidase-peroxygenase superfamily, have unmodified heme *b* at their active site. However, members of the fourth superfamily, the peroxidase-cyclooxygenases, have posttranslationally modified heme *b* which is covalently linked to the protein via one, two or even three covalent bonds that involve aspartate and glutamate residues (1).

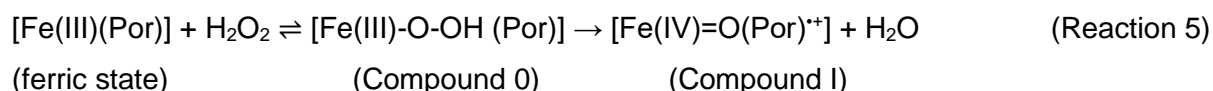
All superfamilies share the peroxidatic reactions, where one-electron donors (AH<sub>2</sub>) are oxidized to their corresponding radical (<sup>•</sup>AH) (Reaction 1). In the halogenation reaction two-electron donors like halides (X<sup>-</sup>) or pseudohalides (e.g SCN<sup>-</sup>) are oxidized to the corresponding (pseudo)hypohalous acids (HOX and HOSCN) (Reaction 2). Specialized (sub)families on the other hand show catalase (Reaction 3) or peroxygenase (Reaction 4) activity (1).



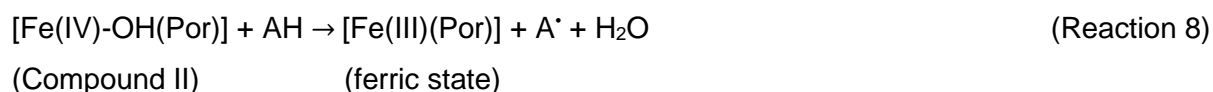
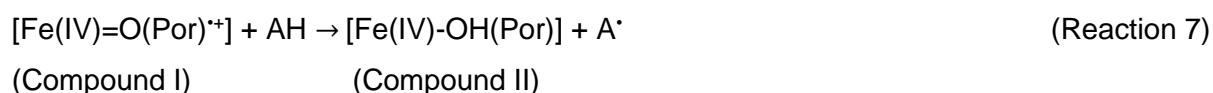
## 1.2 Peroxidase and halogenation cycles

Typically, heme peroxidases follow the peroxidase cycle, which includes the resting state [Fe(III)], Compound I [oxoiron(IV) with a porphyrin radical] and Compound II [oxoiron(IV)] thereby catalyzing Reaction 1. In addition, heme peroxidases (including peroxidases) can follow the halogenation cycle, which includes the resting state and Compound I thereby catalyzing Reaction 2 (3). In both cases the reaction cycle is started by the hydrogen peroxide-mediated oxidation of the resting state to Compound I (Reaction 5) (3). In an initial step, hydrogen peroxide reacts with Fe(III) from the peroxidase to form a very short-lived ferric hydroperoxide (Fe(III)-O-O-H) complex (3). Heterolytic cleavage of the O-O bond leads to the

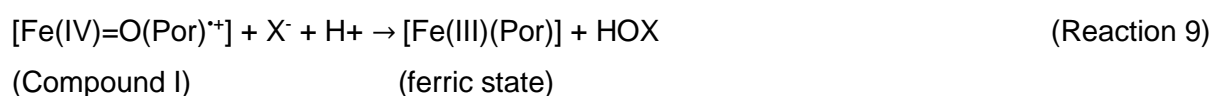
withdrawal of two electrons from the heme (one from the iron, one from the porphyrin backbone) while water is released and Compound I (Reaction 5) is formed (4–7). Compound I is short-lived and characterized by a high redox potential and reactivity. If there are no exogenous electron donors available, electrons are transferred internally from amino acids towards the porphyrin radical leading to the formation of Compound I\* (Reaction 6). The formation of amino acid radicals leads to oxidative damage to the protein which is subsequently inactivated over time (8).



In the presence of one-electron donors (AH), Compound I is readily reduced via Compound II to the ferric resting state by two consecutive electron donations while the substrates are oxidized to their corresponding radicals (Reaction 7+8). Among known physiological one-electron donors are serotonin, ascorbate, tyrosine, nitrite and urate (9–12).



If the substrates can donate two electrons, Compound I is directly reduced to its ferric resting state (Reaction 9).



Typical two-electron donors for peroxidases are halides and pseudo-halides (13, 14). Summing up, the peroxidase cycle includes Reactions 5, 7 and 8, whereas the halogenation cycle includes Reactions 5 and 9.

### 1.3 Chordata peroxidases

The peroxidase-cyclooxygenase superfamily has members in all kingdoms of life and is further divided into seven families (Fig. 1). In the context of this thesis, especially Family 1 (chordata peroxidases) and Family 2 (peroxidasins) are particularly interesting. Myeloperoxidase (MPO), lactoperoxidase (LPO), eosinophil peroxidase (EPO) and thyroid peroxidase (TPO) are the most prominent members of the chordata family.



to be one of the key enzymes in the thyroid hormone biosynthesis. TPO is oxidizing iodide (I<sup>-</sup>) to hypoiodous acid (HOI) that subsequently iodinated distinct tyrosine residues within the protein thyroglobulin (TG) (26). Iodinated TG serves as precursor for the thyroid hormones thyroxin and triiodothyronine (27, 28). The mechanism of the iodination of TG tyrosines by TPO is yet unresolved. It is still under discussion whether TG is iodinated by freely diffusing iodine species released from TPO or whether TPO interacts specifically with distinct TG tyrosines in order to avoid side reactions (29, 30).

## 1.4 Peroxidasins

While chordata peroxidases were first discovered between 1940 (31) and 1970 (32–36), peroxidasin made its first appearance in scientific publications in 1994 (37). Nelson et al. discovered a novel protein that combined a peroxidase domain that was homologous to MPO and EPO with motifs that were found in proteins of the extracellular matrix of *Drosophila melanogaster* (37). However, it took almost another 20 years until the modus operandi of peroxidasin for a physiological relevant reaction was described in detail in 2012. Bhave et al. showed that like TPO, peroxidasins exhibit an important biosynthetic function. They observed that peroxidasin together with hydrogen peroxide is able to generate highly reactive hypohalous acids that are subsequently involved in the formation of an unusual intermolecular sulfilimine (S=N) crosslink within the collagen IV network of basement membranes (38).

### 1.4.1 Phylogeny of peroxidasin

As previously mentioned, peroxidasins are members of Family 2 in the peroxidase-cyclooxygenase superfamily and are closely related to chordata peroxidases (Family 1) and peroxinectins (Family 3) (1, 39) (Fig. 1). Compared to Family 1 peroxidases, peroxidasins are unique since they are multidomain proteins that combine a peroxidase domain with motifs known from the extracellular matrix. These include N-terminal leucine-rich repeat (LRR) domains, immunoglobulin C2-like (Ig) domains and a von Willebrand factor type C (VWC) domain at the C-terminus of the protein (1, 39).

An initial evaluation of peroxidasins phylogeny revealed five distinct subfamilies, where Subfamily 1- 4 covered invertebrate and Subfamily 5 included vertebrate peroxidasins (Fig. 2). The closest neighbor to chordata peroxidases and the origin of multidomain peroxidasins are represented by proteins from hemi- and urochordata species (Subfamily 1). Clearly separated are nematode peroxidasins (Subfamily 2), arthropod peroxidasins (Subfamily 3), a second group of hemi- and urochordata peroxidasins (Subfamily 4) and invertebrate peroxidasins (Subfamily 5). The invertebrate subfamily is further branched into peroxidasin 1 (Pxd1) and

peroxidasin 2 (Pxd2) and in each branch a segregation between mammalian, fish, bird and amphibian species is observed.

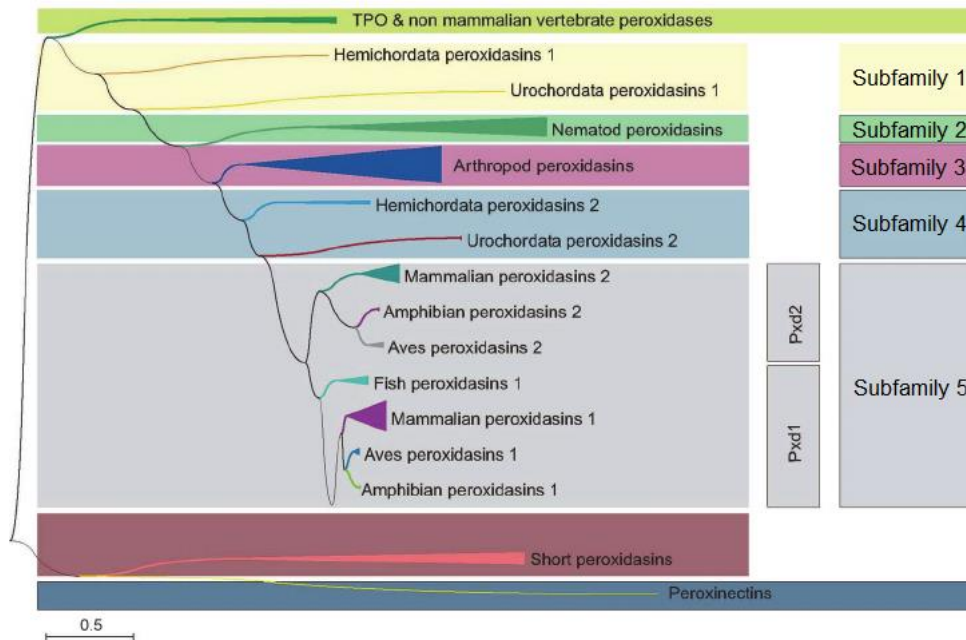


Figure 2 – Reconstructed unrooted phylogenetic tree of selected chordata peroxidases, peroxinectins and peroxidasins. Adapted Modified from Ref. (39) (published under open access)

Two different peroxidasins are expressed in the human genome (hsPxd01 on chromosome 2 and hsPxd02 on chromosome 8) that share a sequence identity of almost 60% (39, 40). Sequence analysis revealed that both human peroxidasins carry a secretion signal and consist of four different subdomains: A LRR domain comprised of five leucine-rich repeats plus an N- and C-terminal capping motif, four consecutive Ig domains, a heme binding peroxidase domain and a C-terminal VWC domain. Those domains except the VWC can also be found in the other subfamilies but vary usually in the number of leucine-rich repeats and Ig domains. From an evolutionary point of view, the VWC domain seems to be the newest addition to peroxidasin as it is absent in Subfamilies 1,2 and 4 (Fig. 3).

#### 1.4.2 Structure of peroxidasin

As previously mentioned, peroxidasin is comprised of LRR domains, Ig domains, one peroxidase domain and a VWC domain with a total theoretical molecular mass of 163 kDa per monomer. The different domains are discussed below. Protomers are covalently bound via disulfide bridges between cysteine residues to form homotrimers. Additionally, it has eleven glycosylation sites of which ten are at least partly occupied which leads to an apparent molecular mass of 504 kDa of the homotrimeric protein. Thus it is the biggest human peroxidasin known so far (41, 42).

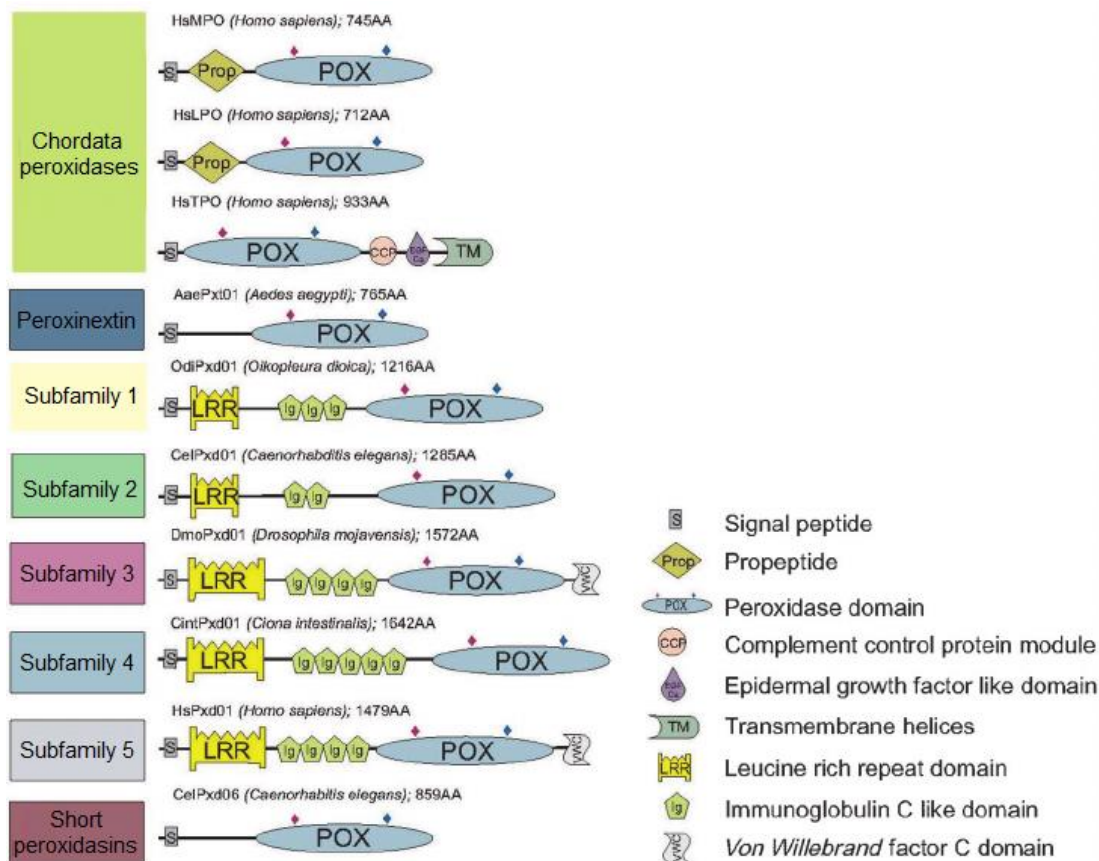


Figure 3 – Schematic presentation of subunit assembly of representatives of invertebrate und vertebrate peroxidasins in comparison to chordata peroxidases. Modified from Ref. (39) (published under open access)

#### 1.4.2.1 Leucine-rich repeat domain

LRRs are usually built from tandems of two or more repeats that contain 20-29 residues that form a solenoid structure and are known to be important for protein-protein interactions such as cell adhesion, platelet aggregation, neuronal development and extracellular matrix assembly (43, 44). One repeat usually comprises a conserved eleven amino acid segment with the consensus sequence (LxxLxLxxNxL), which corresponds to  $\beta$ -sheets that form the concave site of the solenoid. The convex site shows greater variability in structural elements like  $\alpha$ -helices,  $3_{10}$ -helices, polyproline II helices and  $\beta$ -turns. To protect the hydrophobic parts of the first and the last repeat, LRR domains are often flanked by disulphide-bonded caps. The N-terminal capping motif (LRRNT) usually is a single  $\beta$ -strand that runs antiparallel to the main  $\beta$ -sheets and contains four cysteines that form a disulphide knot. The C-terminal capping motif (LRRCT) also contains disulphide-building cysteines and usually forms an  $\alpha$ -helix that covers the hydrophobic core of the last repeat. These caps are very common in extracellular LRR proteins (43, 44). HsPxd01 contains five typical tandem LRRs flanked by a LRRNT and a LRRCT domain. Additionally, four disulfide bridges in the cap regions were confirmed in

LRRNT between Cys36-Cys42 and Cys40-Cys49 and in the LRRCT between Cys196-Cys243 and Cys198-Cys222 (41).

#### 1.4.2.2 Immunoglobulin domain

Immunoglobulin (IG) like domains are most commonly comprised of approximately 100 residues, which fold to a sandwich consisting of two  $\beta$ -sheets that contain antiparallel  $\beta$ -strands with a greek key topology. The immunoglobulin superfamily (IGSF) is nowadays one of the largest known protein superfamilies within vertebrate genomes and the IG fold is recognized to be involved in protein-protein or protein-ligand interactions (45, 46). Based on their sequence, IG domains can be further classified as V-domains (variable domains in antibodies), C1-domains (constant domains in antibodies), C2-domains (domains in non-antibody molecules) and I-domains (intermediate domains) (47).

HsPxd01 has four subsequent C2-like domains. Each is built up by two  $\beta$ -sheets comprised of seven  $\beta$ -strands and one disulfide bridge. However only two disulfide bonds could be found experimentally between Cys267-Cys317 and Cys454-Cys502 (41).

#### 1.4.2.3 Peroxidase domain

The peroxidase domain is the catalytic center of peroxidase. The signature sequence which allows correct assignment of proteins to the peroxidase-cyclooxygenases is **-X-G-Q-X-X-D-H-D-X-** (1). Multiple sequence alignment revealed the presence of those highly conserved residues in peroxidases (39) (Fig. 4+5). This sequence includes the distal catalytic histidine (His827, numbering according to hsPxd01), which is flanked by two aspartates (Asp826, Asp828), which are involved in ester bond formation and  $\text{Ca}^{2+}$  binding. The role for calcium binding is well studied in chordata peroxidases. The calcium binding pocket in MPO and LPO has a typical pentagonal bipyramidal coordination geometry and contains several highly conserved residues that are also found in peroxidases (39, 48, 49) (Fig. 4b). Its role is to stabilize the heme moiety in the catalytic center of the protein. Glutamine (Gln823) is involved in the distal hydrogen bonding network and halide binding (5) in the active site. Other typical distal residues are a catalytic arginine (Arg977) and a glutamate (Glu980) which form the second heme to protein bond with the typical sequence **-X-R-X-X-E-X-** (1) (Fig. 4c). First structural studies on peroxidase suggested that heme is covalently linked via ester bonds to Asp826 and Glu980 (41, 42). The distal His-Arg pair plays a crucial function in the heterolytic cleavage of hydrogen peroxide and is found in all peroxidases from the peroxidase-cyclooxygenase, peroxidase-peroxygenase and peroxidase-catalase superfamilies (1, 2, 5). Except for enzymes from the peroxidase-peroxygenase superfamily, histidine (H1074) serves

as a heme ligand on the proximal site that interacts with an asparagine (Asn1153), which has hydrogen bonds with an arginine (Arg1161). Exchange of asparagine to aspartate in MPO leads to modified spectral changes and diminished catalytic activity, while the exchange of arginine did not allow heme to bind in the active site anymore, underlining the importance of His-Asn-Arg triad for maintenance of overall heme cavity architecture (50, 51).

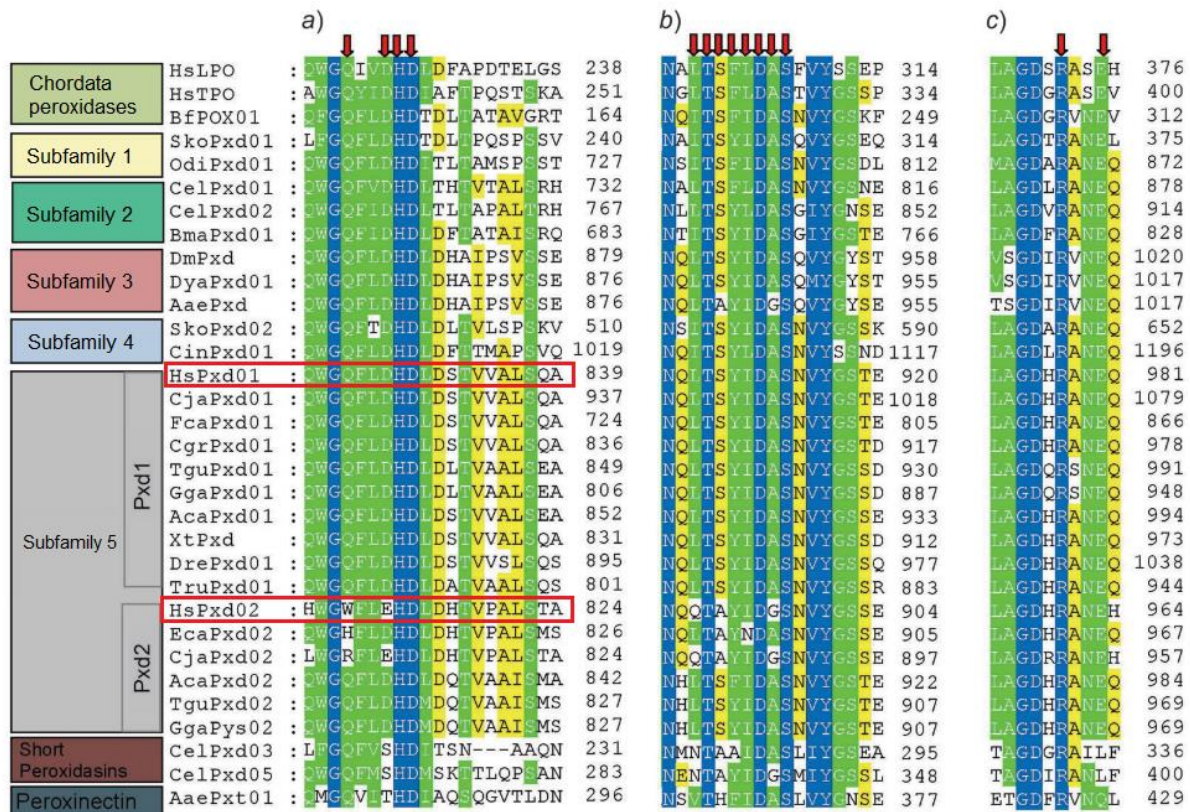


Figure 4 – Multiple sequence alignments of selected chordata peroxidases, peroxidasins and peroxinectins. Human Peroxidase 1 and 2 are highlighted in red boxes. Arrows indicate important amino acids a) conserved distal -X-G-Q-X-X-D-H-D-X sequence - b) Calcium binding pocket sequence c) conserved distal -X-R-X-X-E-X- sequence. modified from Ref. (39) (published under open access)

An overall comparison of the peroxidase domain to the well-studied chordata peroxidases leads to the conclusion that all important residues for peroxidase functionality are present in peroxidasin and suggests a similar overall fold of mainly  $\alpha$ -helices.

By aligning the sequences of hsPxd01 and hsPxd02, critical changes in the active site architecture of hsPxd02 are obvious since Asp826 is exchanged for a glutamate and Gln823 is switched to a tryptophan residue. While the exchange of aspartate to glutamate would not result in the exclusion of a potential ester link, the more crucial change is the implementation of tryptophan instead of the proximal glutamine. Glutamine has an essential role in halide binding in other mammalian peroxidases as previously discussed (5). Exchange of this highly conserved amino acid indicates that hsPxd02 might not have any catalytic function. Lazar et al showed that hsPxd01 carrying a Asp826Glu and Gln823Trp double mutation was catalytically inactive (42). An additional mutation of hsPxd02 at the distal site of Asn1153 to

isoleucine (Fig. 5b) further indicates that hsPxd01 and hsPxd02 should exhibit different catalytic and spectral features. It is therefore possible that hsPxd02 has lost its catalytic peroxidase activity and thus has a different biochemical and physiological function compared to hsPxd01. Studies suggested that hsPxd02 serves as an antagonist by forming heterotrimers with hsPxd01 and thus impairing its functionality (40). Another study indicated, that hsPxd02 can serve as a potential biomarker for breast cancer (52). Furthermore, an alternative splice variant of hsPxd02 with endonuclease activity was proposed (53).

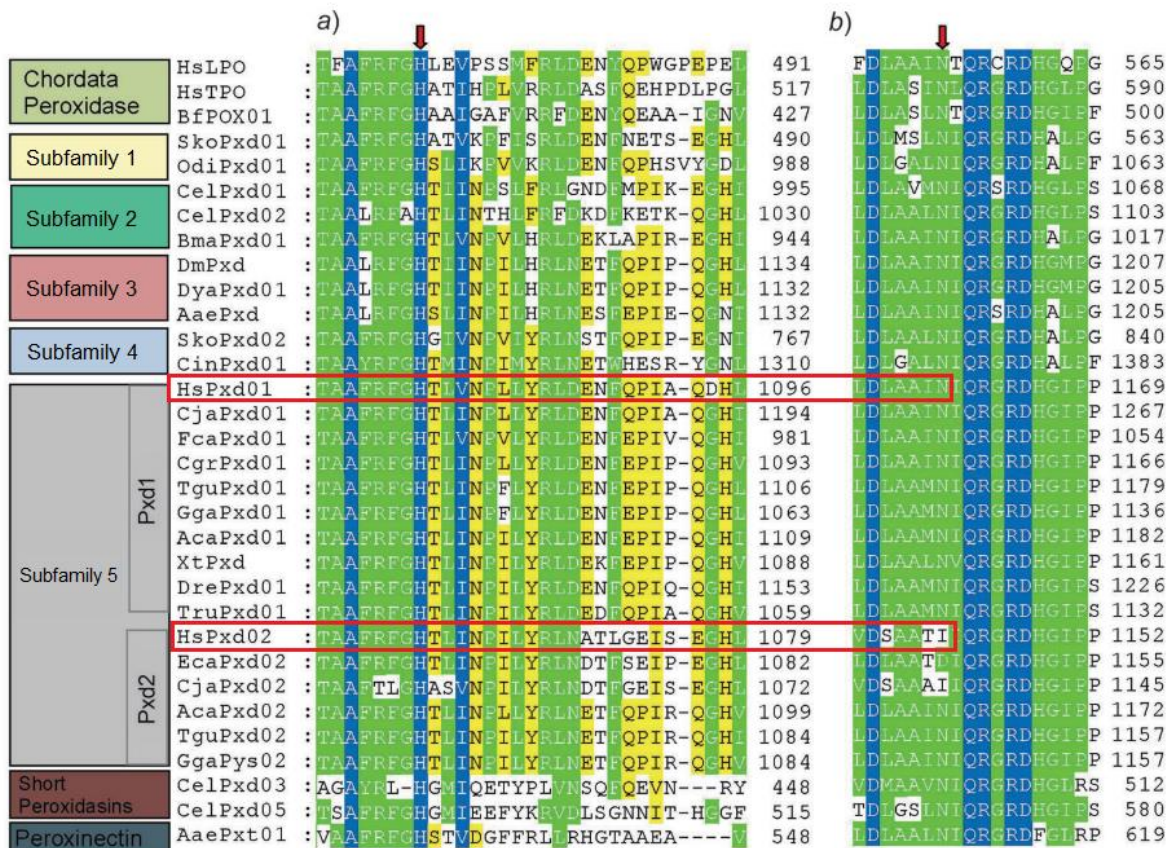


Figure 5– Multiple sequence alignments of selected chordata peroxidases, peroxidasins and peroxinectins. Human peroxidasin 1 and 2 are highlighted in red boxes a) proximal histidine b) proximal asparagine. Modified from Ref. (39) (published under open access)

#### 1.4.2.4 Von Willebrand Factor C like domain

The VWC domain is the most commonly occurring motif and usually contains less than 100 amino acids. It has ten conserved cysteine residues with a consensus sequence of -C-X-X-C-X-C- and -C-C-X-X-C-. The VWC therefore also often is referred to as cysteine-rich domain (CR) (54–56). Besides the cysteine motive, the sequences of VWCs are highly diverse and can be found in so-called CCN (acronym derived from the first three described members CYR61 (cysteine-rich 61), CTGF (connective tissue growth factor) and NOV (nephroblastoma overexpressed)) proteins. These CCN proteins are multifunctional mosaic proteins that among other domains contain one VWC and have critical physiological functions like skeletal

development, mitogenesis, proliferation, angiogenesis etc. (57). Although the VWC is a very common domain its actual function is yet poorly understood. However, it is known to bind bone morphogenic proteins (BMPs) and TGF- $\beta$  and it is believed to be a versatile binding module (54).

The function of VWC in peroxidase remains yet to be identified. A study by Colon et al. proposed that the VWC may serve as an oligomerization domain and a negative regulator of peroxidase activity which is subsequently cleaved off to activate peroxidase by a proprotein convertase (58). However, a study conducted during the course of this thesis could show that the VWC is not necessary for oligomerization (59). It is noteworthy that the proposed proprotein convertase cleavage site (RGRR) situated between the peroxidase domain and the VWC is conserved throughout the Subfamilies 3 and 5 that introduced the VWC in the first place.

## 1.5 Peroxidase and the basement membrane

In a groundbreaking study performed by Bhave and colleagues it was demonstrated that peroxidase and bromide is necessary to catalyze the formation of sulfilimine crosslinks within the collagen IV network of basement membranes (BM) (38, 60). BMs are highly specialized ECMs that lie basolateral to epithelial, endothelial, fat, muscle and peripheral nerve cells. Although BMs are associated with a highly complex set of over 300 proteins and sugars, its core components can be broken down to laminin, collagen IV, nidogen, perlecan, agrin and heparan sulfate proteoglycans (HS) (61–63) (Fig. 6). Besides being a first mechanical barrier that prevents malignant cells from escaping the epithelium and migrating to deeper tissues (64), BMs are considered to be the one of the most important regulators of cellular and tissue function. They are associated with various roles like angiogenesis, blood filtration, muscle homeostasis, cell differentiation and cell survival (61, 63, 65).

BM formation is a self-assembling process that involves cell surface binding, intermolecular binding and polymerization. In an initial step, laminin is binding to the cell surface via cellular receptors (e.g integrins), where it polymerizes to a network-like structure. In a subsequent step, collagen IV, which is the only other molecule besides laminin to form a network within the BM, is incorporated into the ECM and is bridged to laminin via nidogen (entactin) and perlecan (Fig. 6). While the laminin-network builds an early foundation of the BM, the collagen network serves as a scaffold for other BM proteins and provides mechanical strength and contributes to BM stiffness (66–69).

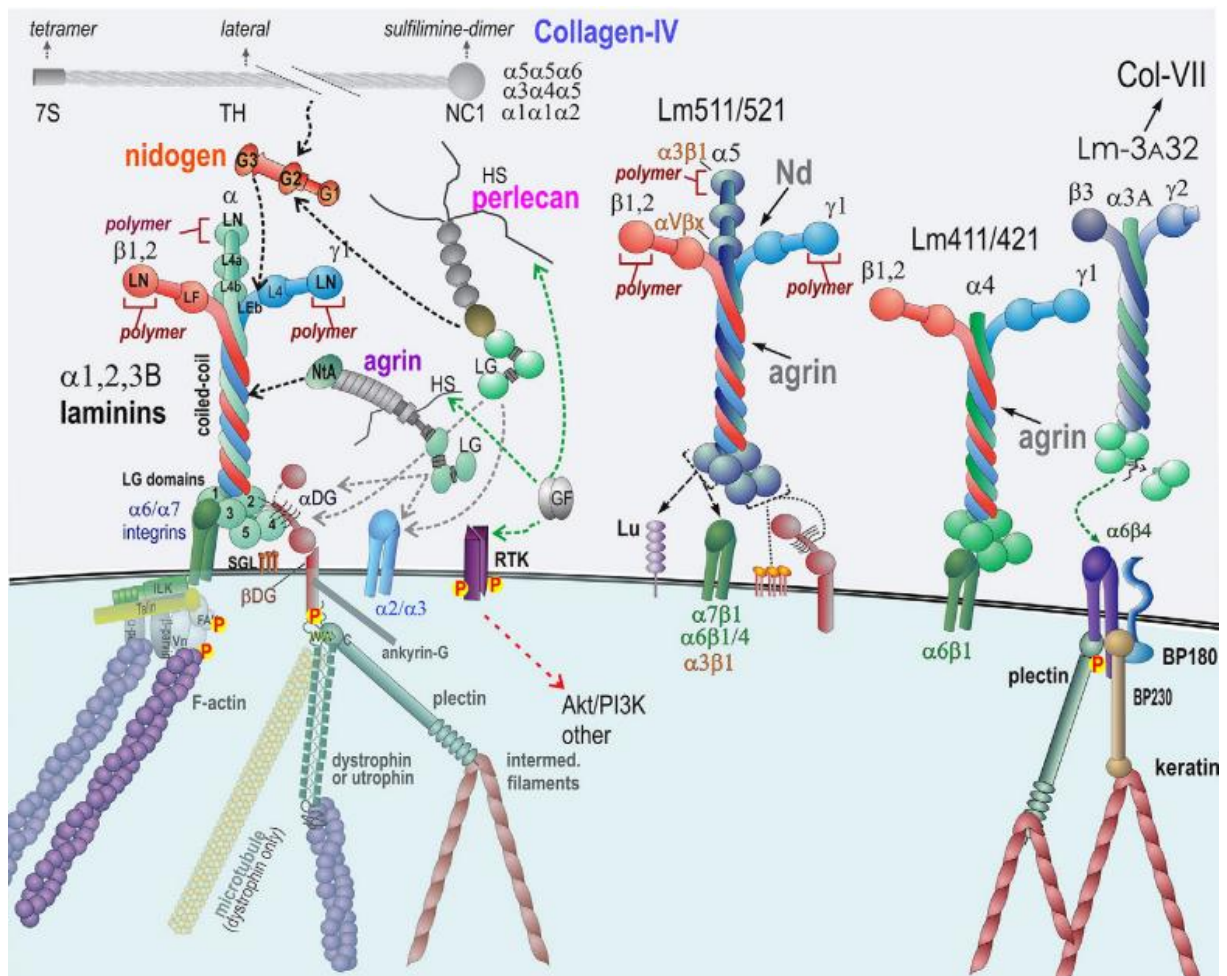


Figure 6 – Core basement membrane components and their interactions. Laminins are required for initiation of basement membrane formation. Laminin binds to cell surface integrins, agrins,  $\alpha$ -dystroglycan ( $\alpha$ DG), nidogen and polymerizes via its N-terminal domains. Collagen-IV and perlecan bind to nidogen, completing the core basement membrane scaffold. Agrin, perlecan and heparan sulfate proteoglycans chains attach to growth factors, promoting their interactions with receptor tyrosine kinases (RTK). Integrin and  $\alpha$ -dystroglycan attach to the cytoskeleton through adaptor proteins. Reprinted with permission from Ref. (61) (Elsevier; # 4852980092775)

### 1.5.1 Collagen IV structure and assembly

Collagens are the most abundant proteins in the human body. The collagen superfamily comprises 28 types in vertebrates which, based on their supramolecular assembly, can be further subdivided into fibrillar, fibril-associated, network-forming, beaded filament-forming, anchoring fibrils and transmembrane collagens (70–73). Collagen IV, one of the network-forming collagens, is predominantly found in BMs where it serves as a protein scaffold and gives the BMs mechanical resilience. It can contain up to six different polypeptide chains  $\alpha$ 1(IV) to  $\alpha$ 6(IV) of which three assemble to a collagen IV protomer (e.g three  $\alpha$ 1 chains form  $\alpha$ 111). This trimerization is triggered at the C-terminal non-collagenous domain (NC1) (74) (Fig. 7A). However, out of the many possible combinations,  $\alpha$ -chains interact with extraordinary specificity to form only three protomers which are  $\alpha$ 1 $\alpha$ 1 $\alpha$ 2(IV),  $\alpha$ 3 $\alpha$ 4 $\alpha$ 5 (IV) and  $\alpha$ 5 $\alpha$ 5 $\alpha$ 6 (IV). While  $\alpha$ 1(IV) and  $\alpha$ 2(IV) chains can be found in all BMs,  $\alpha$ 3(IV),  $\alpha$ 4(IV),  $\alpha$ 5(IV) and  $\alpha$ 6(IV) are

restricted to specific tissues.  $\alpha3\alpha4\alpha5(\text{IV})$  can be found in glomerular BMs of kidneys and in BM of lung, testis and eye while  $\alpha5\alpha5\alpha6(\text{IV})$  is found in skin, smooth muscles and kidney (72). A more recent study suggests that  $\alpha3\alpha4\alpha5(\text{IV})$  and  $\alpha5\alpha5\alpha6(\text{IV})$  are not restricted to specific tissues but are rather low abundant compared to  $\alpha1\alpha1\alpha2(\text{IV})$  (63).

As collagen IV protomers are secreted into the extracellular space, they assemble at their C-terminal NC1 domain (Fig. 7B) and N-terminal 7S domain (Fig. 7C) into a network or scaffold (Fig. 7D) that is reinforced by heavy crosslinking.

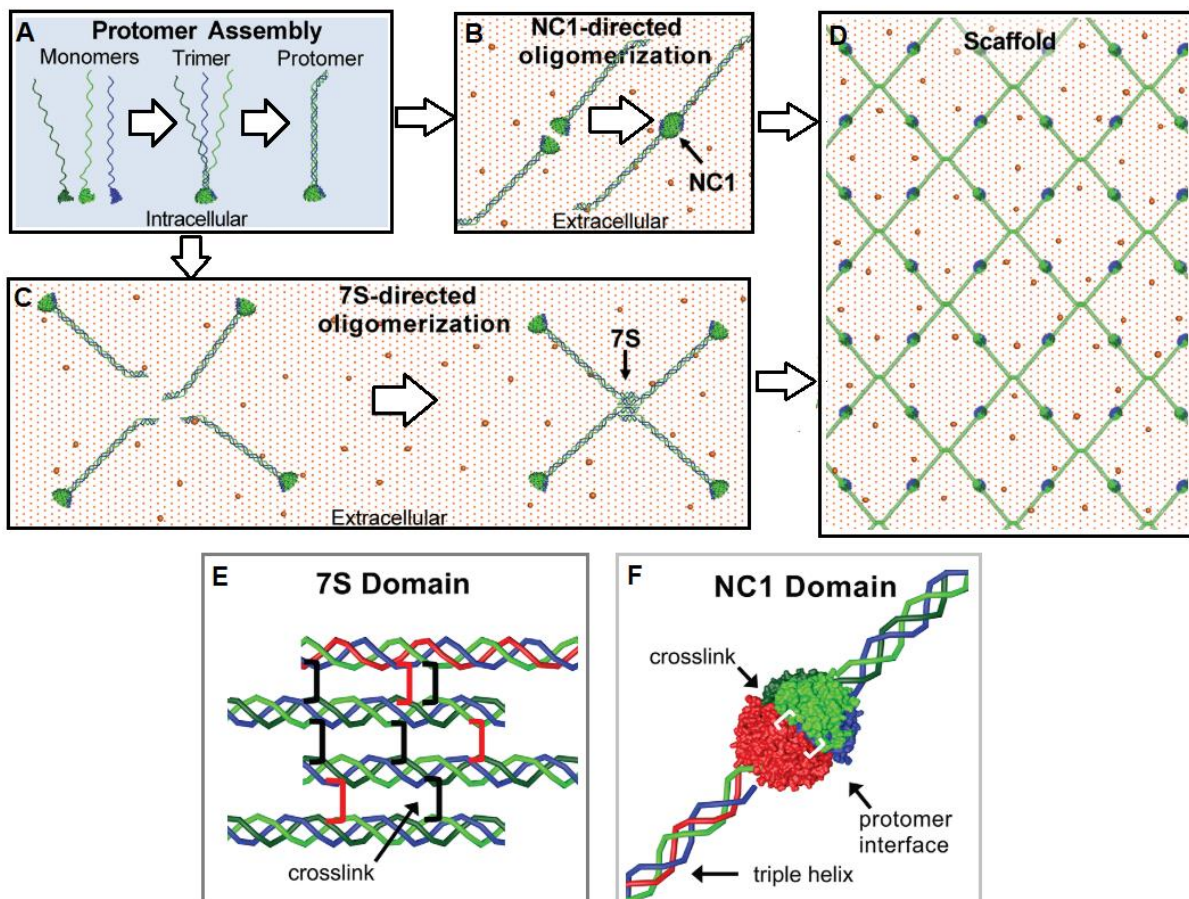


Figure 7 – Assembly of collagen IV into a network. Trimerization of collagen IV monomers into protomers is triggered at their NC1 domain intracellularly (A). Upon secretion, oligomerization of NC1 domains (depending on high chloride concentration) (B) and 7S domains (C) takes place extracellularly to form the final network-like structure (D). Four 7S domains are reinforced by cysteine-bridges (black) and lysine-lysine crosslinks (red) (E). NC1 domains are crosslinked at their protomer interface with sulfilimine bonds (white) (F). Modified from Ref. (66) (published under open access)

7S domains form dodecamers that are stabilized by intra- and interchain disulfide bonds and hydroxylysyl-derived crosslinks (Fig. 7E), while NC1 hexamers are stabilized by sulfilimine crosslinks (Fig. 7F). Both domains and their crosslinks provide BM stability and lack thereof leads to disruption of BM integrity (60, 75–77).

### 1.5.1.1 NC1 domain and mechanism of sulfilimine link formation

As mentioned above, collagen IV protomers ( $\alpha1\alpha1\alpha2(\text{IV})$ ,  $\alpha3\alpha4\alpha5(\text{IV})$  and  $\alpha5\alpha5\alpha6(\text{IV})$ ) are able to selectively associate at their NC1 domains to form  $\alpha1\alpha1\alpha2(\text{IV}) - \alpha1\alpha1\alpha2(\text{IV})$ ,  $\alpha3\alpha4\alpha5(\text{IV}) - \alpha3\alpha4\alpha5(\text{IV})$  and  $\alpha1\alpha1\alpha2(\text{IV}) - \alpha5\alpha5\alpha6(\text{IV})$  networks (78). Upon secretion of collagen IV from cells to the extracellular space, NC1 trimers are exposed to very high  $\text{Cl}^-$  concentrations (120 mM) that triggers the initial oligomerization of two NC1 trimers to hexamers. In a subsequent step, NC1 domains are covalently linked at the protomer interface. In detail, Met93 of one  $\alpha$ -chain forms a sulfilimine bond with Hyl211 of the opposing  $\alpha$ -chain of the second protomer (Fig. 8A). Both, Met93 and Hyl211, are highly conserved in all collagen IV alpha chains. Sulfilimine crosslinks were also detected in  $\alpha3\alpha4\alpha5(\text{IV}) - \alpha3\alpha4\alpha5(\text{IV})$  and  $\alpha1\alpha1\alpha2(\text{IV}) - \alpha5\alpha5\alpha6(\text{IV})$  NC1 hexamers (75, 79, 80).

In major breakthrough studies, it was shown that the catalytic activity of peroxidase in the presence of bromide is essential for the formation of this sulfilimine link (38, 60). It was hypothesized that peroxidase releases hypobromous acid near collagen IV where it would freely diffuse to the NC1 domain generating a bromosulfonium intermediate at Met91 that predominantly interacts with the  $\epsilon\text{-NH}_2$  of Hyl211 to form the sulfilimine link (Fig. 8A and B) (81). Hypochlorous acid on the other hand would lead to a chlorosulfonium intermediate at Met93 that would fail in crosslink formation as the predominant reaction product is methionine sulfoxide (Fig. 8D). It was further shown that the formation of the first crosslink energetically favors the formation of a second sulfilimine bond (Fig. 8C) (81). This was also the first indication that peroxidase is highly selective for bromide, given the fact that high chloride concentrations are crucial for initial NC1 oligomerization while hypochlorous acid fails to form the sulfilimine crosslink. A subsequent study revealed that both MPO and EPO fail to efficiently form the sulfilimine crosslink at the NC1 interface and that the non-catalytic domains of peroxidase were required for the crosslink formation (81). This implicates that the non-catalytic domains of peroxidase have a crucial role in delivering the hypobromous acid towards collagen IV. However, since no stable association of peroxidase with collagen IV was yet detected it was hypothesized that there is most likely a ternary complex with another BM protein to facilitate delivery of freely diffusing HOBr to the NC1 domains of collagen IV (81). However, since HOBr is a highly reactive oxidant, it could also lead to potential oxidative damage in the ECM. The theory of freely diffusing bromide to form a specific reaction product has remarkable similarity with the iodination of tyrosines by TPO, where iodine is also believed to freely diffuse to specific tyrosine residues in thyroid hormone biosynthesis (26). A most recent study could indeed reveal that bromine is enriched in normal BMs of mouse kidneys. In peroxidase knockout mice, the bromine content in kidneys was reduced by 85%. Proteomic analysis further showed that approx. 1.5% of tyrosine-1485 in the NC1 domain of collagen IV was brominated in normal mouse tissue, while this modification was absent in knockout mice

(82). This indicates that the formation is not entirely specific and that “off-target” oxidation events occur.

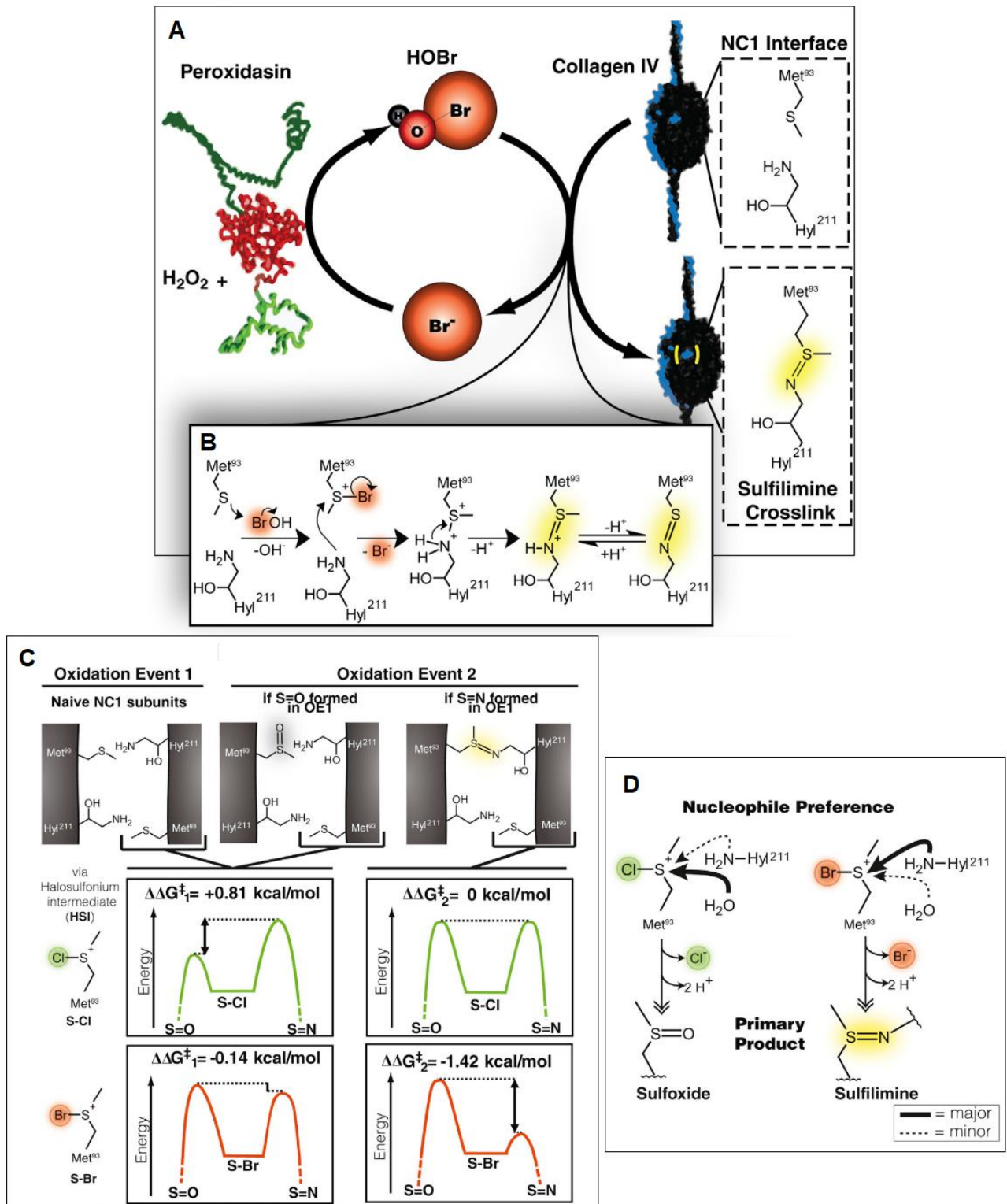


Figure 8 – Mechanism of sulfilimine link formation at the NC1 domain. Schematic representation of hydrogen peroxide, peroxidase, bromide and collagen and their roles in the formation of sulfilimine link (A). Proposed chemical reaction mechanism of sulfilimine link formation by HOBr (B). Free energy landscape for sulfilimine link formation at NC1 interface (C). Intrinsic chemical reactivity of S-Cl and S-Br at Met93 (D). Modified with permission from Ref. (60) (Elsevier, #4853020775500)

### 1.5.2. Laminin – a potential binding partner for peroxidasin

As already outlined in chapter 1.4, laminin (LM) is a core component in BM formation that is required for initiating BM assembly. LMs are large heterotrimeric glycoproteins that assemble from disulphide linked  $\alpha$ -,  $\beta$ - and  $\gamma$ -chains. The human genome carries eleven LM genes that code for five  $\alpha$ -, three  $\beta$ - and three  $\gamma$ - chains leading to a total combination of over 50 potential heterotrimeric isoforms. However, currently only 16 combinations are identified in humans (Fig. 9) (83).

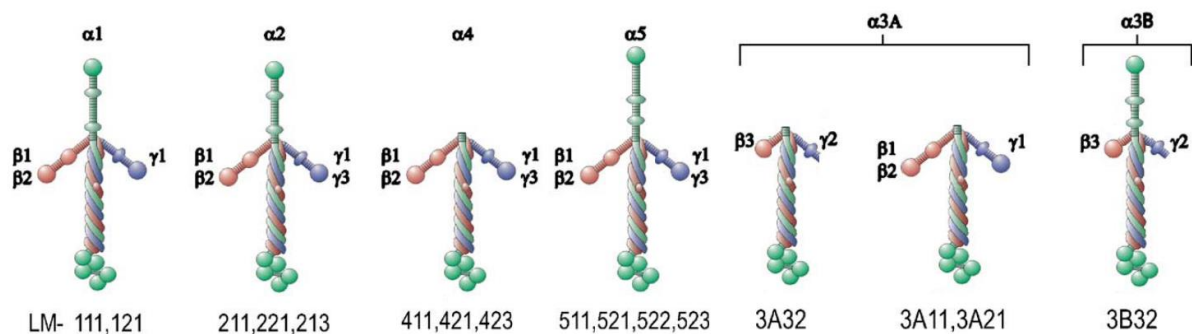


Figure 9 – Schematic overview of 16 known/predicted laminin heterotrimers. Numbers below laminin indicate their trimer composition. A short  $\alpha 3A$  and a long transcript is available for the  $\alpha 3$  chain. Modified with permission from Ref. (84) (Elsevier; #4852990757714)

LMs are essential for organogenesis and early embryonic events (85). While LM-111 is ubiquitous in embryos, the most dominant isoforms of LM in adults are LM-511 and LM-521. LM-211 and 221 are found in BMs of skeletal and cardiac muscles, while LM-411 and 421 are abundant in endothelial BMs, LM-332 is specific for the basal lamina below endothelial tissues (83). As seen in Fig. 9 all LM isoforms resemble a cross-like architecture with one long heavily conserved coiled-coil arm with the C-terminal region and up to three short rod-like N-termini. The C-terminal domain interacts with proteins that are anchored to the cellular surface of cells and thus can pass down signals from the extracellular space into the cell (Fig. 6). The shorter N-terminal arms on the other hand interact with other ECM proteins and molecules (e.g nidogen, collagen IV, perlecan, Fig. 6) and are required for polymerization of LM (67, 83). Given the fact LMs are crucial molecules in every BM and interact with collagen IV and many other ECM proteins, they are a potential candidate as a peroxidasin binding partner.

## 1.6 Biological role of peroxidasin in invertebrates

### 1.6.1 Peroxidase in *Drosophila melanogaster*

As previously mentioned, peroxidase was originally discovered in the BM of *D. melanogaster* (37). Nelson et al. showed that peroxidase is a homotrimeric multidomain protein, which is able to oxidize tyrosine and iodinate other proteins. They further proved that peroxidase is produced by hemocytes in an early embryonic development stage and proposed its use as a potential differentiation marker. Hemocytes are mobile phagocytotic cells that also secrete ECM proteins. Shortly after the initial production of peroxidase in hemocytes, other developmental ECM proteins like papilin, laminin and collagen IV are successively expressed. In later stages of embryogenesis, peroxidase is localized in established BMs. Therefore, peroxidase is a product of the same cell lineage which secretes ECM proteins to build BMs. Already in this first study it was proposed that peroxidase can potentially cross-link and thus stabilize the ECM (37).

Almost 20 years later, Bhave et al. were able to show that peroxidase indeed generates special crosslinks within the network of collagen IV in the ECM (38). Homozygous peroxidase knockouts in *D. melanogaster* were not viable past the third instar larvae stage and showed severely torn and distorted midgut visceral muscles when compared to heterozygous or wild-type larvae. This finding was consistent with a previous study performed in *C. elegans* where peroxidase knockouts also showed defects in the BM integrity (76). It additionally provided a molecular mechanism behind the lethality in homozygous peroxidase knockouts in *C. elegans* and *D. melanogaster* (38). In a subsequent study it was further shown that not only peroxidase knockouts are lethal for larvae but also bromide deficiency leads to a highly similar phenotype of BM defects and larval lethality. This finding not only established a link between peroxidase, bromine and collagen IV but also was the first proof that bromine is an essential trace element for higher organisms. It was further established, that loss of peroxidase slightly reduces elongation in *D. melanogaster* egg development, mimicking a collagen IV deficiency (60).

### 1.6.2 Peroxidase in *Caenorhabditis elegans*

Peroxidase was also identified in a mutagenesis study that screened for defects in embryonic morphogenesis in *C. elegans* (76). Several mutations within the peroxidase gene of *C. elegans* (PXN-2) were identified that expressed different phenotypes, ranging from semi-viable to fully embryonic and early larval lethal. Ultrastructural analysis of the BM revealed that loss of peroxidase function leads to the detachment of the body wall muscles from the epidermis as the cause for early lethality (76). Similar effects were seen in collagen IV mutation studies indicating that tissue integrity is crucial during growth and development (86). Both phenotypes were rescued by providing transgenes containing genomic PXN-2 DNA proving that peroxidase is essential for *C. elegans* embryonic development. However, transgenic

peroxidases lacking the LRR domain or the Ig domains failed or had a significantly reduced rescue ability compared to wild-type peroxidase transgenes, indicating their crucialness for peroxidase functionality. Furthermore PXN-2 not only seems to play a critical role in embryonic morphogenesis but is also required in postembryonic BM integrity (72).

### 1.6.3 Peroxidase in *Chilo suppressalis*

In a recent study, expression patterns of peroxidase were studied in different development stages of *C. suppressalis* (87). It was discovered that peroxidase is expressed in rhythmic waves during metamorphosis. It is highly expressed in eggs and steadily decreases to low levels in the 5<sup>th</sup> instar larvae. A sudden increase of peroxidase expression in the later stage of 6<sup>th</sup> instar larvae occurs when the transformation from larvae to pupa takes place. During the pupa phase, peroxidase levels decrease until the 7<sup>th</sup> day of pupa development, where the next transformation from pupa to adult happens. By knocking down peroxidase with RNA interference (RNAi) in the 6<sup>th</sup> instar larvae, mortality was significantly increased during the molt from larvae to pupa. This indicates that peroxidase might be also involved in the transformation processes during metamorphosis (e.g cuticle sclerotization) (87).

## 1.7 Biological role of peroxidase in vertebrates

### 1.7.1 Peroxidase in *Xenopus tropicalis*

The first study on a vertebrate peroxidase was already performed 2005 by Tindall et al. (88). By studying the expression patterns of peroxidase in the amphibian model organism *X. tropicalis* it was revealed that peroxidase is also expressed in specific tissues like the neural tube and the early pronephric primordium during early development. It was therefore speculated that peroxidase is also involved in the modification of ECM components in vertebrate species (88).

### 1.7.2 Peroxidase in *Mus musculus*

After observing lethal peroxidase mutations in invertebrates, one might think that peroxidase is also essential for the development of higher vertebrates. However, no lethal peroxidase mutations were found in those organisms. It seemed that peroxidase was not essential for general development of vertebrate life. However, a particular eye development defect was associated with peroxidase mutations in mice. An initial study showed that a broad spectrum of ocular dysgenesis phenotypes in humans could be pinned to homozygous mutations in

peroxidase (89), leading to the first indication that peroxidase is important for the development of eyes in vertebrates. A following *in vivo* study on mice showed that peroxidase is indeed a key player in the middle stage of eye development in mice, since a loss of peroxidase function led to anterior eye segment dysgenesis, corneal opacity and lens disorganization (90). Additionally, dramatic changes in the ECM of peroxidase-mutant eyes were observed during embryonic development that were consistent with previous findings in *C. elegans* and *D. melanogaster* (60, 76, 90). It was argued that inability to crosslink collagen IV of peroxidase mutants led to a destabilized ocular BM causing the loss of structural identity of the lens capsule and impairment of lens epithelial adhesion.

A different study which investigated the role of peroxidase in a mouse kidney fibrosis model demonstrated that peroxidase is enriched in the peritubular space of kidneys as fibrosis progresses while it shows low abundance in non-pathologic kidneys (91). Colon and colleagues subsequently showed, that peroxidase knock-out mice show reduced fibroblast activation and renal interstitial fibrosis further indicating a role of peroxidase in fibrosis *in vivo* (92).

### 1.7.3 Peroxidase in *Homo sapiens*

Peroxidase in humans was first described in a study focused on extracted cDNA from p-53-dependent induced apoptotic cells, where it was shown that peroxidase is widely expressed through all tissues except the brain and leukocytes (93). In a different study peroxidase was described as a melanoma associated gene (MG50) by Mitchell et al. since it was discovered in melanoma samples (94). Although the study characterized peroxidase as a potent melanoma-associated antigen, the physiological function remained unstudied. Contradictory to the previous study it was also reported that expression of peroxidase was relatively restricted to tumor tissue and absent from normal tissue (94). In a study conducted by Péterfi et al. in 2009, it was shown that peroxidase is indeed widely expressed (91), confirming the results of the previous study performed by Horikoshi et al. (93). Moreover, they showed for the first time that peroxidase is secreted by myofibroblasts into the extracellular space where it colocalized with fibronectin into a fibril-like network (91).

So far only one pathological condition in humans was reported to be caused by a mutation in the peroxidase gene. Two independent studies could show that mutations in the peroxidase gene can lead to microphthalmia and anterior segment dysgenesis in humans (89, 95). This finding was confirmed by an *in vivo* study conducted in mice (see 1.7.2), which proved that peroxidase plays an important role in eye development (90) in higher mammals. In total six mutations have been found in the peroxidase gene that can cause this pathological phenotype. Out of these six identified mutations, four of them were predicted to cause a stop

or frameshift mutation leading to nonsense-mediated decay. The remaining two affected a highly conserved arginine in the peroxidase domain (Arg880Cys) and a highly conserved glutamine in one of the Ig domains (Gln316Pro) (95).

Peroxidasin has also been reported to be upregulated in several different cancer types including ovarian, bladder, esophageal, prostate, kidney, metastatic melanoma and glioblastoma (94, 96–103). Two studies further indicated that peroxidasin levels were elevated throughout tumor progression and that high peroxidasin levels were associated with a poor prognosis (96, 99). It was additionally suggested that peroxidasin might play a role in angiogenesis and vascularization in (metastatic) tumors (101, 104). This could be confirmed by a recent study which showed that peroxidasin indeed promotes angiogenesis through activation of ERK1/2 (Extracellular-signal Regulated Kinases), PI3K-Akt (Phosphoinositide 3-kinase – Protein Kinase B) and FAK (focal adhesion kinase) pathways (105).

Additionally, peroxidasin is associated with a very rare pulmonary-renal syndrome, the so-called Goodpasture disease. It is an autoimmune disease, where autoantibodies recognize dissociated NC1 domains of the  $\alpha 3$  and  $\alpha 5$  chain in collagen IV. However, peroxidasin-mediated sulfilimine cross-links in collagen IV prevent those autoantibodies from binding, since they provide a constraint against dissociation (106). A recent study showed that patients with Goodpasture disease had also raised autoantibodies against peroxidasin that might inhibit sulfilimine crosslink formation thereby speeding up disease progression (107).

Several studies also indicated that peroxidasin might play a role in the innate immune system like MPO, EPO and LPO. In initial studies it was reported that peroxidasin can kill bacteria based on the production on hypochlorous acid (108, 109). This claim was highly controversial, since it was believed that only MPO was able to generate hypochlorous acid at a reasonable rate at physiological conditions due to its, among peroxidases, unique heme to protein sulfonium linkage (10, 110, 111). In a study conducted during the course of this thesis, it was confirmed that peroxidasin is not able to use chloride as a substrate (112). A recent study showed that peroxidasin might contribute to lung host defense by binding and killing of gram negative bacteria by the release of hypohalous acids (113).

The second human peroxidasin homologue (hsPxd02) is even less studied than hsPxd01. Since hsPxd02 is lacking crucial amino acids in the peroxidase region, it has most likely no catalytic activity. It was first found to be expressed in the heart (40). It was reported that hsPxd01 and hsPxd02 can form heterotrimers and an antagonistic regulation mechanism of hsPxd02 was discussed as this mechanism was also proposed in other species (40, 76). A different study also reported a different splice variant of hsPxd02 leading to a 57 kDa protein with endonuclease activity (53). Most recently a study also suggested that hsPxd02 might serve as a biomarker in breast cancer (52).

## 1.8 The missing source of hydrogen peroxide

As previously established, peroxidase utilizes hydrogen peroxide to oxidize bromide to hypobromous acid (HOBr) (Reaction 5), which further reacts with Met93 of the NC1 domain of collagen IV to form a bromosulfonium intermediate. This intermediate further reacts with an amine group of a hydroxylysine on the opposing protomer to establish a sulfilimine linked NC1 hexamer. (Fig. 8B) (60). However, the source of hydrogen peroxide to initiate the oxidation of bromide by peroxidase is so far unknown. Other human peroxidases cooperate with NOX/DUOX NADPH oxidases that provide hydrogen peroxide to produce hypohalous acids. MPO and EPO for example uses hydrogen peroxide provided by NOX2 to generate HOCl and HOBr in the innate immune system (18, 22) while TPO and LPO on the other hand use hydrogen peroxide provided by DUOX2 (22, 114). It was therefore initially hypothesized that peroxidase also might rely on the production of H<sub>2</sub>O<sub>2</sub> by NOX/DUOX NADPH oxidases. A recent study showed that formation of the sulfilimine crosslink occurs in a NOX/DUOX independent pathway and under low oxygen levels disproving the initial hypothesis (115). Another documented source of extracellular hydrogen peroxide besides NOX members is xanthine oxidase, which is released by hepatocytes and binds to endothelial cells (116). While the intracellular hydrogen peroxide concentration is estimated to be around 2 nM, the extracellular concentrations is approx. 1000 times higher. A very recent review concluded that the extracellular hydrogen peroxide concentration in blood and plasma is estimated to be 2-5 μM (116), which might intrinsically be enough for the formation of sulfilimine links by peroxidase.

## 2. Aims of the thesis

After the initial discovery that peroxidasin was responsible for the important sulfilimine link formation in collagen IV, peroxidasin attracted interest of several researchers across the world. Following studies focused on its role in developmental biology and in diseases (107, 117–120), an initial biochemical characterization (41) and its phylogenetic background (39). However, detailed kinetic studies on the reaction of peroxidasin and its substrates were missing. Moreover, no interaction partner of peroxidasin in the extracellular matrix was known.

Therefore, the first goal of this thesis was to elucidate the pre-steady-state kinetics for the reaction of hsPxd01 with well-known physiological two- and one-electron donors including chloride, bromide, iodide and thiocyanate as well as urate, tyrosine, serotonin and urate. Since peroxidasin is an extracellular protein, the interdependence of the halogenation and peroxidase activities should be elucidated in detail. By using multi-mixing stopped-flow spectroscopy apparent bimolecular rate constants should be determined for the first time and discussed with respect to the proposed physiological functions of hsPxd01.

An initial study suggested that collagen IV might not interact with peroxidasin directly. A mechanism involving a ternary complex with peroxidasin, collagen IV and another protein was proposed (81). Therefore, the second main objective of this thesis was to find an interacting partner within the extracellular matrix. This might shed light on to the exact reaction mechanism of the formation of the sulfilimine link and how damage to the extracellular matrix is avoided.

### 3. Publications

# Pre-steady-state kinetics reveal the substrate specificity and mechanism of halide oxidation of truncated human peroxidasin 1

Martina Paumann-Page, Romy-Sophie Katz, Marzia Bellei, Irene Schwartz, Eva Edenhofer, **Benjamin Sevcnikar**, Monika Soudi, Stefan Hofbauer, Gianantonio Battistuzzi, Paul G. Furtmüller, and Christian Obinger

Research Article

The Journal of Biological Chemistry Vol. 292, No. 11, pp. 4583–4592,  
March 17, 2017  
DOI:10.1074/jbc.M117.775213

# Pre-steady-state Kinetics Reveal the Substrate Specificity and Mechanism of Halide Oxidation of Truncated Human Peroxidase 1\*

Received for publication, January 4, 2017, and in revised form, January 24, 2017. Published, JBC Papers in Press, January 31, 2017, DOI 10.1074/jbc.M117.775213

Martina Paumann-Page<sup>‡</sup>, Romy-Sophie Katz<sup>‡</sup>, Marzia Bellei<sup>§</sup>, Irene Schwartz<sup>‡</sup>, Eva Edenhofer<sup>‡</sup>, Benjamin Sevcnikar<sup>‡</sup>, Monika Soudi<sup>‡</sup>,  Stefan Hofbauer<sup>‡</sup>,  Gianantonio Battistuzzi<sup>¶</sup>,  Paul G. Furtmüller<sup>‡1</sup>, and  Christian Obinger<sup>‡2</sup>

From the <sup>‡</sup>Department of Chemistry, Division of Biochemistry, Vienna Institute of BioTechnology, BOKU-University of Natural Resources and Life Sciences, Muthgasse 18, A-1190 Vienna, Austria and the Departments of <sup>§</sup>Life Sciences and <sup>¶</sup>Chemistry and Geology, University of Modena and Reggio Emilia, 41125 Modena, Italy

Edited by F. Peter Guengerich

Human peroxidase 1 is a homotrimeric multidomain peroxidase that is secreted to the extracellular matrix. The heme enzyme was shown to release hypobromous acid that mediates the formation of specific covalent sulfilimine bonds to reinforce collagen IV in basement membranes. Maturation by proteolytic cleavage is known to activate the enzyme. Here, we present the first multimixing stopped-flow study on a fully functional truncated variant of human peroxidase 1 comprising four immunoglobulin-like domains and the catalytically active peroxidase domain. The kinetic data unravel the so far unknown substrate specificity and mechanism of halide oxidation of human peroxidase 1. The heme enzyme is shown to follow the halogenation cycle that is induced by the rapid H<sub>2</sub>O<sub>2</sub>-mediated oxidation of the ferric enzyme to the redox intermediate compound I. We demonstrate that chloride cannot act as a two-electron donor of compound I, whereas thiocyanate, iodide, and bromide efficiently restore the ferric resting state. We present all relevant apparent bimolecular rate constants, the spectral signatures of the redox intermediates, and the standard reduction potential of the Fe(III)/Fe(II) couple, and we demonstrate that the prosthetic heme group is post-translationally modified and cross-linked with the protein. These structural features provide the basis of human peroxidase 1 to act as an effective generator of hypobromous acid, which mediates the formation of covalent cross-links in collagen IV.

Human peroxidase 1 (hsPxd01)<sup>3</sup> plays a critical role in the stabilization of basement membranes by catalyzing the forma-

tion of covalent cross-links within the collagen IV network (1). Type IV collagen  $\alpha$  chains form triple helical protomers that self-assemble with end-to-end C-terminal associations known as NC1 hexamers. Peroxidase 1 oxidizes bromide to hypobromous acid, which is responsible for the generation of a highly specific sulfilimine bond between opposing methionine and hydroxylysine residues that bridge the trimer-trimer interface of the NCI hexamer thereby structurally reinforcing the collagen IV network (2). Despite these very exciting findings in recent years, relatively little is known about the mechanism of the catalytic reactions, redox intermediates, and substrate specificity of this novel multidomain human heme peroxidase.

Human peroxidase 1 belongs to the peroxidase-cyclooxygenase superfamily (3, 4). In addition to the catalytic peroxidase domain (POX), hsPxd01 comprises a leucine-rich repeat domain (LRR) and four C-like immunoglobulin domains (Ig) at the N terminus and a C-terminal von Willebrand factor type C module (VWC), all known to be important for protein-protein interactions and cell adhesion. Moreover, mature human peroxidase 1 is shown to be highly glycosylated and to form a homotrimer via intermolecular disulfide bonds (5, 6).

The peroxidase domain displays high homology to that of the well characterized chordata peroxidases lactoperoxidase (LPO), myeloperoxidase (MPO), eosinophil peroxidase (EPO), and thyroid peroxidase (TPO) with the highest similarity to LPO. Comparative sequence analysis clearly suggests that in the active site of hsPxd01 all amino acid residues, which are crucial to peroxidase and halogenation activity, are fully conserved (5, 7), including distal His, Arg, and Gln.

It has been reported that the catalytic efficiency of bromide oxidation ( $k_{cat}/K_m$ ) of recombinant full-length hsPxd01 is rather low but increased upon truncation (5). This was confirmed in a recent study that showed the cleavage of trimeric hsPxd01 at Arg<sup>1336</sup> C-terminal of the peroxidase domain by a proprotein convertase (8). The truncation eliminates the von Willebrand factor and renders the peroxidase more active. This proteolytic maturation seems to represent a key regulatory event in hsPxd01 biosynthesis and function because the C-terminal proprotein convertase recognition sequence is evolutionarily conserved throughout the animal kingdom (8).

\* This work was supported by Austrian Science Fund Project P25538 and Doctoral Program Biomolecular Technology of Proteins (BioToP) FWF W1224. The authors declare that they have no conflicts of interest with the contents of this article.

✂ Author's Choice—Final version free via Creative Commons CC-BY license.

<sup>1</sup> To whom correspondence may be addressed. Tel.: 43-1-47654-77277; Fax: 43-1-47654-77059; E-mail: paul.furtmueller@boku.ac.at.

<sup>2</sup> To whom correspondence may be addressed. Tel.: 43-1-47654-77273; Fax: 43-1-47654-77059; E-mail: christian.obinger@boku.ac.at.

<sup>3</sup> The abbreviations used are: hsPxd01, human peroxidase 1; hsPxd01-con4, construct 4 of human peroxidase 1; POX, peroxidase domain; LRR, leucine-rich repeat domain; VWC, von Willebrand factor C; LPO, lactoperoxidase; EPO, eosinophil peroxidase; MPO, myeloperoxidase; CT, charge transfer; DAD, diode array detector.

## Kinetics of Interconversion of Redox Intermediates of Pxd01

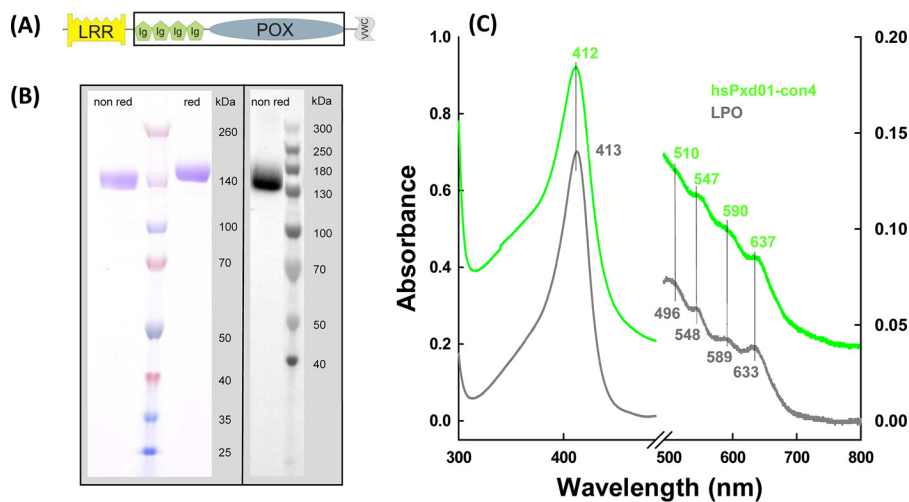


**FIGURE 1. Biochemical characterization of hsPxd01-con4.** A, schematic structure of hsPxd01-con4. It includes four Ig domains (Ig) and the catalytic POX domain as marked by the *black box*, omitting the LRR domain and the VWC module of full-length hsPxd01. B, SDS-PAGE and detection of covalently bound heme by ECL of hsPxd01-con4: 2  $\mu$ g of protein was resolved on a 4–12% gradient gel under non-reducing and under reducing conditions (*left panel*). For ECL 6  $\mu$ g of hsPxd01-con4 was blotted on a nitrocellulose membrane, and covalently bound heme was visualized with enhanced chemiluminescence (*right panel*). C, UV-visible spectra of hsPxd01-con4 and bovine lactoperoxidase: spectra of 8  $\mu$ M per heme hsPxd01-con4 (*green*) and bovine lactoperoxidase (*gray*) were recorded in 100 mM phosphate buffer, pH 7.4.

In this work, to study the reactivity of the peroxidase domain and the effect of other domains on catalysis, several truncated variants of hsPxd01 were expressed recombinantly in HEK cells (5). One monomeric construct composed of the four Ig domains and the peroxidase domain (hsPxd01-con4) (Fig. 1A) was superior in terms of yield, heme insertion, spectroscopic features, and catalytic activity. This allowed for the first time a comprehensive study of the kinetics of interconversion of the relevant redox intermediates of the halogenation cycle. Here, we report the standard reduction potential of the Fe(III)/Fe(II) couple of the peroxidase domain and apparent bimolecular rate constants for cyanide binding as well as the formation and reduction of compound I mediated by hydrogen peroxide, bromide, iodide, and thiocyanate at pH 7.4. Based on the available structural, kinetic, and thermodynamic data of the homologous human peroxidases, we provide a mechanism for the halogenation cycle of human peroxidase 1, and we discuss its relevance for its biosynthetic function in collagen IV cross-linking.

### Results

**Purification, Spectral and Redox Properties of hsPxd01-con4**—Transient expression of hsPxd01-con4 in HEK cells resulted in a yield of purified protein of ~10–20 mg/liter medium. The protein was composed of the amino acid residues Pro<sup>246</sup>–Asp<sup>1314</sup> (numbers referring to full-length hsPxd01, including the signal peptide (5)) with a theoretical molar mass of 121 kDa. The construct included the four immunoglobulin (Ig)-like domains and the POX domain. In SDS-PAGE under both aerobic and reducing conditions, the corresponding band appeared at a slightly higher molar mass (Fig. 1B, *left panel*) because hsPxd01 is highly glycosylated with eight confirmed *N*-glycosylation sites located in the hsPxd01-con4 region (5). The heme of this construct was post-translationally modified and covalently bound to the protein that was clearly demonstrated by SDS-PAGE in combination with the enhanced chemiluminescence staining procedure (Fig. 1B, *right panel*).

Covalent attachment of the prosthetic group could also be confirmed by precipitation of the recombinant protein by acetone at pH 4.5 resulting in colorless supernatants (data not shown). Furthermore, the determined spectral and redox properties clearly suggested the establishment of heme-protein bonds (see below). It is well known that these post-translational modifications considerably influence both the spectral signatures of a heme protein in its ferric state and the standard reduction potential of the Fe(III)/Fe(II) couple (9, 10).

In this context, it is important to note that the purification protocol (see under “Experimental Procedures”) could be significantly improved by including a 48-h incubation step prior to buffer exchange and affinity chromatography. This period seemed to be necessary for establishment of covalent bonds. The modification of the prosthetic group is reflected by a gradual transition of the UV-visible spectrum of freshly purified hsPxd01-con4. Spectral transition included a red-shift of the Soret band from 410 to 412 nm together with establishment of Q-bands at 510, 547, and 590 nm and a charge transfer (CT) band at 637 nm (Fig. 1C, *green spectrum*). This spectrum is reminiscent of that of ferric LPO (Fig. 1C, *gray spectrum*). The peroxidase domain of hsPxd01 has a high amino acid sequence homology with LPO (34% identity and 53% similarity) (5). In the known crystal structure of LPO, continuous electron densities underline the presence of two ester bonds between the modified prosthetic heme group and conserved Asp and Glu residues (7). Sequence alignment and modeling demonstrated that these acidic amino acids are fully conserved in hsPxd01 (*i.e.* Asp<sup>826</sup> and Glu<sup>980</sup>) (3, 5).

Heme modification was also underlined by spectroelectrochemical studies on hsPxd01-con4. Fig. 2 shows a representative redox titration with fully oxidized and fully reduced hsPxd01-con4 depicted in *green* and *brown*, respectively. Upon reduction, the Soret peak of the ferric protein shifted from 412 to 435 nm (Fig. 2) very similar to 5-coordinated ferrous lac-

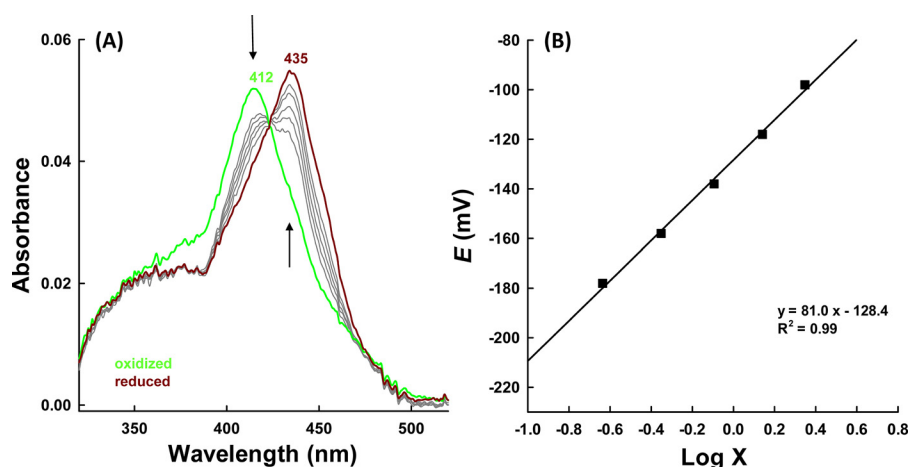


FIGURE 2. **Spectroelectrochemistry of hsPxd01-con4.** A, electronic spectra of hsPxd01-con4 recorded at various potentials in spectroelectrochemical experiments carried out with an OTTLE cell at 25 °C. Conditions: 5  $\mu\text{M}$  hsPxd01-con4 in 100 mM phosphate buffer, pH 7.4, containing 100 mM NaCl, in the presence of the following mediators: 30  $\mu\text{M}$  methyl viologen, 1  $\mu\text{M}$  lumiflavin 3-acetate; methylene blue, phenazine methosulfate; and indigo disulfonate used as mediators. Arrows indicate spectral changes during reduction from ferric (green) to ferrous hsPxd01-con4 (brown). B, corresponding Nernst plot where  $\times$  represents  $(A_{\lambda_{\text{red}}}^{\text{max}} - A_{\lambda_{\text{red}}}) / (A_{\lambda_{\text{ox}}}^{\text{max}} - A_{\lambda_{\text{ox}}})$ , with  $A_{\lambda_{\text{ox}}} = 412 \text{ nm}$  and  $A_{\lambda_{\text{red}}} = 435 \text{ nm}$ , respectively.

toperoxidase and eosinophil peroxidase (11). From the corresponding Nernst plot (Fig. 2B), the standard reduction potential ( $E'^0$ ) of the Fe(III)/Fe(II) couple was calculated to be  $-0.128 \pm 0.006 \text{ V}$  (25 °C and pH 7.4).

**Cyanide Binding**—Before investigating the kinetics of compound I formation and reduction, we probed the accessibility of the heme cavity and the homogeneity of the architecture of the active site by monitoring the kinetics of cyanide binding. It has been demonstrated that the post-translational modification of the prosthetic group in peroxidases from the heme peroxidase-cyclooxygenase superfamily is often not fully established resulting in some structural heterogeneity of the heme cavity that can easily be probed by studying the kinetics of cyanide binding (7, 10). In the case of hsPxd01-con4, cyanide binding resulted in the transition of the high spin ( $S = 5/2$ ) Fe(III) state to the low spin ( $S = 1/2$ ) Fe(III) state (Soret maximum at 431 nm, bands at 558 and 588 nm, and loss of the CT band at 637 nm) with clear isosbestic points at 423, 494, 519, 623, and 666 nm (Fig. 3A). Binding of the ligand was biphasic with a dominating rapid first phase and a slower second phase (Fig. 3B). From the double exponential fit of these time traces, first-order rate constants ( $k_{\text{obs}(1)}$  and  $k_{\text{obs}(2)}$ ) were obtained and plotted versus cyanide concentration. From the corresponding linear plots (Fig. 3C), an apparent second-order rate constant  $k_{\text{on}(1)}$  for the dominating rapid phase was calculated to be  $(7.9 \pm 0.2) \times 10^5 \text{ M}^{-1} \text{ s}^{-1}$  ( $k_{\text{off}} = (3.3 \pm 0.7) \text{ s}^{-1}$  and  $K_D(1) = k_{\text{off}}/k_{\text{on}} = 4.2 \mu\text{M}$ ) at pH 7.4 and 25 °C, which compares with  $1.3 \times 10^6 \text{ M}^{-1} \text{ s}^{-1}$  and  $K_D = 4.3 \mu\text{M}$  for human MPO (12) and  $1.3 \times 10^6 \text{ M}^{-1} \text{ s}^{-1}$  and  $K_D = 23.8 \mu\text{M}$  for bovine LPO (13). From the plot of  $k_{\text{obs}(2)}$  values versus cyanide concentration, an apparent  $k_{\text{on}(2)}$  of  $(8.8 \pm 0.2) \times 10^3 \text{ M}^{-1} \text{ s}^{-1}$  ( $k_{\text{off}(2)} = (0.40 \pm 0.08) \text{ s}^{-1}$  and a  $K_D(2) = 45.5 \mu\text{M}$ ) (data not shown) was calculated for the minor second phase. These binding parameters are comparable with recently reported values for a recombinant bacterial peroxidase from the cyanobacterium *Lyngbya* sp. PCC 8106, which features autocatalytically formed covalent heme to protein links (10). Like the peroxidase domain of hsPxd01, the bacterial peroxidase has a high amino acid sequence homology with LPO, and the prosthetic group is

covalently attached to the protein via two ester bonds. The reaction of the ferric bacterial protein with cyanide also showed a biphasic behavior with a dominating rapid phase. In both cases in a small portion of the protein the post-translational modification of the prosthetic group was not fully accomplished resulting in some heterogeneity of the active site and in consequence in the kinetics and thermodynamics of cyanide binding.

**Hydrogen Peroxide Efficiently Oxidizes hsPxd01-con4 to Compound I**—To act as peroxidase in extracellular cross-linking reactions, peroxidase must be oxidized by peroxides. Here, we showed that hydrogen peroxide efficiently converted the ferric form of hsPxd01-con4 into the redox intermediate compound I. Fig. 4A shows that this reaction was reflected by a spectral transition with isosbestic points at 360 and 443 nm, hypochromicity in the Soret absorbance (maximum at 410 nm), and the establishment of a new band around 670 nm (Fig. 4, red spectrum). Similar to LPO (14), maximum hypochromicity was already achieved with equimolar  $\text{H}_2\text{O}_2$  within 200 ms (Fig. 4A). Analogous to LPO (14), compound I of hsPxd01-con4 was not stable but slowly converted to a compound II-like species (Fig. 4, blue spectrum).

The kinetics of hsPxd01-con4 oxidation mediated by  $\text{H}_2\text{O}_2$  was followed by the decrease of absorbance at 412 nm. The reaction was biphasic with a dominating rapid first phase ( $>80\%$  of  $\Delta A_{412 \text{ nm}}$ ). The corresponding pseudo first-order rate constants  $k_{\text{obs}(1)}$  and  $k_{\text{obs}(2)}$  were obtained from double exponential fits. From the slope of the plots of the respective  $k_{\text{obs}}$  values versus hydrogen peroxide concentration, the apparent bimolecular rate constants for the dominating phase  $k_{\text{app}(1)}$ ,  $(1.8 \pm 0.1) \times 10^7 \text{ M}^{-1} \text{ s}^{-1}$  (Fig. 4C), and the second phase  $k_{\text{app}(2)}$ ,  $(6.9 \pm 0.6) \times 10^5 \text{ M}^{-1} \text{ s}^{-1}$  (data not shown), were calculated, pH 7.4.

Furthermore, we could demonstrate that the rate of compound I formation was invariant within the pH range of 5.0–9.0 (Fig. 4D). A  $\text{p}K_1$  value of 4.7 and a  $\text{p}K_2$  value of 9.0 were calculated from the fit  $k_{\text{app}} = a/(1 + x/b) \times (1 + c/x)$  with  $a$  representing  $k_{\text{internal}}$ ;  $x$  is the concentration of  $\text{H}^+$ ;  $b$  is  $\text{p}K_1$ , and  $c$  is

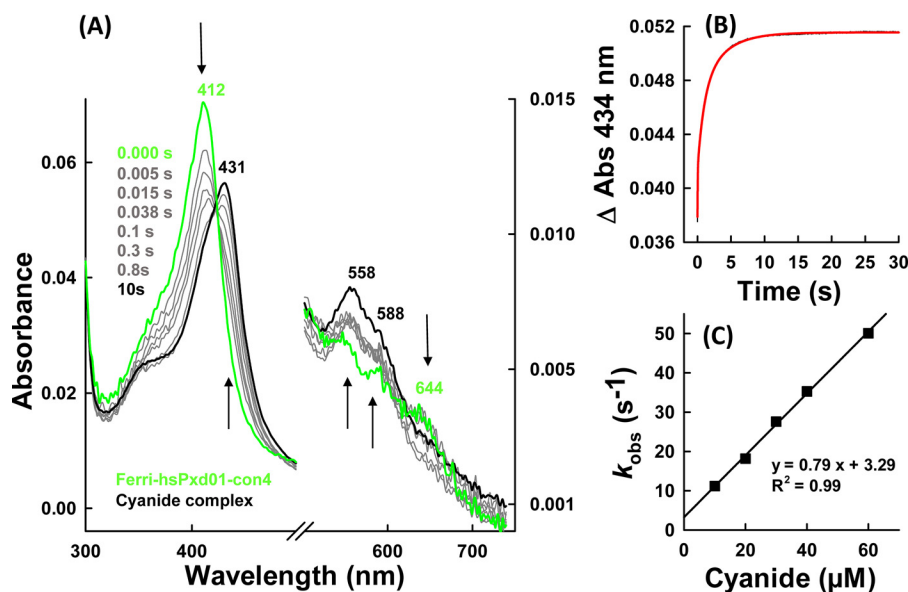


FIGURE 3. **Cyanide binding by ferric hsPxd01-con4.** *A*, spectral changes (arrows) of 1  $\mu\text{M}$  hsPxd01-con4 upon addition of 1 mM sodium cyanide in 100 mM phosphate buffer, pH 7.4. *B*, time trace and fit (red) of 500 nm hsPxd01-con4 after adding 90  $\mu\text{M}$  cyanide in 100 mM phosphate buffer, pH 7.4. Spectral changes were recorded at 434 nm. *C*,  $k_{\text{obs}}$  values for the reaction of 500 nm hsPxd01-con4 reacting with 10–60  $\mu\text{M}$  cyanide in 100 mM phosphate buffer, pH 7.4, plotted against the cyanide concentration for determination of  $k_{\text{on}}$ ,  $k_{\text{off}}$  and  $K_D$ .

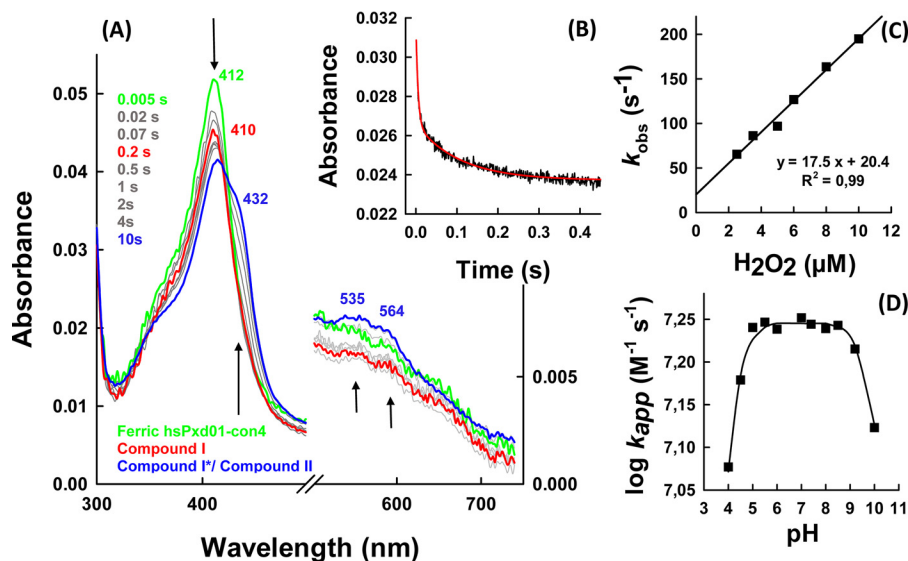


FIGURE 4. **Formation of compound I.** *A*, spectral changes (arrows) of 1  $\mu\text{M}$  hsPxd01-con4 reacting with equimolar hydrogen peroxide in 100 mM phosphate buffer, pH 7.4. *B*, typical time trace of compound I formation followed at 412 nm (black line) with corresponding double exponential fit (red line). *C*, determination of the apparent second-order rate constant at 25 °C: 1  $\mu\text{M}$  hsPxd01-con4 was reacted with 2.5, 3.5, 5, 6, 8, and 10  $\mu\text{M}$  hydrogen peroxide, and the obtained pseudo-first order  $k_{\text{obs}}$  values of the first phase were plotted against the concentration. *D*, pH profile of hsPxd01-con4 compound I formation: the determined  $k_{\text{app}}$  values at pH 4, 4.5, 5, 5.5, 6, 7, 7.4, and 8–10 were plotted against the respective pH values.

$\text{p}K_2$ . The first inflection point might reflect the  $\text{p}K_a$  of the distal histidine that acts as proton acceptor in compound I formation of heme peroxidases (7), whereas the second one could be related with the alkaline transition of hsPxd01-con4. The UV-visible spectrum of the ferric high spin protein is invariant between pH 5 and 8.0 (5) but converts to a low spin spectrum with red-shifted Soret band (430 nm) at pH values  $>8.5$  most probably reflecting the formation of a low spin hydroxide complex.

Addition of excess hydrogen peroxide to ferric hsPxd01-con4 converts the enzyme from the ferric state via compound I to compound II (oxoiron(IV) species) and, finally, to compound

III, which resembles electronically oxyhemoglobin or oxymyoglobin (*i.e.*  $\text{Fe(II)-O}_2 \leftrightarrow \text{Fe(III)-O}_2^-$ ) (Fig. 5). When hsPxd01-con4 was mixed with a 50-fold molar excess of hydrogen peroxide, the formation of predominantly compound II was observed with a heme Soret maximum at 432 nm and a broad Q band at 535 nm with a shoulder at 564 nm (Fig. 5, blue spectrum). With a 1000-fold molar excess of  $\text{H}_2\text{O}_2$ , compound II was converted to compound III resulting in a distinct UV-visible spectrum with a heme Soret maximum at 425 nm and prominent Q-bands at 552 and 588 nm (Fig. 5, cyan spectrum).

It was interesting to see that in contrast to LPO (14) but similar to myeloperoxidase (7), the conversion of compound I

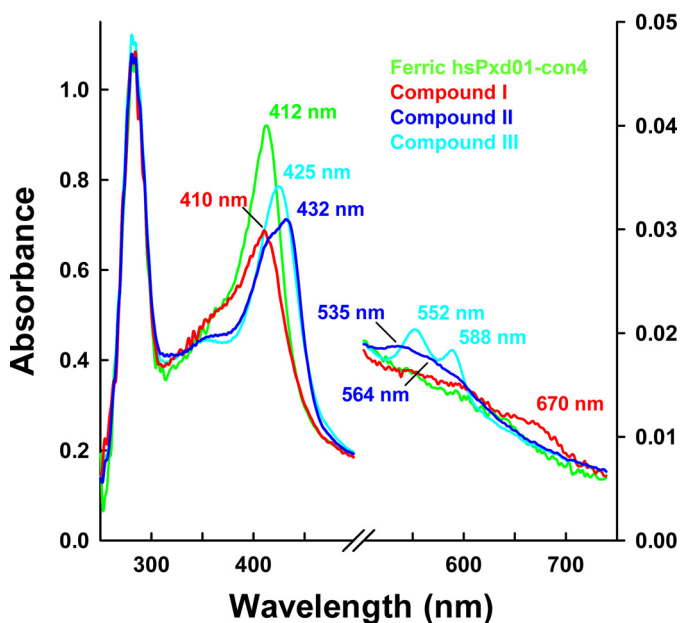


FIGURE 5. UV-visible spectra of compound I, compound II, and compound III.  $1 \mu\text{M}$  hsPxd01-con4 was reacted with varying concentrations of hydrogen peroxide in 100 mM phosphate buffer, pH 7.4. The ferric form of hsPxd01-con4 is depicted in green, and compound I, compound II, and compound III are shown in red, blue, and cyan, respectively. The characteristic Soret peak maxima and bands in the visible region are illustrated in the same color code. Compound II was formed by the addition of  $50 \mu\text{M}$  hydrogen peroxide, and compound III was generated by adding  $1 \text{ mM}$  hydrogen peroxide to the ferric protein.

to compound II was also dependent on the hydrogen peroxide concentration (Fig. 6). After incubating hsPxd01-con4 with equimolar  $\text{H}_2\text{O}_2$  in the aging loop of the stopped-flow instrument for 200 ms, formed compound I was mixed with increasing concentrations of  $\text{H}_2\text{O}_2$ . Formation of compound II clearly depended on the  $\text{H}_2\text{O}_2$  concentration, and from the biphasic time traces (Fig. 6B),  $k_{\text{app}}$  of the dominating initial reaction was calculated to be  $(1.3 \pm 0.03) \times 10^4 \text{ M}^{-1} \text{ s}^{-1}$  (Fig. 6C).

**Reaction of hsPxd01-con4-Compound I with Halides and Thiocyanate**—Next, we probed the reactivity of hsPxd01-con4 compound I with the halides chloride, bromide, iodide, and the pseudo-halide thiocyanate. Again, the sequential mode was used to form compound I by preincubating hsPxd01-con4 with an equimolar concentration of hydrogen peroxide for 200 ms before the halides were added. Fig. 7A shows the direct conversion of compound I back to the ferric enzyme upon addition of bromide. In contrast to the reaction of the ferric enzyme with cyanide and hydrogen peroxide, compound I reduction by bromide was monophasic (Fig. 7B) and allowed the calculation of an apparent bimolecular rate  $k_{\text{app}} = (5.6 \pm 0.4) \times 10^6 \text{ M}^{-1} \text{ s}^{-1}$  at pH 7.4 (Fig. 7C).

Because hypobromous acid formation was reported to be essential for the formation of the sulfilimine link (1, 2), the pH dependence of the kinetics of bromide oxidation was investigated. Fig. 7D depicts the corresponding plot of the logarithm of first-order rate constants  $k_{\text{obs}}$  versus pH. Between pH 4 and pH 6, the reaction was fast and pH-independent but decreased with increasing pH.

Importantly, chloride cannot act as an electron donor for compound I of hsPxd01-con4. Even in the presence of chloride

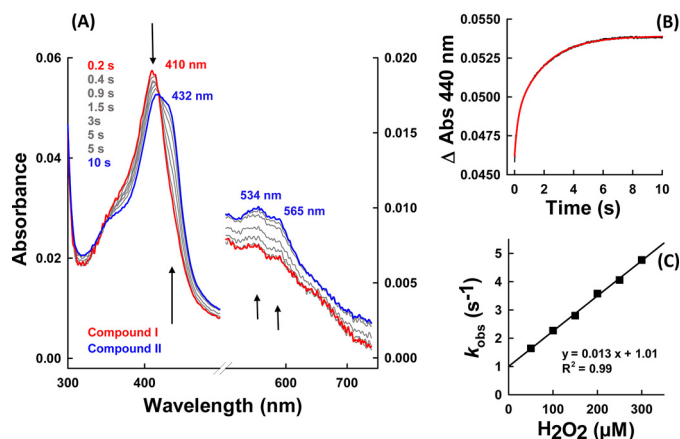


FIGURE 6. Reduction of compound I to compound II mediated by hydrogen peroxide. A, spectral changes (arrows) of  $1 \mu\text{M}$  hsPxd01-con4 compound I reacting with  $50 \mu\text{M}$  hydrogen peroxide. Compound I was formed after 200 ms in the aging loop. B, time trace of reaction between  $500 \text{ nm}$  compound I of hsPxd01-con4 and  $300 \mu\text{M}$  hydrogen peroxide measured in the sequential stopped-flow mode (delay time of 200 ms for compound I formation). The time trace (black line) was fitted double exponentially (red line). C, pseudo first-order rate constant of  $500 \text{ nm}$  hsPxd01-con4 compound I reacting with  $50, 100, 150, 200, 250,$  and  $300 \mu\text{M}$  hydrogen peroxide, respectively.  $k_{\text{obs}}$  values of the first phase were plotted against the concentration of hydrogen peroxide.

concentrations  $\gg 10 \text{ mM}$  added to  $1 \mu\text{M}$  hsPxd01-con4 compound I, no formation of the ferric enzyme could be detected. In the presence of chloride, compound I slowly converted to an intermediate with a compound II-like spectrum (data not shown). However, upon addition of  $5 \mu\text{M}$   $\text{Br}^-$  to  $100 \text{ mM}$   $\text{Cl}^-$ , the direct reduction of compound I to ferric hsPxd01-con4 could be observed (data not shown).

By contrast, the reaction of hsPxd01-con4 compound I with thiocyanate and iodide was very fast and resulted in a direct conversion of compound I to the ferric state. The spectral transition was almost identical to that observed with bromide. Fig. 8, A and B, shows representative monophasic time traces that could be fitted single exponentially. The apparent bimolecular rate constants were calculated to be  $(1.8 \pm 0.07) \times 10^7 \text{ M}^{-1} \text{ s}^{-1}$  and  $(1.7 \pm 0.067) \times 10^7 \text{ M}^{-1} \text{ s}^{-1}$  for the reaction with thiocyanate and iodide at pH 7.4 (Fig. 8, C and D).

## Discussion

For the first time, a truncated variant of hsPxd01 was produced in appreciable yield, good quality, and high activity, which allowed for pre-steady-state kinetic measurements to evaluate the substrate specificity and the mechanism of halide oxidation of human peroxidase 1. So far, only steady-state (5) and end point measurements (1, 2, 5) were published, and it was suggested that the enzyme preferentially generates hypobromous acid as a reactive intermediate to form sulfilimine cross-links in collagen (1, 2). Additionally, some papers reported the generation of hypochlorous acid by hsPxd01 (15, 16).

Human peroxidase 1 is a homotrimeric, highly glycosylated multidomain peroxidase, which so far could only be produced in recombinant form in animal cell cultures in very low amounts of protein with unsatisfactory heme occupancy and incomplete post-translational heme modification and thus low activity (5). However, elimination of the LRR and VWC domains increased the activity of the respective recombinant

## Kinetics of Interconversion of Redox Intermediates of Pxd01

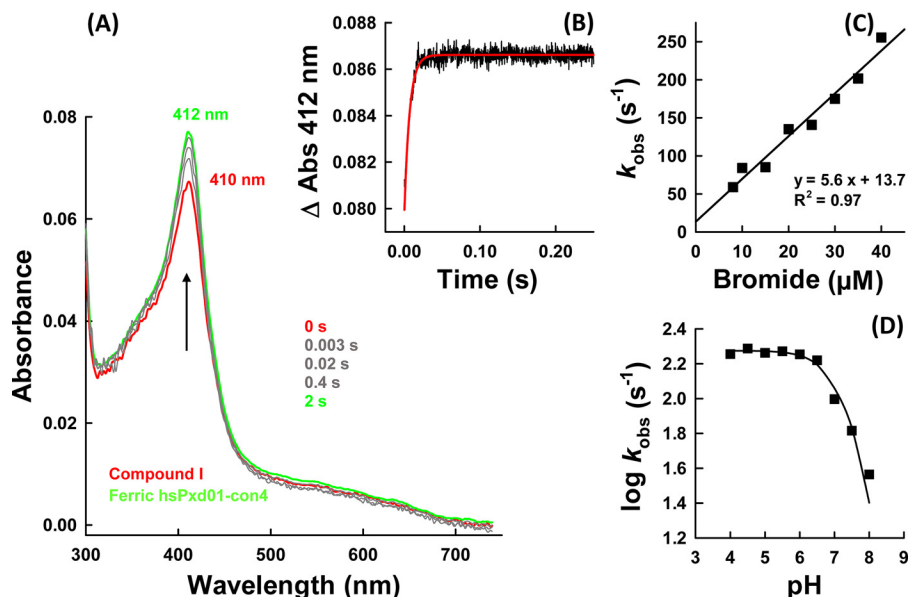


FIGURE 7. **Reaction of compound I with bromide.** *A*, spectral changes of the reaction between 1  $\mu\text{M}$  compound I of hsPxd01-con4 (red spectrum) with 10  $\mu\text{M}$  bromide in 100 mM phosphate buffer, pH 7.4. Compound I was formed with equimolar  $\text{H}_2\text{O}_2$  in the sequential mode (delay time of 200 ms). *B*, time trace (black line) of reaction between 1  $\mu\text{M}$  compound I of hsPxd01-con4 and 20  $\mu\text{M}$  bromide in 100 mM phosphate buffer, pH 7.4, together with single exponential fit (red line). *C*, plot of  $k_{\text{obs}}$  values versus bromide concentration. Conditions: 1  $\mu\text{M}$  hsPxd01-con4 compound I reacting with 8, 10, 15, 20, 25, 30, 35, and 40  $\mu\text{M}$  bromide in 100 mM phosphate buffer, pH 7.4, respectively. *D*, pH dependence of bromide oxidation by compound I. Plot of  $\log k_{\text{obs}}$  values versus pH. Conditions: 1  $\mu\text{M}$  hsPxd01-con4 reacting with 10  $\mu\text{M}$  bromide in the respective 100 mM buffer (pH 4–5.5 citrate phosphate buffer; pH 5.5–8 phosphate buffer; and pH 9 and 10 carbonate buffer).

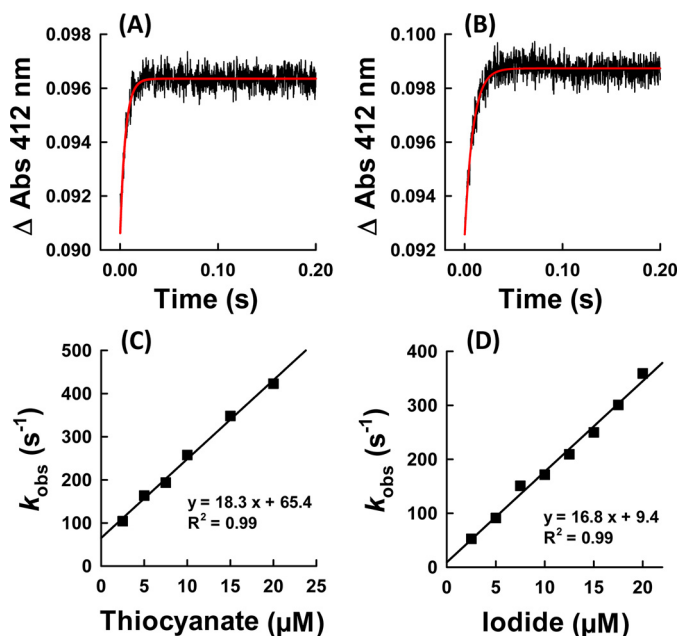


FIGURE 8. **Reaction of compound I with thiocyanate and iodide.** Time traces at 412 nm of reaction between 1  $\mu\text{M}$  compound I of hsPxd01-con4 and 20  $\mu\text{M}$  thiocyanate (*A*) and 5  $\mu\text{M}$  iodide (*B*), respectively. Plots of  $k_{\text{obs}}$  values versus thiocyanate (*C*) and iodide (*D*) concentration. Conditions: 1  $\mu\text{M}$  hsPxd01-con4 compound I reacting with 2.5, 5, 7.5, 10, 15, and 20  $\mu\text{M}$  thiocyanate or 2.5, 5, 7.5, 10, 12.5, 15, 17.5, and 20  $\mu\text{M}$  iodide in 100 mM phosphate buffer, pH 7.4.

construct (5). Recently, Colon and Bhawe (8) demonstrated that proprotein convertase processing enhances peroxidase 1 activity by elimination of the VWC domains and proposed that this event represents a key step in the biosynthesis and function of hsPxd01 to support basic membrane and tissue integrity. These findings motivated us to design several constructs,

including the POX domain only to search for a functional and well folded protein for first comprehensive pre-steady-state kinetic studies. Finally, comparative biochemical studies demonstrated that only the construct hsPxd01-con4 fulfilled the requirements with regard to yield, heme occupancy, and modification. Apparently, the four Ig domains together with the peroxidase domain are the smallest active entity, which is also supported by data from Ero-Tolliver *et al.* (17) that showed that this construct is likewise the smallest unit that mediates efficient sulfilimine cross-linking. The POX domain only was inactive in these studies, which underlines the evolutionarily conserved function of peroxidase in tissue development and integrity and distinguishes peroxidase from other peroxidases, such as LPO, EPO, and MPO, which are composed of fully functional POX domains only.

Our spectral, redox, and kinetic data clearly demonstrate that hsPxd01-con4 has an LPO-like heme environment that was already proposed by sequence alignment and homology modeling (4, 5). It has been demonstrated that one of the most important structural features of halogenating enzymes like LPO, EPO, and MPO is the modification of the 1- and 5-methyl groups on pyrrole rings A and C of the heme group allowing formation of ester linkages with the carboxyl groups of conserved aspartate and glutamate residues (7, 18). Myeloperoxidase is unique in having a third covalent (*i.e.* sulfonium ion) bond (9, 19, 20). Formation of these covalent heme-protein bonds has been proposed to occur autocatalytically (22–24) mediated by (sub)micromolar hydrogen peroxide concentrations and has a deep impact on the biochemical and biophysical properties of these peroxidases (18, 19). Full establishment of the covalent bonds is never achieved even when native proteins are purified from natural sources (20, 22–24). Similarly, in the

TABLE 1

Fe(III)/Fe(II) reduction potential and apparent second-order rate constants of Compound I formation (H<sub>2</sub>O<sub>2</sub>) and reduction (chloride, bromide, thiocyanate, and iodide) reactions of hsPxd01-con4, LPO, EPO and MPO

For hsPxd01-con4, all measurements were performed in 100mM phosphate buffer, pH 7.4, whereas the data displayed for LPO, EPO, and MPO was measured in 10 mM phosphate buffer, pH 7.

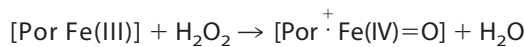
	hsPxd01-con4	LPO	EPO	MPO
Fe(III)/Fe(II) reduction potential	-0.128 V	-0.183 V (11)	-0.176 V (11)	+0.005 V (29)
Substrate	$\times 10^4$ (M <sup>-1</sup> s <sup>-1</sup> )	$\times 10^4$ (M <sup>-1</sup> s <sup>-1</sup> ) (14)	$\times 10^4$ (M <sup>-1</sup> s <sup>-1</sup> ) (31)	$\times 10^4$ (M <sup>-1</sup> s <sup>-1</sup> ) (30)
H <sub>2</sub> O <sub>2</sub>	1800	1100	4300	1400
chloride	-	-	0.31	2.5
bromide	560	4.1	1900	110
iodide	1680	12000	9300	720
thiocyanate	1830	20000	10000	960

case of recombinantly produced members from this superfamily, there was always some heterogeneity that could be diminished to some extent by adding low micromolar amounts of H<sub>2</sub>O<sub>2</sub> (10, 19, 25–27). In human peroxidase 1 Asp<sup>826</sup> and Glu<sup>890</sup> have been proposed to be involved in heme-protein ester bonds (3–5). Freshly purified hsPxd01-con4 showed a red-shifted (compared with unmodified heme b) Soret maximum at 410 nm and a standard reduction potential of the Fe(III)/Fe(II) couple of -0.215 V (5), which already indicated the presence of partially modified heme b. But importantly, simply by keeping the protein under aerobic condition for 48 h prior to purification (see below), the Soret maximum further shifted to 412 nm (Fig. 1), and  $E'^0$  increased to -0.128 V (Fig. 2). Nevertheless, the biphasic behavior of cyanide binding to ferric hsPxd01-con4 (Fig. 3) or compound I formation (Fig. 4) indicated that there is still some heterogeneity left. Considering comparable data about homologous human peroxidases (10, 19, 25–27), it can be speculated that the observed heterogeneity of hsPxd01-con4 also derives from a mixture of molecules with mainly two ester linkages and a small portion having only one covalent bond. It has to be mentioned that this phenomenon is even observed in crystal structures of MPO (20) and LPO (28), which always show fully established Asp ester linkage but split electron densities for the Glu ester bond suggesting the presence of two conformations.

In any case, we could demonstrate that ferric hsPxd01-con4 exhibits spectral features very similar to LPO and EPO and in addition shows similar rates of cyanide binding, which clearly suggests comparable active site architectures. The standard reduction potential  $E'^0$  [Fe(III)/Fe(II)] of our construct follows the hierarchy  $E'^0$  (MPO; +5 mV) >  $E'^0$  (hsPxd01-con4; -128 mV) >  $E'^0$  (EPO; -176 mV) >  $E'^0$  (LPO; -183 mV) (Table 1) (9, 11, 29).

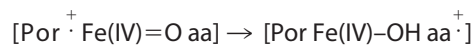
The reaction cycle of hsPxd01 starts by reaction of the Fe(III) form with hydrogen peroxide to form compound I (oxoiron(IV) with porphyrin  $\pi$ -cation radical), which contains two oxidizing equivalents more than the resting enzyme (Reaction 1). The determined  $k_{app}$  value of this bimolecular reaction was similar

to that of other mammalian heme peroxidases with reported  $k_{app}$  values within  $(1.1\text{--}5.6) \times 10^7 \text{ M}^{-1} \text{ s}^{-1}$  (14, 30, 31). Heterolytic cleavage of hydrogen peroxide is supported by a fully conserved distal His-Arg pair (His<sup>827</sup> and Arg<sup>977</sup> in hsPxd01) (30), with His<sup>827</sup> acting as proton acceptor and donor in this redox reaction. Upon its protonation ( $pK_a \sim 4.7$ ) Reaction 1 cannot take place. PorFe is equal to heme or protoporphyrin IX plus iron.



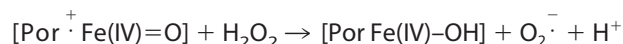
## REACTION 1

Similar to LPO (14) and thyroid peroxidase (TPO) (32), compound I can be produced with equimolar H<sub>2</sub>O<sub>2</sub>. In the absence of an exogenous electron donor, it slowly converts to a compound II-like species, which most probably is compound I\* formed by intramolecular electron transport from the protein matrix (where aa is amino acid) to the prosthetic group (Reaction 2).



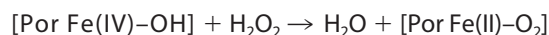
## REACTION 2

Interestingly, hydrogen peroxide also mediates the one-electron reduction of compound I of hsPxd01-con4 to compound II, *i.e.* [Por Fe(IV)-OH] (Reaction 3),



## REACTION 3

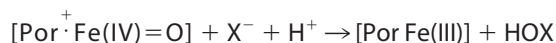
which so far has been described for MPO only (30). At high (>1000) molar excess of H<sub>2</sub>O<sub>2</sub>, compound II is converted to compound III (Reaction 4).



## REACTION 4

However, it is unlikely that this reaction is relevant *in vivo* because the extracellular H<sub>2</sub>O<sub>2</sub> concentration is typically in the low micromolar range. Moreover, it is unknown whether there is a distinct (inducible?) source of hydrogen peroxide in the extracellular matrix for initiation of Reaction 1 and, finally, the halogenation cycle for sulfilimine formation.

It has been reported that the pseudohalide thiocyanate (SCN<sup>-</sup>) and iodide inhibited sulfilimine cross-linking in cell culture, whereas bromide enhanced cross-link formation (2). Now with our stopped-flow data, we can easily explain these observations. Direct reduction of compound I by halides (X<sup>-</sup>) or SCN<sup>-</sup> restores the enzyme in its resting state and releases hypohalous acids (HOX) or hypothiocyanite (HOSCN) (Reaction 5).



## REACTION 5

## Kinetics of Interconversion of Redox Intermediates of Pxd01

At physiological pH 7.4 both thiocyanate ( $1.83 \times 10^7 \text{ M}^{-1} \text{ s}^{-1}$ ) and iodide ( $1.68 \times 10^7 \text{ M}^{-1} \text{ s}^{-1}$ ) are excellent two-electron donors of hsPxd01-con4 compound I and thus effectively compete with bromide. Reduction of compound I to the ferric resting state mediated by bromide ( $5.6 \times 10^6 \text{ M}^{-1} \text{ s}^{-1}$ ) is about 3-times slower compared with  $\text{I}^-$  and  $\text{SCN}^-$ . Importantly, chloride (even at physiological concentrations,  $> 100 \text{ mM}$ ) could not mediate Reaction 5. Moreover, in the presence of chloride only compound I decayed to compound I\* according to Reaction 2, whereas in the presence of  $100 \text{ mM Cl}^-$  and micromolar bromide Reaction 5 was followed. This data fit with (i) the observation that chloride did not support cross-link formation whereas addition of micromolar  $\text{Br}^-$  rescued sulfilimine formation (2) and with (ii) the fact that  $E'^0$  [Fe(III)/Fe(II)] of hsPxd01-con4 is significantly less positive compared with that of MPO, which is the only known human enzyme that is able to oxidize chloride at reasonable rate at neutral pH. This enzymatic property is closely related to the MPO-specific covalent heme-protein sulfonium ion linkage which does not exist in hsPxd01 (3, 4, 9). Nevertheless, hsPxd01-con4 outperforms the reactivity of LPO and MPO toward bromide at neutral pH (Table 1).

Typical normal human serum concentrations of bromide are in the range  $10\text{--}100 \mu\text{M}$ , and the  $\text{Br}^-$  level is maintained via diet and renal excretion (33). *In vitro* studies on sulfilimine formation together with modeling of the cross-linking reaction clearly demonstrated that hypobromous acid is responsible for the formation of a bromosulfonium-ion intermediate that energetically selects for sulfilimine formation (2). Based on the demonstration that (i) bromine deficiency leads to physiological dysfunction, (ii) that repletion of the element reverses dysfunction, and that (iii) biochemical data can explain the physiological function, bromine has to be considered to be an essential trace element in animals (2). Its oxidation by hsPxd01 according to Reaction 5 provides the basis for the biosynthesis of sulfilimine cross-linked collagen IV scaffolds that are central to the formation and function of basement membranes in animals (1, 2).

However, because bromine has not been considered as an essential trace element until recently, systematic investigations on its replacement have not been pursued in various disease states associated with bromide deficiency. Functional  $\text{Br}^-$  deficiency may occur in smokers despite normal  $\text{Br}^-$  levels because of elevated levels of serum  $\text{SCN}^-$ . Normally, the level of thiocyanate in blood plasma varies in individuals from  $20$  to  $120 \mu\text{M}$  depending on their diet but can be significantly increased in smokers (34). Under these conditions,  $\text{SCN}^-$  would be the preferred electron donor for compound I, and reinforcement of collagen IV scaffolds with sulfilimine cross-links may be substantially reduced. Indeed, smoking has been associated with changes in the architecture of basement membranes (35). Oxidation of  $\text{SCN}^-$  generates hypothiocyanate, which is a milder oxidant than hypobromous acid and reacts with thiol residues mainly (36, 37) but cannot mediate the formation of sulfilimine cross-links. Because iodide levels are below micromolar concentrations in blood plasma,  $\text{I}^-$  will not compete with  $\text{Br}^-$  for hsPxd01 compound I.

Summing up, we were able to recombinantly produce a fully functional truncated human peroxidase 1 variant with post-translationally modified and cross-linked heme. It allowed for the first time the determination of apparent bimolecular rate constants of all relevant redox steps of the physiologically relevant halogenation cycle, *i.e.* the  $\text{H}_2\text{O}_2$ -mediated compound I formation followed by two-electron reduction of compound I by bromide, iodide, and thiocyanate. Besides EPO and MPO (Table 1), human peroxidase 1 is shown to be the most effective generator of hypobromous acid in the human body.

### Experimental Procedures

**Materials**—Bovine lactoperoxidase (L2005), sodium chloride, potassium thiocyanate, sodium cyanide, and hydrogen peroxide (30% solution) were purchased from Sigma. The concentration of hydrogen peroxide was determined at  $240 \text{ nm}$  using the molar extinction coefficient of  $39.4 \text{ M}^{-1} \text{ cm}^{-1}$  (38). Potassium bromide and potassium iodide were obtained from Merck. All other chemicals, if not stated otherwise, were purchased from Sigma at the highest grade available.  $\text{H}_2\text{O}_2$  solutions and potassium iodide were prepared fresh before use.

**Cloning of hsPxd01-con4**—Cloning, transient transfection, and expression of hsPxd01-con4 was described previously (5). The work presented here was performed with the N-terminal polyhistidine tag version of hsPxd01-con4, resulting in a translation product of 1069 amino acid residues (Pro<sup>246</sup>–Asp<sup>1314</sup>). All amino acid residue numberings refer to the full-length hsPxd01, including the signal peptide.

**Purification of hsPxd01-con4**—The cell supernatant was harvested and filtrated with a  $0.45\text{-}\mu\text{m}$  PVDF membrane (Durapore) and stored at  $-30^\circ\text{C}$  until further processing. After thawing, the supernatant was stirred for 48 h at  $4^\circ\text{C}$  before the volume was decreased ( $\sim 25$  times), and the cell culture medium was replaced with  $100 \text{ mM}$  phosphate buffer, pH 7.4, using a Millipore LabScale™ TFF diafiltration system.  $5 \text{ ml}$  of HisTrap™ FF columns (GE Healthcare) loaded with nickel chloride were used for the purification of hsPxd01-con4. The column was equilibrated with  $100 \text{ mM}$  phosphate buffer, pH 7.4, containing  $1 \text{ M NaCl}$  and  $5 \text{ mM}$  imidazole. The sample was adjusted to  $1 \text{ M NaCl}$  and  $5 \text{ mM}$  imidazole before loading, and the column was washed with equilibration buffer after sample loading. The protein was eluted by applying two consecutive gradients of  $0\text{--}8\%$  ( $2 \text{ ml/min}$ ,  $10 \text{ min}$ ) and  $8\text{--}70\%$  ( $1 \text{ ml/min}$ ,  $50 \text{ min}$ ) of  $100 \text{ mM}$  phosphate buffer, pH 7.4, containing  $500 \text{ mM NaCl}$  and  $500 \text{ mM}$  imidazole, respectively. Eluted fractions were analyzed by UV-visible spectroscopy, SDS-PAGE, and Western blotting following standard procedures (Penta-His Antibody, BSA-free from Qiagen; anti-mouse antibody, alkaline phosphatase-conjugated).

Enhanced chemiluminescence was used for the detection of covalent heme to protein linkages as described earlier (5). Fractions were pooled accordingly and concentrated in a  $10\text{-kDa}$  molecular mass cutoff dialysis tubing (SnakeSkin™, Thermo Fisher Scientific) by applying PEG ( $20 \text{ kDa}$ ) to the outside of the tubing. Subsequently, the sample was dialyzed against  $100 \text{ mM}$  phosphate buffer, pH 7.4, and stored at  $-30^\circ\text{C}$ .

**Spectral Characterization of hsPxd01-con4**—The extinction coefficients of hsPxd01-con4 were determined to be  $147,500$

$M^{-1} \text{ cm}^{-1}$  at 280 nm and  $101,400 M^{-1} \text{ cm}^{-1}$  at the heme Soret peak, resulting in a theoretical purity number of 0.7 ( $\epsilon_{412 \text{ nm}} / \epsilon_{280 \text{ nm}}$ ). The average purity number obtained by metal affinity chromatography was 0.45–0.55 indicating a 65–80% heme occupancy. Specified hsPxd01-con4 concentrations were always related to heme concentrations.

**Spectroelectrochemistry**—The standard reduction potential ( $E'^0$ ) of the Fe(III)/Fe(II) couple of hsPxd01-con4 was determined as described previously (5). Briefly, the spectroelectrochemical titrations were performed using a homemade OTTLE (optically transparent thin layer spectroelectrochemical) cell. The three-electrode configuration consisted of a gold mini-grid working electrode (Buckbee-Mears), a saturated calomel ( $\text{Hg}_2\text{Cl}_2$ ) microreference electrode (AMEL Electrochemistry), separated from the working solution by a Vycor set, and a platinum wire as counter-electrode (11, 21, 29). All potentials are referenced to the standard hydrogen electrode.

Experiments were performed with  $5 \mu\text{M}$  hsPxd01-con4 in 100 mM phosphate buffer, pH 7.4, containing 100 mM NaCl, 30  $\mu\text{M}$  methyl viologen, and 1  $\mu\text{M}$  lumiflavin 3-acetate, methylene blue, phenazine methosulfate, and indigo disulfonate used as mediators at 25 °C. Nernst plots consisted of at least five points and were invariably linear with a slope consistent with a one-electron reduction process (11, 21, 29). The spectroelectrochemical experiments were performed three times, and the resulting  $E'^0$  values were found to be reproducible within  $\pm 6$  mV.

**Stopped-flow Spectroscopy**—Pre-steady-state spectra were recorded with the stopped-flow apparatus SX.18MV (Applied Photophysics) connected to a diode array detector (DAD) with the first spectrum usually recorded 3 ms after mixing the reactants. The Pi-star-180 apparatus from Applied Photophysics was employed for all single wavelength measurements, and the first data point after mixing two solutions was typically recorded at 1 ms. The optical quartz cell had a volume of 20  $\mu\text{l}$  and a path length of 10 mm. All reactions were followed at single wavelengths and additionally by using the DAD. Polychromatic data were analyzed with the Pro-Kineticist software from Applied Photophysics. Rate constants were determined by fitting single wavelength time traces with the Pro-Data Viewer software (Applied Photophysics). The conventional mode was applied to monitor the reaction of hsPxd01-con4 with hydrogen peroxide by following the decrease of absorbance at 412 nm and cyanide binding by monitoring the increase at 434 nm. All presented rate constants were measured using the sequential mixing mode due to the inherent instability of compound I. A delay time of 200 ms for the formation of compound I was employed.

All reactions with the exception of the pH profiles presented were performed in 100 mM phosphate buffer, pH 7.4, and at 25 °C. Citrate phosphate buffer was used for measurements from pH 4 to 5.5; phosphate buffer was employed for the pH range of 5.5–8, and carbonate buffer was used for pH 9 and 10. Three measurements were performed for each ligand (cyanide), oxidant (hydrogen peroxide), and electron donor (halides and thiocyanate) concentration, respectively. The mean of the first-order rate constants,  $k_{\text{obs}}$ , was used to calculate the apparent second-order rate constant that was obtained from the slope of

the plot of the  $k_{\text{obs}}$  values versus the concentrations of the respective reactants.

**Author Contributions**—P. G. F. and C. O. conceived and coordinated the study and wrote the paper. M. P. P. designed the constructs, performed and analyzed the experiments, and contributed to writing of the paper. R. S. K., I. S., E. E., B. S., and M. S. provided technical assistance and produced and purified the recombinant proteins. M. B. and G. B. performed the spectroelectrochemical experiments, and S. H. probed the homogeneity and conformational stability of the constructs.

## References

- Bhave, G., Cummings, C. F., Vanacore, R. M., Kumagai-Cresse, C., Ero-Tolliver, I. A., Rafi, M., Kang, J.-S., Pedchenko, V., Fessler, L. I., Fessler, J. H., and Hudson, B. G. (2012) Peroxidase forms sulfilimine chemical bonds using hypohalous acids in tissue genesis. *Nat. Chem. Biol.* **8**, 784–790
- McCall, A. S., Cummings, C. F., Bhave, G., Vanacore, R., Page-McCaw, A., and Hudson, B. G. (2014) Bromine is an essential trace element for assembly of collagen IV scaffolds in tissue development and architecture. *Cell* **157**, 1380–1392
- Zamocky, M., Jakopitsch, C., Furtmüller, P. G., Dunand, C., and Obinger, C. (2008) The peroxidase-cyclooxygenase superfamily: reconstructed evolution of critical enzymes of the innate immune system. *Proteins* **72**, 589–605
- Soudi, M., Zamocky, M., Jakopitsch, C., Furtmüller, P. G., and Obinger, C. (2012) Molecular evolution, structure, and function of peroxidases. *Chem. Biodivers.* **9**, 1776–1793
- Soudi, M., Paumann-Page, M., Delporte, C., Pirker, K. F., Bellei, M., Edenhofer, E., Stadlmayr, G., Battistuzzi, G., Boudjeltia, K. Z., Furtmüller, P. G., Van Antwerpen, P., and Obinger, C. (2015) Multidomain human peroxidase 1 is a highly glycosylated and stable homotrimeric high spin ferric peroxidase. *J. Biol. Chem.* **290**, 10876–10890
- Lázár, E., Péterfi, Z., Sirokmány, G., Kovács, H. A., Klement, E., Medzihradszky, K. F., and Geiszt, M. (2015) Structure-function analysis of peroxidase provides insight into the mechanism of collagen IV cross-linking. *Free Radic. Biol. Med.* **83**, 273–282
- Furtmüller, P. G., Zederbauer, M., Jantschko, W., Helm, J., Bogner, M., Jakopitsch, C., and Obinger, C. (2006) Active site structure and catalytic mechanisms of human peroxidases. *Arch. Biochem. Biophys.* **445**, 199–213
- Colon, S., and Bhave, G. (2016) Proprotein convertase processing enhances peroxidase activity to reinforce collagen IV. *J. Biol. Chem.* **291**, 24009–24016
- Battistuzzi, G., Stamper, J., Bellei, M., Vlasits, J., Soudi, M., Furtmüller, P. G., and Obinger, C. (2011) Influence of the covalent heme-protein bonds on the redox thermodynamics of human myeloperoxidase. *Biochemistry* **50**, 7987–7994
- Auer, M., Nicolussi, A., Schütz, G., Furtmüller, P. G., and Obinger, C. (2014) How covalent heme to protein bonds influence the formation and reactivity of redox intermediates of a bacterial peroxidase. *J. Biol. Chem.* **289**, 31480–31491
- Battistuzzi, G., Bellei, M., Vlasits, J., Banerjee, S., Furtmüller, P. G., Sola, M., and Obinger, C. (2010) Redox thermodynamics of lactoperoxidase and eosinophil peroxidase. *Arch. Biochem. Biophys.* **494**, 72–77
- Bolscher, B. G., and Wever, R. (1984) A kinetic study of the reaction between human myeloperoxidase, hydroperoxides and cyanide. Inhibition by chloride and thiocyanate. *Biochim. Biophys. Acta* **788**, 1–10
- Dolman, D., Dunford, H. B., Chowdhury, D. M., and Morrison, M. (1968) The kinetics of cyanide binding by lactoperoxidase. *Biochemistry* **7**, 3991–3996
- Furtmüller, P. G., Jantschko, W., Regelsberger, G., Jakopitsch, C., Arnhold, J., and Obinger, C. (2002) Reaction of lactoperoxidase compound I with halides and thiocyanate. *Biochemistry* **41**, 11895–11900

15. Cheng, G., Salerno, J. C., Cao, Z., Pagano, P. J., and Lambeth, J. D. (2008) Identification and characterization of VPO1, a new animal heme-containing peroxidase. *Free Radic. Biol. Med.* **45**, 1682–1694
16. Shi, R., Hu, C., Yuan, Q., Yang, T., Peng, J., Li, Y., Bai, Y., Cao, Z., Cheng, G., and Zhang, G. (2011) Involvement of vascular peroxidase 1 in angiotensin II-induced vascular smooth muscle cell proliferation. *Cardiovasc. Res.* **91**, 27–36
17. Ero-Tolliver, I. A., Hudson, B. G., and Bhave, G. (2015) The ancient immunoglobulin domains of peroxidasin are required to form sulfilimine cross-links in collagen IV. *J. Biol. Chem.* **290**, 21741–21748
18. Zederbauer, M., Furtmüller, P. G., Brogioni, S., Jakopitsch, C., Smulevich, G., and Obinger, C. (2007) Heme to protein linkages in mammalian peroxidases: impact on spectroscopic, redox and catalytic properties. *Nat. Prod. Rep.* **24**, 571–584
19. Brogioni, S., Stampfer, J., Furtmüller, P. G., Feis, A., Obinger, C., and Smulevich, G. (2008) The role of the sulfonium ion linkage in the stabilization of the heme architecture of the ferrous form of myeloperoxidase: a comparison with lactoperoxidase. *Biochim. Biophys. Acta* **1784**, 843–849
20. Carpena, X., Vidossich, P., Schroettner, K., Calisto, B. M., Banerjee, S., Stampfer, J., Soudi, M., Furtmüller, P. G., Rovira, C., Fita, I., and Obinger, C. (2009) Essential role of proximal histidine-asparagine interaction in mammalian peroxidases. *J. Biol. Chem.* **284**, 25929–25937
21. Battistuzzi, G., Borsari, M., Ranieri, A., and Sola, M. (2002) Redox thermodynamics of the  $\text{Fe}^{3+}/\text{Fe}^{2+}$  couple in horseradish peroxidase and its cyanide complex. *J. Am. Chem. Soc.* **124**, 26–27
22. DePillis, G. D., Ozaki Si, Kuo, J. M., Maltby, D. A., and Ortiz de Montellano, P. R. (1997) Autocatalytic processing of heme lactoperoxidase produces the native protein-bound prosthetic group. *J. Biol. Chem.* **272**, 8857–8860
23. Fayadat, L., Niccoli-Sire, P., Lanet, J., and Franc, J. L. (1999) Role of heme in intracellular trafficking of thyroperoxidase and involvement of  $\text{H}_2\text{O}_2$  generated at the apical surface of thyroid cells in autocatalytic covalent heme binding. *J. Biol. Chem.* **274**, 10533–10538
24. Ortiz de Montellano, P. R. (2008) Mechanism and role of covalent heme binding in the CYP4 family of P450 enzymes and the mammalian peroxidases. *Drug Metab. Rev.* **40**, 405–426
25. Zederbauer, M., Furtmüller, P. G., Bellei, M., Stampfer, J., Jakopitsch, C., Battistuzzi, G., Moguilevsky, N., and Obinger, C. (2007) Disruption of the aspartate to heme ester linkage in human myeloperoxidase: impact on ligand binding, redox chemistry and interconversion of redox intermediates. *J. Biol. Chem.* **282**, 17041–17052
26. Zederbauer, M., Furtmüller, P. G., Ganster, B., Moguilevsky, N., and Obinger, C. (2007) Manipulating the vinyl-sulfonium bond in human myeloperoxidase: impact on compound I formation and reduction by halides and thiocyanate. *Biochem. Biophys. Res. Commun.* **356**, 450–456
27. Auer, M., Gruber, C., Bellei, M., Pirker, K. F., Zamocky, M., Kroiss, D., Teufer, S. A., Hofbauer, S., Soudi, M., Battistuzzi, G., Furtmüller, P. G., and Obinger, C. (2013) A stable bacterial peroxidase with novel halogenating activity and an autocatalytically linked heme prosthetic group. *J. Biol. Chem.* **288**, 27181–27199
28. Singh, P. K., Sirohi, H. V., Iqbal, N., Tiwari, P., Kaur, P., Sharma, S., and Singh, T. P. (2017) Structure of bovine lactoperoxidase with a partially linked heme moiety at 1.98 Å resolution. *Biochim. Biophys. Acta* **1865**, 329–335
29. Battistuzzi, G., Bellei, M., Zederbauer, M., Furtmüller, P. G., Sola, M., and Obinger, C. (2006) Redox thermodynamics of the  $\text{Fe(III)/Fe(II)}$  couple of human myeloperoxidase in its high-spin and low-spin forms. *Biochemistry* **45**, 12750–12755
30. Furtmüller, P. G., Burner, U., and Obinger, C. (1998) Reaction of myeloperoxidase compound I with chloride, bromide, iodide, and thiocyanate. *Biochemistry* **37**, 17923–17930
31. Furtmüller, P. G., Burner, U., Regelsberger, G., and Obinger, C. (2000) Spectral and kinetic studies on the formation of eosinophil peroxidase compound I and its reaction with halides and thiocyanate. *Biochemistry* **39**, 15578–15584
32. Ruf, J., and Carayon, P. (2006) Structural and functional aspects of thyroid peroxidase. *Arch. Biochem. Biophys.* **445**, 269–277
33. van Leeuwen, F. X., and Sangster, B. (1987) The toxicology of bromide ion. *Crit. Rev. Toxicol.* **18**, 189–213
34. Tsuge, K., Kataoka, M., and Seto, Y. (2000) Cyanide and thiocyanate levels in blood and saliva of healthy adult volunteers. *J. Health Sci.* **46**, 343–350
35. Asmussen, I. (1979) Fetal cardiovascular system as influenced by maternal smoking. *Clin. Cardiol.* **2**, 246–256
36. Hawkins, C. L. (2009) The role of hypothiocyanous acid (HOSCN) in biological systems. *Free Radic. Res.* **43**, 1147–1158
37. Lane, A. E., Tan, J. T., Hawkins, C. L., Heather, A. K., and Davies, M. J. (2010) The myeloperoxidase-derived oxidant HOSCN inhibits protein tyrosine phosphatases and modulates cell signaling via the mitogen-activated protein kinase (MAPK) pathway in macrophages. *Biochem. J.* **430**, 161–169
38. Nelson, D. P., and Kiesow, L. A. (1972) Enthalpy of decomposition of hydrogen peroxide by catalase at 25°C (with molar extinction coefficients of  $\text{H}_2\text{O}_2$  solutions in the UV). *Anal. Biochem.* **49**, 474–478

## **Pre-steady-state Kinetics Reveal the Substrate Specificity and Mechanism of Halide Oxidation of Truncated Human Peroxidasin 1**

Martina Paumann-Page, Romy-Sophie Katz, Marzia Bellei, Irene Schwartz, Eva Edenhofer, Benjamin Sevcnikar, Monika Soudi, Stefan Hofbauer, Gianantonio Battistuzzi, Paul G. Furtmüller and Christian Obinger

*J. Biol. Chem.* 2017, 292:4583-4592.

doi: 10.1074/jbc.M117.775213 originally published online January 31, 2017

---

Access the most updated version of this article at doi: [10.1074/jbc.M117.775213](https://doi.org/10.1074/jbc.M117.775213)

Alerts:

- [When this article is cited](#)
- [When a correction for this article is posted](#)

[Click here](#) to choose from all of JBC's e-mail alerts

This article cites 38 references, 10 of which can be accessed free at <http://www.jbc.org/content/292/11/4583.full.html#ref-list-1>

# Reaction of human peroxidase 1 compound I and compound II with one-electron donors

**Benjamin Sevcnikar**, Martina Paumann-Page, Stefan Hofbauer, Vera Pfanzagl, Paul G. Furtmüller and Christian Obinger

Research Article

Archives of Biochemistry and Biophysics Volume 681, 15 March 2020,  
108267

DOI: 10.1016/j.abb.2020.108267



## Reaction of human peroxidasin 1 compound I and compound II with one-electron donors

Benjamin Sevcnikar<sup>a</sup>, Martina Paumann-Page<sup>b</sup>, Stefan Hofbauer<sup>a</sup>, Vera Pfanzagl<sup>a</sup>, Paul G. Furtmüller<sup>a,\*</sup>, Christian Obinger<sup>a,\*</sup>

<sup>a</sup> Department of Chemistry, Institute of Biochemistry, University of Natural Resources and Life Sciences, Vienna, Austria

<sup>b</sup> Centre for Free Radical Research, Department of Pathology and Biomedical Science, University of Otago Christchurch, Christchurch, New Zealand

### ARTICLE INFO

#### Keywords:

Human peroxidasin 1  
Compound I  
Compound II  
Transient-state kinetics  
One-electron donors  
Stopped-flow spectroscopy  
Nitrite

### ABSTRACT

Human peroxidasin 1 (hsPxd01) is a homotrimeric multidomain heme peroxidase embedded in the extracellular matrix. It catalyses the two-electron oxidation of bromide by hydrogen peroxide to hypobromous acid which mediates the formation of essential sulfilimine cross-links between methionine and hydroxylysine residues in collagen IV. This confers critical structural reinforcement to the extracellular matrix. This study presents for the first time transient kinetic measurements of the reactivity of hsPxd01 compound I and compound II with the endogenous one-electron donors nitrite, ascorbate, urate, tyrosine and serotonin using the sequential stopped-flow technique. At pH 7.4 and 25 °C compound I of hsPxd01 is reduced to compound II with apparent second-order rate constants ranging from  $(1.9 \pm 0.1) \times 10^4 \text{ M}^{-1} \text{ s}^{-1}$  (urate) to  $(4.8 \pm 0.1) \times 10^5 \text{ M}^{-1} \text{ s}^{-1}$  (serotonin). Reduction of compound II to the ferric state occurs with apparent second-order rate constants ranging from  $(4.3 \pm 0.2) \times 10^2 \text{ M}^{-1} \text{ s}^{-1}$  (tyrosine) to  $(7.7 \pm 0.1) \times 10^3 \text{ M}^{-1} \text{ s}^{-1}$  (serotonin). The relatively fast rates of compound I reduction suggest that these reactions may take place *in vivo* and modulate bromide oxidation due to formation of compound II. Urate is shown to inhibit the bromination activity of hsPxd01, whereas nitrite stimulates the formation of hypobromous acid. The results are discussed with respect to known kinetic data of homologous mammalian peroxidases and to the physiological role of human peroxidasin 1.

### 1. Introduction

Human peroxidasin 1 (hsPxd01) is a key player in the stabilization of basement membranes. It oxidizes bromide to hypobromous acid, which is further able to promote the formation of a highly specific covalent sulfilimine crosslink within the collagen IV network of basement membranes [1–3]. Trimeric C-terminal non-collagenous (NCl) domains of two collagen IV protomers self-assemble head to head to form a hexameric structure. Subsequently, opposing methionine and lysine residues at the trimer-trimer interface are crosslinked via a sulfilimine (S=N) bond [1,3]. This unusual link not only imparts mechanical strength to the basement membrane, but also enables collagen IV to serve as a scaffold for cell attachment and cell signaling [4–6]. Among mammalian peroxidases, only hsPxd01 is able to efficiently crosslink collagen IV [7]. However, the detailed molecular mechanism

for formation of the sulfilimine by hsPxd01 is not known.

Human peroxidasin 1 (hsPxd01) is a member of Family 2 of the peroxidase-cyclooxygenase superfamily [8,9]. Family 2 is comprised of five clades with hsPxd01 belonging to Clade 5 [10]. It is a highly glycosylated and secreted multidomain homotrimeric heme peroxidase with N-terminal leucine-rich repeats (LRR), four C-like immunoglobulin (Ig) domains, a peroxidase domain and a C-terminal Von Willebrand factor type C domain (VWC). The LRR, Ig and VWC domains are known to mediate protein-protein interaction and cell adhesion [10]. The enzymatically active peroxidase domain is homologous to other well studied (Family 1) chordata peroxidases like myeloperoxidase (MPO) and lactoperoxidase (LPO) having all crucial catalytic amino acids for heterolytic cleavage of hydrogen peroxide and halide oxidation [8,9,11,12]. Moreover, the heme was shown to be posttranslationally modified and covalently linked with the protein [3,11,13].

**Abbreviations:** hsPxd01, human peroxidasin 1; hsPxd01-con4, truncated catalytically active human peroxidasin 1 comprised of the four Ig domains and the peroxidase domain; LPO, lactoperoxidase; EPO, eosinophil peroxidase; MPO, myeloperoxidase; LRR, leucine-rich repeat; Ig, immunoglobulin; VWC, Von Willebrand factor type C domain; con 4, construct 4;  $E^\circ$ , standard reduction potential

\* Corresponding author.

\*\* Corresponding author.

E-mail addresses: [paul.furtmueller@boku.ac.at](mailto:paul.furtmueller@boku.ac.at) (P.G. Furtmüller), [christian.obinger@boku.ac.at](mailto:christian.obinger@boku.ac.at) (C. Obinger).

<https://doi.org/10.1016/j.abbi.2020.108267>

Received 3 December 2019; Received in revised form 10 January 2020; Accepted 13 January 2020

Available online 15 January 2020

0003-9861/ © 2020 Published by Elsevier Inc.

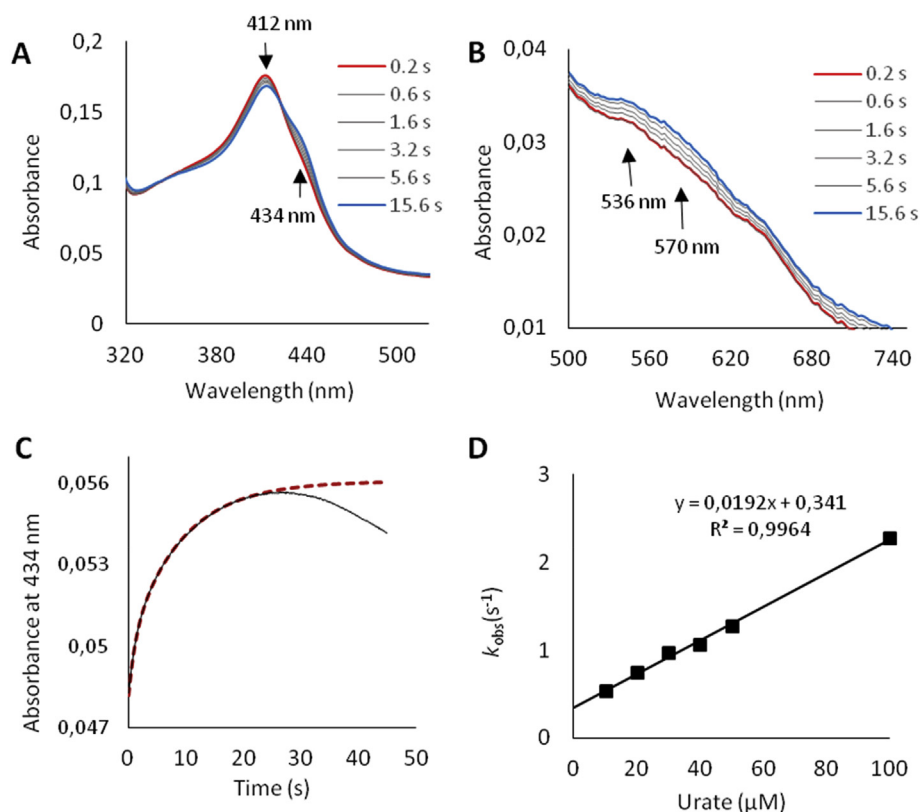


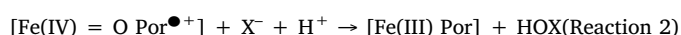
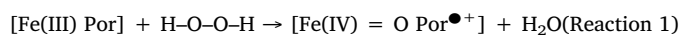
**Fig. 1.** Kinetics of reduction of compound I of hsPxd01-con4 by urate. Spectral changes in the Soret region (A) and in the visible region (B) upon mixing of 2  $\mu\text{M}$  hsPxd01-con4 compound I with 50  $\mu\text{M}$  urate in 100 mM phosphate buffer, pH 7.4. After 15.6 s compound I was fully established. Compound I was pre-formed with equimolar  $\text{H}_2\text{O}_2$  in the sequential-mixing mode. Delay time: 200 ms. (C) Typical time trace at 434 nm reflecting the reaction between 0.75  $\mu\text{M}$  compound I reacting with 10  $\mu\text{M}$  urate in 100 mM phosphate buffer, pH 7.4 (black line), and single exponential fit (dashed red line) of the initial phase representing conversion of compound I to compound II (increase of absorbance at 434 nm). (D) Plot of  $k_{\text{obs}}$  values versus urate concentrations. Conditions: 0.75  $\mu\text{M}$  compound I reacting with 10, 20, 30, 40, 50, 100  $\mu\text{M}$  urate in 100 mM phosphate buffer, pH 7.4. (For interpretation of the references to colour in this figure legend, the reader is referred to the Web version of this article.)

**Table 1**

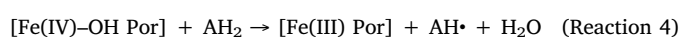
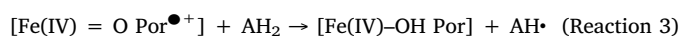
Apparent second-order rate constants for the reaction of compound I and compound II of human peroxidase 1, bovine lactoperoxidase and human myeloperoxidase with the endogenous one-electron donors of serotonin, nitrite, ascorbate, tyrosine and urate. hsPxd01-con4, truncated human peroxidase 1 comprised of four Ig domains and the peroxidase domain; LPO, lactoperoxidase; MPO, myeloperoxidase; n.d., not determined.

	hsPxd-con4		LPO		MPO	
	$k_3$ [ $\text{M}^{-1} \text{s}^{-1}$ ]	$k_4$ [ $\text{M}^{-1} \text{s}^{-1}$ ]	$k_3$ [ $\text{M}^{-1} \text{s}^{-1}$ ]	$k_3$ [ $\text{M}^{-1} \text{s}^{-1}$ ]	$k_3$ [ $\text{M}^{-1} \text{s}^{-1}$ ]	$k_4$ [ $\text{M}^{-1} \text{s}^{-1}$ ]
Serotonin	$(4.8 \pm 0.1) \times 10^5$	$(7.7 \pm 0.1) \times 10^3$	$(2.0 \pm 0.1) \times 10^6$ [36]	$(3.0 \pm 0.1) \times 10^5$ [36]	$(1.7 \pm 0.1) \times 10^7$ [36]	$(1.4 \pm 0.1) \times 10^6$ [36]
Nitrite	$(1.9 \pm 0.1) \times 10^5$	$(4.0 \pm 0.1) \times 10^3$	$(2.3 \pm 0.2) \times 10^7$ [37]	$(3.5 \pm 0.1) \times 10^5$ [37]	$(2.0 \pm 0.2) \times 10^6$ [38]	$(5.5 \pm 0.1) \times 10^2$ [38]
Ascorbate	$(7.2 \pm 0.6) \times 10^4$	$(6.1 \pm 0.6) \times 10^2$	n.d.	n.d.	$(1.6 \pm 0.1) \times 10^6$ [38]	$(1.1 \pm 0.1) \times 10^4$ [38]
Tyrosine	$(2.2 \pm 0.1) \times 10^4$	$(4.3 \pm 0.2) \times 10^2$	$(1.1 \pm 0.1) \times 10^5$ [36]	$(1.0 \pm 0.1) \times 10^4$ [36]	$(7.7 \pm 0.1) \times 10^5$ [36]	$(1.6 \pm 0.6) \times 10^4$ [36]
Urate	$(1.9 \pm 0.1) \times 10^4$	$(5.8 \pm 0.2) \times 10^2$	$(1.1 \pm 0.1) \times 10^7$ [37]	$(8.5 \pm 0.4) \times 10^3$ [37]	$(4.6 \pm 0.4) \times 10^5$ [17]	$(1.7 \pm 0.1) \times 10^4$ [17]

In a previous study, we have elucidated the pre-steady-state kinetics and substrate specificity of halide oxidation of truncated variants of hsPxd01, demonstrating that the minimal fully functional recombinant construct is hsPxd01-con4, which consists of four Ig- and the peroxidase domains [3,14]. Additionally, an *in vivo* study showed that the immunoglobulin domains are required to form the sulfilimine crosslinks in collagen IV [15]. Upon studying hsPxd01-con4 it was demonstrated that the enzyme is able to follow the halogenation cycle (Reactions 1 & 2) which includes hydrogen peroxide-mediated oxidation of the ferric peroxidase to compound I (Reaction 1) and compound I reduction to the resting state by thiocyanate, iodide and bromide (Reaction 2) [3].



Limited information is available about the peroxidase activity of hsPxd01. The peroxidase cycle (Reactions 1, 3 & 4) includes compound I formation (Reaction 1) followed by two one-electron reduction steps via compound II (Reaction 3) to the ferric resting state (Reaction 4).



In a recent study, Bathish and co-workers identified modulatory effects of endogenous and exogenous one- and two-electron donors on the peroxidase-mediated sulfilimine bond formation in isolated extracellular matrix (ECM) [16]. The authors could demonstrate that physiological concentrations of thiocyanate and urate partially inhibit crosslink formation by hypobromous acid suggesting that these alternative electron donors compete with bromide in compound I reduction. Thus, in order to study the impact of the peroxidase activity of hsPxd01 on HOBr formation, we have assessed the transient-state kinetics of the whole peroxidase cycle (Reactions 1, 3 & 4) of hsPxd01-con4 with typical endogenous one-electron donors. For the first time the apparent bimolecular rate constants for compound I and compound II reduction mediated by nitrite, ascorbate, urate, tyrosine and serotonin are presented. The impact of the peroxidase activity of hsPxd01 on extracellular matrix stabilization is discussed.

## 2. Materials and methods

### 2.1. Materials

Hydrogen peroxide (30% solution), sodium nitrite, tyrosine, serotonin, uric acid and L-ascorbic acid were purchased from Sigma-

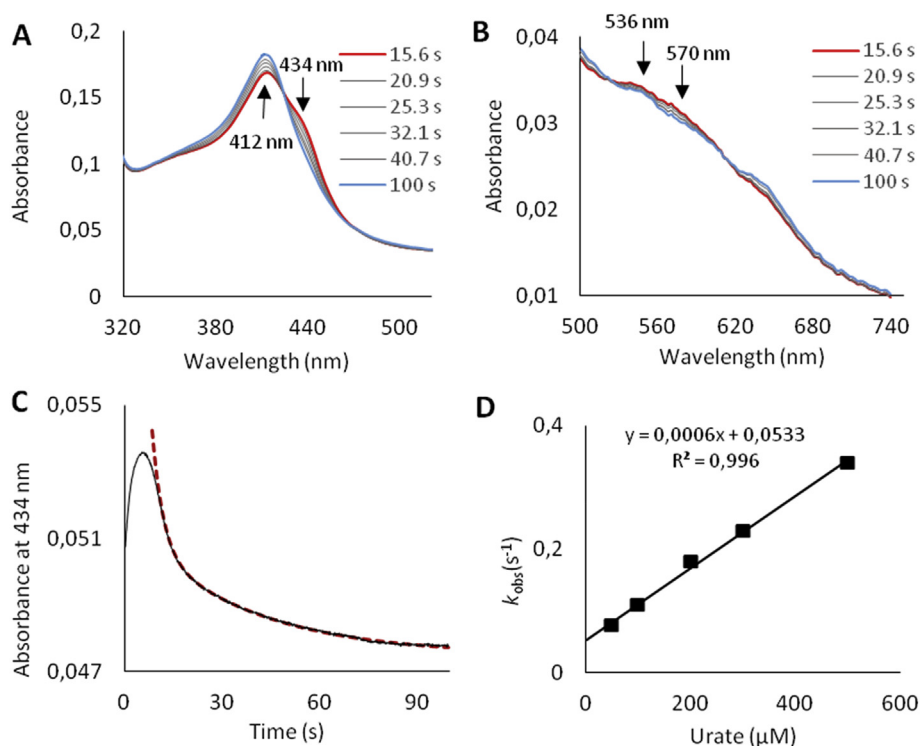


**Fig. 2. Kinetics of reduction of hsPxd01-con4 compound II by urate.** (A) Kinetics of spectral changes in the Soret (A) and the visible region (B) of the reaction between 2  $\mu\text{M}$  hsPxd01-con4 compound I and 50  $\mu\text{M}$  urate in 100 mM phosphate buffer, pH 7.4. Fig. 2A is a continuation of Fig. 1A (15.6–100 s) and shows the transition of compound II to ferric hsPxd01-con4. (C) Typical time trace at 434 nm representing the full reaction between 0.75  $\mu\text{M}$  compound I and 500  $\mu\text{M}$  urate in 100 mM phosphate buffer, pH 7.4 (black line). Decrease in absorbance reflects reduction of compound II and was fitted double-exponentially. (D) Plot of  $k_{\text{obs}}$  values versus urate concentrations.

Aldrich. The concentration of  $\text{H}_2\text{O}_2$  was determined using the absorbance at 240 nm and the molar extinction coefficient of  $39.4 \text{ M}^{-1} \text{ cm}^{-1}$ . Human myeloperoxidase (MPO) was purchased from Planta Natural Products.

## 2.2. Cloning, expression and purification of Pxd01-con4

DNA of hsPxd01-con4 (uniprotkb: Q92626, residues Pro<sub>246</sub>-Asp<sub>1314</sub>) was cloned into a modified gWiz vector (Genlantis) carrying an N-terminal His<sub>6</sub> tag for protein purification. Forward and reverse PCR primer for preparation of hsPxdn01-con4 DNA were as follows: 5' GAGGCTCACCACCACCATCACCATCCCCGAATCACCTCCGAGCCC3' and 5'TAGCCAGAAGTGATCTGGATCTCAGTCCTGCCACACCCGGAGGTC3'. Transformed *E. coli* XL-10 were screened with colony-PCR. Positive clones were selected and validated by DNA sequencing. For expression we chose the HEK 293F (Invitrogen) suspension system. Cells were cultivated according to the Invitrogen User Guideline. Cells were transfected as previously described. Hemin was added to the culture medium to a final concentration of 5  $\mu\text{g}/\text{mL}$  4 h after transfection to improve heme incorporation. Supernatants were harvested 5 days after transfection.

Harvested supernatant was filtrated with a 0.45  $\mu\text{m}$  PVDF membrane (Durapore) and concentrated to 100 mL using a Millipore Labscale TFF diafiltration system. Subsequently, the sample was adjusted to 1 M NaCl and 20 mM imidazole. For purification of the His<sub>6</sub>-tagged protein, 5 mL HisTrap FF columns (GE Healthcare) loaded with nickel chloride were used. After equilibration of the column with 100 mM phosphate buffer, pH 7.4, 1 M NaCl and 20 mM imidazole, sample was loaded and washed with equilibration buffer. Protein was eluted using two consecutive step gradients of 8% and 70% of 20 mM phosphate buffer, pH 7.4, 500 mM NaCl and 500 mM imidazole. Eluted fractions were analyzed by UV-visible spectroscopy and SDS-Page following standard procedures. Fractions were pooled and washed five times with 100 mM phosphate buffer, pH 7.4, using Amicon Ultra-15 with 50 kDa cutoff filters (Merck Milipore).

Quality control of the recombinant heme protein was performed routinely as described recently by Paumann-Page et al. [14] including

SDS-PAGE, size exclusion chromatography combined with multi-angle light scattering and UV-vis spectroscopy.

## 2.3. Transient-state kinetics

The stopped-flow apparatus SX.18 MV (Applied Photophysics) connected to a diode array detector (DAD) was used for recording pre-steady-state spectra. The first spectrum was usually recorded 1 ms after mixing the reactants. For all single wavelength measurements the Pistar-180 apparatus (Applied Photophysics) was used. Both instruments are equipped with an optical quartz cell that had a volume of 20  $\mu\text{L}$  and a path length of 10 mm. All reactions were followed at single wavelengths and additionally by using the DAD. Rate constants were determined by fitting single wavelength time traces with Pro-Data Viewer software (Applied Photophysics). Since hsPxd01-con4 was produced in a different system than previously described, the conventional mode was used to follow the reaction of hsPxd01-con4 with hydrogen peroxide by measuring the decrease of absorbance at 412 nm and cyanide binding by monitoring the increase at 434 nm. Previously published reaction rate constants for cyanide binding, compound I formation as well as the delay time of 200 ms for the formation of compound I could be reproduced (data not shown) [14].

For the determination of rate constants of the reaction of hsPxd01-con4 compound I and compound II with one-electron donors, hsPxd01-con4 (3  $\mu\text{M}$  heme) was premixed with 3  $\mu\text{M}$   $\text{H}_2\text{O}_2$  in the aging loop for 200 ms to form compound I (100 mM phosphate buffer, pH 7.4 at 25  $^\circ\text{C}$ ). Compound I was subsequently allowed to react with one-electron donors to form compound II, which further reacted in a second reaction step with another one-electron donor to the ferric resting state. Compound II formation was monitored as increase in absorbance at 434 nm and monophasic time traces could be fitted single exponentially. Compound II reduction was followed by decrease in absorbance at 434 nm and the respective biphasic time traces were fitted double exponentially with  $k_{\text{obs}}$  values calculated from the dominating rapid phase.

At least three measurements were performed for each electron donor concentration. The mean of the bimolecular rate constants,  $k_{\text{obs}}$ ,

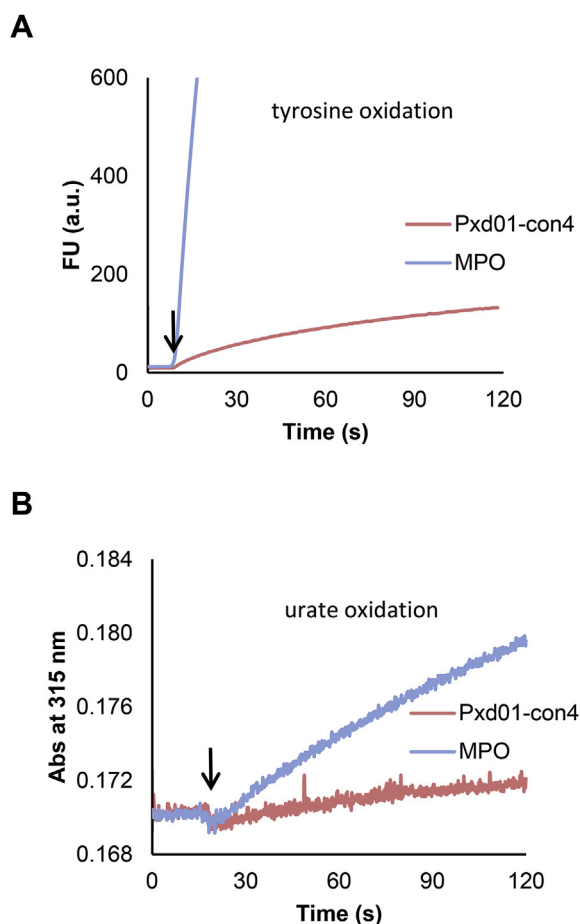


**Fig. 3.** Overall peroxidase activity of hsPxd01-con4 and MPO using the substrates tyrosine (A) and urate (B). (A) Spectrofluorometric detection of dityrosine formation. Conditions: 100  $\mu$ M tyrosine, 100 nM MPO (blue) or 100 nM hsPxd01-con4 (red), 200  $\mu$ M hydrogen peroxide, 100 mM phosphate buffer, pH 7.4. (B) Spectrophotometric monitoring of urate oxidation. Conditions: 100  $\mu$ M urate, 50 nM MPO (blue) or 50 nM hsPxd01-con4 (red), 200  $\mu$ M  $H_2O_2$ , 100 mM phosphate buffer, pH 7.4. Reactions were started by the addition of hydrogen peroxide. (For interpretation of the references to colour in this figure legend, the reader is referred to the Web version of this article.)

was used to calculate the apparent second-order rate constant, which was obtained from the slope of the plot of  $k_{obs}$  values versus the concentration of the respective electron donor.

#### 2.4. Steady-state-kinetics

Urate and tyrosine were used to test the overall peroxidase activity of hsPxd01-con4 in comparison with MPO in 100 mM phosphate buffer, pH 7.4, and 25 °C. In case of urate 100  $\mu$ M substrate was mixed with 50 nM Pxd01-con4 or MPO and the reaction was started by addition of 200  $\mu$ M hydrogen peroxide and followed spectrophotometrically (Hitachi-4500 spectrophotometer) by monitoring the rate of product formation at 315 nm [17]. Dityrosine formation (200  $\mu$ M tyrosine, 100  $\mu$ M  $H_2O_2$ , 100 nM hsPxd01-con4 or MPO, 100 mM phosphate buffer, pH 7.4, and 25 °C) was followed spectrofluorometrically (Hitachi F-7000 spectrofluorometer) using an excitation wavelength of 325 nm and an emission wavelength of 405 nm with 700 mV applied [18].

Bromination activity was measured using dansylglycine, a fluorescent probe which is oxidized by HOBr thereby losing fluorescence [19]. It is important to mention that dansylglycine fluorescence is not quenched by the radicals derived from peroxidase activity [19]. In detail, 50 nM hsPxd01-con4 or 50 nM MPO in 100 mM phosphate

buffer, 7.4, were incubated with 50  $\mu$ M dansylglycine and 100 mM bromide. The reaction was started with addition of 200  $\mu$ M hydrogen peroxide (Hitachi F-7000 spectrofluorometer: 700 mV; excitation wavelength: 340 nm; emission wavelength: 550 nm; excitation and emission slit: 2.5 nm).

Inhibition of bromination activity and determination of  $IC_{50}$  values were performed using the bromination assay as described above in the presence of either nitrite (0–200  $\mu$ M) or urate (0–50  $\mu$ M) at increasing concentrations. The fluorescent signal at the end of the measurement was taken and plotted against the respective one-electron donor concentration. Data was fitted in SigmaPlot 13 using a single rectangular hyperbola function with 3 parameters to determine  $IC_{50}$  values.

### 3. Results

#### 3.1. Purification and spectral properties of transiently expressed hsPxd01-con4

Transient expression of catalytically fully active hsPxd01-con4 in HEK293 freestyle cells led to a yield of purified protein in the range of 10–15 mg  $L^{-1}$  of cell culture medium. The construct (including the signal peptide) was composed of the amino acid residues Pro246–Asp1314 (numbers referring to full-length hsPxd01) with a theoretical molar mass of 121 kDa. As previously described [14], the construct was purified via affinity purification utilizing a His-Tag and Ni-NTA affinity column. The heme of this construct was post-translationally modified and covalently bound to the protein as verified by Western blotting in combination with the enhanced chemiluminescence staining procedure (data not shown). Furthermore the determined spectral and redox properties as well as the kinetics and thermodynamics of cyanide binding of the purified protein were identical to the recombinant protein derived from the previously described expression system [14].

#### 3.2. Reduction of compound I by one electron donors

Before investigating the kinetics of the reaction of one-electron donors with compound I we have re-visited the kinetics of the reaction between ferric Pxd01-con4 and hydrogen peroxide. As shown for previously expressed hsPxd01-con4, ferric peroxidase (Soret maximum at 412 nm) was converted into the redox intermediate compound I (hypochromicity in the Soret region) with equimolar hydrogen peroxide within 200 ms [3]. Similar to previous measurements compound I was not stable but slowly converted to a species with a compound II-like spectrum having a red-shifted Soret maximum at 434 nm. As a consequence, we had to use the sequential-mixing mode to probe the reactivity of hsPxd01-con4 compound I with one-electron donors. In detail, in the sequential mode hsPxd01-con4 was pre-incubated with equimolar concentration of hydrogen peroxide for 200 ms before one-electron donors were added (100 mM phosphate buffer, pH 7.4).

First, we investigated whether urate is able to convert hsPxd01-con4 compound I to compound II. Upon addition of 50  $\mu$ M urate to pre-formed compound I the Soret maximum shifted towards 434 nm with an isobestic point at 421 nm (Fig. 1A). In addition weak Q bands at 536 nm and 570 nm were observed (Fig. 1B). After 15 s compound II was fully established. The spectral signatures of this compound II are very similar to the species, which slowly evolved from compound I in the absence of electron donors [3].

Next we investigated the kinetics of compound I reduction with increasing urate concentrations at 434 nm. Typical time traces showed an overall biphasic character (Fig. 1C) representing compound II formation (first phase, increase of absorbance at 434 nm) and compound II reduction (second phase, decrease of absorbance at 434 nm). Transition of compound I to compound II was monophasic and could be fitted single-exponentially (Fig. 1C, red line). From the linear plot of calculated observed rate constants,  $k_{obs}$ , versus urate concentration (Fig. 1D)

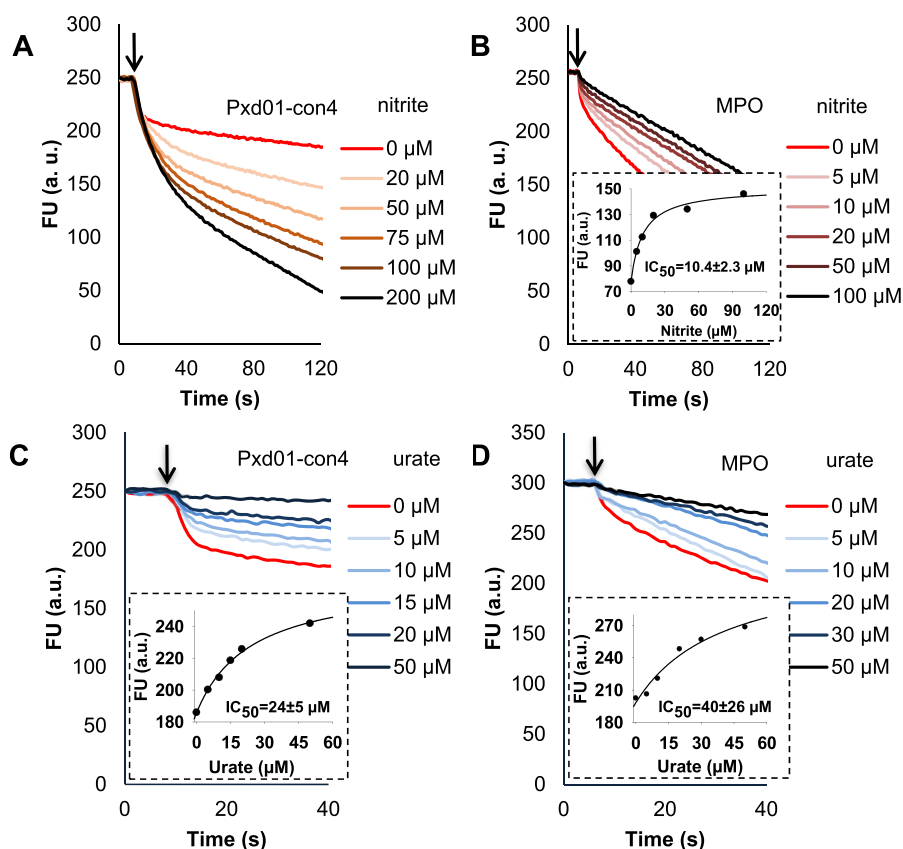


**Fig. 4.** Influence of nitrite and urate on the bromination activity of Pxd01-con4 (A, C) and MPO (B, D). Reaction conditions: 50  $\mu\text{M}$  dansylglycine, 50 nM Pxd01-con4 or MPO, 100 mM KBr and varying nitrite or urate concentrations; 100 mM phosphate buffer, pH 7.4. Reactions were started upon addition of 200  $\mu\text{M}$  hydrogen peroxide. In the absence of bromide no change in fluorescence was observed. Insets to Fig. 4B, C & D shows secondary plots and fits used for calculation of the respective  $\text{IC}_{50}$  values.

an apparent bimolecular rate constant of  $k_{\text{app}} = (1.9 \pm 0.1) \times 10^4 \text{ M}^{-1} \text{ s}^{-1}$  (pH 7.4, 25  $^{\circ}\text{C}$ ) was calculated. The finite intercept of the plot reflects the instability of compound I of hsPxd01.

Next tyrosine, serotonin, ascorbate and nitrite were tested as one-electron donors for compound I. All four endogenous molecules promoted the one-electron reduction of compound I to compound II in a strict concentration-dependent manner. The corresponding apparent biomolecular rate constants ( $k_3$ ) were determined to be  $(4.8 \pm 0.1) \times 10^5 \text{ M}^{-1} \text{ s}^{-1}$  (serotonin),  $(1.9 \pm 0.1) \times 10^5 \text{ M}^{-1} \text{ s}^{-1}$  (nitrite),  $(7.2 \pm 0.6) \times 10^4 \text{ M}^{-1} \text{ s}^{-1}$  (ascorbate) and  $(2.2 \pm 0.1) \times 10^4 \text{ M}^{-1} \text{ s}^{-1}$  (tyrosine), respectively, at pH 7.4 and 25  $^{\circ}\text{C}$  (Table 1).

### 3.3. Reduction of compound II by one-electron donors

As mentioned before, compound II formation and reduction could be followed in one measurement. Spectral changes in Fig. 2A, which is a continuation of Fig. 1A, show compound II reduction by urate to the ferric enzyme. Upon addition of 50  $\mu\text{M}$  urate to compound I transiently (fully) established compound II converted to the ferric resting state within 15 s. The Soret peak shifted from 434 nm back to 412 nm with an isosbestic point at 423 nm, while the Q-bands at 536 nm and at 570 nm disappeared (Fig. 2B). The biphasic decrease of absorbance at 434 nm (Fig. 2C) was fitted with a double exponential function and only the dominant first phase was used for the calculation of the observed rate constants,  $k_{\text{obs}}$  (Fig. 2C). The latter were plotted against the respective urate concentrations and the apparent bimolecular rate constant  $k_{\text{app}} = (5.8 \pm 0.2) \times 10^2 \text{ M}^{-1} \text{ s}^{-1}$  was determined from the slope of the plot (Fig. 2D). The second minor phase of the transition back to the ferric state was not dependent on the urate concentration.

The apparent bimolecular rate constants ( $k_4$ ) for the other one-electron donors were calculated to be  $(7.7 \pm 0.1) \times 10^3 \text{ M}^{-1} \text{ s}^{-1}$  (serotonin),  $(4.0 \pm 0.1) \times 10^3 \text{ M}^{-1} \text{ s}^{-1}$  (nitrite),

$(6.1 \pm 0.6) \times 10^2 \text{ M}^{-1} \text{ s}^{-1}$  (ascorbate) and  $(4.3 \pm 0.2) \times 10^2 \text{ M}^{-1} \text{ s}^{-1}$  (tyrosine), respectively (Table 1). In general, compound II reduction of hsPxd01-con4 for each substrate was significantly slower compared to compound I reduction. The  $k_3/k_4$  ratios varied from 33 (urate) to 118 (ascorbate).

### 3.4. Interplay between peroxidase and bromination activity

Next, for comparison of the oxidation capacity of hsPxd01-con4 with human myeloperoxidase (MPO) we probed the overall peroxidase activity with the substrates tyrosine and urate. Fig. 3A compares di-tyrosine formation mediated by hsPxd01-con4 and myeloperoxidase under identical conditions. It clearly demonstrates that MPO-mediated tyrosine oxidation is 34-times faster compared with hsPxd01-con4. Similarly, urate oxidation mediated by MPO is 37-times higher compared to hsPxd01-con4 at pH 7.4 (Fig. 3B).

Finally, we investigated the impact of urate and nitrite on the bromination activity using the dansylglycine assay [19]. Selection of these substrates was based on the fact that (i) the plasma concentrations of urate are high (200–500  $\mu\text{M}$  in health and > 500  $\mu\text{M}$  in hyperuricemia) [20,21] and that (ii) nitrite is a major product of nitrogen monoxide metabolism [22] and markedly increased nitrite levels have been detected during inflammatory processes, where NO is overproduced. Additionally, as outlined above, nitrite is a much better electron donor for both compound I and compound II compared to urate (Table 1). Again hsPxd01-con4 and MPO were compared under identical conditions.

Interestingly, the bromination activity of hsPxd01-con4 increased with increasing nitrite concentrations (Fig. 4A) whereas it decreased with increasing urate concentrations (Fig. 4C) allowing to calculate an  $\text{IC}_{50}$  value of  $24.0 \pm 5.0 \mu\text{M}$ . By contrast, the bromination activity of myeloperoxidase was inhibited by both urate and nitrite with  $\text{IC}_{50}$  values of  $40 \pm 26 \mu\text{M}$  and  $10.4 \pm 2.3 \mu\text{M}$ , respectively (Fig. 4D & B).

#### 4. Discussion

This work together with the data presented in Paumann-Page et al. [3] clearly demonstrate that Family 2 multidomain human peroxidase 1 is able to follow both the halogenation cycle (Reactions 1 & 2) and the peroxidase cycle (Reaction 1, 3 & 4). The common redox intermediate in both cycles is compound I. Recently we have demonstrated that - similar to LPO [23] and EPO [24] - hsPxd01-con4 compound I can be produced with equimolar  $\text{H}_2\text{O}_2$ . Similar to LPO and EPO, hsPxd01-con4 slowly converts to a species with compound II-like spectral signatures, which most probably is compound I\* [i.e. oxoiron(IV) amino acid radical], formed by (unspecific) intramolecular electron transport from the protein matrix to the prosthetic group [3]. This side reaction takes place in the absence of exogenous one-electron donors and is responsible for apparent inactivation of halogenation activity of human peroxidases and hsPxd01-con4 in the course of reaction. As a consequence good electron donors for compound II like nitrite are able to stimulate the bromination activity of hsPxd01-con4.

The physiological role of hsPxd01 is closely related to its halogenation activity, which includes the two-electron reduction of compound I directly to the ferric resting state (Reaction 2). Recently, we have elucidated the kinetics of compound I reduction ( $k_2$ ) by thiocyanate ( $1.8 \times 10^7 \text{ M}^{-1} \text{ s}^{-1}$ ), iodide ( $1.7 \times 10^7 \text{ M}^{-1} \text{ s}^{-1}$ ) and bromide ( $5.6 \times 10^6 \text{ M}^{-1} \text{ s}^{-1}$ ) demonstrating that peroxidase compound I is an excellent oxidant of these two-electron donors [3]. By contrast, chloride even at 100 mM could not mediate reduction of compound I [3]. These data fit with the fact that chloride did not support crosslink formation *in vivo* [1], whereas iodide and thiocyanate do not cause cross-linking of collagen IV but effectively compete with bromide and thus inhibit the formation of sulfilimine bonds. Moreover,  $E^\circ[\text{Fe(III)/Fe(II)}]$  of hsPxd01-con4 is significantly less positive ( $-128 \text{ mV}$ ) compared to that of MPO ( $+5 \text{ mV}$ ) [25–27], which is the only human enzyme that is able to oxidize chloride at reasonable rates [28].

The  $E^\circ$  value of the redox couple  $[\text{Fe(III)/Fe(II)}]$  of hsPxd01-con4 is similar to EPO ( $-126 \text{ mV}$ ) and more positive than LPO ( $-176 \text{ mV}$ ) [29]. With MPO, EPO and LPO it has been demonstrated that the hierarchy of  $E^\circ[\text{Fe(III)/Fe(II)}]$ , namely  $\text{MPO} > \text{EPO} > \text{LPO}$ , follows the same trend that was observed for  $E^\circ$  of the compound I/Fe(III) couple, that is,  $\text{MPO} (1160 \text{ mV}) > \text{EPO} (1100 \text{ mV}) > \text{LPO} (1090 \text{ mV})$  [30–33]. This suggests that within a defined peroxidase the same molecular factors influence the redox properties of the heme iron at different oxidation states and this, most probably, also applies to hsPxd01. The unique features of MPO are closely related to the MPO-specific covalent heme-protein sulfonium ion linkage [34,35] which does not exist in LPO, EPO and hsPxd01 [8–13]. Posttranslational modification of heme *b* in EPO, LPO and hsPxd01 enables the formation of two ester bonds between the protein and the prosthetic group [3,11,30]. Nevertheless, hsPxd01-con4 outperforms the reactivity of MPO towards bromide at neutral pH [3] suggesting that, besides thermodynamics, also structural factors like accessibility of the heme cavity and architecture of the access channel contributes to the kinetics of substrate oxidation by human peroxidases (Table 1). This applies to halide oxidation but is even more pronounced in oxidation of bulkier aromatic, aliphatic or inorganic electron donors.

Compound I is the redox intermediate that links the halogenation cycle with the peroxidase cycle. Whether hsPxd01 compound I reacts with bromide or with a one-electron donor is dictated by the concentration of the respective substrate and the second-order rate constants for compound I reduction to either the ferric state or compound II. Thus peroxidase substrates have the ability to divert the enzyme away from the halogenation cycle to compound II and thus to modulate the bromination activity and consequently sulfilimine cross-linking. This has been demonstrated by Bathish et al. [16] who investigated cross-linking by peroxidase embedded in extracellular matrix isolated from cultured epithelial cells. The authors observed partial inhibition of cross-link formation in the presence of alternative substrates like urate.

The present study provides the kinetic basis for understanding this interference between oxidation of bromide and endogenous one-electron donors. Table 1 compares the calculated apparent second-order rate constants of compound I ( $k_3$ ) and compound II ( $k_4$ ) reduction of hsPxd01-con4 with kinetic data known from the homologous human peroxidases LPO and MPO [36–40]. For both reduction of compound I and compound II the hierarchy of the respective apparent bimolecular rate constants was serotonin > nitrite > ascorbate > tyrosine & urate with  $k_3/k_4$  ratios of 62 (serotonin), 48 (nitrite), 118 (ascorbate), 51 (tyrosine) and 33 (urate). Since reduction of compound II ( $k_4$ ) represents the rate limiting step in the peroxidase cycle, serotonin and nitrite can be regarded as moderate peroxidase substrates of human peroxidase 1, whereas tyrosine and urate are poor peroxidase substrates at physiological pH (Table 1, Fig. 3).

Urate has already been shown to be a physiological substrate for both LPO [37] and MPO [17] with a plasma concentration ranging between 200 and 500  $\mu\text{M}$  [40], which can be significantly enhanced in inflammatory diseases and neurodegenerative disorders [41]. This compares with a bromide concentration of 60–75  $\mu\text{M}$  in plasma [42]. Although bromide is a 263-times better reductant of compound I at pH 7.4, the higher urate concentration together with its low reactivity at compound II promotes accumulation of compound II during turnover and in consequence reversible inhibition of bromide oxidation. The  $\text{IC}_{50}$  value of  $24.0 \pm 5.0 \mu\text{M}$  determined with the dansylglycine assay (Fig. 4) very well fits with the observation that urate partially inhibited crosslink formation of hsPxd01 embedded in extracellular matrix with an  $\text{IC}_{50}$  value of 20  $\mu\text{M}$  [16]. Future studies have to probe whether pathophysiological urate concentrations have an adverse impact on mechanical strength of extracellular matrix *in vivo*. The inhibitory effect of urate on bromide oxidation was also seen for MPO, which is in agreement with a previous study of Meotti et al. [17].

In contrast to urate, nitrite has been shown to promote the bromination activity of hsPxd01. Bromide is a 29-times better reductant of compound I at pH 7.4 than nitrite. Nitrite is known to derive from nitrogen monoxide produced by nitric oxide synthases [43]. Expression of nitric oxide synthases is induced during inflammatory processes as a defense mechanism against microorganisms. However, excessive production of reactive nitrogen species can also have adverse effects on host tissue [43,44]. Under inflammatory and pathophysiological conditions the nitrite concentration in plasma exceeds that of bromide and nitrite efficiently converts hsPxd01 compound I to compound II similar to MPO [38] (Table 1) thereby producing  $\text{NO}_2$  radicals which promote nitrotyrosine formation [45]. By contrast, lactoperoxidase was reported to mediate the two-electron oxidation of nitrite to peroxynitrite [37]. Interestingly, compound II of hsPxd01 is a 7-times better oxidant compared to compound II of MPO (Table 1). As a consequence hsPxd01 is an excellent source of nitrogen dioxide in human blood plasma. Nitrite promotes the turnover of compound II and therefore does not inhibit bromide oxidation mediated by hsPxd01 despite competing with bromide in reaction with compound I. By contrast, the bromination activity of MPO is inhibited by nitrite (Fig. 4).

In summary, we have demonstrated that hsPxd01 is able to follow both the halogenation cycle (Reactions 1 & 2) and the peroxidase cycle (Reaction 1, 3 & 4) and, for the first time, have determined apparent bimolecular rate constants for compound I and compound II reduction with various endogenous one-electron donors. Depending of the respective rate constants ( $k_3$  and  $k_4$ ) and their concentration these blood constituents either act as inhibitors (like urate) or promoters (like nitrite) of hypobromous acid formation by hsPxd01 and consequently of sulfilimine bond formation in basement membranes. Our study also demonstrated that hsPxd01 is a source of nitrogen dioxide in the extracellular matrix and could contribute to host tissue injury and oxidative modifications.

## Author statement

Conceptualization: PGF, CO.

Data curation: BS, MPP, PGF.

Formal analysis: BS, MPP, PGF, SH, VP.

Funding acquisition: CO.

Roles/Writing – original draft: BS, PGF.

Writing – review & editing: BS, MPP, SH, VP, PGF, CO.

## Acknowledgements

This project was supported by the Austrian Science Fund, FWF [Doctoral Program BioToP - Molecular Technology of Proteins (W1224) and project P25538].

## References

- [1] G. Bhavé, C.F. Cummings, R.M. Vanacore, C. Kumagai-Cresse, I.A. Ero-Tolliver, M. Rañ, J.S. Kang, V. Pedchenko, L.I. Fessler, J.H. Fessler, B.G. Hudson, *Nat. Chem. Biol.* 8 (2012) 784–790.
- [2] A.S. McCall, C.F. Cummings, G. Bhavé, R. Vanacore, A. Page-McCaw, B.G. Hudson, *Cell* 157 (2014) 1380–1392.
- [3] M. Paumann-Page, R.S. Katz, M. Bellei, I. Schwartz, E. Edenhofer, B. Sevcnikar, M. Soudi, S. Hofbauer, G. Battistuzzi, P.G. Furtmüller, C. Obinger, *J. Biol. Chem.* 292 (2017) 4583–4592.
- [4] A.L. Fidler, R.M. Vanacore, S.V. Chetyrkin, V.K. Pedchenko, G. Bhavé, V.P. Yin, C.L. Stothers, K.L. Rose, W.H. McDonald, T.A. Clark, D.B. Borza, R.E. Steele, M.T. Ivy, Aspirin, J.K. Hudson, B.G. Hudson, *Proc. Natl. Acad. Sci.* 111 (2014) 331–336.
- [5] G. Bhavé, S. Colon, N. Ferrell, *Am. J. Physiol. Physiol.* 313 (2013) F596–F602.
- [6] H. Medfai, A. Kalil, A. Rousseau, V. Nuyens, M. Paumann-Page, B. Sevcnikar, P.G. Furtmüller, C. Obinger, N. Moguilevsky, O. Peulen, M. Herfs, V. Castronovo, M. Amri, P. Van Antwerpen, L. Vanhamme, K.Z. Boudjeltia, *Cardiovasc. Res.* 115 (2019) 463–475.
- [7] E. Lázár, Z. Péterfi, G. Sirokmány, H.A. Kovács, E. Klement, K.F. Medzihradszky, M. Geiszt, *Free Radic. Biol. Med.* 83 (2015) 273–282.
- [8] M. Zamocky, C. Jakopitsch, P.G. Furtmüller, C. Dunand, C. Obinger, *Proteins* 72 (2008) 589–605.
- [9] M. Zámocký, S. Hofbauer, I. Schaffner, B. Gasselhuber, A. Nicolussi, M. Soudi, K.F. Pirker, P.G. Furtmüller, C. Obinger, *C3. Arch. Biochem. Biophys.* 574 (2015) 108–119.
- [10] M. Soudi, M. Zamocky, C. Jakopitsch, C. Obinger, *Chem. Biodivers.* 9 (2012) 1776–1793.
- [11] M. Soudi, M. Paumann-Page, C. Delporte, K.F. Pirker, M. Bellei, E. Edenhofer, G. Stadlmayr, G. Battistuzzi, K.Z. Boudjeltia, P.G. Furtmüller, P. Van Antwerpen, C. Obinger, *J. Biol. Chem.* 290 (2015) 10876–10890.
- [12] P.G. Furtmüller, M. Zederbauer, W. Jantschko, J. Helm, M. Bogner, C. Jakopitsch, C. Obinger, *Arch. Biochem. Biophys.* 445 (2006) 199–213.
- [13] A. Nicolussi, M. Auer, B. Sevcnikar, M. Paumann-Page, V. Pfanzagl, M. Zámocký, S. Hofbauer, P.G. Furtmüller, C. Obinger, *C. Arch. Biochem. Biophys.* 643 (2018) 12–23.
- [14] M. Paumann-Page, R. Tscheliessnig, R.-S. Katz, I. Schwartz, S. Hofbauer, V. Pfanzagl, P.G. Furtmüller, C. Obinger, *Biochim. Biophys. Acta Protein Proteomics* 1868 (2020) 140249.
- [15] I. Ero-Tolliver, B.G. Hudson, G. Bhavé, *J. Biol. Chem.* 290 (2015) 21741–21748.
- [16] B. Bathish, R. Turner, M. Paumann-Page, A.J. Kettle, C.C. Winterbourn, *Arch. Biochem. Biophys.* 646 (2018) 120–127.
- [17] F.C. Meotti, G.N. Jameson, R. Turner, D.T. Harwood, S. Stockwell, M.D. Rees, S.R. Thomas, A.J. Kettle, *Biol. Chem.* 286 (2011) 12901–12911.
- [18] L. Marquez-Curtis, H. Dunford, *J. Biol. Chem.* 270 (1995) 338–350.
- [19] L. Bertozzi, M.L. Zeraik, V.F. Ximenes, *Anal. Biochem.* 532 (2017) 29–37.
- [20] A. Enomoto, H. Kimura, A. Chairoungdua, Y. Shigeta, P. Jutabha, S.H. Cha, M. Hosoyamada, M. Takeda, T. Sekine, T. Igarashi, H. Matsuo, Y. Kikuchi, T. Oda, K. Ichida, T. Hosoya, K. Shimokata, T. Niwa, Y. Kanai, H. Endou, *Nature* 417 (2002) 447–452.
- [21] B.F. Becker, *Free Radic. Biol. Med.* 14 (1993) 615–631.
- [22] M.L. Brennan, W. Wu, X. Fu, Z. Shen, W. Song, H. Frost, C. Vadseth, L. Narine, E. Lenkiewicz, M.T. Borchers, A.J. Lusis, J.J. Lee, N.A. Lee, H.M. Abu-Soud, H. Ischiroopoulos, S.L. Hazen, *J. Biol. Chem.* 277 (2002) 17415–17427.
- [23] P.G. Furtmüller, W. Jantschko, G. Regelsberger, C. Jakopitsch, J. Arnhold, C. Obinger, *Biochemistry* 41 (2002) 11895–11900.
- [24] P.G. Furtmüller, W. Jantschko, G. Regelsberger, C. Obinger, *Biochim. Biophys. Acta* 1548 (2001) 121–128.
- [25] G. Battistuzzi, M. Bellei, M. Zederbauer, P.G. Furtmüller, M. Sola, C. Obinger, *Biochemistry* 45 (2006) 12750–12755.
- [26] J. Arnhold, E. Monzani, P.G. Furtmüller, M. Zederbauer, L. Casella, C. Obinger, *J. Inorg. Chem.* 19 (2006) 3801–3811.
- [27] G. Battistuzzi, J. Stampfer, M. Bellei, J. Vlasits, M. Soudi, M. Sola, P.G. Furtmüller, C. Obinger, *Biochemistry* 50 (2011) 7987–7994.
- [28] P.G. Furtmüller, U. Burner, C. Obinger, *Biochemistry* 37 (1998) 17923–17930.
- [29] G. Battistuzzi, M. Bellei, J. Vlasits, S. Banerjee, P.G. Furtmüller, S. Sola, C. Obinger, *Arch. Biochem. Biophys.* 494 (2010) 72–77.
- [30] J. Arnhold, P.G. Furtmüller, C. Obinger, *Redox Rep.* 8 (2003) 179–186.
- [31] J. Arnhold, P.G. Furtmüller, G. Regelsberger, C. Obinger, *Eur. J. Biochem.* 268 (2001) 5142–5148.
- [32] P.G. Furtmüller, J. Arnhold, W. Jantschko, H. Pichler, C. Obinger, *Biochem. Biophys. Res. Commun.* 301 (2003) 551–557.
- [33] P.G. Furtmüller, J. Arnhold, W. Jantschko, M. Zederbauer, C. Jakopitsch, C. Obinger, *J. Inorg. Biochem.* 99 (2005) 1220–1229.
- [34] M. Zederbauer, P.G. Furtmüller, S. Brogioni, C. Jakopitsch, G. Smulevich, C. Obinger, *Nat. Prod. Rep.* 24 (2007) 571–584.
- [35] X. Carpena, P. Vidossich, K. Schroettner, B.M. Calisto, S. Banerjee, J. Stampfer, M. Soudi, P.G. Furtmüller, C. Rovira, I. Fita, C. Obinger, *J. Biol. Chem.* 284 (2009) 25929–25937.
- [36] W. Jantschko, P.G. Furtmüller, M. Allegra, M.A. Livrea, C. Jakopitsch, G. Regelsberger, C. Obinger, *Arch. Biochem. Biophys.* 398 (2002) 12–22.
- [37] T.B. Brück, R.J. Fielding, M.C.R. Symons, P.J. Harvey, *Eur. J. Biochem.* 268 (2001) 3214–3222.
- [38] U. Burner, P.G. Furtmüller, A.J. Kettle, W.H. Koppenol, C. Obinger, *J. Biol. Chem.* 275 (2000) 20597–20601.
- [39] Y. Hsuanyu, H.B. Dunford, *Arch. Biochem. Biophys.* 368 (1999) 413–420.
- [40] F. Martinon, V. Pétrilli, A. Mayor, A. Tardivel, J. Tschopp, *Nature* 440 (2006) 237–241.
- [41] M.K. Kutzling, B.L. Firestein, *J. Pharmacol. Exp. Ther.* 324 (2007) 1–7.
- [42] H.A. Olszowy, J. Rossiter, J. Hegarty, P. Geoghegan, *J. Anal. Toxicol.* 22 (1998) 225–230.
- [43] J.N. Sharma, A. Al-Omran, S.S. Parvathy, *Inflammopharmacology* 15 (2007) 252–259.
- [44] G. Degendorfer, C.Y. Chuang, H. Kawasaki, A. Hammer, E. Malle, F. Yamakura, M.J. Davies, *Free Radic. Biol. Med.* 97 (2016) 602–615.
- [45] W.A. Prütz, H. Mönig, J. Butler, E.J. Land, *Arch. Biochem. Biophys.* 243 (1985) 125–134.

# The leucine-rich repeat domain of human peroxidasin 1 promotes binding to laminin in basement membranes

**Benjamin Sevcnikar**, Irene Schaffner, Christine Y. Chuang, Luke Gamon, Martina Paumann-Page, Stefan Hofbauer, Michael J. Davies, Paul G. Furtmüller and Christian Obinger

Research Article

Archives of Biochemistry and Biophysics Volume 689, 15 August 2020,  
108433

DOI: [10.1016/j.abb.2020.108443](https://doi.org/10.1016/j.abb.2020.108443)



## The leucine-rich repeat domain of human peroxidasin 1 promotes binding to laminin in basement membranes

Benjamin Sevcnikar<sup>a</sup>, Irene Schaffner<sup>a</sup>, Christine Y. Chuang<sup>b</sup>, Luke Gamon<sup>b</sup>,  
Martina Paumann-Page<sup>c</sup>, Stefan Hofbauer<sup>a</sup>, Michael J. Davies<sup>b</sup>, Paul G. Furtmüller<sup>a,\*\*</sup>,  
Christian Obinger<sup>a,\*</sup>

<sup>a</sup> Department of Chemistry, Institute of Biochemistry, BOKU – University of Natural Resources and Life Sciences, Muthgasse 18, A-1190, Vienna, Austria

<sup>b</sup> Department of Biomedical Sciences, University of Copenhagen, Copenhagen, Denmark

<sup>c</sup> Department of Pathology and Biomedical Science, University of Otago, Christchurch, New Zealand

### ARTICLE INFO

#### Keywords:

Human peroxidasin 1  
Extracellular matrix  
Basement membrane  
Type-IV collagen  
Laminin  
Immunoprecipitation  
Surface plasmon resonance spectroscopy

### ABSTRACT

Human peroxidasin 1 (PXDN) is a homotrimeric multidomain heme peroxidase and essential for tissue development and architecture. It has a biosynthetic function and catalyses the hypobromous acid-mediated formation of specific covalent sulfilimine (S=N) bonds, which cross-link type IV collagen chains in basement membranes. Currently, it is unknown whether and which domain(s) [i.e. leucine-rich repeat domain (LRR), immunoglobulin domains, peroxidase domain, von Willebrand factor type C domain] of PXDN interact with the polymeric networks of the extracellular matrix (ECM), and how these interactions integrate and regulate the enzyme's cross-linking activity, without imparting oxidative damage to the ECM. In this study, we probed the interactions of four PXDN constructs with different domain compositions with components of a basement membrane extract by immunoprecipitation. Strong binding of the LRR-containing construct was detected with the major ECM protein laminin. Analysis of these interactions by surface plasmon resonance spectroscopy revealed similar kinetics and affinities of binding of the LRR-containing construct to human and murine laminin-111, with calculated dissociation constants of 1.0 and 1.5  $\mu\text{M}$ , respectively. The findings are discussed with respect to the recently published in-solution structures of the PXDN constructs and the proposed biological role of this peroxidase.

### 1. Introduction

Basement membranes (BMs) are widely-distributed cell-adherent specialized extracellular matrices (ECMs), that provide a complex framework that segregates polarized epithelial or endothelial cells from the underlying mesenchyme [1,2]. The emergence of BMs coincided with the origin of multicellularity in animals, suggesting that they are essential for the formation of tissues. BMs provide structural support to tissues and play active roles in many developmental processes including organogenesis, angiogenesis and tissue repair [3]. Their sheet-like structure derives from two independent polymeric networks derived from two major protein classes: the laminins and type IV collagen [4]. These (independent) networks interact with each other via additional ECM proteins including agrin, nidogen, entactin and perlecan [3].

Laminins are cross-shaped heterotrimers ( $\alpha\beta\gamma$ ) that share a common structure with a number of globular and rod-like domains [5,6]. In vertebrates, five  $\alpha$ , three  $\beta$ , and three  $\gamma$  chains are assembled in

different combinations generating a large variety of isoforms which are believed to have distinct functions in embryogenesis, vascular maturation, and neuromuscular development [7]. For example, the isoform laminin-111 (i.e.  $\alpha1\beta1\gamma1$ ) plays an important role in the early embryonic development in mammals [7].

Previous studies have shown that the ECM proteins are highly susceptible to oxidative damage due to their high abundance, their low rate of turnover, and the relatively low levels of extracellular antioxidants, repair and catabolic systems [8]. Oxidants can induce structural and functional changes to laminins and other ECM materials, with damage evident in multiple tissue samples, including human atherosclerotic lesions [9–11]. It has been hypothesized that co-localisation of hypohalous acid-producing myeloperoxidase (MPO) with ECM components might be involved in the observed oxidative damage, since MPO undergoes transcytosis across endothelial cells and binds tightly to sub-endothelial and glomerular BM [12] and particularly fibronectin [13]. MPO also directly binds to perlecan via an electrostatic

\* Corresponding author.

\*\* Corresponding author.

E-mail addresses: [paul.furtmueller@boku.ac.at](mailto:paul.furtmueller@boku.ac.at) (P.G. Furtmüller), [christian.obinger@boku.ac.at](mailto:christian.obinger@boku.ac.at) (C. Obinger).

<https://doi.org/10.1016/j.abbi.2020.108443>

Received 25 February 2020; Received in revised form 26 May 2020; Accepted 27 May 2020

Available online 30 May 2020

0003-9861/ © 2020 The Authors. Published by Elsevier Inc. This is an open access article under the CC BY-NC-ND license

(<http://creativecommons.org/licenses/by-nc-nd/4.0/>).

**Abbreviations**

PXDN	human peroxidase 1
LRR	leucine-rich repeat domain
Ig	immunoglobulin domain
VWC	C-terminal von Willebrand factor type C
POX	peroxidase domain
ECM	extracellular matrix
BM	basement membrane
BME	basement membrane extract
LN	laminin
huLN	human laminin
muLN	murine laminin

MPO	myeloperoxidase
LPO	lactoperoxidase
EPO	eosinophil peroxidase
TPO	thyroid peroxidase
PBS	phosphate buffer-saline
PBST	phosphate buffer-saline + Tween 20
IP	immunoprecipitation
SAXS	small-angle X-ray scattering
SPR	surface plasmon resonance
SEC-MALS	size exclusion chromatography combined with multi-angle light scattering
MCK	multi-cycle kinetics

interaction established between cationic MPO and the anionic side chains of perlecan [14].

Recently, a related human peroxidase, peroxidase 1 (PXDN) was detected within the ECM network [15,16]. In contrast to MPO (which exhibits antimicrobial activity and is part of the innate immune system), PXDN has been shown to have a biosynthetic function and to mediate the formation of specific covalent sulfilimine (S=N) bonds that cross-link type IV collagen chains in BMs. In contrast to MPO (and other homologous human peroxidases), PXDN is a multi-domain, highly-glycosylated, homotrimeric peroxidase [17,18] and a member of Family 2 of the peroxidase-cyclooxygenase superfamily [19,20]. It catalyses the hydrogen peroxide-mediated oxidation of bromide to hypobromous acid [21], which mediates S=N bond formation between specific (hydroxy)lysine and methionine residues at the interface of two NC1-domain trimers of type IV collagen [15,16,22]. Removal of the substrate bromide, and hence prevention of cross-linking, is embryonically lethal in *Drosophila melanogaster* and *Caenorhabditis elegans* [16]. Thus, peroxidase 1 catalyses a post-translational modification that is essential for tissue development and architecture.

To date, it is unknown how peroxidase 1 is embedded in the ECM, and how it is able to catalyse the formation of specific sulfilimine bonds in type IV collagen without inducing (collateral) oxidative damage to other sites on the collagen chains, or other BM molecules. In particular, the role(s) of specific PXDN-typical domains, including the N-terminal leucine-rich repeat domain (LRR), the immunoglobulin domains (Ig), and the C-terminal von Willebrand factor type C module (VWC) [17,18], which are all known to be important for protein-protein interactions and cell adhesion [22], are unknown. Therefore, we have designed and produced four recombinant and truncated PXDN variants with different domain compositions in order to identify potential BM binding partners by co-immunoprecipitation (IP). We have unambiguously identified laminin as a binding partner of PXDN and demonstrate that the LRR domain promotes high affinity binding to murine and human laminin-111 with very similar  $K_D$  values, as determined by surface plasmon resonance (SPR) spectroscopy.

**2. Material and methods****2.1. Materials**

High purity murine laminin (muLN111) free of entactin (Corning® Ultrapure Laminin) was purchased from Corning Incorporated, USA. Human laminin isoforms (huLN111, huLN411) were from Biolamina AB, Sweden. Laminin concentrations were determined via the UV-vis absorption at 280 nm and based on molar masses of 900 and 713 kDa (muLN111 and huLN111) or 579 kDa (huLN411). Murine basement membrane extract (BME) with reduced growth factors (Cultrex) was purchased from Trevigen. Protein G Dynabeads were obtained from ThermoFisher. The anti-His<sub>6</sub> antibody monoclonal antibody and rabbit anti-laminin polyclonal antibody, were purchased from Abcam, and the secondary anti-rabbit IgG conjugated with horseradish peroxidase antibody was purchased from GE. Other chemicals were purchased from Sigma at the highest grade available.

**2.2. Cloning, expression and purification of constructs**

We have cloned and recombinantly produced four PXDN constructs, namely PXDN-con2, PXDN-con3, PXDN-con4, and PXDN-con5 (Fig. 1). UniProt KB (<http://www.uniprot.org/>) data on human peroxidase 1 (Q92626) provided the basis for primer design. DNA of PXDN-con 2 (Pro<sup>246</sup>-Leu<sup>1471</sup>), PXDN-con 3 (Val<sup>27</sup>-Asp<sup>1314</sup>), PXDN-con 4 (Pro<sup>246</sup>-Asp<sup>1314</sup>) and PXDN-con 5 (Gly<sup>619</sup>-Asp<sup>1314</sup>) were cloned into a modified gWiz vector (Genlantis) carrying an N-terminal His<sub>6</sub> tag for protein purification. Forward and reverse PCR primers were as follows: PXDN-con2: 5'-gaggctcaccac-caccatcac catccccaatcaccctccgagccc -3' and 5'-agccagaagtgatctgga-tcaagcagactggacagcaggc-3'; PXDN-con3: 5'-gaggctcaccaccaccatcaccatgtgg-tggcccagaagccggg-3' and 5'-tagccagaagtgatctgga-tcagtcctgccaccgccggagtc-3'; PXDN-con4: 5'-gctctgggtccagggtccactggccatcaccatcaccatggagatcc-gttgtagctacctcatcg-3' and 5'-gccagaggtcgaggtcggggatccttatcagtcctcca-caccggaggtccaccctgggg-3'; PXDN-con5: same forward primer as for PXDN-con5 and 5'-gccagaggtcgaggtcggggatccttaactgag-cggtgattcaagttctttatc-3'. Transformed *E. coli* XL-10 were screened via colony-PCR and positive clones were selected and validated by DNA sequencing.

Construct	Domain composition of the constructs	MW (kDa)	Oligomeric structure
PXDN -con2		138	Trimer
PXDN -con3		145	Monomer
PXDN -con4		120	Monomer
PXDN -con5		81	Monomer

**Fig. 1. Overview of the investigated constructs of human peroxidase-1.** PXDN-con2 comprises four immunoglobulin (Ig) domains and the peroxidase domain (POX) as well as the C-terminal von Willebrand factor type C (VWC) domain and forms trimers; PXDN-con3 is monomeric and comprises the leucine rich repeat domain (LRR), the Ig domains and POX; PXDN-con4 is monomeric and consists of the four Ig domains and POX; PXDN-con5 is monomeric and consists of the catalytic peroxidase domain only.

For recombinant expression, we chose the HEK 293F (Invitrogen) suspension system. Cells were cultivated according to the Invitrogen User Guideline. Cells were transfected as reported previously [21]. Hemin chloride was added to the culture medium to a final concentration of  $5 \mu\text{g mL}^{-1}$  4 h after transfection to improve heme incorporation. Supernatants were harvested 5 days after transfection. Purification of the different constructs (Fig. 1) followed a procedure described previously [21,23]. In short, the harvested supernatant was filtrated through a  $0.45 \mu\text{m}$  PVDF membrane (Durapore) and concentrated to 100 mL using a Millipore Labscale TFF diafiltration system. Subsequently, the sample was adjusted to 1 M NaCl and 20 mM imidazole.

For purification of the His<sub>6</sub>-tagged proteins, 5 mL HisTrap FF columns (GE Healthcare) loaded with nickel chloride were used. After equilibration of the column with 100 mM sodium phosphate buffer (pH 7.4) containing 1 M NaCl and 20 mM imidazole, the sample was loaded and washed with equilibration buffer. The protein was eluted using two consecutive step gradients of 8% and 70% of 20 mM sodium phosphate buffer, pH 7.4, 500 mM NaCl and 500 mM imidazole. Eluted fractions were analysed by UV-vis spectroscopy and SDS-PAGE. Appropriate fractions were pooled and washed 5 times with 100 mM sodium phosphate buffer, pH 7.4, using Amicon Ultra-15 50 kDa cut-off centrifugal filters (Merck Milipore).

### 2.3. Immunoprecipitation

Murine basement membrane extract (BME; 20  $\mu\text{g}$ ) was mixed with 10  $\mu\text{g}$  of each construct and incubated at 21 °C for 1 h. Protein G Dynabeads (ThermoFisher) were coupled with an anti-His<sub>6</sub> antibody (Abcam mouse 1  $\times$  Anti-6  $\times$  His tag<sup>®</sup>) according to the manufacturer's protocol and was washed once with 0.05% v/v Tween 20 in PBS (PBST). The BME-construct mix was subsequently added to the coupled Dynabeads and immunoprecipitated overnight with rotation at 4 °C. On the next day, samples were washed 3 times with PBST, transferred into clean tubes and eluted from the Protein G Dynabeads using the elution buffer as per manufacturer's protocol to collect the immunoprecipitate.

### 2.4. Silver staining and immunoblotting

Immunoprecipitated samples were treated with NuPAGE reducing buffer (1:10 dilution; ThermoFisher) and heat denatured for 10 min at 70 °C in the presence of the NuPAGE sample buffer (1:4 dilution; ThermoFisher) and loaded onto NuPAGE 3–8% Tris-acetate gels run under constant voltage (160 V) for 70 min. High molecular mass protein markers (HMW HiMark; 460–31 kDa; ThermoFisher) were used as calibration standards. Protein bands were detected by both silver staining and immunoblotting using a rabbit polyclonal anti-laminin antibody (Abcam ab11575, 1:2000 dilution) and an anti-rabbit-HRP conjugated secondary antibody (1:5000 dilution), with the blots developed using a commercial chemiluminescence (ECL) reagent (PerkinElmer, MA, USA), and imaged using a chemiluminescence imager (Syngene, MD, USA).

### 2.5. Surface plasmon resonance

Surface plasmon resonance (SPR) experiments were performed on a Biacore T200 instrument (GE Healthcare). Laminin variants ( $10 \mu\text{g mL}^{-1}$  in 10 mM sodium acetate buffer, pH 4.5) were covalently immobilized on flow cells 2, 3 and 4 (immobilization levels: muLN111 ~ 2650 RU; huLN111 ~ 2015 RU; huLN411 ~ 1615 RU), on a commercially available CM5 chip (GE Healthcare) using the amine coupling kit according to the manufacturer's protocol (GE Healthcare). In short, the flow cells were activated with 1-ethyl-3-[3-dimethylaminopropyl] carbodiimide (EDC)/N-hydroxysulfosuccinimide (NHS) and excess reactive carboxyl groups were blocked with ethanolamine. Flow cell 1 was activated and blocked in the same way and served as reference surface (without ligand). Multi-cycle kinetics (MCK) experiments were performed at 25 °C using increasing concentrations of PXDN-con3, PXDN-con4, and PXDN-con5 respectively (0.14; 0.281; 0.5625; 1.125; 2.25; 4.5; 9  $\mu\text{M}$ ). 1  $\times$  PBS supplemented with 0.05% Tween 20 was used as running buffer. Double referencing was accomplished by subtracting the signal from injections of running buffer. The flow rate was set to  $30 \mu\text{L min}^{-1}$ , association time was 7 min, dissociation was monitored for 20 min. Complete regeneration of laminin variants was achieved by one injection of glycine-HCl, pH 1.5 (30 s,  $30 \mu\text{L min}^{-1}$ ) followed by four injections of 10 mM NaOH (30 s each,  $30 \mu\text{L min}^{-1}$ )

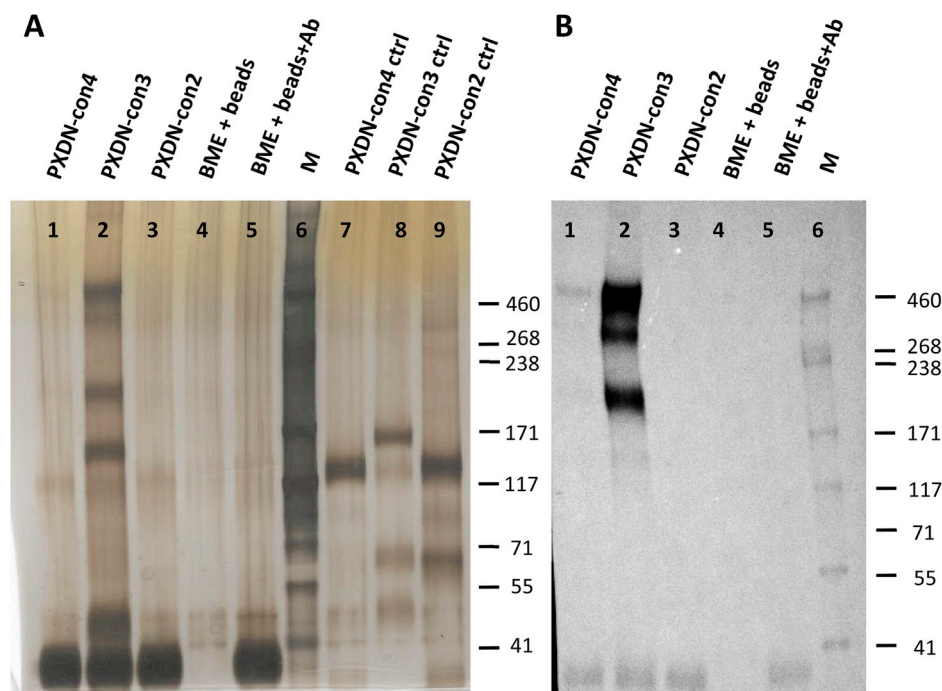


**Fig. 2. Immunoprecipitation of truncated human peroxidasin-1 variants and basement membrane extracts.** (A) Silver-stained SDS-PAGE under reducing conditions. Lanes 1–3 show immunoprecipitates containing monomeric PXDN-con4, monomeric PXDN-con3 or trimeric PXDN-con2. Lanes 4 and 5 represent negative controls. BME, basement membrane extract; Ab, anti-His<sub>6</sub> antibody. Lane 6: marker proteins. Lanes 7–9: SDS-PAGE of recombinant glycosylated constructs only (ctrl, control). (B) Immunoblot using anti-laminin polyclonal antibody. Lanes 1–3 show immunoprecipitates containing monomeric PXDN-con4, monomeric PXDN-con3 or trimeric PXDN-con2. Lanes 4 and 5 represent negative controls and lane 6 marker proteins. All gels and blots are representatives of at least three independent experiments.

after every cycle. The integrity of the various ligands within one titration experiment was ensured by testing reproducibility of the 1.125  $\mu\text{M}$  analyte binding curve after application of the highest analyte concentration. Data were analysed with the Biacore Evaluation Software version 3.1 (GE Healthcare). To determine the dissociation constant  $K_D$ , steady-state response units were plotted against analyte concentrations and the data were fitted to a steady-state affinity model. All MCK experiments were performed in triplicates.

### 3. Results

The truncated constructs PXDN-con2, PXDN-con3, PXDN-con4, and PXDN-con5 (Fig. 1) with an N-terminal His<sub>6</sub> tag were purified using affinity chromatography and preparative size exclusion chromatography (SEC). PXDN-con2 forms trimers, whereas PXDN-con3, PXDN-con4 and PXDN-con5 are monomeric proteins. Importantly, full length homotrimeric PXDN is not included in this study because we (and also other groups) have not been able to obtain sufficient amounts of correctly folded protein. The correct folding of the recombinant proteins were probed routinely by SEC coupled to multi-angle light scattering

(MALS), circular dichroism and UV-vis spectroscopy as described recently [21,23].

#### 3.1. Laminin is a specific binding partner of human peroxidasin 1 (PXDN)

Purified distinct His<sub>6</sub>-tagged PXDN constructs were mixed with murine extracellular basement membrane extract (which contains laminins, collagen IV, entactin and heparan sulphate proteoglycans) and incubated with protein G coated with an anti-His<sub>6</sub> antibody. The mixture was immunoprecipitated, the attached proteins released, and these then separated by electrophoresis under reducing conditions. Fig. 2A compares the silver-stained IP mixtures with positive controls (ctrl) of pure recombinant glycosylated constructs 2, 3 and 4 which have molar masses of 130–170 kDa (right side of panel A). It has been demonstrated that the full length PXDN has ten confirmed N-glycosylation sites [seven on the peroxidase domain (POX), one on the Ig domains, one in the C-terminal linker region between POX and the VWC module and one on the VWC module] [18]. From the IP mixtures, only PXDN-con3 (molar mass of glycosylated protein ~170 kDa) showed three additional bands at molar masses  $\gg$  170 kDa suggesting co-

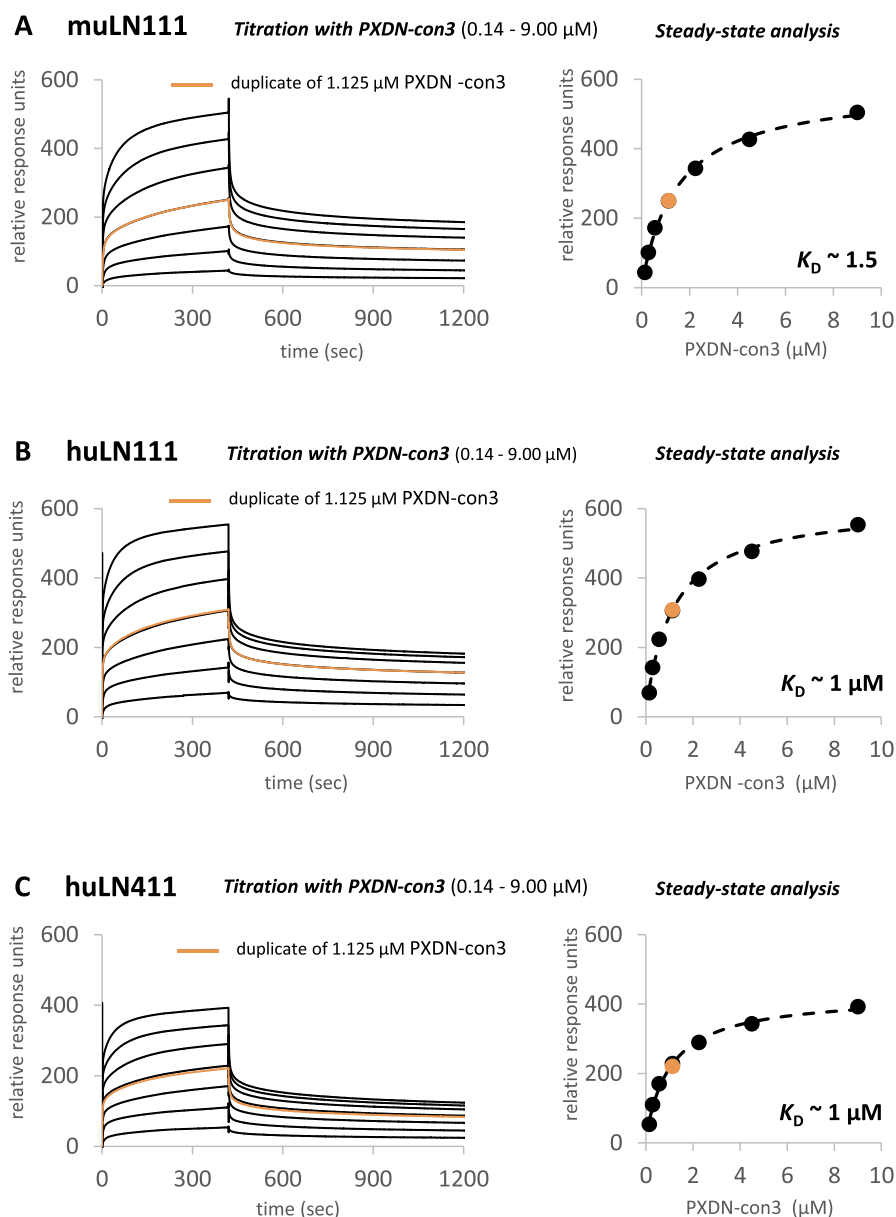


Fig. 3. Kinetics and affinity of binding of human peroxidasin-1 construct, PXDN-con3, to murine and human laminins. Determination of the dissociation constants ( $K_D$ ) for the interaction of different laminin isoforms with PXDN-con3 via steady-state analysis of double-referenced multi-cycle kinetics SPR experiments. Left: Titrations of (A) murine laminin-111 (muLN111), (B) human laminin-111 (huLN111) and (C) human laminin-411 (huLN411) with 7 different concentrations of PXDN-con3 (0.14–9.00  $\mu\text{M}$ ). Right: Corresponding plots of analyte concentrations versus steady-state responses and the affinities ( $K_D$ ) determined thereof. All plots are representatives of 3 independent measurements.

precipitation of BME proteins. By contrast, trimeric construct 2 and monomeric construct 4 (Fig. 2A) and monomeric construct 5 (not shown) did not interact with BME under the applied conditions indicating that the LRR domain plays an important role in binding of BME proteins.

Next, we screened the IP mixtures with antibodies raised against laminin resulting in the discovery of laminin as an interacting partner of peroxidasin construct PXDN-con3 (Fig. 2B). Typically, under reducing conditions, the three glycosylated chains of laminin appear as two bands on the gel, one at ~300 kDa corresponding to the  $\beta$ -chain and  $\gamma$ -chain (theoretical protein molar masses of 230 kDa and 220 kDa, respectively) and ~500 kDa indicative of the  $\alpha$ -chain (theoretical protein molar mass ~400 kDa) [24,25]. The band at around 200 kDa may represent a proteolytic fragment of laminin, which is still recognized by the anti-laminin antibody. It should also be noted that the IP mixture containing PXDN-con4 also showed a faint band at ~500 kDa upon staining with the anti-laminin antibody, suggesting a weak interaction of this construct with laminin.

### 3.2. The leucine-rich repeat domain of human peroxidasin 1 promotes binding to laminin

The interaction of PXDN-con3 with murine and human laminin-111 was confirmed and characterised by SPR spectroscopy, with laminin-111 serving as the ligand covalently coupled to the chip. Multi-cycle kinetics (MCK) experiments were performed using increasing concentrations of PXDN-con3. Fig. 3A (left) shows the sensorgram of PXDN-con3 associating with, and dissociating from, murine laminin-111 (muLN111), the best characterised laminin isoform [24,25]. Both the association and the dissociation occur in a multi-phasic manner, most probably as a consequence of the heterogeneous orientation of the amine coupled ligand on the chip surface, and the resulting variations in accessibility of the binding site(s). The double-referenced MCK experiments were analysed by plotting the response values 4 s before the injection stop (i.e. under steady-state conditions) against the respective PXDN-con3 concentration. The entire data set was then fitted to a steady-state affinity model resulting in a dissociation constant ( $K_D$ ) of 1.5  $\mu$ M, confirming that PXDN-con3 interacts specifically with laminin, and quantifying this binding (Fig. 3A, right).

To probe whether laminin binding to PXDN-con3 is species or isoform-dependent, human laminin-111 (huLN111) and human laminin-411 (huLN411) were covalently coupled to the chip surface and titrated

with PXDN-con3 as described above for muLN111. Similar binding curves to those obtained for muLN111, were obtained for huLN111 and huLN411 (Fig. 3B and C, left). Steady-state evaluation of the concentration dependent and saturable response curves (Fig. 3B and C, right) resulted in very similar  $K_D$  values, clearly indicating that the modes of binding of PXDN-con3 to muLN111 and huLN111, as well as isoform huLN411, are almost identical.

Since the immunoblots of the IP mixture containing PXDN-con4 also indicated some weak interaction with laminin, SPR measurements were also performed with PXDN-con4 and PXDN-con5 with muLN111. Fig. 4A depicts the sensorgram of the interaction of PXDN-con4 with muLN111. The shapes of the response curves are similar to PXDN-con3, but the maximum experimental response (~61 RU) was only ~14% of the maximum theoretical calculated response (~446 RU). Nevertheless, steady-state analysis resulted in a similar dissociation constant (2.0  $\mu$ M) as for PXDN-con3 (Fig. 4B). The titration with PXDN-con5 (Fig. 4C and D) gave 60% of the maximum theoretical response, but the  $K_D$  value was ~10 fold higher (i.e.: ~15  $\mu$ M) compared to the PXDN-con3 and PXDN-con4 constructs.

## 4. Discussion

Human peroxidasin 1 is an indispensable player in the basement membrane synthesis [15,16,22]. Loss of integrity of the BM is associated with severe developmental defects and pathologies [2,3]. Assembly of collagen IV generates one of the two major protein networks of BMs. It assembles through oligomerization and non-covalent interactions, and is subsequently stabilized by covalent cross-links including the sulfilimine bonds synthesized by PXDN, and the allysine-derived cross-links generated by lysyl oxidase and lysyl oxidase-like enzymes [26]. However, it unknown how the highly reactive and potentially damaging hypobromous acid [27] released by PXDN is able to generate specific S=N bonds between adjacent collagen IV protomers, without damaging neighbouring sites on collagen IV, or other BM molecules.

Together with thyroid peroxidase (TPO), PXDN catalyses an anabolic reaction. In contrast to (diffusible) lactoperoxidase (LPO), eosinophil peroxidase (EPO) and MPO, that each consist solely of a peroxidase domain, and are involved in non-specific immune defense reactions, TPO is a membrane-anchored peroxidase, and PXDN contains several non-enzymatic domains that might be expected to integrate and regulate the peroxidase activity of peroxidasin 1. Although differing in their structural composition, the main enzymatic reaction of all five

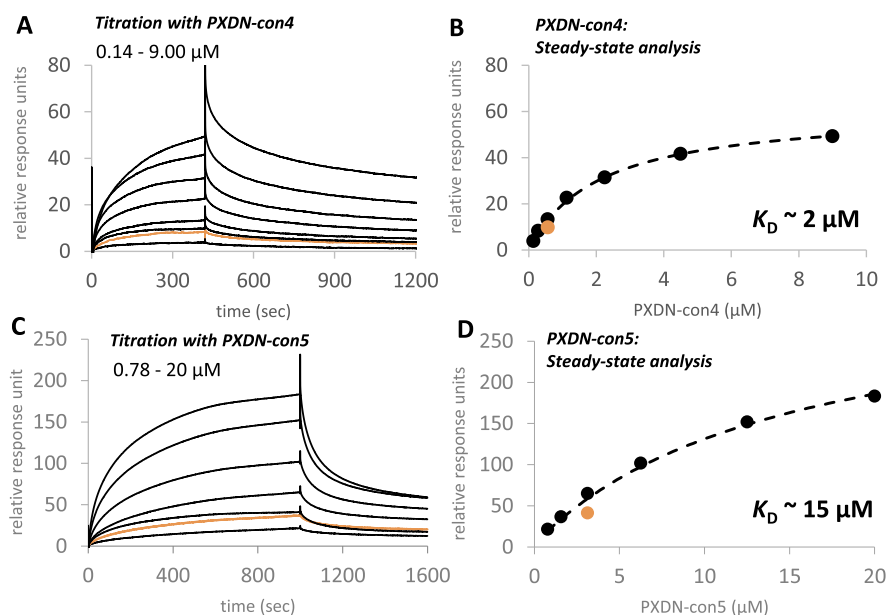


**Fig. 4.** Interaction between murine laminin-111 with human peroxidasin-1 constructs PXDN-con4 and PXDN-con5. Titration of murine laminin-111 (muLN111) with 0.14–9.00  $\mu$ M PXDN-con4 and 0.78–20  $\mu$ M PXDN-con5, respectively. Double-referenced multi-cycle kinetics SPR experiments with PXDN-con4 (A) and PXDN-con5 (C). Corresponding plots of the equilibrium response units versus PXDN-con4 (B) and PXDN-con5 (D) concentrations and the determined  $K_D$  values. The orange curves represent duplicates of 0.5625  $\mu$ M of PXDN-con4, and 3.15  $\mu$ M of PXDN-con5, respectively. (For interpretation of the references to colour in this figure legend, the reader is referred to the Web version of this article.)

human heme peroxidases is two-electron oxidation of halide and pseudohalide (thiocyanate) anions to the corresponding hypohalous acids and hypothiocyanite, which are diffusible antimicrobial oxidants. The capacity of those peroxidases to oxidize different anions depends strongly on the post-translational modifications of the heme and consequent alterations to the redox properties of the heme iron [21,28–32]. Human peroxidase 1 is able to efficiently oxidize bromide to hypobromous acid (HOBr), but not chloride to hypochlorous acid (HOCl) [21]. To date it is unknown as whether, and how, the PXDN-typical domains might restrict its mobility within the ECM, and foster the colocalisation of the peroxidase domain with the NC1 domains of collagen IV to avoid unspecific reactions of HOBr. So far, potential interaction partners of the ECM networks and associated proteins could not be identified.

In the present study, we have produced four different recombinant constructs of PXDN with distinct domain compositions (Fig. 1). One of the constructs, PXDN-con2 is trimeric, since it contains the alpha-helical linker region and redox-sensitive cysteines close to the C-terminus of the peroxidase domain, which are responsible for trimerization [23]. In contrast, PXDN-con3, PXDN-con4 and PXDN-con5 are monomeric proteins [23]. Upon association of these four His-tagged proteins with the anti-His<sub>6</sub> antibody coupled Dynabeads and mixing with BME, only laminin was immunoprecipitated, as demonstrated by SDS-PAGE and immunoblotting using polyclonal antibodies raised against laminin (Fig. 2). This supports and confirms the conclusion that type IV collagen does not form a stable complex with peroxidase 1, as reported recently [33]. These data suggest that interaction of PXDN with collagen IV and its NC1 domains, may be transient in nature or mediated by another ECM protein, such as the laminin isoforms described here.

The LRR domain in PXDN-con3 (Fig. 2B, lane 2) appears to be essential for efficient immunoprecipitation of laminin. Neither trimeric PXDN-con2, nor monomeric PXDN-con4 were able to promote precipitation of ECM proteins. The affinity of PXDN-con3 towards human and mouse laminin-111 (i.e.  $\alpha 1\beta 1\gamma 1$ ) was almost identical, suggesting the presence of conserved binding motif(s). Moreover, laminin-411 ( $\alpha 4\beta 1\gamma 1$ ), which contains a shorter  $\alpha$ -chain due to an N-terminal truncation, also bound to PXDN-con3 with a similar affinity. This suggests that the N-terminal region of the  $\alpha$ -chain of laminin is not essential for binding of PXDN.

To date, there is an absence of high resolution structural data of full length homotrimeric PXDN, or truncated variants. A potential reason for this lack of structural data is the high flexibility of both the monomeric and homotrimeric structures as demonstrated recently by small-angle X-ray scattering (SAXS) [23]. This SAXS data indicates that the POX domain (i.e. PXDN-con5) has an N-terminal flexible propeptide region and a compact globular core catalytic structure, similar to that of proMPO [34]. The monomeric construct PXDN-con4, which includes the four Ig domains located N-terminally of the propeptide region of the POX domain, is highly catalytically active [21,35]. The Ig domains have been shown to support correct folding of the POX domain [18,21] and thus to be essential for efficient sulfilimine bond formation in collagen IV [33]. Both SAXS data and rotary shadowing images suggest significant interaction of the Ig domains with the peroxidase domain and with each other [34]. The homotrimeric construct PXDN-con2 differs from PXDN-con4 at the C-terminus, with PXDN-con2 containing the additional VWC domain. The latter is not involved in trimerization, and is removed before secretion of peroxidase 1 to the ECM [36]. It should be noted that in the expression system used here, this processing step does not, or only partially, occurs [34]. In any case, trimerization is promoted by the amphipathic helix as well as by the conserved cysteines C736 and C1315. SAXS data as well as rotary shadowing, suggest a triangular arrangement of the three compact core peroxidase domains [34]. Moreover, modelling suggests free access for substrates (hydrogen peroxide and bromide) to the respective heme cavities in this trimeric construct [34]. A triangular arrangement of the POX domains is also obvious by inspection of micrograph data of full length trimeric

peroxidase from *Drosophila* [37]. The structures show a relatively compact core similar to the triangular POX domains as seen in the SAXS data [23,34]. The POX domains extend into three flexible arms, which are most likely composed of the LRR and Ig domains [37].

Unfortunately, an in-solution structure of PXDN-con3 is not available so far, nor is anything known about the molecular basis of the affinity of this construct to huLN111, muLN111 or huLN411. However, our SPR data indicate that the POX domain must be involved in binding to laminin. The measured SPR responses and calculated  $K_D$  values of PXDN-con4 and PXDN-con5 can be discussed on the basis of the available structural data of peroxidase variants outlined above. In general, the binding capacity of the SPR chip surface depends on the levels of immobilized laminin. The term maximum response ( $R_{max}$ ) describes the binding capacity of the surface in terms of the response at saturation. A theoretical  $R_{max}$  value can be calculated assuming 1:1 binding and both the immobilized ligand and the analyte (i.e. PXDN constructs) are active and fully accessible:

$$\text{Theoretical } R_{max} = \frac{\text{analyte MW}}{\text{ligand MW}} \times \text{RU}_{\text{immobilized ligand}}$$

The theoretical  $R_{max}$  for binding of PXDN-con3 to muLN111 is ~532 RU, whereas the experimental value was measured as ~524 RU, which is about 99% of the theoretical value. This is consistent with fully active ligand and analyte. Compared to the theoretical  $R_{max}$  of 446 RU of PXDN-con4 binding to muLN111, the experimental  $R_{max}$  is 61 RU, which is only 14% of the theoretical  $R_{max}$ . The POX domain in PXDN-con4 is well folded but highly shielded by the very flexible Ig domains as seen in the SAXS data [23]. As a consequence, there is a steric hindrance for the interaction between muLN111 and the POX domain in PXDN-con4. Keeping in mind the high flexibility of the protein, it can be assumed that at a distinct time point, only in a certain fraction of PXDN-con4 molecules, the arrangement of Ig and POX domains allows binding to laminin. In contrast, in the absence of the Ig domains (i.e. PXDN-con5), the accessibility to the POX domain for laminin is higher (reflected by 60% of the measured response), but the affinity is significantly lower due to partial misfolding of the catalytic domain in the absence of the stabilizing Ig domains. This might also apply to trimeric PXDN-con2, which lacks both Ig and LRR domains and was not able to immunoprecipitate laminin (Fig. 2). As mentioned above, we could not study the interaction between laminin and full length homotrimeric PXDN, which may alter the thermodynamics of binding. Based on the available data, we hypothesize that the presence of the LRR domain in PXDN-con3 impairs intimate interaction between the Ig domains, thereby providing accessibility to the correctly folded catalytic domain, which is supported by the micrograph of full length peroxidase from *Drosophila* described above and in Ref. [37]. Thus, the LRR domain appears to promote high affinity binding of laminin-111 to the POX domain of human peroxidase 1.

Whilst these data provide compelling information on the binding of human peroxidase 1 to laminins, a number of critical questions remain. These include the binding site(s) and chains from the laminin that are involved, and the mode of interaction of the laminin-peroxidase complex with type IV collagen, and specifically the NC1 domains. Furthermore, the source of hydrogen peroxide, which is essential for the catalytic activity of PXDN and bromide oxidation is unclear, with recent studies appearing to eliminate NADPH oxidases as a source [38,39]. Structural studies on potential complexes in-solution and/or by electron microscopy would clearly be beneficial.

## Acknowledgements

This work was supported by the Austrian Science Fund, FWF [Doctoral Program BioToP-Molecular Technology of Proteins (W1224) and project P25538]. Additional financial support from the Novo Nordisk Foundation and Danmarks Frie Forskningsfond (grants NNF13OC0004294 and DFF-7014-00047, respectively, to MJD) is

gratefully acknowledged. The SPR equipment was kindly provided by the EQ-BOKU VIBT GmbH and the BOKU Core Facility Biomolecular & Cellular Analysis.

## References

- [1] S. Colon, P. Page-McCaw, G. Bhave, *Antioxidants Redox Signal.* 27 (2017) 839–854.
- [2] A. Pozzi, P.D. Yurchenco, R.V. Iozzo, *Matrix Biol.* 57–58 (2017) 1–11.
- [3] R. Jayadev, D.R. Sherwood, *Curr. Biol.* 27 (2017) R207–R211.
- [4] E. Hohenester, P.D. Yurchenco, *Cell Adhes. Migrat.* 7 (2013) 56–63.
- [5] M. Durbeej, *Cell Tissue Res.* 339 (2010) 259–268.
- [6] M. Aumailley, L. Bruckner-Tuderman, W.G. Carter, R. Deutzmann, D. Edgar, P. Ekblom, J. Engel, E. Engvall, E. Hohenester, J.C. Jones, H.K. Kleinman, M.P. Marinkovich, G.R. Martin, U. Mayer, G. Meneguzzi, J.H. Miner, K. Miyazaki, M. Patarroyo, M. Paulsson, V. Quaranta, J.R. Sanes, Z. Sasaki, K. Sekiguchi, L.M. Sorokin, J.F. Talts, K. Tryggvason, J. Uitto, I. Virtanen, K. von der Mark, U.M. Wewer, Y. Yamada, P.D. Yurchenco, *Matrix Biol.* 24 (2005) 326–332.
- [7] J.H. Miner, *Microsc. Res. Tech.* 71 (2008) 349–356.
- [8] C.Y. Chuang, G. Degendorfer, M.J. Davies, *Free Radic. Res.* 48 (2014) 970–989.
- [9] G. Degendorfer, C.Y. Chuang, A. Hammer, E. Malle, M.J. Davies, *Free Radic. Biol. Med.* 89 (2015) 721–733.
- [10] G. Degendorfer, C.Y. Chuang, M. Mariotti, A. Hammer, G. Hoefler, P. Hagglund, E. Malle, S.G. Wise, M.J. Davies, *Free Radic. Biol. Med.* 115 (2018) 219–231.
- [11] T. Nybo, S. Dieterich, L.F. Gamon, C.Y. Chuang, A. Hammer, G. Hoefler, E. Malle, A. Rogowska-Wrzesinska, M.J. Davies, *Redox Biol.* 20 (2019) 496–513.
- [12] S. Baldus, J.P. Eiserich, A. Mani, L. Castro, M. Figueroa, P. Chumley, W. Ma, A. Tousson, C.R. White, D.C. Bullard, M.L. Brennan, A.J. Lusis, K.P. Moore, B.A. Freeman, *J. Clin. Invest.* 108 (2001) 1759–1770.
- [13] H. Cai, C.Y. Chuang, C.L. Hawkins, M.J. Davies, *Sci. Rep.* 10 (2020) 666.
- [14] M.D. Rees, J.M. Whitelock, E. Malle, C.Y. Chuang, R.V. Iozzo, A. Nilasaroya, M.J. Davies, *Matrix Biol.* 29 (2012) 63–73.
- [15] G. Bhave, C.F. Cummings, R.M. Vanacore, C. Kumagai-Cresse, I.A. Ero-Tolliver, M. Rafi, J.S. Kang, V. Pedchenko, L.I. Fessler, J.H. Fessler, B.G. Hudson, *Nat. Chem. Biol.* 8 (2012) 784–790.
- [16] A.S. McCall, C.F. Cummings, G. Bhave, R. Vanacore, A. Page-McCaw, B.G. Hudson, *Cell* 157 (2014) 1380–1392.
- [17] M. Soudi, M. Zamocky, C. Jakopitsch, P.G. Furtmüller, C. Obinger, *Chem. Biodivers.* 9 (2012) 1776–1793.
- [18] M. Soudi, M. Paumann-Page, C. Delporte, K.F. Pirker, M. Bellei, E. Edenhofer, G. Stadlmayr, G. Battistuzzi, K.Z. Boudjeltia, P.G. Furtmüller, P. Van Antwerpen, C. Obinger, *J. Biol. Chem.* 290 (2015) 10876–10890.
- [19] M. Zamocky, S. Hofbauer, I. Schaffner, B. Gasselhuber, A. Nicolussi, M. Soudi, K.F. Pirker, P.G. Furtmüller, C. Obinger, *Arch. Biochem. Biophys.* 574 (2015) 108–119.
- [20] M. Zamocky, C. Jakopitsch, P.G. Furtmüller, C. Dunand, C. Obinger, *Proteins* 72 (2008) 589–605.
- [21] M. Paumann-Page, R.S. Katz, M. Bellei, I. Schwartz, E. Edenhofer, B. Sevcnikar, M. Soudi, S. Hofbauer, G. Battistuzzi, P.G. Furtmüller, C. Obinger, *J. Biol. Chem.* 292 (2017) 4583–4592.
- [22] E. Lazar, Z. Peterfi, G. Sirokmany, H.A. Kovacs, E. Klement, K.F. Medzihradszky, M. Geiszt, *Free Radic. Biol. Med.* 83 (2015) 273–282.
- [23] M. Paumann-Page, R. Tscheliessnig, B. Sevcnikar, R.S. Katz, I. Schwartz, S. Hofbauer, V. Pfanzagl, P.G. Furtmüller, C. Obinger, *Biochim. Biophys. Acta* (2019) 140249.
- [24] R. Timpl, H. Rohde, P.G. Robey, S.I. Rennard, J.M. Foidart, G.R. Martin, *J. Biol. Chem.* 254 (1979) 9933–9937.
- [25] T. Sasaki, R. Fassler, E. Hohenester, *J. Cell Biol.* 164 (2004) 959–963.
- [26] C. Añazco, A.J. López-Jiménez, M. Rafi, L. Vega-Montoto, M.-Z. Zhang, B.G. Hudson, R.M. Vanacore, *J. Biol. Chem.* 291 (2016) 25999–26012.
- [27] D.I. Pattison, M.J. Davies, *Biochemistry* 43 (2004) 4799–4809.
- [28] J. Arnhold, P.G. Furtmüller, C. Obinger, *Redox Rep.* 8 (2003) 179–186.
- [29] P.G. Furtmüller, J. Arnhold, W. Jantschko, C. Jakopitsch, C. Obinger, *J. Inorg. Biochem.* 99 (2005) 1220–1229.
- [30] J. Arnhold, E. Monzani, P.G. Furtmüller, L. Casella, M. Zederbauer, C. Obinger, *Eur. J. Inorg. Chem.* 19 (2006) 3801–3811.
- [31] G. Battistuzzi, M. Bellei, P.G. Furtmüller, M. Zederbauer, M. Sola, C. Obinger, *Biochemistry* 45 (2006) 12750–12755.
- [32] G. Battistuzzi, J. Stampfer, M. Bellei, J. Vlasits, M. Soudi, P.G. Furtmüller, C. Obinger, *Biochemistry* 50 (2011) 7987–7994.
- [33] L.A. Ero-Tolliver, B.G. Hudson, G. Bhave, *J. Biol. Chem.* 290 (2015) 21741–21748.
- [34] I. Grishkovskaya, M. Paumann-Page, R. Tscheliessnig, J. Stampfer, S. Hofbauer, M. Soudi, B. Sevcnikar, C. Oostenbrink, P.G. Furtmüller, K. Djinović-Carugo, W.M. Nauseef, C. Obinger, *J. Biol. Chem.* 292 (2017) 8244–8261.
- [35] B. Sevcnikar, M. Paumann-Page, S. Hofbauer, V. Pfanzagl, P.G. Furtmüller, C. Obinger, *Arch. Biochem. Biophys.* 681 (2020) 108267.
- [36] S. Colon, G. Bhave, *J. Biol. Chem.* 291 (2016) 24009–24016.
- [37] R.E. Nelson, L.I. Fessler, Y. Takagi, B. Blumberg, D.R. Keene, P.F. Olson, C.G. Parker, J.H. Fessler, *EMBO J.* 13 (1994) 3438–3447.
- [38] G. Sirokmany, H.A. Kovács, E. Lázár, K. Kónya, A. Donkó, B. Enyedi, H. Grasberger, M. Geiszt, *Redox Biol.* 16 (2018) 314–321.
- [39] G. Sirokmany, M. Geiszt, *Front. Immunol.* 10 (2019) 394.

## 4. Conclusion

While previous studies focused on the biological relevance of peroxidasin in developmental biology and its role in diseases, the main objective of this thesis was (i) to elucidate the reaction mechanism of hsPxd01 with one- and two-electron donors and (ii) to identify potential interaction partners within the extracellular matrix. Since there was contradicting data published over the course of the last years claiming that peroxidasin was able to oxidize chloride, it was of priority to clarify the reaction kinetics of peroxidasin towards halides. Furthermore, it was unclear how peroxidasin interacts with the extracellular matrix to form this specific sulfilimine link at the interfaces of collagen IV molecules.

Consequently, in the beginning of the thesis, we focused on the acquisition of pre-steady-state kinetics of peroxidasin with various substrates. So far only steady-state kinetics and endpoint measurements were available (38, 41, 60) that suggested bromide as the primary substrate of hsPxd01 while other studies reported the generation of hypochlorous acid (109, 121) by peroxidasin.

As the production of full length peroxidasin in mammalian cell factories (CHO and HEK) led to recombinant protein of low yield and activity, we had to focus on the production of truncated variants that were lacking specific domains. This approach was further supported by publications, which suggested that the smallest functional unit of peroxidasin were four Ig domains combined with the peroxidase domain and that the VWC domain is cleaved off by a proprotein convertase (58, 81). By utilizing a transient transfection system in HEK cells, we managed to produce a highly active truncated peroxidasin construct (hsPxd01-con4) with which we were able to perform pre-steady state kinetic studies on peroxidasin 1 in this thesis. We showed that truncated peroxidasin has similar spectral features compared to LPO and EPO. Furthermore, cyanide is binding in a similar rate to the heme cofactor of peroxidasin compared to LPO and EPO, which indicates a comparable heme cavity architecture.

The apparent second-order rate constant ( $k_{app}$ ) for the initial oxidation of ferric peroxidasin to Compound I by hydrogen peroxide ( $1.8 \times 10^7 \text{ M}^{-1} \text{ s}^{-1}$ ) was very similar to the reported  $k_{app}$  values of other mammalian heme peroxidases ( $(1.1 - 5.6) \times 10^7 \text{ M}^{-1} \text{ s}^{-1}$ ). Compound I, which can be fully established with equimolar hydrogen peroxide concentrations, has been shown to slowly convert to Compound I\* in the absence of electron donors. This side reaction is responsible for apparent inactivation of halogenation activity of human peroxidases and hsPxd01-con4. In the presence of halides and pseudohalides, Compound I is quickly converted into the ferric resting state. While iodide, bromide and thiocyanate were proven to be good substrates for hsPxd01, chloride failed to react with Compound I and could not restore the ferric resting state. This observation was supported by the electrochemical potential  $E^\circ$  [Fe(III)Fe(II)] couple of peroxidasin that is much less positive compared to MPO, which has an additional heme-protein

sulfonium link and is the only known human enzyme to oxidize chloride (122). However, although peroxidasin has less potent electrochemical properties, it outperforms MPO in the oxidation of bromide, which indicates that not only thermodynamics but also structural features like accessibility to the heme pocket influence the kinetics of substrate oxidation. The rate constants for thiocyanate ( $1.8 \times 10^7 \text{ M}^{-1} \text{ s}^{-1}$ ) and iodide ( $1.7 \times 10^7 \text{ M}^{-1} \text{ s}^{-1}$ ) additionally explain why both substrates showed inhibitory effects in sulfilimine link formation *in vitro*, as they compete with bromide, which is approximately three times slower ( $5.6 \times 10^6 \text{ M}^{-1} \text{ s}^{-1}$ ). While blood plasma concentrations of iodide are below the micromolar range and will therefore not compete with bromide (10-100  $\mu\text{M}$ ) *in vivo*, thiocyanate might interfere with sulfilimine link formation as its plasma concentration ranges from 20-100  $\mu\text{M}$  and can be significantly elevated in smokers. Smoking is further associated with hypervascularization and fragmentation of pulmonary basement membranes (123, 124).

Subsequently, we were probing the reactivity of peroxidasin towards one-electron donors, which follow the peroxidase cycle (Reactions 5, 7 and 8). As previously mentioned, Compound I serves as a common base for either the halogenation cycle or the peroxidase cycle. Whether peroxidasin reacts with halides or one-electron substrates depends on the concentration and the second-order rate constant of the respective substrate to either Compound II or the ferric resting state. One-electron donors therefore have the ability to redirect peroxidasin from the halogenation cycle into Compound II of the peroxidase cycle (Reaction 7) and thus influence the bromination activity and subsequently sulfilimine link formation. In a recent study it was shown that alternative substrates like urate can partially inhibit sulfilimine crosslink formation (125). Using pre-steady-state kinetic analysis, we determined rate constants for reduction of Compound I and Compound II of hsPxd01 with various one-electron donors. The hierarchy of the respective apparent second-order rate constants was serotonin > nitrite > ascorbate > tyrosine > urate. As the reduction of Compound II is the rate limiting step in this reaction cycle, serotonin and nitrite can be seen as mediocre substrates, while tyrosine and urate can be considered as poor substrates at pH 7.4. As urate is a known physiological substrate for MPO and LPO (9, 126) and its plasma concentration is rather high with 200 to 500  $\mu\text{M}$  (127) we further tested its impact on bromination activity of peroxidasin. Although urate is approx. 200 times less potent to reduce Compound I compared to bromide at pH 7.4, its higher concentration and low reactivity with Compound II leads to accumulation of Compound II. It therefore reversibly inhibits bromination activity of peroxidasin, as less Compound I is available for the halogenation cycle. This effect was described for MPO in previous study (9) and could be confirmed by this study. Our observed  $\text{IC}_{50}$  value for inhibition of bromination activity of peroxidasin by urate of  $24 \pm 5 \mu\text{M}$  fits well with the data observed for partial inhibition of induced crosslink formation in extracellular matrix *in vitro* with an  $\text{IC}_{50}$  value of 20  $\mu\text{M}$ . Further studies are necessary to investigate if pathophysiological concentrations of urate indeed have a

negative impact on the mechanical stability of extracellular matrices. Nitrite on the other hand, promoted the bromination activity of peroxidase while inhibiting MPO. *In vivo*, nitrite is derived from nitrogen monoxide, which is produced by nitric oxide synthetases during inflammatory processes from the immune system. Excessive production of reactive nitric species, however, can damage host tissues and is associated with atherosclerosis and other inflammatory diseases (128, 129). Under these pathological conditions, the concentration of nitrite can exceed the concentration of bromide and thus efficiently reacts with Compound I of peroxidase to produce NO<sub>2</sub> radicals, as it was observed for MPO (10, 130). These NO<sub>2</sub> radicals subsequently induce the formation of nitro-tyrosines (131). Interestingly, Compound II of peroxidase is seven times more potent to oxidize nitrite when compared to MPO and thus makes it a potential source of reactive nitrogen species and oxidative damage in the extracellular matrix.

As it is unclear, if and how peroxidase is co-localized with the NC1 domains of collagen IV to form the sulfilimine link, it was a clear goal of this thesis to find potential interacting partners. We therefore produced additional truncated constructs (hsPxd01-con2, hsPxd01-con3, hsPxd01-con4 and hsPxd01-con5) with varying domain combinations and probed basement membrane extracts using immunoprecipitation. We were able to identify laminin, a major protein of basement membranes, as a potential interacting partner for peroxidase and collagen IV. It was recently reported that NC1 domains of collagen co-localize with laminin at the epithelial layer, which establishes a further link between the laminin, collagen and peroxidase triangle (132). Ero-Tolliver et al. additionally suggested that peroxidase interacts with the NC1 domain of collagen IV in either a transient way or forming a ternary complex with other basement membrane proteins such as laminin (81). The LRR domain of peroxidase (hsPxd01-con3) appeared to be essential for successfully immunoprecipitating laminin from the extract, as constructs lacking the LRRs failed to precipitate ECM proteins. Further analysis with SPR revealed that the affinity between hsPxd01-con3 and murine laminin was almost identical to human laminin, which indicates conserved binding motifs. Furthermore, it appears that the N-terminus of the laminin  $\alpha$ -chain is not essential for binding, as laminin-411 binds with the same affinity to hsPxd01-con3. Other constructs lacking the LRR domain were also able to bind to laminin but with either a ten-fold increased  $K_d$  value or with only 15% of binding response which further indicates the necessity of LRR for proper binding between laminin and peroxidase.

In summary, this work aimed for a better understanding of biochemical properties of peroxidase and the identification of potential binding partners. By analyzing pre-steady-state kinetics of peroxidase and two-electron donors, we were able to show that peroxidase is following the halogenation cycle of other mammalian peroxidases. While it is not able to oxidize chloride, it can act as a source of HOBr, HOSCN and HOI. Additionally, peroxidase is able to

follow the peroxidase cycle by utilizing one-electron donors that are able to modulate halogenation activity. We showed that urate is negatively impacting the bromination activity of peroxidase while nitrite is able to enhance it. Furthermore, we could identify laminin, as a binding partner for peroxidase and determine the dissociation constant of 1  $\mu\text{M}$ . The LRR domain seems to play an important role in the mode of binding between laminin and peroxidase. Although many questions were answered in the course of this thesis, even more questions arose that will need further investigation.

## 5. References

1. Zámocký, M., Hofbauer, S., Schaffner, I., Gasselhuber, B., Nicolussi, A., Souidi, M., Pirker, K. F., Furtmüller, P. G., and Obinger, C. (2015) Independent evolution of four heme peroxidase superfamilies. *Arch. Biochem. Biophys.* **574**, 108–119
2. Zamocky, M., Jakopitsch, C., Furtmüller, P. G., Dunand, C., and Obinger, C. (2008) The peroxidase-cyclooxygenase superfamily: Reconstructed evolution of critical enzymes of the innate immune system. *Proteins Struct. Funct. Genet.* **72**, 589–605
3. Derat, E., Terner, J., Shaik, S., and Schlichting, I. (2007) Structure and quantum chemical characterization of chloroperoxidase compound 0 , a common reaction intermediate of diverse heme enzymes. **104**, 99–104
4. Poulos, T. L., and Kraut, J. (1980) The Stereochemistry of Peroxidase Catalysis \*
5. Furtmüller, P. G., Zederbauer, M., Jantschko, W., Helm, J., Bogner, M., Jakopitsch, C., and Obinger, C. (2006) Active site structure and catalytic mechanisms of human peroxidases. *Arch. Biochem. Biophys.* **445**, 199–213
6. Rodri, J. N., Lowe, D. J., Herna, J., Hiner, A. N. P., and Garci, F. (2001) Mechanism of Reaction of Hydrogen Peroxide with Horseradish Peroxidase: Identification of Intermediates in the Catalytic Cycle
7. Wirstam, M., Blomberg, M. R. A., and Siegbahn, P. E. M. (1999) Reaction Mechanism of Compound I Formation in Heme Peroxidases : A Density Functional Theory Study. 10.1021/ja991997c
8. Gunther, M. R. (2004) Probing the free radicals formed in the metmyoglobin–hydrogen peroxide reaction. *Free Radic. Biol. Med.* **36**, 1345–1354
9. Meotti, F. C., Jameson, G. N. L., Turner, R., Harwood, D. T., Stockwell, S., Rees, M. D., Thomas, S. R., and Kettle, A. J. (2011) Urate as a physiological substrate for myeloperoxidase: Implications for hyperuricemia and inflammation. *J. Biol. Chem.* **286**, 12901–12911
10. Arnhold, J., Monzani, E., Furtmüller, P. G., Zederbauer, M., Casella, L., and Obinger, C. (2006) Kinetics and thermodynamics of halide and nitrite oxidation by mammalian heme peroxidases. *Eur. J. Inorg. Chem.* 10.1002/ejic.200600436
11. Hsuanyu, Y., and Dunford, H. B. (1999) Oxidation of clozapine and ascorbate by myeloperoxidase. *Arch. Biochem. Biophys.* **368**, 413–420
12. Dunford, H. B., and Hsuanyu, Y. (1999) Kinetics of oxidation of serotonin by myeloperoxidase compounds I and II. *Biochem. Cell Biol.* **77**, 449–457

13. Furtmüller, P. G., Jantschko, W., Regelsberger, G., Jakopitsch, C., Arnhold, J., and Obinger, C. (2002) Reaction of lactoperoxidase compound I with halides and thiocyanate. *Biochemistry*. **41**, 11895–11900
14. Furtmuller, P. G., Burner, U., and Obinger, C. (1998) Reaction of myeloperoxidase compound I with chloride, bromide, iodide, and thiocyanate. *Biochemistry*. **37**, 17923–17930
15. Nicolussi, A., Auer, M., Sevcnikar, B., Paumann-Page, M., Pfanzagl, V., Zámocký, M., Hofbauer, S., Furtmüller, P. G., and Obinger, C. (2018) Posttranslational modification of heme in peroxidases – Impact on structure and catalysis. *Arch. Biochem. Biophys.* **643**, 14–23
16. Ueda, T., Sakamaki, K., Kuroki, T., Yano, I., and Nagata, S. (1997) Molecular cloning and characterization of the chromosomal gene for human lactoperoxidase. *Eur. J. Biochem.* **243**, 32–41
17. Meeusen, E. N. T., and Balic, A. (2000) Do eosinophils have a role in the killing of helminth parasites? *Parasitol. Today*. **16**, 95–101
18. Wang, J., and Slungaard, A. (2006) Role of eosinophil peroxidase in host defense and disease pathology. *Arch. Biochem. Biophys.* **445**, 256–260
19. Hampton, M. B., Kettle, A. J., and Winterbourn, C. C. (1998) Inside the neutrophil phagosome: Oxidants, myeloperoxidase, and bacterial killing. *Blood*. **92**, 3007–3017
20. Thomas, E. L., Milligan, T. W., Joyner, R. E., and Jefferson, M. M. (1994) Antibacterial activity of hydrogen peroxide and the lactoperoxidase- hydrogen peroxide-thiocyanate system against oral streptococci. *Infect. Immun.* **62**, 529–535
21. Malik, A., and Batra, J. K. (2012) Antimicrobial activity of human eosinophil granule proteins: Involvement in host defence against pathogens. *Crit. Rev. Microbiol.* **38**, 168–181
22. Klebanoff, S. J. (2005) Myeloperoxidase: Friend and foe. *J. Leukoc. Biol.* **77**, 598–625
23. Davies, M. J., Hawkins, C. L., Pattison, D. I., and Rees, M. D. (2008) Mammalian heme peroxidases: from molecular mechanisms to health implications. *Antioxid. Redox Signal.* **10**, 1199–234
24. Ihalin, R., Loimaranta, V., and Tenovuo, J. (2006) Origin, structure, and biological activities of peroxidases in human saliva. *Arch. Biochem. Biophys.* **445**, 261–268
25. Kimura, S., Kotani, T., McBride, O. W., Umeki, K., Hirai, K., Nakayama, T., and Ohtaki, S. (1987) Human thyroid peroxidase: Complete cDNA and protein sequence,

- chromosome mapping, and identification of two alternately spliced mRNAs. *Proc. Natl. Acad. Sci. U. S. A.* **84**, 5555–5559
26. Carvalho, D. P., and Dupuy, C. (2017) Thyroid hormone biosynthesis and release. *Mol. Cell. Endocrinol.* **458**, 6–15
  27. Dunn, J. T., and Dunn, A. D. (1999) The importance of thyroglobulin structure for thyroid hormone biosynthesis. *Biochimie.* **81**, 505–509
  28. Dunn, J. T., and Dunn, A. D. (2001) Update on intrathyroidal iodine metabolism. *Thyroid.* **11**, 407–414
  29. Kessler, J., Obinger, C., and Eales, G. (2008) Factors influencing the study of peroxidase-generated iodine species and implications for thyroglobulin synthesis. *Thyroid.* **18**, 769–774
  30. TAUROG, A. (1970) Thyroid Peroxidase and Thyroxine Biosynthesis. in *Recent Progress in Hormone Research* (ASTWOOD, E. B. B. T.-P. of the 1969 L. H. C. ed), pp. 189–247, Academic Press, Boston, **26**, 189–247
  31. AGNER, K. (1941) Verdoperoxidase : a ferment isolated from leucocytes. *Acta Physiol. Scand.* **2**, 1–64
  32. Hosoya, T., and Morrison, M. (1967) The Isolation and Purification of Thyroid Peroxidase. *J. Biol. Chem.* **242**, 2828–2836
  33. Taurog, A. (1970) Thyroid peroxidase-catalyzed iodination of thyroglobulin; inhibition by excess iodide. *Arch. Biochem. Biophys.* **139**, 212–220
  34. Nauseef, W. M. (2014) Myeloperoxidase in human neutrophil host defence. *Cell. Microbiol.* **16**, 1146–1155
  35. Archer, G. T., Air, G., Jackas, M., and Morell, D. B. (1965) Studies on rat eosinophil peroxidase. *Biochim. Biophys. Acta - Enzymol. Biol. Oxid.* **99**, 96–101
  36. ARCHER, G. T. (1962) Release of Peroxidase from Eosinophil Granules in vitro. *Nature.* **194**, 973–974
  37. Nelson, R. E., Fessler, L. I., Takagi, Y., Blumberg, B., Keene, D. R., Olson, P. F., Parker, C. G., and Fessler, J. H. (1994) Peroxidasin: a novel enzyme-matrix protein of *Drosophila* development. *EMBO J.* **13**, 3438–3447
  38. Bhave, G., Cummings, C. F., Vanacore, R. M., Kumagai-Cresse, C., Ero-Tolliver, I. a, Rafi, M., Kang, J.-S., Pedchenko, V., Fessler, L. I., Fessler, J. H., and Hudson, B. G. (2012) Peroxidasin forms sulfilimine chemical bonds using hypohalous acids in tissue genesis. *Nat. Chem. Biol.* **8**, 784–790

39. Soudi, M., Zamocky, M., Jakopitsch, C., and Obinger, C. (2012) Molecular Evolution, Structure, and Function of Peroxidasins. *Chem. Biodivers.* **9**, 1776–1793
40. Péterfi, Z., Tóth, Z. E., Kovács, H. A., Lázár, E., Sum, A., Donkó, Á., Sirokmány, G., Shah, A. M., and Geiszt, M. (2014) Peroxidasin-like protein: a novel peroxidase homologue in the human heart. *Cardiovasc. Res.* **101**, 393–399
41. Soudi, M., Paumann-Page, M., Delporte, C., Pirker, K. F., Bellei, M., Edenhofer, E., Stadlmayr, G., Battistuzzi, G., Boudjeltia, K. Z., Furtmüller, P. G., Van Antwerpen, P., and Obinger, C. (2015) Multidomain Human Peroxidasin 1 Is a Highly Glycosylated and Stable Homotrimeric High Spin Ferric Peroxidase. *J. Biol. Chem.* **290**, 10876–10890
42. Lázár, E. E., Péterfi, Z., Sirokmány, G., Kovács, H. A., Klement, E., Medzihradszky, K. F., and Geiszt, M. (2015) Structure–function analysis of peroxidasin provides insight into the mechanism of collagen IV crosslinking. *Free Radic. Biol. Med.* **83**, 273–282
43. Bella, J., Hindle, K. L., Mcewan, P. A., and Lovell, S. C. (2008) Review The leucine-rich repeat structure. **65**, 2307–2333
44. Kobe, B., and Kajava, A. V (2001) The leucine-rich repeat as a protein recognition motif. *Curr. Opin. Struct. Biol.* **11**, 725–732
45. Biologie, M., Ura, C., Marie-curie, U. P., and Jussieu, P. (1998) The Immunoglobulin Superfamily: An Insight on Its Tissular , Species , and Functional Diversity. <https://doi.org/10.1007/PL00006318>
46. Barclay, A. N. (2003) Membrane proteins with immunoglobulin-like domains — a master superfamily of interaction molecules. **15**, 215–223
47. Smith, D. K., and Xue, H. (1997) Sequence Profiles of Immunoglobulin and Immunoglobulin-like Domains
48. Fiedler, T. J., Davey, C. A., and Fenna, R. E. (2000) X-ray crystal structure and characterization of halide-binding sites of human myeloperoxidase at 1.8 Å resolution. *J. Biol. Chem.* **275**, 11964–11971
49. Singh, A. K., Singh, N., Sharma, S., Singh, S. B., Kaur, P., Bhushan, A., Srinivasan, A., and Singh, T. P. (2008) Crystal Structure of Lactoperoxidase at 2.4 Å Resolution. *J. Mol. Biol.* **376**, 1060–1075
50. Capena, X., Vidossich, P., Schrottner, K., Calisto, B. M., Banerjee, S., Stampler, J., Soudi, M., Furtmüller, P. G., Rovira, C., Fita, I., and Obinger, C. (2009) Essential role of proximal histidine-asparagine interaction in mammalian peroxidases. *J. Biol. Chem.* **284**, 25929–25937

51. Stampler, J., Bellei, M., Soudi, M., Gruber, C., Battistuzzi, G., Furtmüller, P. G., and Obinger, C. (2011) Manipulating the proximal triad His-Asn-Arg in human myeloperoxidase. *Arch. Biochem. Biophys.* **516**, 21–28
52. Li, Y., Jiao, Y., Luo, Z., Li, Y., and Liu, Y. (2019) High peroxidase-like expression is a potential and independent prognostic biomarker in breast cancer. *Medicine (Baltimore)*. **98**, e17703
53. Gu, S., Bakthavachalu, B., Han, J., Patil, D. P., Otsuka, Y., Guda, C., and Schoenberg, D. R. (2012) Identification of the human PMR1 mRNA endonuclease as an alternatively processed product of the gene for peroxidase-like protein. 10.1261/rna.031369.111.5
54. Zhang, J. L., Huang, Y., Qiu, L. Y., Nickel, J., and Sebald, W. (2007) Von Willebrand factor type C domain-containing proteins regulate bone morphogenetic protein signaling through different recognition mechanisms. *J. Biol. Chem.* **282**, 20002–20014
55. O’Leary, J. M., Hamilton, J. U., Deane, C. M., Valeyev, N. V., Sandell, L. J., and Downing, A. K. (2004) Solution structure and dynamics of a prototypical chordin-like cysteine-rich repeat (von Willebrand factor type C module) from collagen IIA. *J. Biol. Chem.* **279**, 53857–53866
56. Holbourn, K. P., Acharya, K. R., and Perbal, B. (2008) The CCN family of proteins: structure-function relationships. *Trends Biochem. Sci.* **33**, 461–473
57. Holbourn, K. P., Perbal, B., and Ravi Acharya, K. (2009) Proteins on the catwalk: Modelling the structural domains of the CCN family of proteins. *J. Cell Commun. Signal.* **3**, 25–41
58. Colon, S., and Bhave, G. (2016) Proprotein convertase processing enhances peroxidase activity to reinforce collagen IV. *J. Biol. Chem.* **291**, 24009–24016
59. Paumann-Page, M., Tscheliessnig, R., Sevcnikar, B., Katz, R. S., Schwartz, I., Hofbauer, S., Pfanzagl, V., Furtmüller, P. G., and Obinger, C. (2020) Monomeric and homotrimeric solution structures of truncated human peroxidase 1 variants. *Biochim. Biophys. Acta - Proteins Proteomics.* **1868**, 140249
60. McCall, a S., Cummings, C. F., Bhave, G., Vanacore, R., Page-McCaw, A., and Hudson, B. G. (2014) Bromine is an essential trace element for assembly of collagen IV scaffolds in tissue development and architecture. *Cell.* **157**, 1380–92
61. Pozzi, A., Yurchenco, P. D., and Iozzo, R. V. (2017) The nature and biology of basement membranes. *Matrix Biol.* **57–58**, 1–11
62. Mayorca-Guiliani, A. E., Madsen, C. D., Cox, T. R., Horton, E. R., Venning, F. A., and Erler, J. T. (2017) ISDoT: In situ decellularization of tissues for high-resolution imaging

- and proteomic analysis of native extracellular matrix. *Nat. Med.* **23**, 890–898
63. Randles, M. J., Humphries, M. J., and Lennon, R. (2017) Proteomic definitions of basement membrane composition in health and disease. *Matrix Biol.* **57–58**, 12–28
  64. Liotta, L. A., Tryggvason, K., Garbisa, S., Hart, I., Foltz, C. M., and Shafie, S. (1980) Metastatic potential correlates with enzymatic degradation of basement membrane collagen. *Nature.* **284**, 67–68
  65. Hynes, R. O. (2009) The Extracellular Matrix: Not Just Pretty Fibrils. *Science (80- ).* **326**, 1216–1219
  66. Brown, K. L., Cummings, C. F., Vanacore, R. M., and Hudson, B. G. (2017) Building collagen IV smart scaffolds on the outside of cells. *Protein Sci.* **26**, 2151–2161
  67. Hohenester, E., and Yurchenco, P. D. (2013) Laminins in basement membrane assembly. *Cell Adhes. Migr.* **7**, 56–63
  68. Bhave, G., Colon, S., and Ferrell, N. (2017) The sulfilimine cross-link of collagen IV contributes to kidney tubular basement membrane stiffness. *Am. J. Physiol. - Ren. Physiol.* **313**, F596–F602
  69. Pöschl, E., Schlötzer-Schrehardt, U., Brachvogel, B., Saito, K., Ninomiya, Y., and Mayer, U. (2004) Collagen IV is essential for basement membrane stability but dispensable for initiation of its assembly during early development. *Development.* **131**, 1619–1628
  70. Lullo, G. A. Di, Sweeney, S. M., Ko, J., Ala-kokko, L., and Antonio, J. D. S. (2002) Mapping the Ligand-binding Sites and Disease-associated Mutations on the Most Abundant Protein in the Human , Type I Collagen \*. **277**, 4223–4231
  71. Ricard-Blum, S., and Ruggiero, F. (2005) The collagen superfamily: from the extracellular matrix to the cell membrane. *Pathol. Biol.* **53**, 430–442
  72. Khoshnoodi, J., Pedchenko, V., and Hudson, B. G. (2008) Mammalian collagen IV. *Microsc. Res. Tech.* **71**, 357–70
  73. Wu, Y., and Ge, G. (2019) Complexity of type IV collagens: From network assembly to function. *Biol. Chem.* **400**, 565–574
  74. Boutaud, A., Borza, D.-B., Bondar, O., Gunwar, S., Netzer, K.-O., Singh, N., Ninomiya, Y., Sado, Y., Noelken, M. E., and Hudson, B. G. (2000) Type IV collagen of the glomerular basement membrane: Evidence that the chain specificity of network assembly is encoded by the noncollagenous NC1 domains. *J. Biol. Chem.* **275**, 30716–30724

75. Fidler, A. L., Vanacore, R. M., Chetyrkin, S. V., Pedchenko, V. K., Bhave, G., Yin, V. P., Stothers, C. L., Rose, K. L., McDonald, W. H., Clark, T. A., Borza, D.-B., Steele, R. E., Ivy, M. T., Hudson, J. K., and Hudson, B. G. (2014) A unique covalent bond in basement membrane is a primordial innovation for tissue evolution. *Proc. Natl. Acad. Sci.* **111**, 331–336
76. Gotenstein, J. R., Swale, R. E., Fukuda, T., Wu, Z., Giurumescu, C. A., Goncharov, A., Jin, Y., and Chisholm, A. D. (2010) The *C. elegans* peroxidase PXN-2 is essential for embryonic morphogenesis and inhibits adult axon regeneration. *Development.* **137**, 3603–3613
77. Añazco, C., López-Jiménez, A. J., Rafi, M., Vega-Montoto, L., Zhang, M.-Z., Hudson, B. G., and Vanacore, R. M. (2016) Lysyl Oxidase-like-2 Cross-links Collagen IV of Glomerular Basement Membrane. *J. Biol. Chem.* **291**, 25999–26012
78. Borza, D. B., Bondar, O., Ninomiya, Y., Sado, Y., Naito, I., Todd, P., and Hudson, B. G. (2001) The NC1 Domain of Collagen IV Encodes a Novel Network Composed of the  $\alpha 1$ ,  $\alpha 2$ ,  $\alpha 5$ , and  $\alpha 6$  Chains in Smooth Muscle Basement Membranes. *J. Biol. Chem.* **276**, 28532–28540
79. Vanacore, R., Ham, A.-J. L., Voehler, M., Sanders, C. R., Conrads, T. P., Veenstra, T. D., Sharpless, K. B., Dawson, P. E., and Hudson, B. G. (2009) A Sulfilimine Bond Identified in Collagen IV. *Science (80- )*. **325**, 1230 LP – 1234
80. Robertson, W. E., Rose, K. L., Hudson, B. G., and Vanacore, R. M. (2014) Supramolecular Organization of the  $\alpha 121$ - $\alpha 565$  Collagen IV Network. *J. Biol. Chem.* **289**, 25601–25610
81. Ero-Tolliver, I. A., Hudson, B. G., and Bhave, G. (2015) The Ancient Immunoglobulin Domains of Peroxidase Are Required to Form Sulfilimine Cross-links in Collagen IV. *J. Biol. Chem.* **290**, 21741–21748
82. He, C., Song, W., Weston, T. A., Tran, C., Kurtz, I., Zuckerman, J. E., Guagliardo, P., Miner, J. H., Ivanov, S. V., Bougoure, J., Hudson, B. G., Colon, S., Voziyan, P. A., Bhave, G., Fong, L. G., Young, S. G., and Jiang, H. (2020) Peroxidase-mediated bromine enrichment of basement membranes. *Proc. Natl. Acad. Sci. U. S. A.* **117**, 15827–15836
83. Aumailley, M. (2013) The laminin family. *Cell Adhes. Migr.* **7**, 48–55
84. Aumailley, M., Bruckner-tuderman, L., Carter, W. G., Deutzmann, R., Edgar, D., Ekblom, P., Engvall, E., Hohenester, E., Jones, J. C. R., Kleinman, H. K., Marinkovich, M. P., Martin, G. R., Mayer, U., Meneguzzi, G., Miner, J. H., Miyazaki, K., Patarroyo, M.,

- Paulsson, M., Quaranta, V., Sanes, J. R., Sasaki, T., Sekiguchi, K., Sorokin, L. M., Talts, J. F., Tryggvason, K., Uitto, J., Virtanen, I., Mark, K. Von Der, Wewer, U. M., Yamada, Y., and Yurchenco, P. D. (2005) A simplified laminin nomenclature. *Matrix Biol.* **24**, 326–332
85. Durbeej, M. (2009) Laminins. *Cell Tissue Res.* **339**, 259
86. Gupta, M. C., Graham, P. L., and Kramer, J. M. (1997) Characterization of alpha1(IV) collagen mutations in *Caenorhabditis elegans* and the effects of alpha1 and alpha2(IV) mutations on type IV collagen distribution. *J. Cell Biol.* **137**, 1185–1196
87. Ma, C. P., Guo, Z. M., Zhang, F. L., and Su, J. Y. (2020) Molecular identification, expression and function analysis of peroxidasin in *Chilo suppressalis*. *Insect Sci.* 10.1111/1744-7917.12743
88. Tindall, A. J., Pownall, M. E., Morris, I. D., and Isaacs, H. V (2005) *Xenopus tropicalis* peroxidasin Gene Is Expressed Within the Developing Neural Tube and Pronephric Kidney. 10.1002/dvdy.20226
89. Khan, K., Rudkin, A., Parry, D. A., Burdon, K. P., McKibbin, M., Logan, C. V., Abdelhamed, Z. I. A., Muecke, J. S., Fernandez-Fuentes, N., Laurie, K. J., Shires, M., Fogarty, R., Carr, I. M., Poulter, J. A., Morgan, J. E., Mohamed, M. D., Jafri, H., Raashid, Y., Meng, N., Piseth, H., Toomes, C., Casson, R. J., Taylor, G. R., Hammerton, M., Sheridan, E., Johnson, C. A., Inglehearn, C. F., Craig, J. E., and Ali, M. (2011) Homozygous mutations in PDXN cause congenital cataract, corneal opacity, and developmental glaucoma. *Am. J. Hum. Genet.* **89**, 464–473
90. Yan, X., Sabrautzki, S., Horsch, M., Fuchs, H., Gailus-Durner, V., Beckers, J., de Angelis, M. H., and Graw, J. (2014) Peroxidasin is essential for eye development in the mouse. *Hum. Mol. Genet.* **23**, 5597–5614
91. Péterfi, Z., Donkó, A., Orient, A., Sum, A., Prókai, A., Molnár, B., Veréb, Z., Rajnavölgyi, E., Kovács, K. J., Müller, V., Szabó, A. J., and Geiszt, M. (2009) Peroxidasin is secreted and incorporated into the extracellular matrix of myofibroblasts and fibrotic kidney. *Am. J. Pathol.* **175**, 725–35
92. Colon, S., Luan, H., Liu, Y., Meyer, C., Gewin, L., and Bhave, G. (2019) Peroxidasin and eosinophil peroxidase, but not myeloperoxidase, contribute to renal fibrosis in the murine unilateral ureteral obstruction model. *Am. J. Physiol. Physiol.* **316**, F360–F371
93. Horikoshi, N., Cong, J., Kley, N., and Shenk, T. (1999) Isolation of Differentially Expressed cDNAs from p53- Dependent Apoptotic Cells: Activation of the Human Homologue of the *Drosophila* Peroxidasin Gene. *Biochem. Biophys. Res. Commun.*

94. Mitchell, M. S., Kan-mitchell, J., Mineev, B., Edman, C., and Deans, R. J. (2000) A Novel Melanoma Gene ( MG50 ) Encoding the Interleukin 1 Receptor Antagonist and Six Epitopes Recognized by Human Cytolytic T Lymphocytes 1. <https://doi.org/10.1006/bbrc.1999.1123>
95. Choi, A., Lao, R., Ling-Fung Tang, P., Wan, E., Mayer, W., Bardakjian, T., Shaw, G. M., Kwok, P. Y., Schneider, A., and Slavotinek, A. (2015) Novel mutations in PXDN cause microphthalmia and anterior segment dysgenesis. *Eur. J. Hum. Genet.* **23**, 337–341
96. Zheng, Y. Z., and Liang, L. (2018) High expression of PXDN is associated with poor prognosis and promotes proliferation, invasion as well as migration in ovarian cancer. *Ann. Diagn. Pathol.* **34**, 161–165
97. Di, Y., Chen, D., Yu, W., and Yan, L. (2019) Bladder cancer stage-associated hub genes revealed by WGCNA co-expression network analysis. *Hereditas.* **156**, 7
98. Cai, X., Yang, X., Jin, C., Li, L., Cui, Q., Guo, Y., Dong, Y., Yang, X., Guo, L., and Zhang, M. (2018) Identification and verification of differentially expressed microRNAs and their target genes for the diagnosis of esophageal cancer. *Oncol. Lett.* **16**, 3642–3650
99. Dougan, J., Hawsawi, O., Burton, L. J., Edwards, G., Jones, K., Zou, J., Nagappan, P., Wang, G., Zhang, Q., Danaher, A., Bowen, N., Hinton, C., and Odero-Marah, V. A. (2019) Proteomics-metabolomics combined approach identifies peroxidasin as a protector against metabolic and oxidative stress in prostate cancer. *Int. J. Mol. Sci.* [10.3390/ijms20123046](https://doi.org/10.3390/ijms20123046)
100. Jayachandran, A., Prithviraj, P., Lo, P. H., Walkiewicz, M., Anaka, M., Woods, B. L., Tan, B. S., Behren, A., Cebon, J., and McKeown, S. J. (2016) Identifying and targeting determinants of melanoma cellular invasion. *Oncotarget.* **7**, 41186–41202
101. Liu, Y., Carson-Walter, E. B., Cooper, A., Winans, B. N., Johnson, M. D., and Walter, K. a (2010) Vascular gene expression patterns are conserved in primary and metastatic brain tumors. *J. Neurooncol.* **99**, 13–24
102. Castronovo, V., Waltregny, D., Kischel, P., Roesli, C., Elia, G., Rybak, J. N., and Neri, D. (2006) A chemical proteomics approach for the identification of accessible antigens expressed in human kidney cancer. *Mol. Cell. Proteomics.* **5**, 2083–2091
103. Supiot, S., Gouraud, W., Campion, L., Jezéquel, P., Buecher, B., Charrier, J., Heymann, M. F., Mahé, M. A., Rio, E., and Chérel, M. (2013) Early dynamic transcriptomic changes during preoperative radiotherapy in patients with rectal cancer: A feasibility study. *World J. Gastroenterol.* **19**, 3249–3254

104. Tauber, S., Jais, A., Jeitler, M., Haider, S., Husa, J., Lindroos, J., Knöfler, M., Mayerhofer, M., Pehamberger, H., Wagner, O., and Bilban, M. (2010) Transcriptome analysis of human cancer reveals a functional role of Heme Oxygenase-1 in tumor cell adhesion. *Mol. Cancer*. **9**, 200
105. Medfai, H., Khalil, A., Rousseau, A., Nuyens, V., Paumann-Page, M., Sevcnikar, B., Furtmüller, P. G., Obinger, C., Moguilevsky, N., Peulen, O., Herfs, M., Castronovo, V., Amri, M., Van Antwerpen, P., Vanhamme, L., and Zouaoui Boudjeltia, K. (2019) Human peroxidase 1 promotes angiogenesis through ERK1/2, Akt, and FAK pathways. *Cardiovasc. Res.* **115**, 463–475
106. Vanacore, R., Pedchenko, V., Bhave, G., and Hudson, B. G. (2011) Sulphilimine cross-links in Goodpasture's disease. *Clin. Exp. Immunol.* **164 Suppl**, 4–6
107. McCall, A. S., Bhave, G., Pedchenko, V., Hess, J., Free, M., Little, D. J., Baker, T. P., Pendergraft, W. F., Falk, R. J., Olson, S. W., and Hudson, B. G. (2018) Inhibitory anti-peroxidase antibodies in pulmonary-renal syndromes. *J. Am. Soc. Nephrol.* **29**, 2619–2625
108. Li, H., Cao, Z., Moore, D. R., Jackson, P. L., Barnes, S., Lambeth, J. D., Thannickal, V. J., and Cheng, G. (2012) Microbicidal activity of vascular peroxidase 1 in human plasma via generation of hypochlorous acid. *Infect. Immun.* **80**, 2528–2537
109. Li, H., Cao, Z., Zhang, G., Thannickal, V. J., and Cheng, G. (2012) Vascular peroxidase 1 catalyzes the formation of hypohalous acids: Characterization of its substrate specificity and enzymatic properties. *Free Radic. Biol. Med.* **53**, 1954–1959
110. Furtmüller, P. G., Arnhold, J., Jantschko, W., Pichler, H., and Obinger, C. (2003) Redox properties of the couples compound I/compound II and compound II/native enzyme of human myeloperoxidase. *Biochem. Biophys. Res. Commun.* **301**, 551–557
111. Zederbauer, M., Furtmüller, P. G., Brogioni, S., Jakopitsch, C., Smulevich, G., and Obinger, C. (2007) Heme to protein linkages in mammalian peroxidases: Impact on spectroscopic, redox and catalytic properties. *Nat. Prod. Rep.* **24**, 571–584
112. Paumann-Page, M., Katz, R. S., Bellei, M., Schwartz, I., Edenhofer, E., Sevcnikar, B., Soudi, M., Hofbauer, S., Battistuzzi, G., Furtmüller, P. G., and Obinger, C. (2017) Pre-steady-state kinetics reveal the substrate specificity and mechanism of halide oxidation of truncated human peroxidase 1. *J. Biol. Chem.* **292**, 4583–4592
113. Shi, R., Cao, Z., Li, H., Graw, J., Zhang, G., Thannickal, V. J., and Cheng, G. (2018) Peroxidase contributes to lung host defense by direct binding and killing of gram-negative bacteria. *PLoS Pathog.* **14**, 1–19

114. GEISZT, M., WITTA, J., BAFFI, J., LEKSTROM, K., and LETO, T. L. (2003) Dual oxidases represent novel hydrogen peroxide sources supporting mucosal surface host defense. *FASEB J.* **17**, 1502–1504
115. Sirokmány, G., Kovács, H. A., Lázár, E., Kónya, K., Donkó, Á., Enyedi, B., Grasberger, H., and Geiszt, M. (2018) Peroxidasin-mediated crosslinking of collagen IV is independent of NADPH oxidases. *Redox Biol.* **16**, 314–321
116. Forman, H. J., Bernardo, A., and Davies, K. J. A. (2016) What is the concentration of hydrogen peroxide in blood and plasma? *Arch. Biochem. Biophys.* **603**, 48–53
117. Cho, I., Hwang, G. J., and Cho, J. H. (2015) pxn-1 and pxn-2 May Interact Negatively during Neuronal Development and Aging in *C. elegans*. **38**, 729–733
118. Lee, J. I. J., Bandyopadhyay, J., Lee, J. I. J., Cho, I., Park, D., and Cho, J. H. (2014) A role for peroxidasin PXN-1 in aspects of *C. elegans* development. *Mol. Cells.* **38**, 51–57
119. Manral, P., Colon, S., Bhave, G., Zhao, M. H., Jain, S., and Borza, D. B. (2019) Peroxidasin Is a Novel Target of Autoantibodies in Lupus Nephritis. *Kidney Int. Reports.* **4**, 1004–1006
120. McAdoo, S. P., and Pusey, C. D. (2018) Peroxidasin—a Novel Autoantigen in Anti-GBM Disease? *J. Am. Soc. Nephrol.* **29**, ASN.2018090946
121. Cheng, G., Salerno, J. C., Cao, Z., Pagano, P. J., and Lambeth, J. D. (2008) Identification and characterization of VPO1, a new animal heme-containing peroxidase. *Free Radic. Biol. Med.* **45**, 1682–94
122. Battistuzzi, G., Stampler, J., Bellei, M., Vlasits, J., Soudi, M., Furtmüller, P. G., and Obinger, C. (2011) Influence of the covalent heme-protein bonds on the redox thermodynamics of human myeloperoxidase. *Biochemistry.* **50**, 7987–7994
123. Tsuge, K., Kataoka, M., and Seto, Y. (2000) Cyanide and thiocyanate levels in blood and saliva of healthy adult volunteers. *J. Heal. Sci.* **46**, 343–350
124. Soltani, A., Reid, D. W., Sohal, S. S., Wood-Baker, R., Weston, S., Muller, H. K., and Walters, E. H. (2010) Basement membrane and vascular remodelling in smokers and chronic obstructive pulmonary disease: A cross-sectional study. *Respir. Res.* **11**, 1–8
125. Bathish, B., Turner, R., Paumann-Page, M., Kettle, A. J., and Winterbourn, C. C. (2018) Characterisation of peroxidasin activity in isolated extracellular matrix and direct detection of hypobromous acid formation. *Arch. Biochem. Biophys.* **646**, 120–127
126. Seidel, A., Parker, H., Turner, R., Dickerhof, N., Khalilova, I. S., Wilbanks, S. M., Kettle, A. J., and Jameson, G. N. L. (2014) Uric acid and thiocyanate as competing substrates

- of lactoperoxidase. *J. Biol. Chem.* **289**, 21937–21949
127. Martinon, F., Pétrilli, V., Mayor, A., Tardivel, A., and Tschopp, J. (2006) Gout-associated uric acid crystals activate the NALP3 inflammasome. *Nature.* **440**, 237
  128. Mohiuddin, I., Chai, H., Lin, P. H., Lumsden, A. B., Yao, Q., and Chen, C. (2006) Nitrotyrosine and Chlorotyrosine: Clinical Significance and Biological Functions in the Vascular System. *J. Surg. Res.* **133**, 143–149
  129. Degendorfer, G., Chuang, C. Y., Kawasaki, H., Hammer, A., Malle, E., Yamakura, F., and Davies, M. J. (2016) Peroxynitrite-mediated oxidation of plasma fibronectin. *Free Radic. Biol. Med.* **97**, 602–615
  130. Burner, U., Furtmüller, P. G., Kettle, A. J., Koppenol, W. H., and Obinger, C. (2000) Mechanism of reaction of myeloperoxidase with nitrite. *J. Biol. Chem.* **275**, 20597–20601
  131. Prütz, W. A., Mönig, H., Butler, J., and Land, E. J. (1985) Reactions of nitrogen dioxide in aqueous model systems: Oxidation of tyrosine units in peptides and proteins. *Arch. Biochem. Biophys.* **243**, 125–134
  132. Halfter, W., Oertle, P., Monnier, C. A., Camenzind, L., Reyes-Lua, M., Hu, H., Candiello, J., Labilloy, A., Balasubramani, M., Henrich, P. B., and Plodinec, M. (2015) New concepts in basement membrane biology. *FEBS J.* **282**, 4466–4479

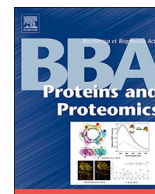
## 6. Appendices

# Monomeric and homotrimeric solution structures of truncated human peroxidasin 1 variants

Paumann-Page M, Tscheliessnig R, **Sevcnikar B**, Katz RS, Schwartz I, Hofbauer S, Pfanzagl V, Furtmüller PG, and Obinger C.

Research Article

Biochimica et Biophysica Acta (BBA) - Proteins and Proteomics, Volume 1868, Issue 1, January 2020, 140249  
DOI: 10.1016/j.bbapap.2019.07.002



## Monomeric and homotrimeric solution structures of truncated human peroxidasin 1 variants



Martina Paumann-Page<sup>a</sup>, Rupert Tscheliessnig<sup>b</sup>, Benjamin Sevcnikar<sup>a</sup>, Romy-Sophie Katz<sup>a</sup>, Irene Schwartz<sup>a</sup>, Stefan Hofbauer<sup>a</sup>, Vera Pfanzagl<sup>a</sup>, Paul G. Furtmüller<sup>a,\*</sup>, Christian Obinger<sup>a,\*</sup>

<sup>a</sup> Department of Chemistry, Division of Biochemistry, BOKU - University of Natural Resources and Life Sciences, 1190 Vienna, Austria

<sup>b</sup> ACIB, Austrian Centre of Industrial Biotechnology, Muthgasse 11, 1190 Vienna, Austria,

### ARTICLE INFO

#### Keywords:

Human peroxidasin 1  
Extracellular matrix  
Basement membrane  
Solution structure  
Rotary shadowing  
Small-angle X-ray scattering

### ABSTRACT

Human peroxidasin 1 is a multidomain peroxidase situated in the basement membrane. The iron enzyme with covalently bound heme oxidizes bromide to hypobromous acid which facilitates the formation of distinct sulfilimine cross-links in the collagen IV network and therefore contributes to its mechanical stability. Additional to the catalytically active peroxidase domain peroxidasin comprises a leucine rich repeat domain, four Ig domains and a C-terminal von Willebrand factor type C module (VWC). Peroxidasin has been shown to form homotrimers involving two redox-sensitive cysteine residues and to undergo posttranslational C-terminal proteolytic cleavage. The present study on several recombinantly produced truncated peroxidasin variants showed that the VWC is not required for trimer formation whereas the alpha-helical linker region located between the peroxidase domain and the VWC is crucial for trimerization. Our data furthermore implies that peroxidasin oligomerization occurs intracellularly before C-terminal cleavage. For the first time we present overall solution structures of monomeric and trimeric truncated peroxidasin variants which were determined by rotary shadowing combined with transmission electron microscopy and by small-angle X-ray scattering (SAXS). A triangular arrangement of the peroxidase domains to each other within the homotrimer was revealed and this structure was confirmed by a model of trimeric peroxidase domains. Our SAXS data showed that the Ig domains are highly flexible and interact with the peroxidase domain and that within the homotrimer each alpha-helical linker region interacts with the respective adjacent peroxidase domain. The implications of our findings on the structure-function relationship of peroxidasin are discussed.

### 1. Introduction

The five human heme peroxidases belong to the peroxidase-cyclooxygenase superfamily [1,2]. Representatives of Family 1 (i.e. chordata peroxidases) are monomeric or homodimeric peroxidases composed of the catalytic peroxidase domain only and are involved in the innate immune system (myeloperoxidase, MPO; eosinophil peroxidase, EPO; and lactoperoxidase, LPO) or in hormone biosynthesis (thyroid peroxidase, TPO). The recently detected member of Family 2 of the peroxidase-cyclooxygenase superfamily, i.e. peroxidasin 1 (hsPxd01, referred to as peroxidasin), is a homotrimeric multidomain peroxidase [3–5], which plays an important role in providing mechanical stability to basement membranes by oxidizing bromide to hypobromous acid, which subsequently mediates the formation of covalent sulfilimine links between a specific methionine and hydroxylysine residue in the collagen IV network [6–10]. Furthermore,

peroxidasin was demonstrated to promote angiogenesis through ERK1/2, Akt and FAK pathways [11].

The prosthetic heme group of peroxidasin is posttranslationally modified allowing the formation of two heme to protein ester bonds and efficient two-electron oxidation of bromide by peroxidasin Compound I [10]. Each monomer of peroxidasin comprises motifs typical for mediation of interactions in the extracellular matrix (ECM) in addition to the catalytically active peroxidase domain (POX) [4,12]. The non-catalytic domains, namely the leucine-rich-repeat domain (LRR) and the four C-like immunoglobulin domains (Ig) at the N-terminus of POX as well as the C-terminal von Willebrand factor type C module (VWC) are all well recognized for their functions in protein-protein interactions and cell adhesion. Fig. 1A schematically illustrates the domain structure of peroxidasin whereas Fig. 1B shows the detailed amino acid sequence of full length peroxidasin with accentuated residues of special interest as well as the amino acid sequence of the

\* Corresponding authors.

E-mail addresses: [paul.furtmueller@boku.ac.at](mailto:paul.furtmueller@boku.ac.at) (P.G. Furtmüller), [christian.obinger@boku.ac.at](mailto:christian.obinger@boku.ac.at) (C. Obinger).

<https://doi.org/10.1016/j.bbapap.2019.07.002>

Received 15 February 2019; Received in revised form 3 July 2019; Accepted 3 July 2019

Available online 08 July 2019

1570-9639/© 2019 The Author(s). Published by Elsevier B.V. This is an open access article under the CC BY license (<http://creativecommons.org/licenses/by/4.0/>).

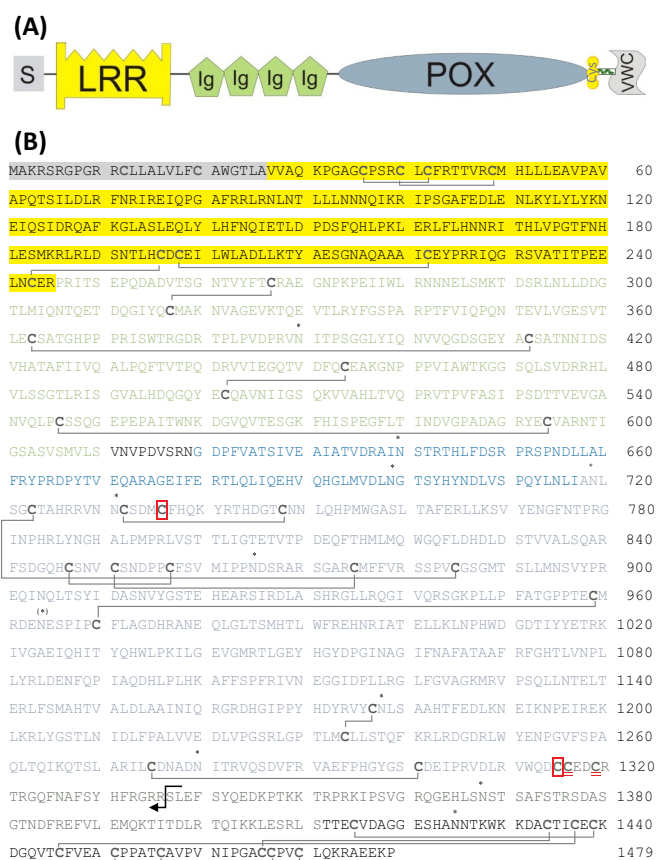


**Fig. 1.** Schematic presentation of domain assembly (A) and amino acid sequence (B) of peroxidasin and truncated variants. (A) Domain assembly of peroxidasin. The signal peptide (S) is depicted in grey, the leucine rich repeat region (LRR) in yellow, the four immunoglobulin (Ig)-like domains are shown in green, the peroxidase domain (POX) is depicted in blue and the VWC domain is shown in grey. The three cysteine residues at the C-terminus of the POX domain are illustrated in yellow and marked with Cys and the alpha helix that follows the three cysteine residues is depicted as green helix. (B) Amino acid sequence of hsPxd01. The domains of the sequence are shown in the same colour code as in the scheme above. Cysteine residues are depicted in bold grey letters and cysteine residues of disulfide bridges are connected with each other. The two cysteine residues responsible for trimer formation are boxed in red, whereas the two other free cysteines are underlined in red. Glycosylation sites are marked with \*. The one asparagine residue that is a predicted glycosylation site but was found not to be glycosylated experimentally is marked with (\*). The disulfide bridges are based on homology models for the LRR, Ig, POX and VWC region based on structures with the PDB codes 206S, 3B43, 2R5L and 1U5M, respectively, as templates. hsPxd01-con4 starts at amino acid residue Pro246 and ends with Asp1314. hsPxd01-con5 comprises the peroxidase domain from residue Gly620 to Asp1314. hsPxd01-con5-VWC consists of amino acid residues Gly620-Pro1479. Both hsPxd01-con5-helix and hsPxd01-con5-cys also start at Gly620 but end with residue Ser1411 and Ala1327, respectively. The black cascaded arrow indicates the proprotein convertase cleavage site.

truncated variants.

Mature peroxidasin is a highly glycosylated protein, which forms disulfide linked homotrimers [5,12]. The two cysteine residues 736 and 1315 were identified to be responsible for disulfide formation between peroxidasin monomers. Furthermore, trimerization was shown to be required for the adhesion of peroxidasin to the cellular surface [5]. Interestingly, the trimeric structure was not mandatory for sulfilimine link formation in the collagen IV NC1 domains [5,8]. Moreover, it was demonstrated that the C-terminus of peroxidasin was post-translationally cleaved by the protease proprotein convertase after Arg1336, which enhanced both catalytic activity and sulfilimine link formation.

In contrast to extracellular peroxidasin, intracellular peroxidasin was shown not to be truncated [13].

Several studies have been conducted to reveal the significance of protein trimerization and domain structure on the enzymatic activity, sulfilimine link formation and the interaction with ECM components. The smallest identified catalytically functional unit is the peroxidase domain plus the four N-terminal Ig domains (construct 4, hsPxd01-con4) (Figs. 1B & 2). It was demonstrated that this variant exhibits increased peroxidase and halogenation activity when compared to full length peroxidasin or other truncated variants [4,8,10]. Furthermore, hsPxd01-con4 is displaying increased sulfilimine link formation [8]. However, still many questions about the structure-function relationships of this enzyme are unanswered and no high resolution structure of peroxidasin is available to date.

The here presented work focused on structural studies of several highly purified truncated peroxidasin variants (Figs. 1B & 2). Our protein expression data demonstrated that (i) the alpha-helical linker region (Cys1315 – Ser1411) plays a decisive role in efficient trimer formation and confirmed that (ii) the VWC is not required for trimerization [5]. Moreover our data implies that (iii) oligomerization occurs intracellularly before C-terminal cleavage. Rotary shadowing (RS) in combination with transmission electron microscopy (TEM) was used to visualize the overall solution structures of the monomeric peroxidase domain (hsPxd01-con5), the peroxidase domain plus the four Ig domains (hsPxd01-con4) and of two trimerized variants [i.e. peroxidase domain plus C-terminal VWC domain (hsPxd01-con5-VWC) and peroxidase domain plus alpha-helical linker region (hsPxd01-con5-helix)]. Small-angle X-ray scattering (SAXS) data confirmed RS-TEM results showing that (i) trimerized peroxidasin variants display a triangular arrangement of the peroxidase domains. (ii) The revealed structural arrangement was corroborated by a model of trimeric peroxidasin composed of peroxidase domains linked via the identified Cys residues 736 and 1315. The SAXS data furthermore showed that (iii) the Ig domains interact with the peroxidase domain in a highly flexible manner and that (iv) in the homotrimer the alpha-helical linker regions interact with the respective adjacent peroxidase domain and (v) do not form a triple coiled coil of alpha helices as suggested by Nelson et al. [3]. Finally, we will discuss the relevance of these structural data with respect to peroxidasin biosynthesis, catalytic activity and its physiological role(s).

## 2. Results

### 2.1. Oligomerization states of peroxidasin constructs

The constructs hsPxd01-con5, hsPxd01-con4, hsPxd01-con5-helix and hsPxd01-con5-VWC (Figs. 1B and 2) were highly purified using affinity chromatography and subsequent preparative size exclusion chromatography. The oligomerization state of the various purified constructs was examined using non-reducing and reducing SDS-PAGE (Fig. 3A, left and middle panel). The structural motifs of the respective variants including their theoretical molar masses and oligomerization state determined by non-reducing SDS PAGE are summarized in Fig. 2. Peroxidasin is a highly glycosylated protein with ten confirmed N-glycosylation sites, one of them situated on the second Ig module, seven on the peroxidase domain (POX), one in the C-terminal linker region between POX and the VWC module and one glycosylation site located on the VWC module (Fig. 1B) [4]. Therefore on SDS PAGE the variants exhibited higher molar masses when compared to the theoretical masses of the unglycosylated proteins.

The construct hsPxd01-con5, which consists of the POX domain only, is a monomer (Fig. 3A, left and middle panel). SDS-PAGE resulted in one protein band with a molar mass of ~95 kDa when resolved under non-reducing and reducing conditions (theoretical molar mass: 81 kDa). The construct hsPxd01-con4, which comprises the four Ig-domains and POX, has a theoretical molar mass of 121 kDa. When resolved on SDS

hsPxd Constructs	Structural motifs of constructs	MW (kDa)	Oligomerization SDS PAGE non red
hsPxd01-con5		81	Monomer (~ 95 kDa)
hsPxd01-con4		121	Monomer (~ 135 kDa)
hsPxd01-con5-VWC		98	Trimer (~ 300 kDa)
hsPxd01-con5-helix		91	Trimer (~ 300 kDa)
hsPxd01-con5-cys		82	Monomer (Dimer, Trimer)* (~ 100, 200, 300 kDa)

**Fig. 2.** Overview of investigated constructs of peroxidasin. hsPxd01-con5 consists only of the peroxidase domain. hsPxd01-con4 comprises the four Ig domains and the peroxidase domain. hsPxd01-con5-VWC features additionally to the peroxidase domain the linker region with the three free cysteine residues, the  $\alpha$ -helical stretch and the VWC domain C-terminally. In hsPxd01-con5-helix the VWC domain is omitted, whereas hsPxd01-con5-cys contains the peroxidase domain and the three cysteine residues at its C-terminus. Theoretical molar masses of the peroxidasin variants are indicated as well as the approximate molar masses of the constructs on non-reducing SDS PAGE including their oligomerization states.

PAGE under both non-reducing and reducing conditions protein bands of ~140 kDa were observed, confirming the monomeric state of hsPxd01-con4 (Fig. 3A, left and middle panel). On the other hand hsPxd01-con5-VWC, which consists of the POX domain, the linker region and the VWC domain, formed redox sensitive trimers of a molar mass of ~300 kDa. When resolved on SDS PAGE under reducing conditions the monomeric form appeared at a molar mass of ~100 kDa. Importantly, hsPxd01-con5-helix, which comprises the peroxidase domain and the C-terminal alpha-helical linker region but excludes the VWC module, also formed redox sensitive trimers (~300 kDa), which appeared on a reducing SDS PAGE at ~100 kDa (Fig. 3A, left and middle panel). These results clearly demonstrated and confirmed that the VWC domain is not required for the assembly of the trimer and for the formation of disulfide bridges between peroxidasin monomers.

Furthermore, we probed whether the oligomeric structure affects the posttranslational modification of the heme prosthetic group of the POX domain by using the enhanced chemiluminescence (ECL) method [14]. Fig. 3A (right panel) showed that each of the constructs was posttranslationally modified and had the heme group covalently bound to the protein.

In order to elucidate if the alpha-helical linker region is essential for trimer formation an additional peroxidasin variant was generated. hsPxd01-con5-cys comprises the POX domain including 13 C-terminal amino acid residues ending with Ala1327. It lacks the predicted alpha-

helix of the linker region (Figs. 1 & 2) but includes the three free cysteine residues adjacent to the C-terminus of the POX domain. Interestingly, under non-reducing conditions this variant formed mainly monomeric protein and to a small degree dimers and trimers as visualized by Western blotting of a ~20 fold concentrated cell supernatant which was not further purified (Fig. 3B, left panel). For comparison the cell supernatant containing hsPxd01-con5-helix was concentrated to the same degree and blotted. The resulting Western blot confirmed that hsPxd01-con5-helix formed trimers only under non-reducing conditions (Fig. 3B, left panel), whereas both variants displayed one single protein band at approximately 100 kDa under reducing conditions (Fig. 3B, right panel). hsPxd01-con5-VWC and hsPxd01-con5-helix migrate very similarly to hsPxd01-con5 under reducing conditions. This could be due to the inhomogeneous glycosylation, which makes it impossible to determine accurate molecular masses on SDS-PAGES and/or the proprotein convertase processing is incomplete. Due to the oligomerization heterogeneity hsPxd01-con5-cys has not been included in later structural studies.

Next the molar mass and oligomeric composition of the different peroxidasin variants in solution was investigated by SEC-MALS. As depicted in Fig. 4 (A–D) all variants eluted as one main single peak at different retention times confirming a high degree of monodispersity. The molar mass of hsPxd01-con5 was determined by MALS to be 105 kDa (elution time: 16.8 min). For hsPxd01-con4, hsPxd01-con5-

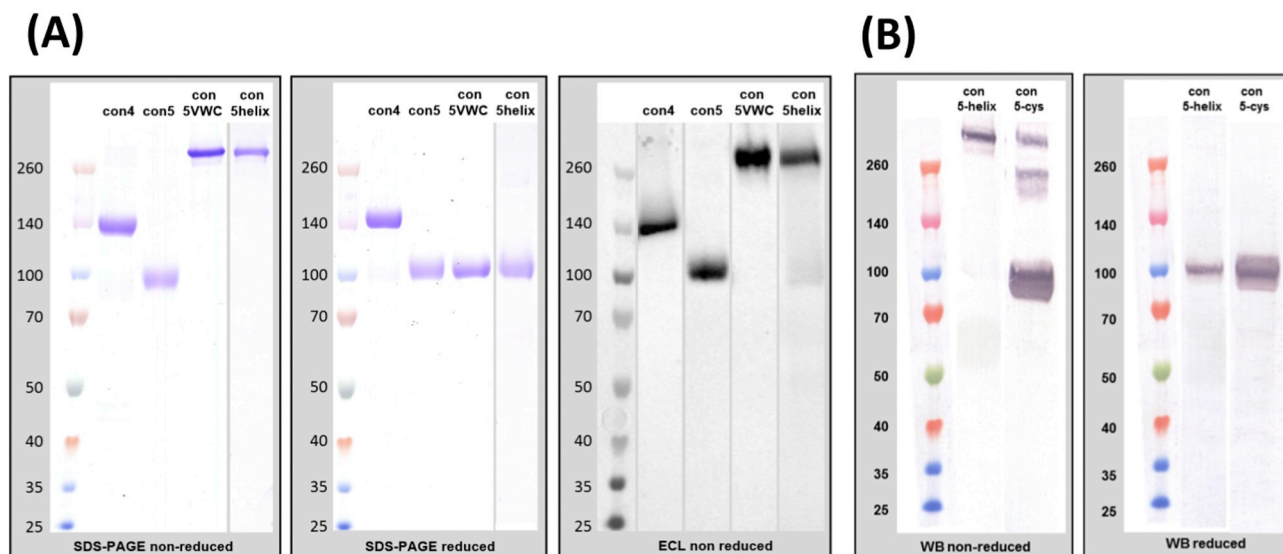


**Fig. 3.** Heme modification and oligomeric structure under reducing and non-reducing conditions. (A) SDS PAGE and enhanced chemiluminescence (ECL) of purified peroxidasin constructs. Peroxidasin variants resolved under non-reducing (left panel) and reducing (middle panel) conditions. Both hsPxd01-con5-VWC and hsPxd01-con5-helix form trimers. Approximate molar masses of the left panel are summarized in Fig. 2. The right panel depicts peroxidasin constructs blotted on nitrocellulose and reacted with ECL solution for visualization of covalently bound heme. (B) Western blots of hsPxd01-con5-helix and hsPxd01-con5-cys. Cell supernatants of HEK293-6E cells expressing hsPxd01-con5-helix and hsPxd01-con5-cys were resolved under non-reducing (left panel) and reducing (right panel) conditions, blotted and visualized. All gels and blots are representative of at least three independent experiments.

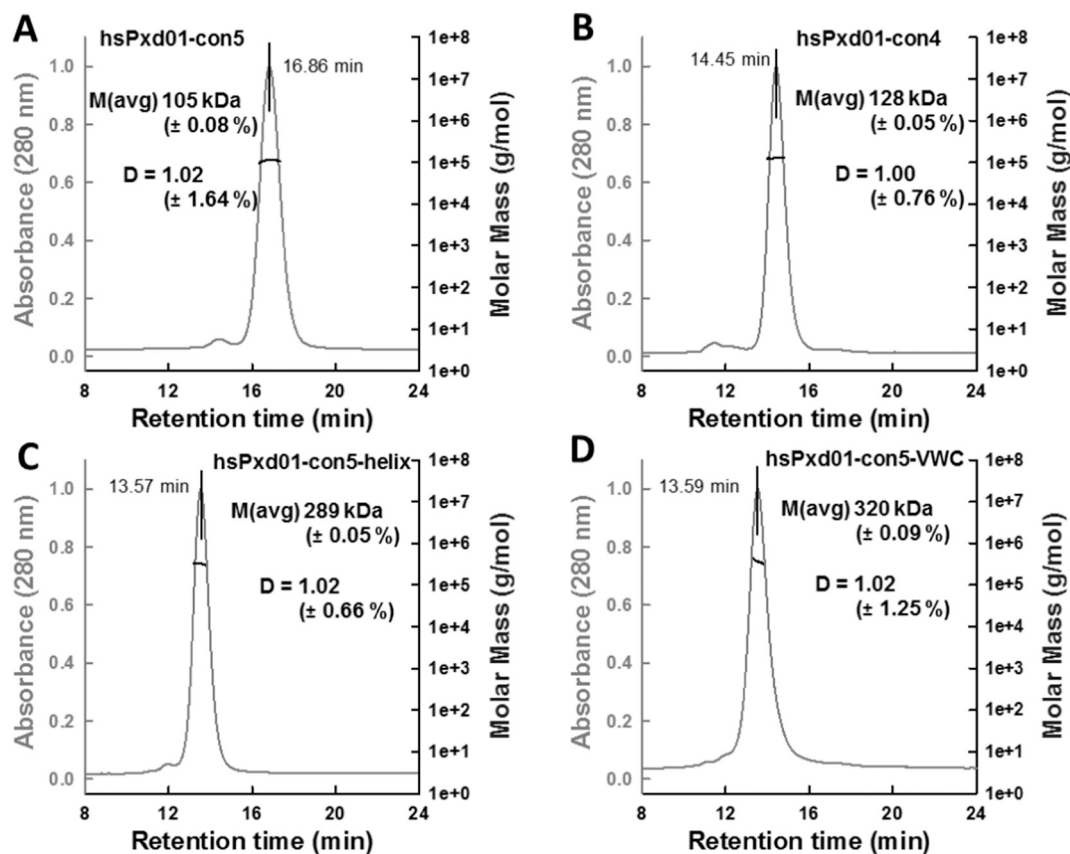


**Fig. 4.** HPLC-SEC-MALS measurements of peroxidasin constructs purified for SAXS experiments. HPLC-SEC elution profiles (grey) as well as molar masses (black) determined using MALS (software ASTRA) for hsPxd01-con5 (A), hsPxd01-con4 (B), hsPxd01-con5-helix (C) and hsPxd01-con5-VWC (D). Prior proteins were purified using affinity chromatography (His-tag) and preparative SEC before samples were run on HPLC-SEC in PBS buffer containing 200 mM NaCl, pH 7.4.

helix and hsPxd01-con5-VWC the measured molar masses were 128 kDa, 289 kDa and 320 kDa, respectively (retention times: 14.45 min, 13.57 min and 13.59 min, respectively). This data affirmed that hsPxd01-con5 and hsPxd01-con4 were monomeric and both hsPxd01-con5-helix and hsPxd01-con5-VWC were homotrimeric proteins.

Furthermore, dynamic light scattering (DLS) was employed to ensure monodispersity of the purified peroxidasin variants under condition used for SAXS measurements (see below). Like for the above HPLC-SEC-MALS analysis 200 mM NaCl was present to prevent interactions of the variants with the column matrix. The autocorrelation functions of hsPxd01-con5, hsPxd01-con4, hsPxd01-con5-helix and hsPxd01-con5-VWC are depicted on the left hand side of Fig. 5 (A–D). Corresponding mass weighted size distribution of each variant is shown on the right. The hydrodynamic radii determined for hsPxd01-con5, hsPxd01-con4, hsPxd01-con5-helix and hsPxd01-con5-VWC were determined to be 3.63 nm, 4.86 nm, 5.47 nm and 4.41 nm, respectively. The presented data demonstrated the monodispersity of the peroxidasin variants and confirm their suitability for further structural analysis, in particular SAXS measurements.

## 2.2. Electron micrographs of peroxidasin constructs

To visualize the peroxidasin variants rotary shadowing (RS) combined with transmission electron microscopy was utilized. As shown in Fig. 6A, hsPxd01-con5 displayed a mainly spherical shape, with a diameter of 11.5 nm. Based on available X-ray structures of lactoperoxidase [15], myeloperoxidase [16] and promyeloperoxidase [17], a globular shape would be expected. hsPxd01-con4, which also comprises the four Ig domains additionally to the peroxidase domain, displayed an oval shape of 16.1 nm length and 11.1 nm width as depicted in Fig. 6B.

As shown in Fig. 6C and D both hsPxd01-con5-helix and hsPxd01-con5-VWC form trimers of triangular peroxidase monomer arrangement with very similar dimensions. Interestingly, in both structures the monomers forming the trimers appeared to be more compact with a monomer diameter of 8.2 nm and 7.9 nm for hsPxd01-con5-helix and hsPxd01-con5-VWC, respectively. This result could imply that the interaction of the monomers in the trimer cause conformational changes. Note that in general rotary shadowing structures appear larger than their actual size due to the layers of platinum and carbon which were vaporized onto the visualized structures.

## 2.3. SAXS structures of peroxidasin constructs

For three-dimensional visualization of the experimentally determined scattering intensity we used the homologous three-dimensional model of the hsPxd01-con5 trimer to compute the corresponding pair density distribution (Fig. 7). The models of the individual peroxidase domains were created using the structure of homologous goat lactoperoxidase as template. For detail please see Experimental Procedures.

In Figs. 8–11 scattering intensities,  $I(Q)$ , are given as function of the scattering wave vector ( $Q$ ) in 1/nm. All signals were of low electronic contrast. In order to minimize unspecific protein-protein interactions both protein concentrations (Fig. 11) and/or pH (Fig. 8–10) of the samples were varied. For all data Guinier fits were computed in order to probe nonlinearity at low  $Q$  values which indicates unspecific protein-protein interaction(s) or protein aggregation. Except for hsPxd01-con5-helix (Fig. 10), the Guinier plots for all constructs are linear in the low  $Q$  regime and the slopes ( $D$ ) are comparable (Figs. 8, 9 and 11). In case of hsPxd01-con5-helix non-linearity might indicate protein-protein interactions, but could also be attributed to rather flexible conformations

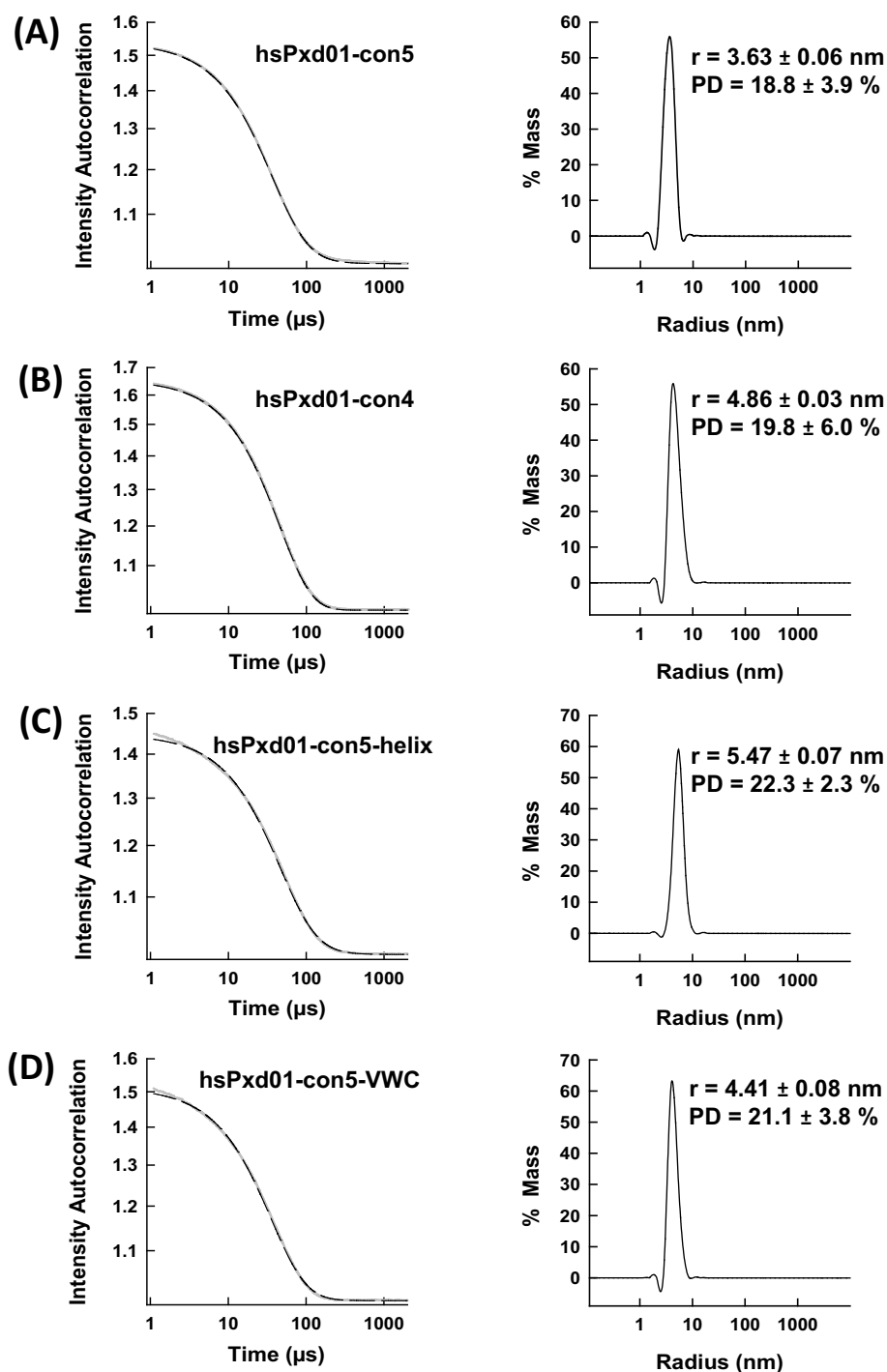


**Fig. 5.** Dynamic light scattering (DLS) data of peroxidasin variants. All variants were analyzed at a protein concentration of 1 mg/mL in phosphate buffer saline at pH 7.4. The left panels depict the autocorrelation function of hsPxd01-con5 (A), hsPxd01-con4 (B), hsPxd01-con5-helix (C) and hsPxd01-con5-VWC (D) in grey colour with their respective cumulative fit (black dashed line). The right panels show the corresponding mass weighted size distribution, the determined hydrodynamic radius based on an isotropic spheres model, as well as the polydispersity (PD) of the samples ( $n \geq 3$ , mean  $\pm$  STDEV).

or very weakly interacting domains. Indeed rotary shadowing (RS) data support the latter interpretation as we identified a plethora of different conformations.

Fig. 8 shows the scattering intensities and Guinier plots (Fig. 8A), as well as pair density distributions and scale corrected data of hsPxd01-con 5 at various pH values. The data suggest that the solution structure of this construct is invariable in the pH regime pH 5–9 and that the scattering contrast in the propeptide region is low, indicating less compactness of the propeptide and loose interaction with the core-

peroxidase domain. Top panel of Fig. 8 depicts two potential conformations of hsPxd01-con5 with stretched and compact propeptide.

Fig. 9 lists different projections of the trimeric model of hsPxd01-con5-VWC. The model is based on the red colored pair density distribution given in Fig. 9C and D (left panels, each). It was designed on basis of the scattering data presented in Fig. 9A & C. The pair density distributions computed from the scattering data clearly indicated a trimeric structure at pH 9. For lower pH values, at bigger spatial distances pair densities have displayed tails (blue and red line in Fig. 9B,

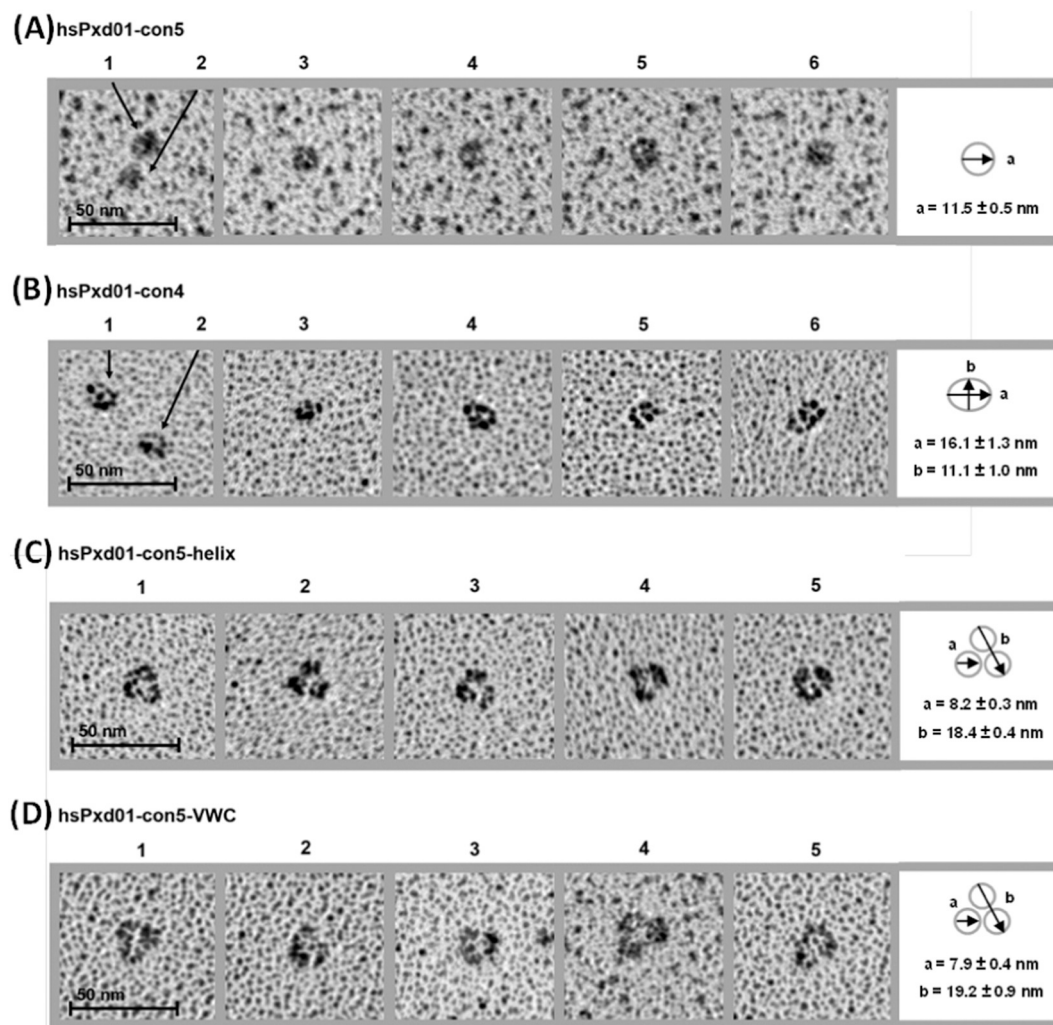


**Fig. 6.** Rotary shadowing and TEM of peroxidasin constructs. Peroxidasin constructs (A–D) were visualized using rotary shadowing and TEM. 100  $\mu\text{g}/\text{mL}$  protein in 50 mM phosphate buffer pH 7.4 was diluted to 50  $\mu\text{g}/\text{mL}$  with 100 mM ammonium acetate and 30% (v/v) glycerol pH 7.4. Samples were sprayed on mica chips and coated with platinum at 5–6° and carbon at 90° and visualized using TEM. Image 1 was used to determine the diameter of individual particles.

left panel), which can be attributed either to a flexible trimeric structure or to pair wise interactions of individual trimers. Considering the HPLC-SEC-MALS (Fig. 4D) and RS results (Fig. 6D), we favored flexible trimer structures as cause for the tails of the pair densities at bigger spatial distances. And indeed, corrected scaling of the scattering data gives a single pair density distribution for all three pH values.

The scattering data of hsPxd01-con5-helix and the resulting SAXS model are presented in Fig. 10. From HPLC-SEC-MALS data (Fig. 4C) and RS data (Fig. 6D) we would expect less tailed pair density distributions than we observe. A flexible trimeric structure could again be the cause for the strong tailing of the pair density distribution. However, the tailing at bigger spatial distances is exceptionally strong. In contrast the RS images of hsPxd01-con5-helix (Fig. 6C) and hsPxd01-con5-VWC (Fig. 6D) are comparable. Thus we conclude that the truncation of the VWC domain leads to stronger interactions between individual trimers. Additionally, it is important to mention that the shown trimeric models of both hsPxd01-con5-helix and hsPxd01-con5-VWC clearly suggest unrestricted access to the active site of the three peroxidase domains (compare Fig. 7 with models of Figs. 9 & 10).

In Fig. 11 we plotted the scattering intensities of hsPxd01-con4 at different variant concentrations in order to analyze possible pair wise interactions. We do not see significant differences in scattering data. The corresponding pair densities (colour code) show a characteristic shoulder at bigger distances. This shoulder might be due to an

elongated conformation of the 4 Ig-domains (Fig. 11, top panel conformation 1). Again we compared the obtained model with the corresponding RS images and HPLC-SEC-MALS data, which favor a compact conformation of the Ig-domains and exclude the presence of dimers. We could scale the scattering data correctly and calculated thereof a pair density (red line in Fig. 11 D, right panel), resulting in computation of a compact protein conformation (Fig. 11, top panel conformation 2) in line with the RS data (Fig. 6B).

### 3. Discussion

Peroxidasin is a multidomain peroxidase that is secreted to the extracellular matrix where it is integrated into the collagen IV scaffold of basement membranes. Next to the catalytically active POX domain peroxidasin comprises typical ECM motifs (a leucine rich repeat domain and four Ig domains at the N-terminus and a C-terminal VWC module), which usually enable protein-protein interactions (Fig. 1). Peroxidasin uses hydrogen peroxide to oxidize bromide to generate HOBr, which facilitates the generation of a sulfilimine cross link in NC1 domains of collagen IV. The sulfilimine link plays a crucial role in basement membrane stability and functionality [6,7]. How peroxidasin conveys this highly specific covalent bond between two distinct opposing amino acid residues, a methionine and a hydroxylysine residue, is still unknown. Spatial proximity of HOBr release and sulfilimine link

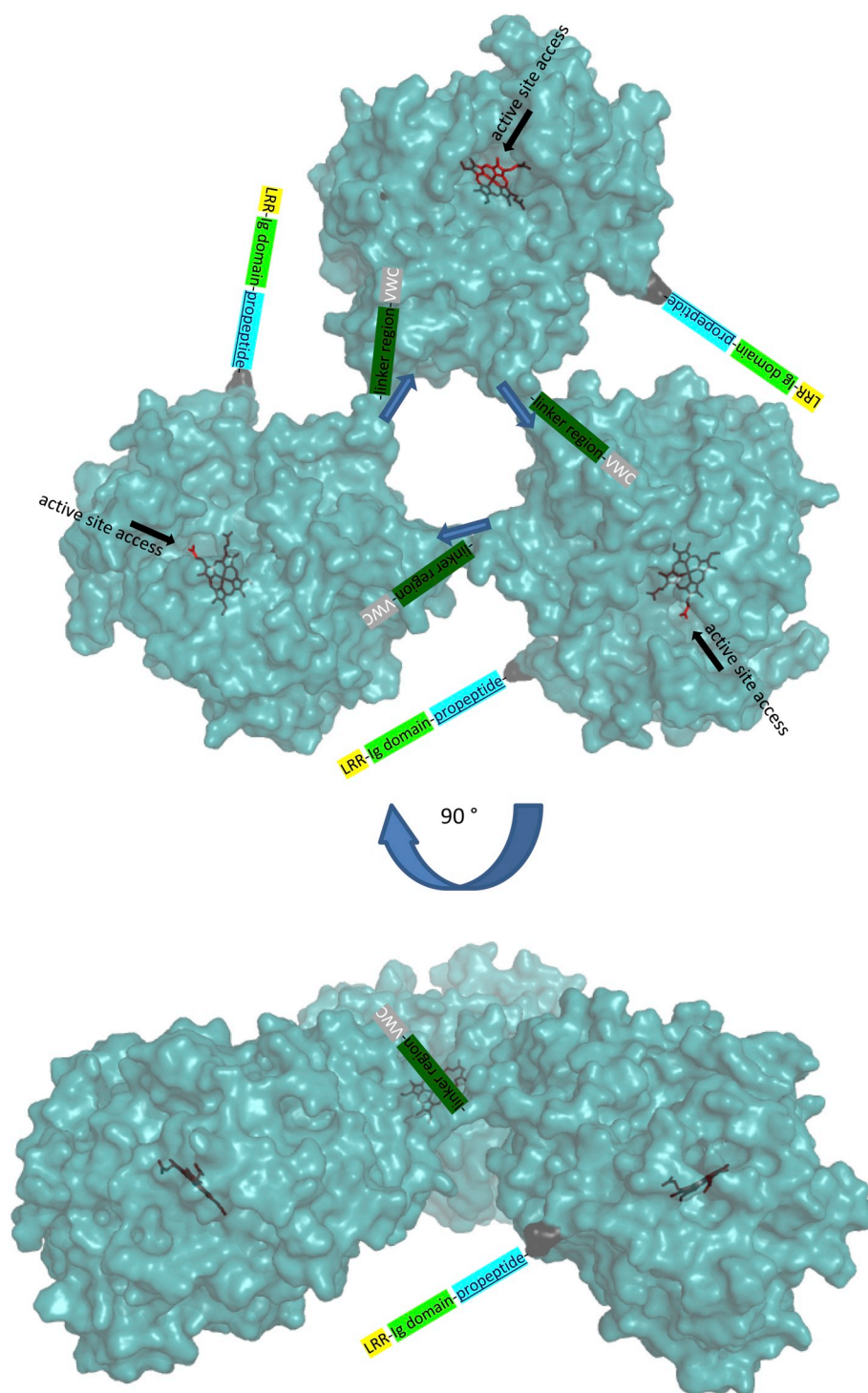


**Fig. 7.** Model of the peroxidase domain trimer of peroxidasin. The model of the peroxidase domain of peroxidasin was created with SWISS model using the structure of goat LPO (PDB code 2R5L) as a template. The model comprises the amino acid residues Ala718 – Asp1314 of peroxidasin. The cysteine residue 1315 was added at the C-terminus of the model, which was then used to introduce the three disulfide bridges which link the monomers to a trimeric structure. Colour code according to Fig. 1. Blue arrows mark the linker region between monomers; black arrows mark the access to the active site.

formation appears to be critical for specificity and efficient NC1 domain cross-linking. MPO and EPO were shown to be able to form the sulfilimine link to a highly reduced degree [7], presumably due to the lack of interacting ECM domains. As a consequence HOBr released from MPO or EPO will react mainly non-specifically with other biomolecules instead of forming the sulfilimine link. However, despite the high specificity of peroxidasin for sulfilimine formation, some HOBr was shown to be released from the enzyme [20].

Presumably these additional ECM domains of peroxidasin facilitate specific protein-protein interactions, which would position peroxidasin in close proximity of the NC1 domain of collagen IV. Peroxidasin does not seem to form a stable complex with collagen IV [8]. The interaction with collagen IV may be either of transient nature or mediated by a tertiary ECM protein. However, a protein binding to peroxidasin could induce conformational changes which may either affect the reactivity of peroxidasin, and act as a switch between catalytically active or inactive

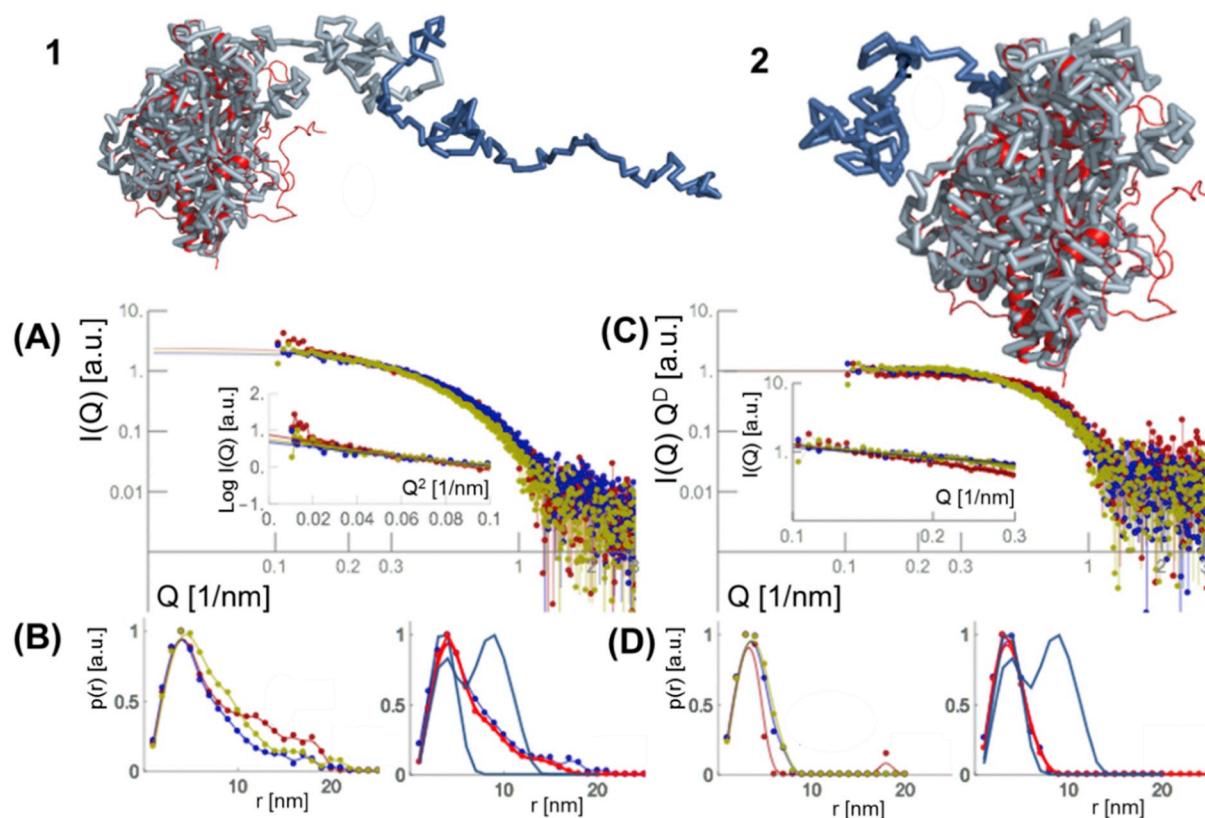


**Fig. 8.** SAXS data and model of hsPxd01-con5. Top panel: SAXS models are shown as transparent chain models. 1) SAXS model with stretched propeptide and 2) with compact propeptide. The peroxidase domain (POX) is depicted in grey and the POX propeptide region is shown in blue. The homologous model of the POX domain is indicated as red cartoon. (A) Plot of scattering intensity  $I(Q)$  at pH 5 (red), pH 7.4 (blue) and pH 9 (green), respectively, and fits versus scattering vector ( $Q$ ). Insert: Guinier plots. The logarithm of scattering intensity,  $\log I(Q)$ , of peroxidase is given as a function of  $Q^2$  at the corresponding pH values including fits. (B) Left panel: Pair density distributions,  $p(r)$ , plotted against the distance ( $r$ ) at pH 5 (red dotted line), pH 7.4 (blue dotted line) and pH 9 (green dotted line). Right panel: The pair density distribution  $p(r)$  computed from the SAXS model (red dotted line), the  $p(r)$  of the monomer and trimer model computed from the homologous models (blue lines) and the  $p(r)$  at pH 7.4 (blue dotted line) were plotted against ( $r$ ). (C) The  $I(Q) Q^{3-D^*}$  ( $D = 3-D^*$ ) values that are the scale corrected scattering data [ $D^* = 2.09$  (pH 5, red), 2.52 (pH 7.4, blue), 2.35 (pH 9, green)] are plotted against the scattering vector ( $Q$ ). Insert: Linear double logarithmic plot with the slope,  $D$  of  $I(Q)$ . (D) Left panel: pair density distribution  $p(r)$  computed from scale corrected data at different pH plotted against the distance ( $r$ ). Right panel: the pair density distribution  $p(r)$  (red dotted line), the  $p(r)$  of the monomer and trimer model computed from the homologous models (blue lines) and the  $p(r)$  at pH 7.4 (blue dotted line) plotted against ( $r$ ). Colour code as in (B).

forms, or influence the accessibility of the active site and the release of HOB<sub>r</sub>.

So far no high resolution structure of peroxidase is available. One very likely cause could be the high flexibility of both monomeric and homotrimeric structures, as demonstrated in the present work. Pair density distributions computed from SAXS data had considerable tailing at bigger spatial distances which usually is an indication for pairwise interactions of individual constructs. Neither pH nor concentration had a significant impact on the tailing of the scattering profile of the investigated constructs (except for hsPxd01-con5). These results indicate that all monomeric and trimeric constructs are considerably flexible and sample a vast number of self-similar conformations. A consequence of the flexibility of peroxidase and its truncated variants in solution could be the difficulty in finding the right condition for crystallization. Nevertheless, based on our SAXS measurements, peroxidase shows its most compact conformation in the slightly basic pH regime.

The peroxidase domain (POX) of peroxidase displays high sequence similarity with Family 1 peroxidases (MPO, LPO, EPO). Lactoperoxidase exhibits the highest homology to the POX domain of peroxidase. All Family 1 peroxidases feature a propeptide which is proteolytically removed during maturation [17,21,22]. Peroxidase also possesses a propeptide like structure (Fig. 1B, comprising Gly620 – Ile717) located at the N-terminus of the POX domain. In contrast to Family 1 peroxidases the propeptide is not cleaved off and remains an integrated part

of the structure. Interestingly, a truncated variant consisting of the POX domain only excluding the propeptide (Fig. 1B, Ala718 – Asp1314) could be recombinantly expressed but was unstable and prone to form polymers [4]. In the presence of the propeptide region (hsPxd01-con5) the protein is stable and monomeric and has a globular structure as visualized by RS-TEM (Fig. 6A). This was to be expected based on crystal structures of homologous Family 1 peroxidases and homology modelling of the POX domain on LPO (Fig. 7). The SAXS structure of hsPxd01-con5 confirms the overall globular shape of the POX domain and suggests that the propeptide region is rather flexible, which is consistent with the crystal structure and SAXS data obtained for proMPO [17]. Importantly, in hsPxd01-con5 and all other investigated recombinant constructs the heme prosthetic group is covalently linked to the protein suggesting that the peroxidase typical additional domains as well as the oligomerization state have no impact on this posttranslational modification.

Variant hsPxd01-con4 which includes the four Ig domains and the POX domain (Fig. 1B, Pro186 – Asp1314 and Fig. 2) is highly catalytically active. Its spectral and halide oxidation properties have been characterized in detail [10] and rate constants of the halogenation cycle are comparable to MPO, LPO and EPO. The construct hsPxd01-con4 is monomeric (Figs. 2, 3A, 4B and 5B) and RS revealed an oval shape (Fig. 6B). As depicted in the SAXS data, Ig3 and Ig4 are likely to interact with each other and Ig4 is in close contact with the POX domain.

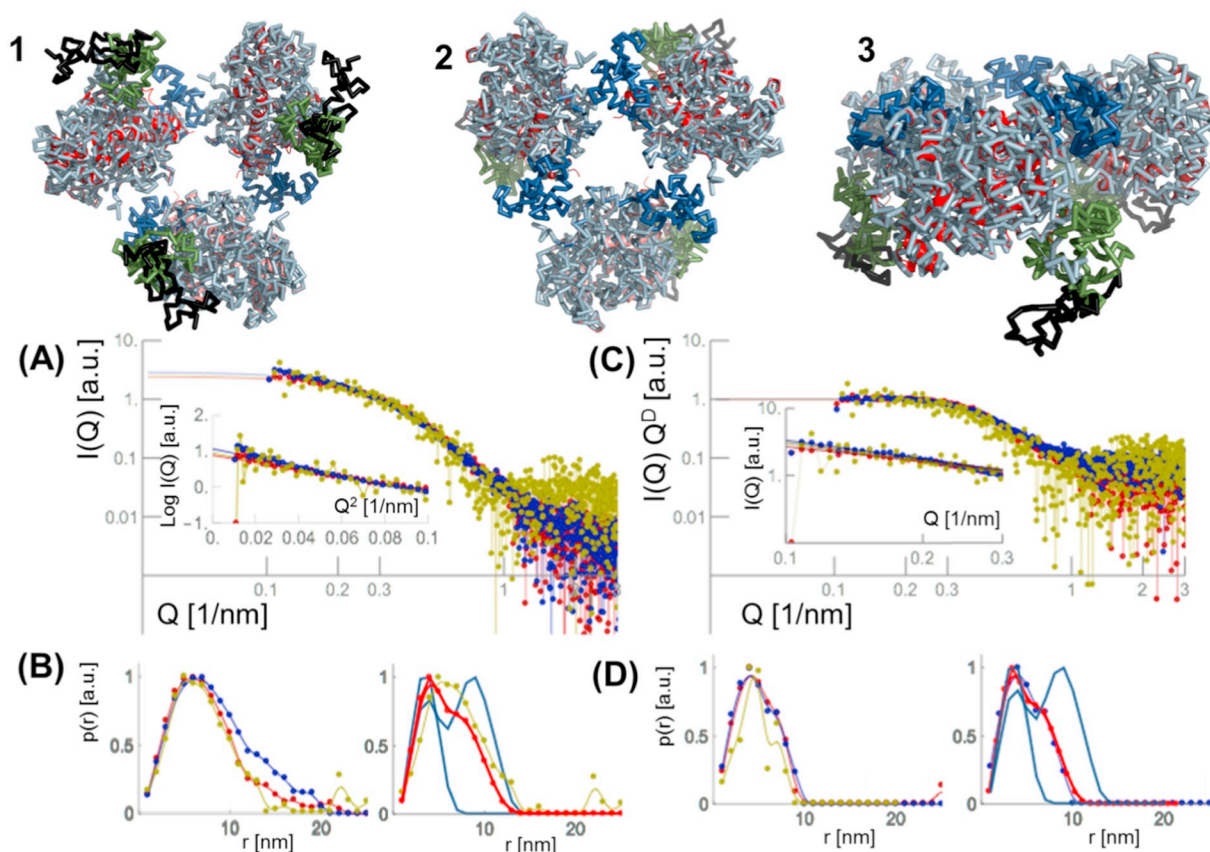


**Fig. 9.** SAXS data and model of hsPxd01-con5-VWC. Top panel: SAXS model is shown as transparent chain model, 1) the C-termini (VWC domains) of the trimeric hsPxd01-con5-VWC facing up, 2) C-termini of the trimer facing down, and 3) position 2 rotated by 90°. The peroxidase domain (POX) is depicted in grey, the POX propeptide region is shown in blue, the linker region between POX domain and VWC is shown in green and the VWC domain is depicted in black. The homologous model of the POX domain is indicated as red cartoon. (A) Plot of scattering intensity  $I(Q)$  at pH 5 (red), pH 7.4 (blue) and pH 9 (green), respectively, and fits versus scattering vector ( $Q$ ). Inset: Guinier plots. The logarithm of scattering intensity,  $\log I(Q)$ , of hsPxd01-con5-VWC is given as a function of  $Q^2$  at the corresponding pH values including fits. (B) Left panel: Pair density distributions,  $p(r)$ , plotted against the distance ( $r$ ) at pH 5 (red dotted line), pH 7.4 (blue dotted line) and pH 9 (green dotted line). Right panel: The pair density distribution  $p(r)$  of the calculated SAXS model (red dotted line), the  $p(r)$  of the monomer and trimer computed from the homologous models (blue lines) and the  $p(r)$  at pH 9 (green dotted line) is plotted against the distance ( $r$ ). (C) The  $I(Q)Q^{3-D^*}$  ( $D = 3-D^*$ ) values, which are the scale corrected scattering data [ $D^* = 2.27$  (pH 5, red), 2.08 (pH 7.4, blue), 2.09 (pH 9, green)], are plotted against the scattering vector ( $Q$ ). Inset: Linear double logarithmic plot with the slope,  $D$  of  $I(Q)$ . (D) Left panel: pair density distribution  $p(r)$  computed from scale corrected data at different pH values plotted against the distance ( $r$ ). Right panel: the pair density distribution  $p(r)$  (red dotted line), the  $p(r)$  of the monomer and trimer computed from the homologous models (blue lines) and the  $p(r)$  at pH 9 (green dotted line) plotted against ( $r$ ). Colour code as in (B).

Homology modelling of the isolated Ig1 and Ig2 domains as well as Ig1 – 4 may resulted in several probable sandwiched structures where Ig1 interacts with Ig2 or Ig1 sandwiches with Ig4 and Ig2 interacts with Ig3 (data not shown). The rotary shadowing images are compact and therefore also suggest the interaction of Ig domains with the peroxidase domain and possibly with each other. The presence and potentially the interaction of the Ig domains with POX impacts greatly on catalytic activity, as hsPxd01-con4 has been shown to be highly catalytically active [10]. This is in accordance with results that showed that the Ig domains and POX were required for efficient sulfilimine bond formation in collagen IV [8].

The hsPxd01-con5-cys variant (Gly620 – Ala1327), which includes the three C-terminal free cysteine residues but omits the alpha helical region between POX and VWC has clearly demonstrated, that the alpha helical region is of crucial importance for effective trimer formation. It has been suggested previously that the amphipathic alpha helix of this region would form a homotrimeric coiled coil [3] thereby facilitating trimerization via conserved cysteines C736 and C1315 [11]. Our results demonstrate, that in the absence of the helix mostly monomeric recombinant protein was produced (Figs. 2 and 3B), whereas in the presence of the helical region, as in variant hsPxd01-con5-helix, only trimers were detected (Figs. 2, 3A and B, 4C and 5C). This is in

accordance with data from Lázár et al., which demonstrated earlier that the VWC module is not involved in trimerization [5].

Moreover, it has been shown recently, that *in vivo* peroxidase is processed after amino acid residue Arg1336 by proprotein convertase A, removing most of the amphipathic alpha-helix and the VWC domain [13]. The cleavage site is located nine amino acids away from the C-terminus of the variant hsPxd01-con5-cys (Ala1327). As hsPxd01-con5-cys predominantly forms monomers, we conclude that trimerization has to take place before proteolytic cleavage. Moreover, this processing step is supposed to occur at the cytoplasmic membrane and therefore our results demonstrate that trimer formation has to take place intracellularly before secretion to the ECM. It has to be mentioned that in our expression system the proposed processing by proprotein convertase A has either not occurred or was incomplete (VWC tryptic peptide of hsPxd01-con5-VWC was detected by mass spectrometric analysis, data not shown).

The rotary shadowing data for hsPxd01-con5-helix and hsPxd01-con5-VWC are comparable, however, the trimer in the latter appeared less densely packed compared to hsPxd01-con5-helix (Fig. 6C and D). SAXS data of the two trimeric variants confirm the triangular arrangement of the POX monomers to each other (supporting absent or incomplete proteolytic processing of the VWC module in our expression

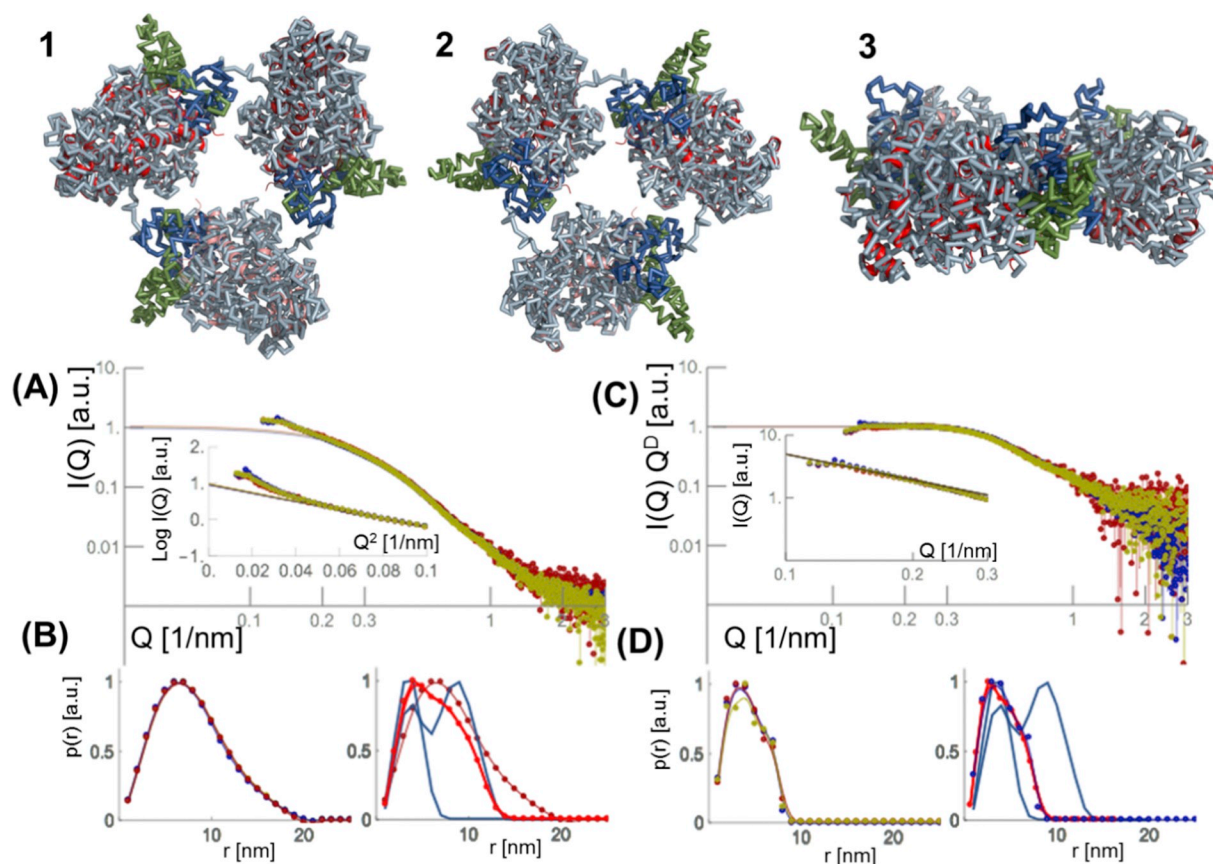


Fig. 10. SAXS data and model of hsPxd01-con5-helix. With the exception of the lack of the VWC domain presentation of data is identical to Fig. 9. [(D = 3-D\*), D\* = 1.28 (pH 5, red), 1.31 (pH 7.4, blue), 1.31 (pH 9, green)].

system). Our model of the POX domain trimer, based on previously identified free cysteines residues C736 and C1315 [5], confirms the triangular arrangement and suggests free access of hydrogen peroxide and bromide to the respective heme cavities (Fig. 7). The triangular arrangement of the POX domains is furthermore in agreement with micrograph data of full length trimeric peroxidase from drosophila [3]. The structures shows a relatively compact core similar to our triangular POX domains from which three flexible arms extend, which are most likely composed of the LRR and Ig domains. Moreover, the micrograph structures support our finding of the high flexibility of the peroxidase structure, which is reflected in various self-similar micrograph formations.

Summing up, crosslinking of collagen IV protomers between interfacing NC1 domains by the formation of distinct sulfilimine links mediated by peroxidase leads to the formation of a scaffold that interacts with other basement membrane proteins. Peroxidase biosynthesis includes heme insertion, modification and covalent linkage to the protein together with core glycosylation of POX and Ig domains in the endoplasmic reticulum. Homotrimerization most probably occurs intracellularly and needs an amphipathic alpha-helical region between the POX and VWC domains for steric alignment and intermolecular disulphide bridge formation between highly conserved C736 and C1315 [5]. Lastly, *in vivo*, a proprotein convertase A presumably located at the cytoplasmic membrane removes most of the amphipathic alpha-helix and the VWC domain [13] before secretion of the truncated but fully active homotrimeric enzyme to the ECM. Our recent studies demonstrated that except POX all monomeric and trimeric constructs exhibit reliable bromide oxidation activity *in vitro* [4,10]. In a physiological setting, however, the monomeric forms were shown to be less effective suggesting that optimal coupling of NC1 domains requires trimerization of hsPxd01 [5]. So far it is unclear whether trimeric peroxidase

interacts directly with the NC1 domains or in a complex with other ECM proteins. The high flexibility of trimeric hsPxd01-con5-helix as well as of monomeric hsPxd01-con4 structures - as demonstrated by SAXS - suggest the establishment of a variety of conformations for potential specific interactions of N-terminal leucine-rich repeat and immunoglobulin domains of processed peroxidase with ECM proteins which might help to reduce the distance between HOBr release by the peroxidase domains and the coupling reaction at the NC1 domains.

Further experiments on potential interactions of peroxidase or truncated variants with ECM proteins will be essential for understanding the mechanism of reaction and the role of peroxidase in the synthesis and function of basement membranes. Moreover, the source of hydrogen peroxide, which is essential for bromide oxidation mediated by hsPxd01, and its role in this biosynthetic pathway is currently also unknown.

## 4. Experimental procedures

### 4.1. Cloning, transient transfection and expression of peroxidase constructs

Data provided by UniProtKB (<http://www.uniprot.org/>) on human peroxidase 1 (Q92626) was used to evaluate primer design for the production of peroxidase variants. Furthermore information from multiple sequence alignments of the peroxidase peroxidase domain and other homologous human peroxidases (myeloperoxidase (MPO), lactoperoxidase (LPO), eosinophil peroxidase (EPO) and thyroid peroxidase (TPO)) was employed for the design of the truncated peroxidase variants.

PCR amplified DNA of truncated peroxidase variants was cloned into a modified pTT5 vector (NRC-BRI). All primers were designed for cloning with Gibson Assembly (New England Biolabs) and an N-

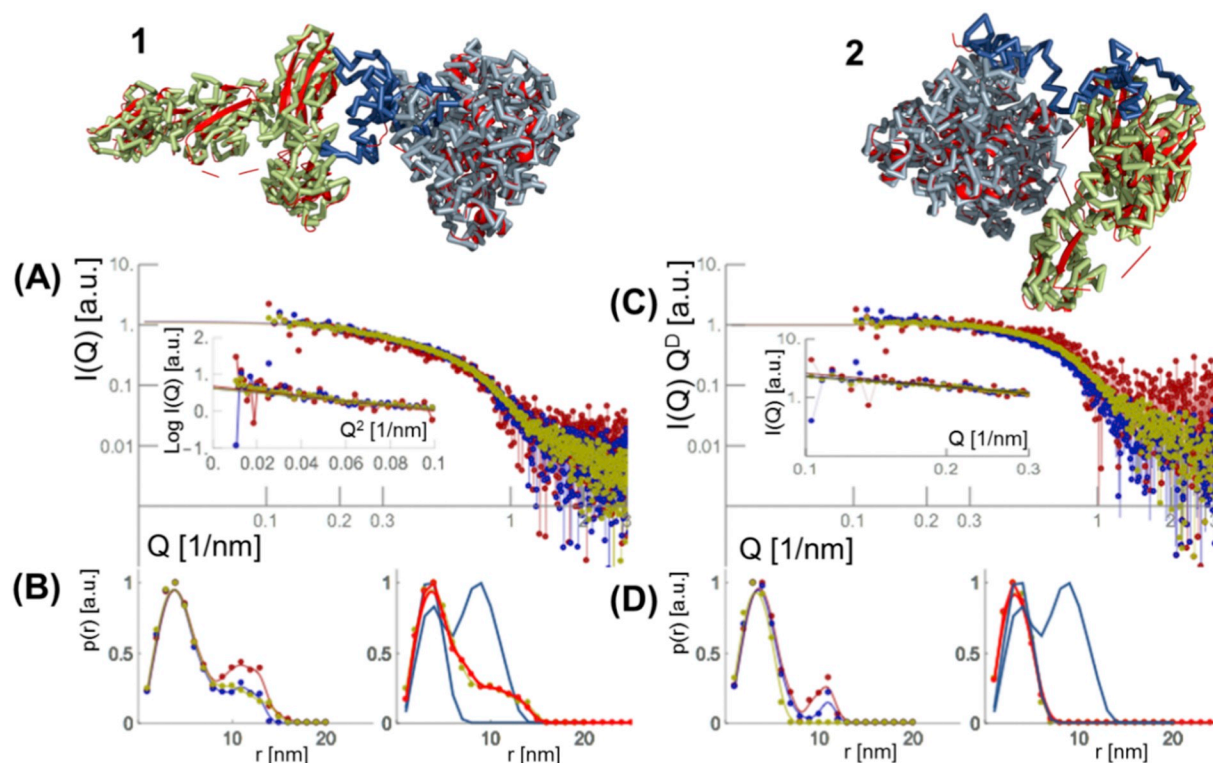


**Fig. 11.** SAXS data and model of hsPxd01-con4. Top panel: two possible conformations of the four Ig domains of the SAXS model are shown as transparent chain model. 1) Ig domains facing away from the POX domain, 2) Ig domains wrapping around the POX domain. The peroxidase domain (POX) is depicted in grey, the POX propeptide region is shown in blue, and the four Ig domains are shown in green. The homologous model of the POX domain is indicated as red cartoon. (A) Plot of scattering intensity  $I(Q)$  with different construct concentration [0.5 mg/mL (red) 1 mg/mL (blue) 2 mg/mL (green)] and fits versus scattering vector ( $Q$ ). Insert: Guinier plots. The logarithm of scattering intensity,  $\log(I(Q))$ , of hsPxd01-con4 is given as a function of  $Q^2$  at the corresponding concentrations including fits. (B) Left panel: Pair density distributions,  $p(r)$ , plotted against the distance ( $r$ ) with 0.5 mg/mL (red dotted line), 1 mg/mL (blue dotted line) and 2 mg/mL (green dotted line) construct. Right panel: Pair density distribution  $p(r)$  from the SAXS model (red dotted line),  $p(r)$  of the monomer and trimer from the homologous models (blue lines) and  $p(r)$  with 1 mg/mL (green dotted line) plotted against  $r$ . (C) The  $I(Q) Q^{3-D^*}$  ( $D = 3-D^*$ ) which are the scale corrected scattering data of different protein concentrations (0.5 mg/mL, red), (1 mg/mL, blue), (2 mg/mL, green) are plotted against the scattering vector ( $Q$ ) [ $D^* = 2.77$  (pH 5, red), 2.71 (pH 7.4, blue), 2.54 (pH 9, green)]. Insert: Linear double logarithmic plot with the slope,  $D$  of  $I(Q)$ . (D) Left panel: pair density distribution  $p(r)$  computed from scale corrected data at different pH plotted against the distance ( $r$ ). Right panel: Pair density distribution at different construct concentrations,  $p(r)$  of the monomer and trimer model from the homologous models (blue lines) and  $p(r)$  at pH 7.4 (blue dotted line) plotted against the distance ( $r$ ). Colour code as in (B).

terminal poly-histidine tag was introduced with the individual forward primers as stated below. The forward and reverse primer pairs used for the preparation of the respective constructs were: 5'-ATCGCTAGCCA TCATCACCATCACCATCACCATCTGGAAGTACTTTTCAGGGGCCCCCGGATCACCTCCGAGCCCCAGGACGCAGA-TGTGACC-3' and 5'-ATGC GCGGCCGCTTATCAATGGT GATGGTGATGATGGTCCTGCCACA -CCC GGAGGTCCACCCTGGG-3' for hsPxd01-con4 which features a His<sub>8</sub>-tag and a HRV-3C cleavage site for tag removal [4]; 5'-GCTCTGGGTT CCAGTTCCACTGGCCATCATCACCATCACCATGGAGATCCGTTTGTA GCTACCTCCATCG-3' and 5'-GCCAGAGGTCGAGGTCGGGGGATCCTTA TCAGTCTGCCACACCCGGAGG TCCACCCTGGG-3' for hsPxd01-con5; same forward primer as for hsPxd01-con5 and reverse primer 5'-GCCAGAGGTCGAGGTCGGGGGATCCTTATCAACTGAGCCGTGATTC AAGTTTCTTTATC-3' for hsPxd01-con5-helix; same forward primer as for hsPxd01-con5 and reverse primer 5'-GCCAGAGGTCGAGGTCGGGG GATCCTTATCAGGCATTGAACTGCCCCCTGGTCTACAGTCTTCAC AGC-3' for hsPxd01-con5-cys; same forward primer as for hsPxd01-con5 and reverse primer 5'-GCCAGAGGTCGAGGTCGGGGGATCCTTAT CAGGCTTTTCTCCGCCCTCTTCTGTAAGCAGACTGG-3' for hsPxd01-con5-VVC.

*Escherichia coli* Top10 cells were used for plasmid preparation and all respective constructs were validated by DNA sequencing. Transient transfection and expression of peroxidasin constructs was described previously [4].

#### 4.2. Purification of peroxidasin constructs

The cell supernatant was harvested and filtrated with a 0.45  $\mu$ m PVDF membrane (Durapore) and stored at  $-30^\circ\text{C}$  until further processing. After thawing the supernatant was stirred for 48 h at  $4^\circ\text{C}$  before the volume was decreased ( $\sim 25$  times) and the cell culture medium was replaced with 100 mM phosphate buffer pH 7.4 using a Millipore Labscale™ TFF System diafiltration. 5 mL His-Trap™ FF columns (GE Healthcare and Life Sciences) loaded with nickel chloride were used for the purification of the respective peroxidasin variants. The column was equilibrated with 100 mM phosphate buffer pH 7.4 containing 1 M NaCl and 5 mM imidazole. The sample was adjusted to 1 M NaCl and 5 mM imidazole before loading and the column was washed with equilibration buffer after sample loading. The protein was eluted by applying two consecutive gradients of 0–7% (2 mL/min, 10 min) and 7–70% (1 mL/min, 50 min) of 100 mM phosphate buffer pH 7.4 containing 500 mM NaCl and 500 mM imidazole. Eluted fractions were analyzed by UV-visible spectroscopy, SDS-PAGE and Western blotting following standard procedures (Penta-His Antibody, BSA-free from Qiagen; Anti-mouse antibody, alkaline phosphatase conjugated). Enhanced chemiluminescence was used for the detection of covalent heme to protein linkages as described earlier [4]. Fractions were pooled accordingly and concentrated in a 10 kDa MWCO dialysis tubing (SnakeSkin™, Thermofisher) by applying PEG (20 kDa) to the outside of the tubing. Subsequently the sample was dialysed against 100 mM phosphate buffer

pH 7.4 and stored at  $-30^{\circ}\text{C}$ .

#### 4.3. Quantification of hsPxd01-constructs

Specified concentrations were always related to protein concentrations using a molar extinction coefficient at 280 nm. For hsPxd01-con4 and hsPxd01-con5 the molar extinction coefficient at 280 nm were determined to be  $147500\text{ M}^{-1}\text{ cm}^{-1}$  and  $115600\text{ M}^{-1}\text{ cm}^{-1}$ , respectively. For hsPxd01-con5-cys the same extinction coefficient as for hsPxd01-con5 was used. Molar concentrations of hsPxd01-con5-helix and hsPxd01-con5-VWC were determined using an extinction coefficient at 280 nm of  $117000\text{ M}^{-1}\text{ cm}^{-1}$  and  $123000\text{ M}^{-1}\text{ cm}^{-1}$ , respectively.

#### 4.4. Preparative size exclusion chromatography (SEC)

Concentrated affinity purified peroxidase constructs were further purified by loading onto a HighLoad 16/600 Superdex 200 prep grade (GE Healthcare and Life Sciences) to obtain a highly monodisperse protein, which is a prerequisite for all light scattering methods as well as for SAXS measurements. A flow rate of 1 mL/min was applied and 20 mM phosphate buffer containing 500 mM NaCl adjusted to pH 7.4 was used. The respective monomeric peak fractions were pooled and concentrated using 15 mL Amicon Ultra-15 centrifugal filter units (Millipore) with a molecular weight cut off of 100 kDa for hsPxd01-con5-helix and hsPxd01-con5-VWC and a 50 kDa cut off for the two other variants. For smaller volumes Amicon Ultra-0.5 centrifugal filter units (Millipore) were used. In order to avoid aggregate formation protein solutions were not concentrated any higher than 1 mg/mL and snap frozen in liquid nitrogen and stored at  $-80^{\circ}\text{C}$  if not used freshly for further experiments.

#### 4.5. HPLC-size exclusion chromatography and MALS analysis of monodisperse protein samples

Purified protein samples were further analyzed by HPLC SEC chromatography coupled to detectors of UV-visible and multi-angle light scattering (MALS). For instrumentation, HPLC (Shimadzu prominence LC20) and MALS (WYATT Helios Dawn8+ plus QELS; software ASTRA 6) were used. Columns were WYATT SEC Columns ( $7.8 \times 5$  and  $7.8\text{ mm} \times 300\text{ mm}$ ; particle size  $5\text{ }\mu\text{m}$ , pore size  $300\text{ }\text{\AA}$ ) with corresponding guard column (WTC030S5G). The SEC buffer used was Dulbecco's PBS plus 200 mM NaCl at a flow rate of 0.5 mL/min and  $20\text{ }\mu\text{g}$  of protein was injected for each run.

#### 4.6. Dynamic light scattering (DLS)

DLS was utilized to ensure monodispersity of the samples under the same conditions as used for subsequent SAXS measurements (1 mg/mL protein in PBS buffer pH 7.4). DLS is a widely used technique to measure the size and dispersity of proteins, particles and other molecules in solution. The translational diffusion coefficient ( $D_T$ ) of particle movement is determined by measuring dynamic fluctuations of light scattering intensity which is caused by the Brownian motion of the particle [23]. This method provides a hydrodynamic radius ( $R_h$ ) to be calculated via the Stokes-Einstein equation. For instrumentation a DynaPro NanoStar™ (Wyatt Technology) was employed using disposable cuvettes (Wyatt Technology). The samples were filtered prior to the measurement using  $0.02\text{ }\mu\text{m}$  Whatman Anotop syringe filters.

#### 4.7. Rotary shadowing (RS) and transmission electron microscopy (TEM)

Samples with a concentration of 0.1 mg/mL in 50 mM phosphate buffer pH 7.4 were diluted to a final concentration of  $50\text{ }\mu\text{g/mL}$  in spraying buffer, containing 100 mM ammonium acetate and 30% ( $v/v$ ) glycerol, pH adjusted to 7.4. After dilution, the samples were sprayed

onto freshly cleaved mica chips (Christine Gröpl, Austria) and immediately transferred into a BAL-TEC MED020 high vacuum evaporator (BAL-TEC, Liechtenstein) equipped with electron guns. The rotating samples were coated with 0.6 nm Platinum (BALTIC, Germany) at an angle of  $5-6^{\circ}$ , followed by 6 nm Carbon (Balzers, Liechtenstein) at  $90^{\circ}$ . The obtained replicas were floated off from the mica chips, picked up on 400 mesh Cu/Pd grids (Agar Scientific, UK), and inspected in an FEI Morgagni 268D TEM (FEI, The Netherlands) operated at 80 kV. Images were acquired using an 11 megapixel Morada CCD camera (Olympus-SIS, Germany).

#### 4.8. Small-angle X-ray scattering (SAXS)

In the present work we interpreted the scattering data in terms of fractal pair densities. For details about deduction of the working equation please see Supplemental Material. In order to access the respective pair density distribution we minimized the  $L_2$  norm of

$$\min \|Q(I(Q) - \mathcal{F}(p(\lambda r))[Q]Q^{D-3})\|_2$$

with  $I(Q)$  resembling the scattering intensity,  $\mathcal{F}(p(\lambda r))[Q]$  the Fourier transform of the pair density,  $\lambda$  indicating the scaling factor,  $D$  reflecting the fractal dimension and  $Q$  the scattering wave vector. All peroxidase constructs were measured at a concentration of 1 mg/mL at pH 5, pH 7.4 and pH 9 to investigate the effect of charge on protein interactions. Scattering intensities of hsPxd01-con4 were also measured at different variant concentrations (0.5 mg/mL, 1 mg/mL and 2 mg/mL) to analyze possible pair wise interactions.

For three-dimensional reconstruction we applied different state-of-the-art techniques. First we followed a typical approach and computed ab initio models with the programs GNOM and DAMMIN [18,19], that resulted in considerably rough models which unfortunately could be vaguely interpreted in terms of individual domains.

Complementary, as we generated homologous three-dimensional models in particular for hsPxd01-con5 and individual Ig domains, we could speculate that (if the individual arrangements of these domains were known) we could recover the experimental pair density distribution and thus compute the corresponding scattering intensity. Consequently, we joined the individual con5 domains via the identified residues Cys736 and Cys1315 and formed a 3D model (Fig. 7). While the shapes of the con5 domains were kept constant, the amino acids that joined the individual domains were randomly bent to allow for different possible conformations. For each conformation we computed the pair density distribution. Following the theoretical section in the Supplemental Material we assumed that the pair density distribution was re-scalable by a factor  $\lambda$  and the fractal dimension  $D$ . Therefore we coded a search algorithm that took into account the effect of scaling. This search algorithm sampled different conformations and stopped if the RMS of the pair density distributions computed from the 3D model and computed from the scattering data dropped below a given threshold. The benefit of this approach was that it enabled an interpretation of scattering data at a much higher model detail. We only changed the arrangement of domains and thus were limited in the possible models. For the final refinement we varied weights of the scattering sites. Stable regions were heavy weighted whereas flexible regions were lower weighted. In terms of potentials this meant that heavy weight scattering sites may be sites with high electronic contrast and strong scattering potential and low weighted scattering sites may be sites of low electronic contrast and thus weak scattering potential.

#### Acknowledgements

This work was supported by the Austrian Science Fund, FWF [Doctoral Program BioToP-Molecular Technology of Proteins (W1224) and project P25538], the Federal Ministry for Digital and Economic Affairs (BMWD), the Federal Ministry for Transport, Innovation and Technology (BMVT), the Styrian Business Promotion Agency SFG, the

Standortagentur Tirol, Government of Lower Austria and ZIT - Technology Agency of the City of Vienna through the COMET-Funding Program managed by the Austrian Research Promotion Agency FFG. The funding agencies had no influence on the conduct of this research.

Rotary shadowing and TEM was performed by the EM Facility of the Vienna Biocenter Core Facilities GmbH (VBCF), member of Vienna Biocenter (VBC), Austria.

#### Declaration of Competing Interest

None.

#### Appendix A. Supplementary data

Supplementary data to this article can be found online at <https://doi.org/10.1016/j.bbapap.2019.07.002>.

#### References

- [1] M. Zámocký, C. Jakopitsch, P.G. Furtmüller, C. Dunand, C. Obinger, The peroxidase-cyclooxygenase superfamily: reconstructed evolution of critical enzymes of the innate immune system, *Proteins* 72 (2008) 589–605.
- [2] M. Zámocký, S. Hofbauer, I. Schaffner, B. Gasselhuber, A. Nicolussi, M. Soudi, K.F. Pirker, P.G. Furtmüller, C. Obinger, Independent evolution of four heme peroxidase superfamilies, *Arch. Biochem. Biophys.* 574 (2015) 108–119.
- [3] R.E. Nelson, L.I. Fessler, Y. Takagi, B. Blumberg, D.R. Keene, P.F. Olson, C.G. Parker, J.H. Fessler, Peroxidasin: a novel enzyme-matrix protein of *Drosophila* development, *EMBO J.* 13 (15) (1994) 3438–3447.
- [4] M. Soudi, M. Paumann-Page, C. Delporte, K.F. Pirker, M. Bellei, E. Edenhofer, G. Stadlmayr, G. Battistuzzi, K.Z. Boudjeltia, P.G. Furtmüller, P. Van Antwerpen, C. Obinger, Multidomain human peroxidasin 1 is a highly glycosylated and stable homotrimeric high spin ferric peroxidase, *J. Biol. Chem.* 290 (17) (2015) 10876–10890.
- [5] E. Lázár, Z. Péterfi, G. Sirokmány, H.A. Kovács, E. Klement, K.F. Medzihradzky, M. Geiszt, Structure-function analysis of peroxidasin provides insight into the mechanism of collagen IV crosslinking, *Free Radic. Biol. Med.* 83 (2015) 273–282.
- [6] G. Bhave, C.F. Cummings, R.M. Vanacore, C. Kumagai-Cresse, I.A. Ero-Tolliver, M. Rafi, J.-S. Kang, V. Pedchenko, L.I. Fessler, J.H. Fessler, B.G. Hudson, Peroxidasin forms sulfilimine chemical bonds using hypohalous acids in tissue genesis, *Nat. Chem. Biol.* 8 (9) (2012) 784–790.
- [7] A.S. McCall, C.F. Cummings, G. Bhave, R. Vanacore, A. Page-McCaw, B.G. Hudson, Bromine is an essential trace element for assembly of collagen IV scaffolds in tissue development and architecture, *Cell* 157 (6) (2014) 1380–1392.
- [8] I.A. Ero-Tolliver, B.G. Hudson, G. Bhave, The ancient immunoglobulin domains of peroxidasin are required to form sulfilimine cross-links in collagen IV, *J. Biol. Chem.* 290 (35) (2015) 21741–21748.
- [9] A.L. Fidler, R.M. Vanacore, S.V. Chetyrkin, V.K. Pedchenko, G. Bhave, V.P. Yin, C.L. Stothers, K.L. Rose, W.H. McDonald, T.A. Clark, D.-B. Borza, R.E. Steele, M.T. Ivy, J.K. Hudson, B.G. Hudson, A unique covalent bond in basement membrane is a primordial innovation for tissue evolution, *Proc. Natl. Acad. Sci.* 111 (1) (2014) 331–336.
- [10] M. Paumann-Page, R.S. Katz, M. Bellei, I. Schwartz, E. Edenhofer, B. Sevcnikar, M. Soudi, S. Hofbauer, G. Battistuzzi, P.G. Furtmüller, C. Obinger, Pre-steady-state kinetics reveal the substrate specificity and mechanism of halide oxidation of truncated human peroxidasin 1, *J. Biol. Chem.* 292 (11) (2017) 4583–4592.
- [11] H. Medfai, A. Khalil, A. Rousseau, V. Nuyens, M. Paumann-Page, B. Sevcnikar, P.G. Furtmüller, C. Obinger, N. Moguilevsky, O. Peulen, M. Herfs, V. Castronovo, M. Amri, P. Van Antwerpen, L. Vanhamme, K.Z. Boudjeltia, Human peroxidasin 1 promotes angiogenesis through ERK1/2, Akt, and FAK pathways, *Cardiovasc. Res.* 115 (2) (2019) 463–475.
- [12] M. Soudi, M. Zámocký, C. Jakopitsch, P.G. Furtmüller, C. Obinger, Molecular evolution, structure, and function of peroxidasins, *Chem. Biodivers.* 9 (2012) 1776–1793.
- [13] S. Colon, G. Bhave, Proprotein convertase processing enhances peroxidasin activity to reinforce collagen IV, *J. Biol. Chem.* 291 (46) (2016) 24009–24016.
- [14] R. Feissner, Y. Xiang, R.G. Kranz, Chemiluminescent-based methods to detect subpicomole levels of c-type cytochromes, *Anal. Biochem.* 315 (1) (2003) 90–94.
- [15] A.K. Singh, N. Singh, S. Sharma, S.B. Singh, P. Kaur, A. Bhushan, A. Srinivasan, T.P. Singh, Crystal structure of lactoperoxidase at 2.4 Å resolution, *J. Mol. Biol.* 376 (4) (2008) 1060–1075.
- [16] T.J. Fiedler, C.A. Davey, R.E. Fenna, X-ray crystal structure and characterization of halide-binding sites of human myeloperoxidase at 1.8 Å resolution, *J. Biol. Chem.* 275 (16) (2000) 11964–11971.
- [17] I. Grishkovskaya, M. Paumann-Page, R. Tscheliessnig, J. Stampfer, S. Hofbauer, M. Soudi, B. Sevcnikar, C. Oostenbrink, P.G. Furtmüller, K. Djinović-Carugo, W.M. Nauseef, C. Obinger, Structure of human promyeloperoxidase (proMPO) and the role of the propeptide in processing and maturation, *J. Biol. Chem.* 292 (20) (2017) 8244–8261.
- [18] D.I. Svergun, Determination of the regularization parameter in indirect-transform methods using perceptual criteria, *J. Appl. Crystallogr.* 25 (1992) 495–503.
- [19] D.I. Svergun, Restoring low resolution structure of biological macromolecules from solution scattering using simulated annealing, *Biophys. J.* 76 (6) (1999) 2879–2886.
- [20] B. Bathish, R. Turner, M. Paumann-Page, A.J. Kettle, C.C. Winterbourn, Characterisation of peroxidasin activity in isolated extracellular matrix and direct detection of hypobromous acid formation, *Arch. Biochem. Biophys.* 646 (2018) 120–127.
- [21] M. Hansson, I. Olsson, W.M. Nauseef, Biosynthesis, processing, and sorting of human myeloperoxidase, *Arch. Biochem. Biophys.* 445 (2) (2006) 214–224.
- [22] P.G. Furtmüller, M. Zederbauer, W. Jantschko, J. Helm, M. Bogner, C. Jakopitsch, C. Obinger, Active site structure and catalytic mechanisms of human peroxidases, *Arch. Biochem. Biophys.* 445 (2) (2006) 199–213.
- [23] K.S. Schmitz, *An Introduction to Dynamic Light Scattering by Macromolecules*, 1990 Academic Press, Boston, 1990.

# Human peroxidase 1 promotes angiogenesis through ERK1/2, Akt, and FAK pathways

Hayfa Medfai, Alia Khalil, Alexandre Rousseau, Vincent Nuyens, Martina Paumann-Page, **Benjamin Sevcnikar**, Paul G Furtmüller, Christian Obinger, Nicole Moguilevsky, Olivier Peulen, Michael Herfs, Vincent Castronovo, Mohamed Amri, Pierre Van Antwerpen, Luc Vanhamme, and Karim Zouaoui Boudjeltia

Research Article

Cardiovascular Research, Volume 115, Issue 2, , Pages 463–475, 01  
February 2019  
DOI: 10.1093/cvr/cvy179

# Human peroxidasin 1 promotes angiogenesis through ERK1/2, Akt, and FAK pathways

Hayfa Medfai<sup>1,2</sup>, Alia Khalil<sup>1</sup>, Alexandre Rousseau<sup>1</sup>, Vincent Nuyens<sup>1</sup>,  
Martina Paumann-Page<sup>3</sup>, Benjamin Sevcnikar<sup>3</sup>, Paul G. Furtmüller<sup>3</sup>,  
Christian Obinger<sup>3</sup>, Nicole Moguelevsky<sup>1</sup>, Olivier Peulen<sup>4</sup>, Michael Herfs<sup>5</sup>,  
Vincent Castronovo<sup>4</sup>, Mohamed Amri<sup>2</sup>, Pierre Van Antwerpen<sup>6</sup>,  
Luc Vanhamme<sup>7†</sup>, and Karim Zouaoui Boudjeltia<sup>1\*†</sup>

<sup>1</sup>Laboratory of Experimental Medicine (ULB 222 Unit), Faculté de Médecine, CHU de Charleroi, A. Vésale Hospital, Université Libre de Bruxelles, Hôpital André Vésale, 706, Rue de Gozée, 6110 Montigny-le-Tilleul, Charleroi, Belgium; <sup>2</sup>Department of Biological Sciences, Laboratory of Functional Neurophysiology and Pathology, UR/11ES09, Université de Tunis El Manar, Faculté des Sciences de Tunis, 20 Rue de Tolède, 2092 Manar II, Tunis, Tunisia; <sup>3</sup>Division of Biochemistry, Department of Chemistry, BOKU, University of Natural Resources and Life Sciences, Muthgasse 18, A-1190 Vienna, Austria; <sup>4</sup>Metastasis Research Laboratory, Giga-Cancer, University of Liege, Quartier Hopital, Avenue de l'Hopital, 11, 4000 Liège, Belgium; <sup>5</sup>Department of Pathology, Laboratory of Experimental Pathology, Giga-Cancer, University of Liege, Quartier Hopital, Avenue de l'Hopital, 11, 4000 Liège, Belgium; <sup>6</sup>Pharmacognosy, Bioanalysis and Drug Discovery and Analytical Platform of the Faculty of Pharmacy, Faculty of Pharmacy, Université Libre de Bruxelles, Campus de la plaine CP205/09, Boulevard du Triomphe, 1050 Bruxelles, Belgium; and <sup>7</sup>Laboratory of Molecular Parasitology, IBMM, Faculty of Sciences, Université Libre de Bruxelles, Rue Adrienne Bolland 8, 6041 Gosselies, Belgium

Received 12 April 2018; revised 4 June 2018; editorial decision 29 June 2018; accepted 3 July 2018; online publish-ahead-of-print 4 July 2018

Time for primary review: 23 days

## Aims

The term angiogenesis refers to sprouting of new blood vessels from pre-existing ones. The angiogenic process involves cell migration and tubulogenesis requiring interaction between endothelial cells and the extracellular matrix. Human peroxidasin 1 (hsPxd01) is a multidomain heme peroxidase found embedded in the basement membranes. As it promotes the stabilization of extracellular matrix, we investigated its possible role in angiogenesis both *in vitro* and *in vivo*.

## Methods and results

We analysed the effects of peroxidasin 1 gene silencing and supplementation by recombinant hsPxd01 in TeloHAEC endothelial cells on cell migration, tubulogenesis in matrigel, and intracellular signal transduction as assessed by kinase phosphorylation and expression of pro-angiogenic genes as measured by qRT-PCR. We further evaluated the angiogenic potential of recombinant peroxidasin in a chicken chorioallantoic membrane model. RNA silencing of endogenous hsPxd01 significantly reduced tube formation and cell migration, whereas supplementation by the recombinant peroxidase promoted tube formation *in vitro* and stimulated vascularization *in vivo* through its catalytic activity. Moreover, recombinant hsPxd01 promoted phosphorylation of Extracellular signal-Regulated Kinases (ERK1/2), Protein kinase B (Akt), and Focal Adhesion Kinase (FAK), and induced the expression of pro-angiogenic downstream genes: Platelet Derived Growth Factor Subunit B (PDGFB), endothelial-derived Heparin Binding EGF-like growth factor (HB-EGF), CXCL-1, Hairy-Related Transcription Factor 1 (HEY-1), DNA-binding protein inhibitor (ID-2), Snail Family Zinc Finger 1 (SNAIL-1), as well as endogenous hsPxd01. However, peroxidasin silencing significantly reduced Akt and FAK phosphorylation but induced ERK1/2 activation after supplementation by recombinant hsPxd01. While hsPxd01 silencing significantly reduced expression of HEY-1, ID-2, and PDGFB, it did not affect expression of SNAIL-1, HB-EGF, and CXCL-1 after supplementation by recombinant hsPxd01.

## Conclusion

Our findings suggest a role of enzymatically active peroxidasin 1 as a pro-angiogenic peroxidase and a modulator of ERK1/2, Akt and FAK signalling.

## Keywords

Human peroxidasin 1 • Angiogenesis • Extracellular-signal-regulated kinase 1/2 • Akt • Focal adhesion kinase

\* Corresponding author. Tel: +32 71 924705; fax: +32 71 92 47 10, E-mail: kzouaoui@ulb.ac.be

† The last two authors are co-directors of this work.

Published on behalf of the European Society of Cardiology. All rights reserved. © The Author(s) 2018. For permissions, please email: journals.permissions@oup.com.

## 1. Introduction

During angiogenesis, new blood vessels sprout from pre-existing ones. This mechanism requires the co-ordination of multiple steps that involve dynamic interactions between endothelial cells, vascular smooth muscle cells, pericytes, extracellular matrix, and vascular growth factors.<sup>1</sup> Once proangiogenic factors activate endothelial surface receptors, proteases are released into the extracellular space to degrade the basement membrane underlying the endothelium. Subsequently, endothelial cells proliferate, migrate and differentiate into a capillary-like tube network.<sup>2,3</sup> As for many epithelias, the endothelium is supported by the basement membrane, a specialized form of extracellular matrix. Blood vessels sprouting is partially regulated by this basement membrane.<sup>4</sup> Indeed, the dynamic remodelling of the extracellular matrix, and its interactions with endothelial cells regulate sprouts behaviour during the different stages of angiogenesis including endothelial capillary morphogenesis and cell migration.<sup>5–8</sup> Under physiological conditions, angiogenesis is driven by a balance between pro- and anti-angiogenic factors, that regulate embryonic development, organ growth, wound healing, and reproduction.<sup>3,9</sup> However, the disruption of this angiogenic balance, leads to an abnormal vascularization that can contribute to pathological conditions including inflammation, autoimmune diseases, and cancer.<sup>10</sup>

Human peroxidase 1 (hsPxd01) has recently been shown to contribute to stabilization and stiffness of this basement membrane. The multi-domain heme peroxidase was originally found to be expressed in the cardiovascular system, but nowadays is known to be widely expressed.<sup>11–14</sup> The metalloenzyme is secreted into the extracellular space and the circulating plasma and embedded in the basement membranes.<sup>11,14</sup> In addition, a study has demonstrated the localization of peroxidase 1 within the endoplasmic reticulum and in the cell surface of Cos 7 cells expressing human recombinant peroxidase.<sup>15</sup> Peroxidase 1 belongs to Family 2 of the peroxidase-cyclooxygenase superfamily.<sup>16</sup> It is a homotrimeric highly glycosylated heme enzyme which—in addition to the catalytic peroxidase domain—comprises a leucine-rich repeat domain (LRR), four C-like immunoglobulin domains (Ig) at the N-terminus, and a C-terminal von Willebrand factor type C module (VWC).<sup>17</sup> Those non-catalytic domains are known to mediate protein-protein interactions.<sup>18</sup>

Peroxidase 1 was originally described as an enzyme essential for extracellular matrix consolidation and structural tissue integrity during the early steps of embryogenesis and larval development in *Drosophila melanogaster*.<sup>19</sup> This was related to its capacity to catalyze the formation of sulfilimine bonds (S=N) in the NC1 hexamers of collagen IV, the predominant constituent of basement membrane.<sup>15,20,21</sup> The biosynthesis of these covalent bonds was shown to depend on the presence of hydrogen peroxide and bromide.<sup>20,21</sup> Furthermore, recent studies have demonstrated the correlation between clinical conditions such as congenital cataract, corneal opacity, and developmental glaucoma; and hsPxd01 mutations that affect the immunoglobulin and the peroxidase domains,<sup>22</sup> suggesting a crucial role for hsPxd01 in the stabilization of the ocular basement membrane. Finally, hsPxd01 has been identified as a glioma, melanoma, and renal carcinoma marker or determinant,<sup>23,24</sup> suggesting its possible involvement in the regulation of tumour angiogenesis.

During angiogenesis, endothelial cells interact with extracellular matrix components, and form filopodia or lamellipodia. This process initially involves proteolytic degradation of the extracellular matrix, which allows endothelial cells to proliferate and invade the extracellular matrix. The latter establish capillary tubules covered with a newly assembled basement membrane matrix, providing stabilization for the neoformed

vessels. As a consequence, this delicate balance between degradation and assembly of the extracellular matrix is critical for an optimal angiogenic response.<sup>25,26</sup> The angiogenic mechanism is mimicked in culture by the formation of tubule-like structures, a process called tubulogenesis.<sup>27,28</sup>

Although the enzymatic role of hsPxd01 in extracellular matrix remodelling is already characterized to some extent, its direct involvement in angiogenesis is not documented. This role has been proposed for homologous Family 1 peroxidases such as myeloperoxidase (MPO) and eosinophil peroxidase (EPO),<sup>29</sup> which are composed of peroxidase domains only and are typically stored within granules in leukocytes. This prompted us to investigate whether hsPxd01 is implicated in the regulation of the angiogenic process. In this article, we demonstrate that hsPxd01 exhibits a pro-angiogenic function both *in vitro* and *in vivo* through the modulation of ERK1/2, Akt, and Focal Adhesion Kinase (FAK) signalling pathways.

## 2. Methods

### 2.1 Cell culture

hTERT immortalized human aortic endothelial cells (TeloHAEC) were purchased from ATCC, and cultivated at 37°C, 5% CO<sub>2</sub> in vascular cell basal medium (ATCC), supplemented with vascular endothelial cell growth kit-VEGF (ATCC).

### 2.2 Cell transfection

TeloHAEC were grown to 70% confluency, and transiently transfected with universal negative control siRNA or siRNA targeting human hsPxd01 (Sigma), using GeneXPlus transfection reagent (ATCC). Cells were incubated at 37°C, 5% CO<sub>2</sub> for 48 h in culture medium devoid of heparin sulfate and antibiotics.

### 2.3 Cloning, expression, and purification of full length hsPxd01 and truncated constructs

Full length hsPxd01 was expressed and purified from a stable transfected HEK293 cells as described previously by Soudi et al.<sup>17</sup> DNA of hsPxd01-con4 (uniprotkb: Q92626, residues Pro246-Asp1314) was cloned into a modified gWiz vector (Genlantis) carrying an N-terminal His6 tag for protein purification.

Forward and reverse polymerase chain reaction (PCR) primers for preparation of hsPxd01-con4 DNA were as follows: 5'-GAGGCT CACCACCACCATCACCATCCCCGAATCACCTCCGAGCCC-3' and 5'-TAGCCAGAAGTGATCTGGATCTCAGTCCTGCCACACCC GGAGGTC-3'.

Transformed *Escherichia coli* XL-10 cells were screened with colony-PCR. Positive clones were selected and validated by DNA sequencing. HsPxd01-con4 in gWiz vector served as template for site directed mutagenesis. In order to obtain inactive hsPxd01-con4 (hsPxd01-con4 Q823A) the highly conserved glutamine residue 823 in the active site (which is crucial for halide binding<sup>30,31</sup>) was exchanged by an alanine. Site directed mutagenesis primer were as follows: 5'-GCTGATGCA GTGGGGCGCCTTCTGGACCACGACCTCG-3' and 5'-CGAGGT CGTGGTCCAGGAAGGCGCCCCACTGCATCAGC-3'.

QuickChange Lightning Site Directed Mutagenesis Kit was used according to manufacturing guidelines (Agilent Technologies). Active and inactive hsPxd01-con4 were expressed in the HEK 293F

(Invitrogen) suspension cell system. Cells were cultivated according to the 'FreeStyle 293F-Cells User Guide' and transfected as previously described.<sup>32</sup> Heme was added to the culture medium to a final concentration of 5 µg/mL, 4 h after transfection to improve heme incorporation. Supernatants were harvested 5 days after transfection. Harvested supernatant was filtrated with a 0.45 µm PVDF membrane (Durapore) and concentrated to 100 mL using a Millipore Labscale TFF diafiltration system. Subsequently, the sample was adjusted to 1 M NaCl and 20 mM imidazole. For purification of the His6-tagged protein, 5 mL HisTrap FF columns (GE Healthcare) loaded with nickel chloride were used. After equilibration of the column with 100 mM phosphate buffer, pH 7.4, 1 M NaCl, and 20 mM imidazole, sample was loaded and washed with equilibration buffer. Protein was eluted using two consecutive step gradients of 8% and 70% of 20 mM phosphate buffer, pH 7.4, 500 mM NaCl, and 500 mM imidazole. Eluted fractions were analysed by UV-visible spectroscopy and SDS-PAGE following standard procedures. Fractions were pooled and washed for five times with 100 mM phosphate buffer, pH 7.4, using Amicon Ultra-15, 30 kDa cut-off centrifugal filters (Merck Milipore). Bromination activities were tested spectrophotometrically by measuring the halogenation of NADH as described by Soudi *et al.*<sup>17</sup>

## 2.4 Tubulogenesis assay

Angiogenesis wells (Ibidi) were coated with 10 µL of growth factor reduced matrigel (ThermoFisher), then allowed to polymerize for 30 min at 37°C. Next, 10<sup>4</sup> cells were seeded per well, incubated at 37°C, 5% CO<sub>2</sub> and observed for tubule formation after 5 h. Pictures were taken from different fields with the ×10 objective using phase contrast microscopy (Nikon, Eclipse Ti). Vessel morphometric parameters including length of vessels and density of junctions were measured using AngioTool software.

## 2.5 Scratch assay

A total of 3 × 10<sup>4</sup> cells were seeded into two well silicone insert defining a cell-free gap (Ibidi) and incubated overnight in growth medium at 37°C, 5% CO<sub>2</sub> to allow cell attachment. Inserts were then removed allowing cells to migrate and fill the gap, and fresh growth medium was added. Photographs were taken from different fields with the ×10 objective using light microscopy (PixelINK PL-A642 Megapixel FireWire Camera). The cell-free wound surface was measured using the ImageJ software.

## 2.6 Cell proliferation assay

Cell proliferation was evaluated using Cell Proliferation Reagent WST-1 (Sigma) based on the measurement of the glycolytic production of NADH directly correlated to the number of active cells. A total of 25 × 10<sup>3</sup> cells were cultured in growth medium (5% CO<sub>2</sub>) for 24 h at 37°C, and 10 µL of WST-1 reagent were added per well.

## 2.7 Chicken chorioallantoic membrane angiogenesis assay

Fertilized eggs were opened at embryonic day E3. On embryonic day E7, 3 mm sterile PVA microsphere (Netcell surgical sponge Ref 30–380) loaded with 20 µL of full length hsPxd01, both active and inactive hsPxd01-con4 (C4 active and C4 inactive) at a concentration of 1 µM, were laid onto the egg chorioallantoic membrane. Vehicle or VEGF (5 µg/mL) (Sigma) were used as negative and positive controls, respectively. At embryonic day E10, chicken chorioallantoic membranes (CAMs) were collected. After image binarization, blood vessel density

(relative % of blood vessel area) and length density (relative percentage of blood vessel length) were evaluated in a region located from 2 to 6 mm away from the microsphere boundary using Fiji. CAMs were then fixed (4% formalin) for 24 h and paraffin embedded. In order to identify blood vessels, immunohistochemical analyses were performed using the following primary antibody: anti-alpha smooth muscle actin (SMA) 1:600 (Abcam). The rabbit Envision kit (Dako, Glostrup, Denmark) was used for the secondary reaction. Five CAMs were analysed in each group. Whole tissue sections were finally digitalized (Ventana iScan HT, Ventana Medical Systems, Tucson, AZ, USA) and the relative alpha SMA-positive vessel areas were quantified by computerized counts QuPath 0.1.2 software.

## 2.8 RNA extraction and quantitative real-time-PCR

Total RNA was extracted from cells using spin columns (Qiagen) according to the manufacturer's instructions. Purity was assessed through absorption ratio (260/280 nm) measurements. One microgram of total RNA was treated with DNAase and reverse-transcribed using PrimeScript RT reagent Kit (Takara-Clontech). Quantitative real-time PCR (qRT-PCR) was performed using LightCycler<sup>®</sup> 480 SYBR Green I Master (Roche). Glyceraldehyde-3-phosphate dehydrogenase (GAPDH) was used as a housekeeping gene for gene expression quantification. The relative expression was calculated according to the comparative ΔΔCt method. Primer sequences are listed in [Supplementary material online, Table S1](#).

## 2.9 Western blot

Whole cell protein lysates were extracted in RIPA lysis buffer (Sigma) supplemented with protease inhibitor (Roche). They were centrifuged at 12 000 g, 4°C for 15 min, and protein concentration was measured using the bicinchoninic acid assay kit (ThermoFisher). Proteins were separated on SDS-PAGE under reducing conditions and transferred onto nitrocellulose membrane (GE Healthcare Life Sciences). After saturation with 5% milk, the membrane was incubated overnight at 4°C with primary antibodies: custom anti-hsPxd01 1:1000, or commercial anti-Phospho ERK1/2 1:5000, anti-total ERK 1/2 1:10 000, anti-Phospho Akt 1:5000, anti-total Akt 1:10 000, anti-Phospho FAK 1:1000, and anti-total FAK 1:1000 (Abcam), washed, incubated with (HRP-conjugated) secondary antibody for 1 h at room temperature and revealed using the ECL substrate (PerkinElmer). Monoclonal anti-β-actin-peroxidase antibody 1:80 000 (Sigma) was used for protein loading control.

## 2.10 Software tools and statistics

The AngioTool software<sup>33</sup> is an open source validated tool that allows quantifications of different morphological parameters by assessing the variation in foreground and background pixel density across a microscopic image. QuPath 0.1.2 software is an open source software for digital pathology image analysis. Image J software is a tool allowing image analysis and processing.

Data were expressed as mean ± standard error of mean (SEM). For comparison of two groups, unpaired t-test was used. Differences between multiple groups were evaluated using one-way or two-way ANOVA as appropriate, followed by Bonferroni *post hoc* test for multiple comparison. The significance level was chosen as *P*-value: <0.05 (\*), <0.01 (\*\*), and <0.001 (\*\*\*)). Experiments were repeated five times independently. All calculations were performed with GraphPad Prism 5.01.

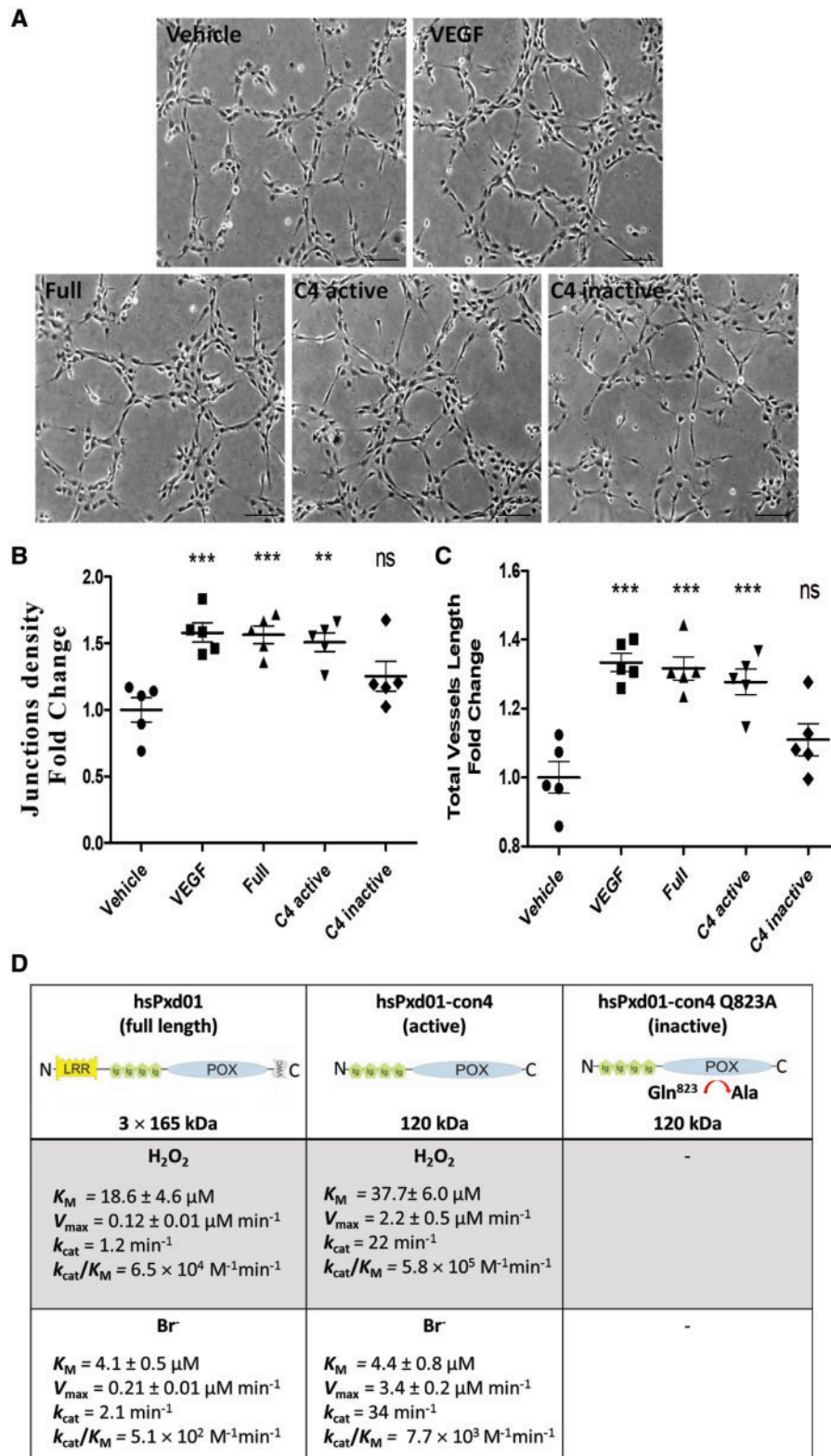


**Figure 1** Peroxidase 1 promotes tubulogenesis through its catalytic activity. (A) TeloHAEC cells ( $10^4$ ) were treated with the indicated hsPxd01 protein constructs (D) at a concentration of  $1 \mu\text{M}$ , or with VEGF-A ( $100 \text{ ng/mL}$ ) and seeded onto matrigel for 5 h. Micrographs were taken at  $\times 10$  magnification. Scale bars represent  $200 \mu\text{m}$ . (D) Domain architecture and kinetic parameters of bromination activity of full length hsPxd01 and the truncated variants. Junction density (B) and total vessels length (C) were quantified using the AngioTool software. Results are expressed as fold change over the vehicle control. Results are expressed as mean  $\pm$  SEM of five independent experiments. Statistics were analysed using one-way ANOVA, followed by Bonferroni's multiple comparison test (\*\* $P < 0.01$ , \*\*\* $P < 0.001$ ;  $n = 5$ ). ns, non-significant.

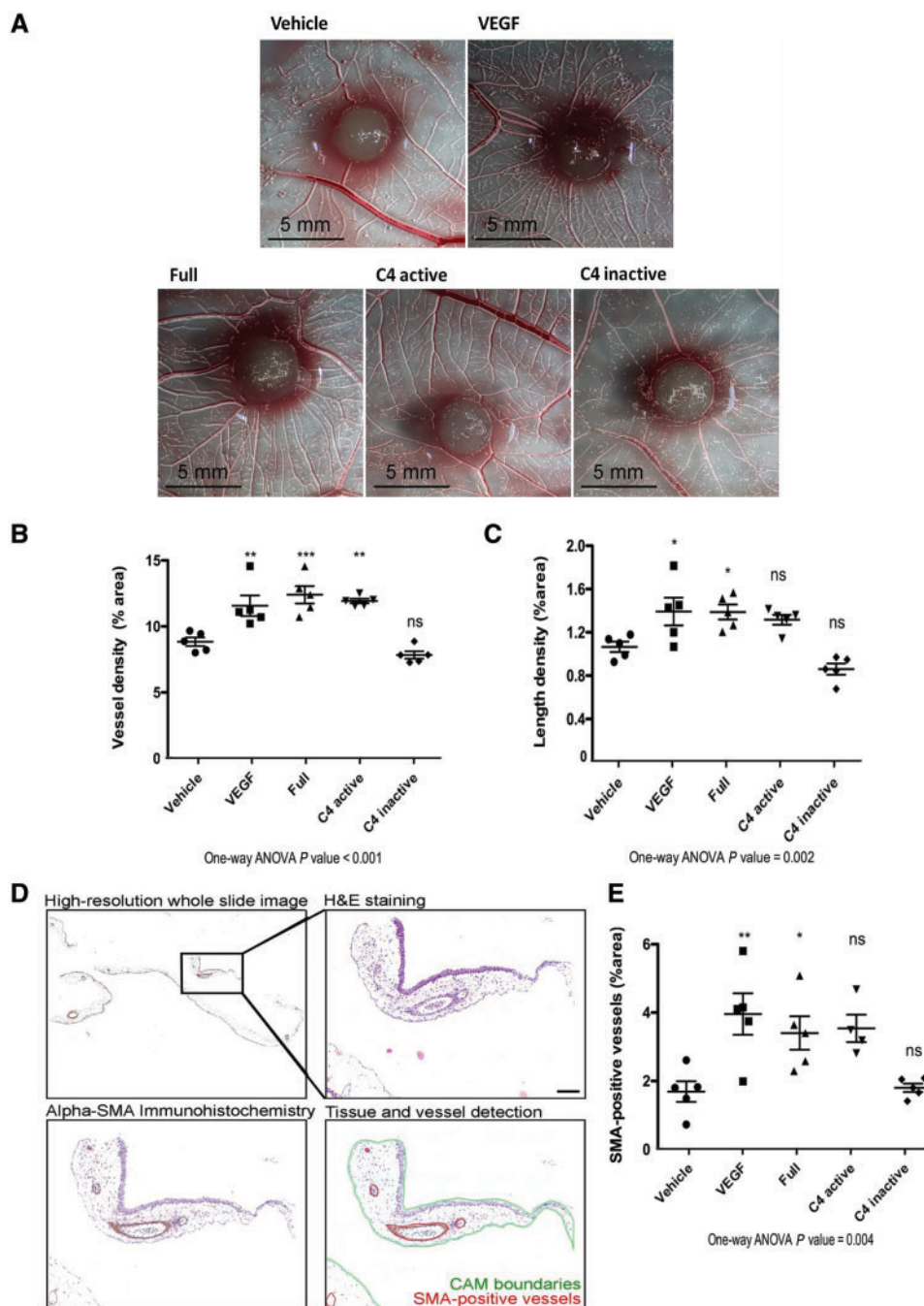


**Figure 2** Peroxidasin 1 promotes angiogenesis in the CAM assay through its catalytic activity. (A) Merge of native and binarized macroscopic images of CAM at E10. Scale bars represent 5 mm (B and C) Fiji quantification of blood vessel density (relative % of blood vessel area) and blood vessel length density (relative % of blood vessel length). (D) Quantification procedure of SMA-positive vessel in CAM. Scale bars represent 200  $\mu$ m. (E) SMA-positive vessels quantification. Results are expressed as mean  $\pm$  SEM of five independent experiments. Statistics were analysed using one-way ANOVA, followed by Bonferroni's multiple comparison test (\* $P < 0.05$ , \*\* $P < 0.01$ , \*\*\* $P < 0.001$ ;  $n = 5$ ). ns, non-significant.

## 3. Results

### 3.1 Peroxidasin 1 promotes tubulogenesis *in vitro* and *in vivo* via its catalytic activity

TeloHAEC cells were seeded on matrigel supplemented with the recombinant full length homotrimeric protein ( $3 \times 163$  kDa), and both active and

inactive monomeric (120 kDa) truncated constructs (hsPxd01-con4 and hsPxd01-con4 Q823A: C4-active and C4-inactive) at a physiological dose ( $1 \mu$ M)<sup>11</sup> for 5 h (Figure 1A). The truncated variants lack the LRR and VWC domains as schematically depicted in Figure 1D.

It has to be noted that hsPxd01 efficiently oxidizes bromide to hypobromous acid but is unable to use chloride as electron donor.<sup>17,34</sup>

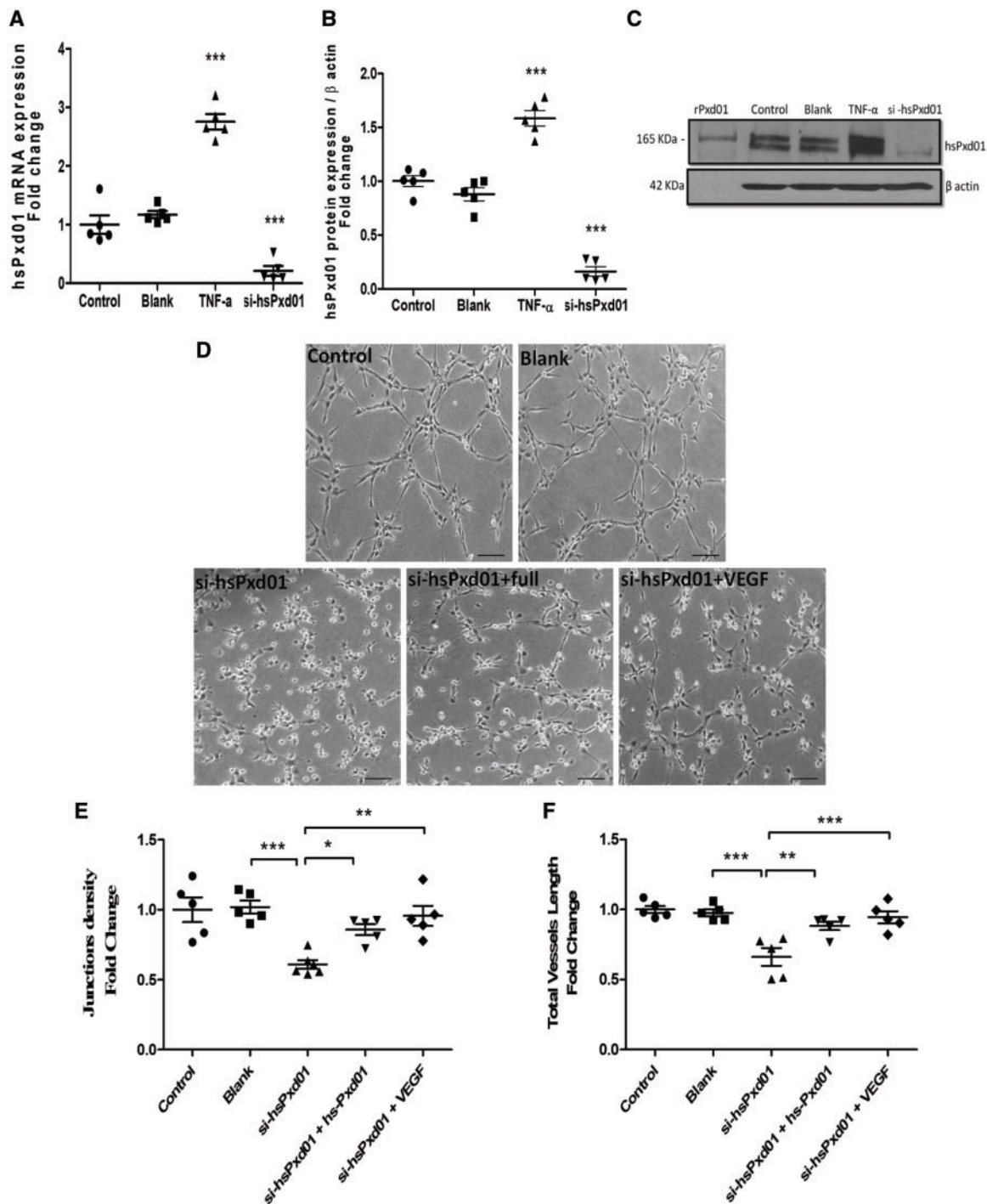


**Figure 3** Effects of knockdown of peroxidasin 1 and supplementation by recombinant hsPxd01 on tubulogenesis. (A–C) Validation of knockdown efficiency using siRNA hsPxd01 in TeloHAEC cells. TeloHAEC cells ( $8 \times 10^4$ ) were transfected with siRNA targeting human hsPxd01 (si-hsPxd01) or scrambled siRNA (Blank). (A) mRNA were extracted at 48 h post-transfection and analysed by qRT–PCR. Relative hsPxd01 mRNA expression levels were normalized to GAPDH. Results are expressed as fold change to the control. (C) Representative western blot analysis using anti hsPxd01 antibody, and quantification (graph) (B) show the drop of hsPxd01 protein level normalized to  $\beta$ -actin. Recombinant hsPxd01 (rPxd01) and TNF- $\alpha$  stimulation (10 ng/mL, 24 h) were used as positive controls. (D) Effects of hsPxd01 silencing and supplementation on tube formation. TeloHAEC cells ( $10^4$ ) were transfected with siRNA targeting hsPxd01 (si-hsPxd01) or scrambled siRNA (Blank), then treated with the full length hsPxd01 at a concentration of 1  $\mu$ M, and seeded onto matrigel for 5 h. Micrographs were taken at  $\times 10$  magnification. Scale bars represent 200  $\mu$ m. Junctions density (E) and total vessels length (F) were quantified using the AngioTool software, and expressed as fold change over the Blank. Results are expressed as mean  $\pm$  SEM of five independent experiments. Statistics were analysed using one-way ANOVA, followed by Bonferroni's multiple comparison test (\* $P < 0.05$ , \*\* $P < 0.01$ , \*\*\* $P < 0.001$ ;  $n = 5$ ).

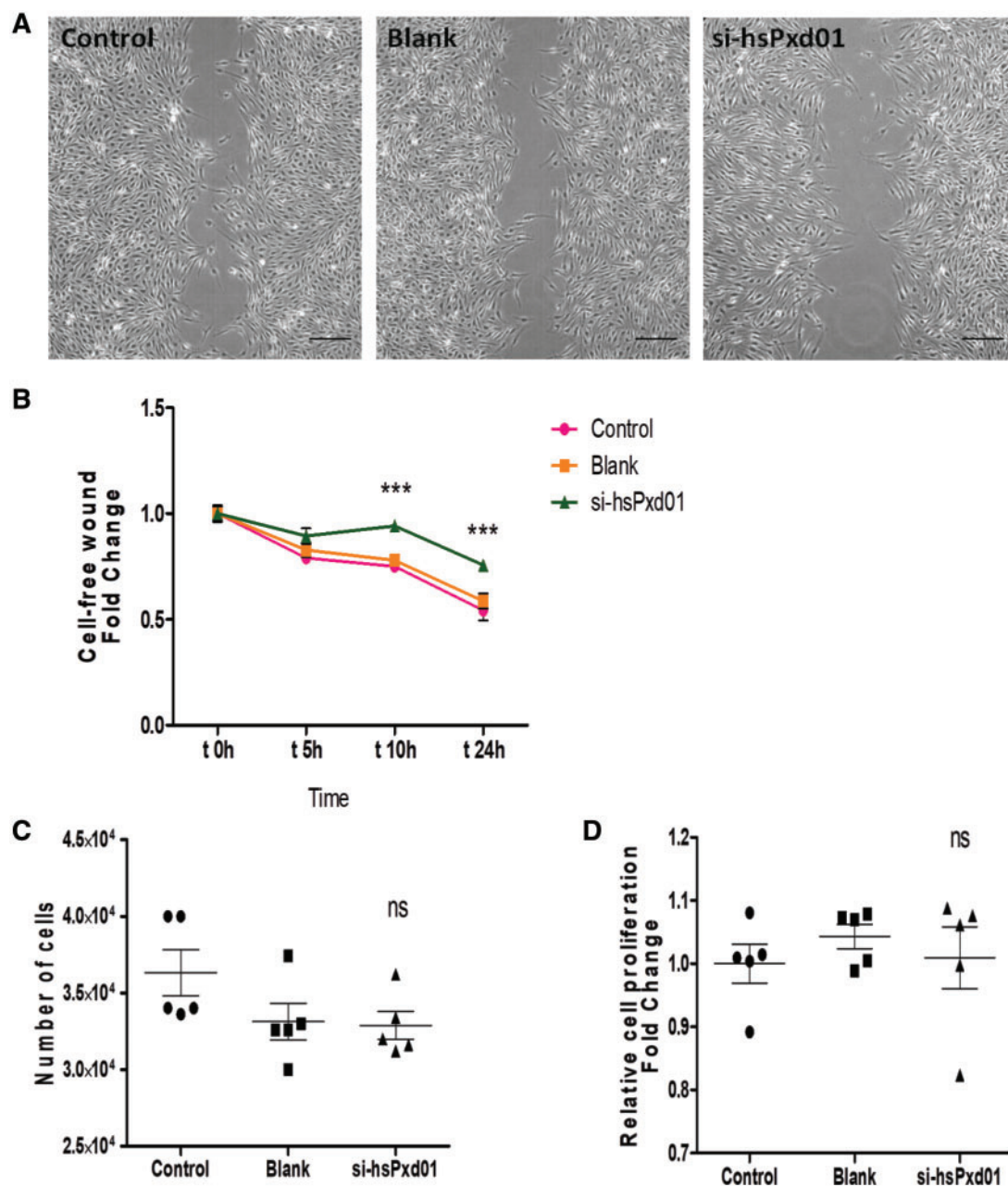


**Figure 4** Peroxidasin 1 is required for endothelial cell migration. (A) TeloHAEC cells ( $3 \times 10^4$ ) were transfected with hsPxd01 siRNA (si-hsPxd01) or scrambled siRNA (Blank), then seeded into two well culture insert and allowed to migrate for 24 h. Micrographs were taken at  $\times 10$  magnification. Scale bars represent 200  $\mu\text{m}$ . (B) The relative change in the cell-free gap surfaces was measured at different time points and expressed as fold change over the control. Cells were counted (C) and the proliferation rate was evaluated at t24 h (D). Results are expressed as fold change and are shown as mean  $\pm$  SEM of five independent experiments. Statistics were analysed using two-way ANOVA, followed by Bonferroni's multiple comparison test ( $***P < 0.001$ ;  $n = 5$ ). ns, non-significant.

The  $K_M$  values for bromide were similar for both full length homotrimeric hsPxd01 (4.1 mM) and the monomeric construct hsPxd01-con4 (4.4 mM), which reflects similar heme cavity structure, whereas the catalytic efficiency for bromide oxidation ( $k_{\text{cat}}/K_M$ ) increased upon truncation (Figure 1D).<sup>17</sup> Importantly, upon exchange of the highly conserved halide-binding glutamine residue at the position 823 by alanine, the construct hsPxd01-con4 completely lost its capacity to oxidize bromide

(C4-inactive).<sup>16</sup> Treatment of TeloHAEC cells with recombinant full length hsPxd01 promoted tube formation with a maximal 1.5- and 1.3-fold increase in junctions density and total vessels length respectively when compared with vehicle control. Similarly, active hsPxd01-con4 (C4 active) induced tube formation with a maximal 1.5- and 1.2-fold increase in junctions density and total vessels length respectively. However, no significant effect was observed with C4-inactive when compared with

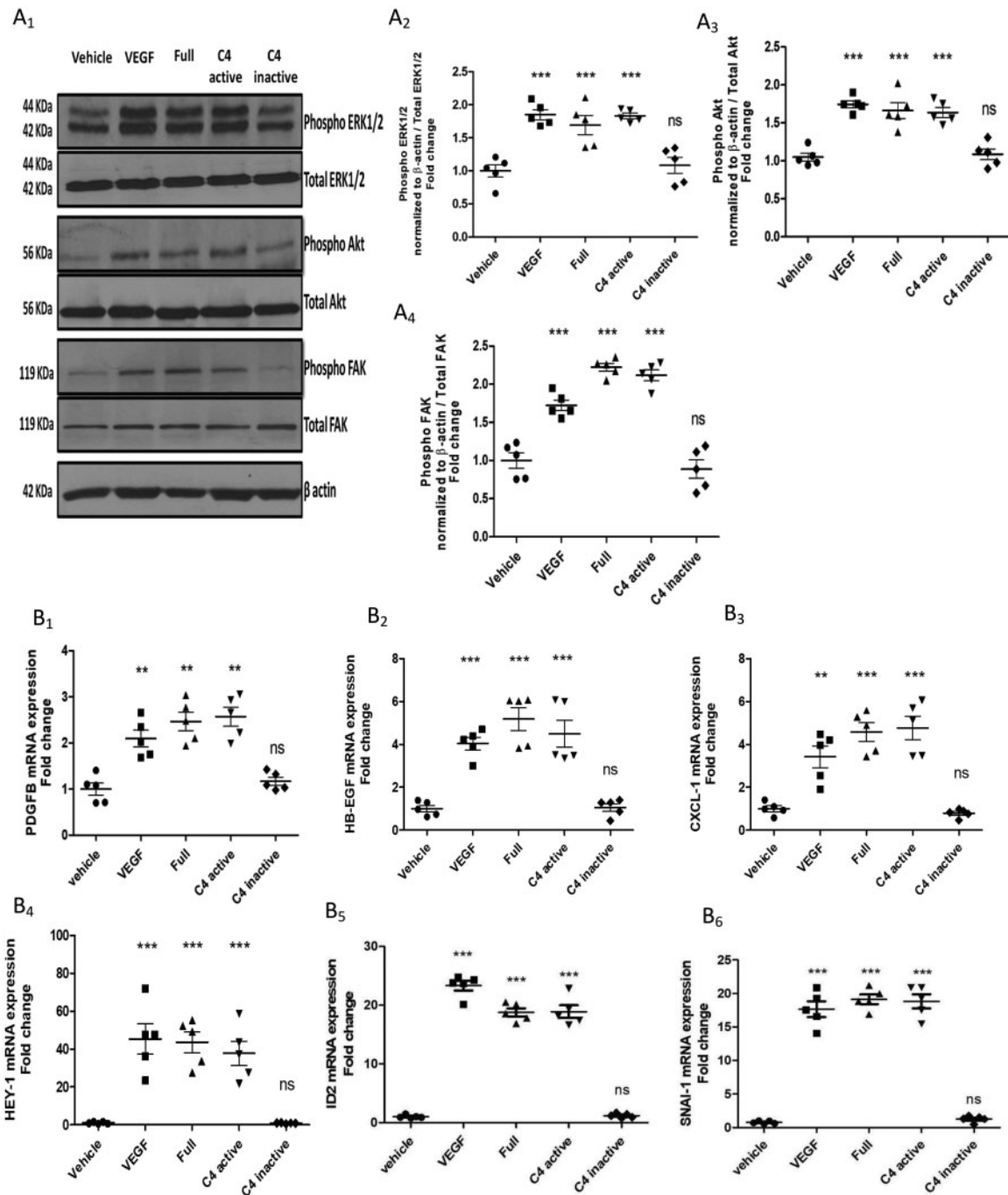


**Figure 5** Peroxidase 1 activates angiogenic signalling pathways and expression of pro-angiogenic downstream genes via its catalytic activity. (A1) TeloHAEC cells ( $4 \times 10^5$ ) were treated with the full length hsPxd01 and the truncated variants C4-active and C4-inactive ( $1 \mu\text{M}$ ), or with VEGF ( $100 \text{ ng/mL}$ ) for 1 h. Representative western blots analysis of protein extracts were performed using the indicated antibodies. Graphs (A2, A3, A4) show the quantification of phosphorylation levels of the indicated kinases normalized to  $\beta$ -actin and total kinase expression. Results are expressed as fold change over vehicle control and shown as mean  $\pm$  SEM of five independent experiments. (B1, B2, B3, B4, B5, B6) TeloHAEC cells ( $9 \times 10^4$ ) were treated with the full length hsPxd01 or the truncated variants C4-active and C4-inactive ( $1 \mu\text{M}$ ), or with VEGF ( $100 \text{ ng/mL}$ ) for 1 h. mRNA were extracted and analysed by qRT-PCR using primers targeting the indicated genes. Relative mRNA expression levels were normalized to GAPDH. Results are expressed as fold change over vehicle control, and are shown as mean  $\pm$  SEM of five independent experiments. Statistics were analysed using one-way ANOVA, followed by Bonferroni's multiple comparison test (\*\* $P < 0.01$ , \*\*\* $P < 0.001$ ;  $n = 5$ ). ns, non-significant.

the vehicle control (Figure 1B and C). For comparison, VEGF (100 ng/mL)—known to promote tube formation—increased junctions density and total vessels length by 1.5- and 1.3-fold, respectively (Figure 1B and C). These findings suggest that hsPxd01 promotes tubulogenesis via its catalytic activity. Neither loss of its oligomeric state nor of the LRR and VWC domains did affect hsPxd01-mediated tubulogenesis.

Next, we assessed the capacity of hsPxd01 to stimulate angiogenesis *in vivo* by using the chicken chorioallantoic membrane (CAM) assay. Macroscopic vessel and length densities were evaluated between 2 and 6 mm remote from the microsphere boundary. Upon treatment with full length hsPxd01 or C4-active vessel density increased when compared with vehicle control (Figure 2B). Interestingly, this increase in vessel density was similar to that observed upon treatment with VEGF (5 µg/mL) (Figure 2B). However, addition of C4-inactive (1 µM) did not induce angiogenesis (Figure 2B).

Increase in length density was only observed when CAMs were treated with full length hsPxd01 or VEGF (Figure 2C). Whereas treatment of CAMs with full length hsPxd01 significantly increased both vessel and length densities when compared with vehicle control (Figure 2B and C), addition of C4-active showed a significant increase in blood vessel density only (Figure 2B). Considering microscopic SMA-positive vessels, results are in agreement with those obtained at macroscopic level (Figure 2E). Taken together, our data show that full length recombinant hsPxd01 and the construct C4-active are able to induce angiogenesis *in vivo*.

### 3.2 Effects of knockdown of endogenous peroxidasin 1 and supplementation by recombinant hsPxd01 on tubulogenesis

In order to determine the role of endogenous hsPxd01 in endothelial tube formation, we transfected TeloHAEC cells with hsPxd01 siRNA. Knockdown was achieved to around 80% of the control level for both mRNA (Figure 3A) and protein levels (Figure 3B and C). Scrambled siRNA was used as a control and did not show any significant effect (Blank). In contrast, knockdown of hsPxd01 affected the formation of tubular structures on matrigel (Figure 3D). Both junctions density and total vessels length were decreased by ~40% (Figure 3E and F) when compared with wild-type cells.

Next, we probed whether addition of recombinant hsPxd01 is able to counteract the effects of hsPxd01 knockdown. Consequently, si-hsPxd01 cells were seeded on matrigel and supplemented with recombinant full length hsPxd01 (1 µM) for 5 h (Figure 3D). As Figure 3D–F depict, addition of recombinant full length hsPxd01 partially restored tube formation in si-hsPxd01 cells with a maximal 1.4- and 1.3-fold increase in junctions density and total vessels length respectively when compared with untreated si-hsPxd01 cells. For comparison, we found that VEGF (100 ng/mL) rescued tube formation in si-hsPxd01 cells with a maximal 1.6- and 1.4-fold increase in junctions density and total vessels length respectively when compared with untreated si-hsPxd01 cells (Figure 3E and F).

### 3.3 Peroxidasin 1 is required for endothelial cell migration

As angiogenesis *in vivo* also requires cell motility, we assessed the effect of knockdown of hsPxd01 on endothelial cell migration. TeloHAEC cells were seeded into two well culture insert and allowed to migrate (Figure 4A). Cell-free gap surfaces were measured at different time points. Figure 4B shows that knockdown of hsPxd01 as opposed to

scrambled siRNA (Blank) and control cells, significantly slows down the closure of the cell free gap by 25% after 24 h. Knockdown of hsPxd01 did not affect cell proliferation (Figure 4C and D) excluding an impact of hsPxd01 knockdown on the cell cycle.

### 3.4 Peroxidasin 1 activates angiogenic signalling pathways and expression of pro-angiogenic downstream genes through its catalytic activity

As hsPxd01 affects endothelial cell migration and tube formation, which are characteristics for angiogenesis *in vivo*, we aimed to understand the underlying molecular mechanism. First, we investigated the ability of full length hsPxd01, C4-active and C4-inactive as well as VEGF to activate Extracellular signal-Regulated Kinases (ERK1/2), Protein kinase B (Akt), and FAK, actors of the major angiogenic signalling pathways. Treatment of TeloHAEC cells with both full length hsPxd01 and C4 active increased the phosphorylation of ERK1/2, Akt and FAK when compared with vehicle control. This effect is comparable to that seen with VEGF. However, no significant effect on kinases activation has been observed with C4-inactive (Figure 5A1, A2, A3, A4).

Next, we analysed the effect of recombinant full length hsPxd01, C4-active and C4-inactive on expression of downstream angiogenic genes encoding growth factors such as Platelet Derived Growth Factor Subunit B (PDGFB), endothelial-derived Heparin Binding EGF-like growth factor (HB-EGF), CXCL-1, a pro-angiogenic chemokine, and some of the “key” transcriptional regulators such as Hairy-Related Transcription Factor 1 (HEY-1), DNA-binding protein inhibitor (ID-2), and Snail Family Zinc Finger 1 (SNAI-1).

Treatment of TeloHAEC cells with the full length hsPxd01 and C4-active significantly enhanced the expression of PDGFB (2.4, 2.5)-fold, HB-EGF (5, 4.5)-fold, CXCL-1 (4.5, 4.7)-fold, HEY-1 (43, 37)-fold, ID-2 (17.8, 16.6)-fold, and SNAI-1 (19, 18)-fold, respectively. These genes were also induced with VEGF (100 ng/mL) used as a positive control. However, addition of C4-inactive had no impact on expression of these genes when compared with vehicle control cells (Figure 5B1, B2, B3, B4, B5, B6). Our findings clearly suggest that addition of active recombinant hsPxd01 (either full-length homotrimeric or truncated monomeric) stimulates ERK1/2, Akt and FAK phosphorylation, and induces the expression of downstream angiogenic genes via its catalytic activity.

In addition, we examined the phosphorylation level of ERK1/2, Akt, and FAK in si-hsPxd01 treated cells. Phosphorylation of Akt and FAK was reduced in si-hsPxd01 cells compared with scrambled siRNA treated cells upon hsPxd01 stimulation (Figure 6A1, A4, A5). Interestingly, there was a significant increase of ERK1/2 phosphorylation in si-hsPxd01 cells after addition hsPxd01 when compared with hsPxd01-treated scrambled siRNA cells (Figure 6A1, A3). However, silencing of hsPxd01 did not affect ERK1/2, Akt and FAK activation upon stimulation by VEGF (Supplementary material online, Figure S1 A1, A3, A4, A5). Furthermore, we probed whether endogenous hsPxd01 regulates downstream angiogenic gene expression. Knockdown of hsPxd01 did not alter the basal level of PDGFB, HB-EGF, CXCL-1, HEY-1, ID-2 and SNAI-1 expression (Figure 6B2, B3, B4, B5, B6, B7), whereas expression of HEY-1, ID-2, and PDGFB was reduced by 29-fold, 7-fold, and 1.3-fold respectively in hsPxd01-treated si-hsPxd01 cells when compared with hsPxd01-treated scrambled siRNA cells (Figure 6B5, B6, B2). Moreover, addition of recombinant hsPxd01 induced the expression of endogenous hsPxd01 both at mRNA (Figure 7A) and protein levels (Figure 7B and C) in wild-type cells. Taken together, these results suggest

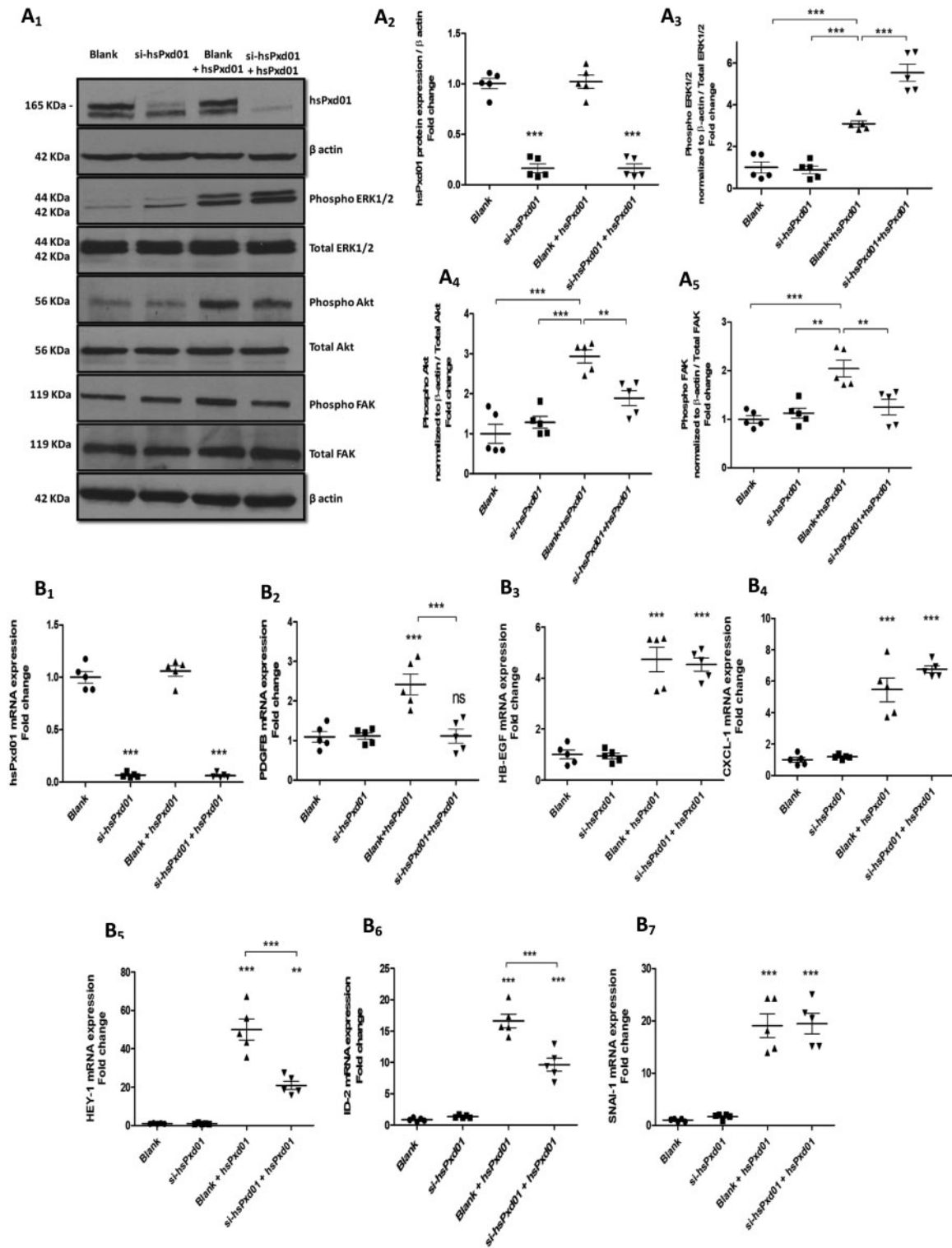


**Figure 6** Peroxidasin 1 activates angiogenic signalling pathways and expression of pro-angiogenic downstream genes via endogenous peroxidasin 1. (A1) Scrambled siRNA (blank) and si-hsPxd01-transfected cells ( $4 \times 10^5$ ) were treated with the full length recombinant hsPxd01 ( $1 \mu\text{M}$ ) for 1 h. Representative western blots analysis of protein extracts were performed using the indicated antibodies. Graphs (A2, A3, A4, A5) show the quantification of hsPxd01 protein level and phosphorylation levels of the indicated kinases normalized to  $\beta$ -actin and total kinase expression, and expressed as fold change over Blank. (B1, B2, B3, B4, B5, B6, B7) Scrambled siRNA (Blank) and si-hsPxd01-transfected cells ( $9 \times 10^4$ ) were treated with the full length recombinant hsPxd01 ( $1 \mu\text{M}$ ) for 1 h. mRNA were extracted and analysed by qRT-PCR using primers targeting the indicated genes. Relative mRNA expression levels were normalized to GAPDH. Results are expressed as fold change over blank and are shown as mean  $\pm$  SEM of five independent experiments. Statistics were analysed using one-way ANOVA, followed by Bonferroni's multiple comparison test. (\*\* $P < 0.01$ , \*\*\* $P < 0.001$ ;  $n = 5$ ). ns: non-significant.

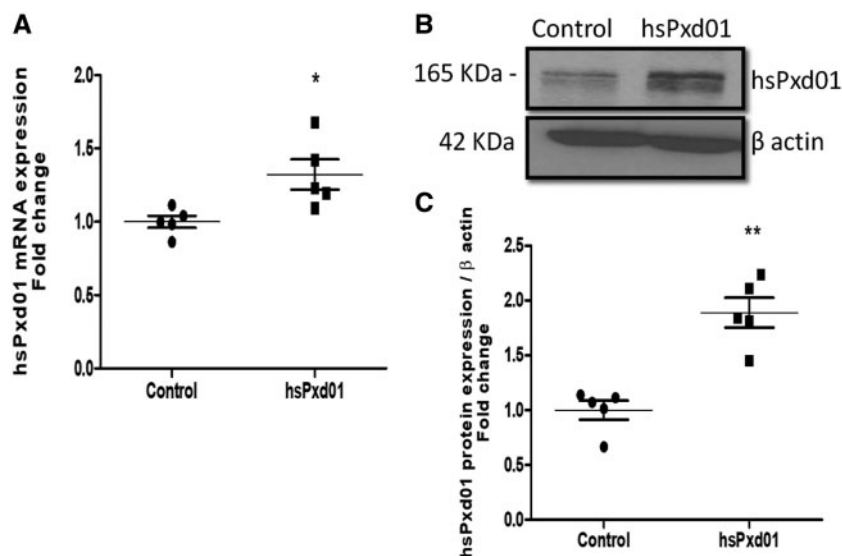


**Figure 7** Extracellular peroxidasin 1 induces its own endogenous expression. TeloHAEC cells ( $3.5 \times 10^5$ ) were treated full length hsPxd01 (1  $\mu$ M) for 48 h. (A) mRNA were extracted and analysed by qRT-PCR. Relative hsPxd01 mRNA expression levels were normalized to GAPDH. (B) Representative western blot analysis using anti-hsPxd01 antibody and quantification (graph) (C) show the induction of expression of endogenous hsPxd01 after 48 h of addition of full length recombinant hsPxd01. Results are expressed as fold change over control, and are shown as mean  $\pm$  SEM of five independent experiments. Statistics were analysed using unpaired *t*-test (\* $P < 0.05$ , \*\* $P < 0.01$ ;  $n = 5$ ).

that extracellular hsPxd01 regulates the expression of some angiogenic genes (e.g. HEY-1, ID-2, and PDGFB) via expression of endogenous hsPxd01, while it controls another gene pack through a pathway independent of endogenous hsPxd01. In the same context, VEGF (100 ng/mL, 48 h) had no effect on the expression of the endogenous hsPxd01 (Supplementary material online, Figure S2 A, B, C). Moreover, hsPxd01 silencing did not affect downstream genes expression upon VEGF stimulation (Supplementary material online, Figure S1 B2, B3, B4, B5, B6, B7), suggesting that endogenous hsPxd01 does not interfere in pro-angiogenic response induced by VEGF. This may explain the rescue effect of exogenously added VEGF in hsPxd01 knockdown cells on both tube formation and cell migration (Figure 3D–F and Supplementary material online, Figure S3A and B, respectively). Taken together, our study suggests that hsPxd01 and VEGF promote angiogenesis independently.

## 4. Discussion

During angiogenesis, endothelial cells interact with extracellular matrix components. The present work proposes a role of human peroxidasin in this highly coordinated process. This multidomain peroxidase was originally described as an enzyme essential for extracellular matrix consolidation and remodelling by catalyzing the formation of sulfilimine bonds in collagen IV (the predominant constituent of basement membrane) via the  $H_2O_2$ -mediated oxidation of bromide to hypobromous acid.<sup>15,19–21</sup>

Among the many processes involved in angiogenesis, tube formation and cell migration are amenable to experimentation in culture through tubulogenesis and scratch assays. Our data clearly demonstrated that addition of recombinant hsPxd01 stimulated tube formation in endothelial cells as well as in the chicken embryo chorioallantoic membrane (CAM) assay. The recombinant enzyme significantly induced vascularization,

associated with an increase of alpha-smooth muscle actin-positive vessels. Importantly, both full length homotrimeric hsPxd01 and the monomeric construct C4-active (which lacks the LRR and VWC domains) promoted tubulogenesis both *in vitro* and *in vivo*, whereas the enzymatically inactive construct (C4-inactive) had no impact. This corroborates recent studies demonstrating that LRR and VWC domains are not required for efficient sulfilimine cross-links formation in collagen IV mediated by various hsPxd01 constructs.<sup>21</sup> Moreover, it has been demonstrated that the proteolytic elimination of the VWC domain by proprotein convertase *in vivo* enhances the catalytic activity of hsPxd01 and represents a key regulatory process in the physiological function of human peroxidasin 1.<sup>35</sup> Along the same line, a recent report has shown that the pro-angiogenic effect of two other heme peroxidase family members MPO and EPO was reduced using a specific peroxidase inhibitor, highlighting the importance of the catalytic activity for peroxidase-mediated angiogenesis.<sup>29</sup> Furthermore, we confirmed the importance of endogenous hsPxd01 in angiogenesis, since its silencing reduced both tube formation and cell migration. These findings are supported by recent studies showing that melanoma and choriocarcinoma cells migratory behaviour and invasion were reduced as a consequence of hsPxd01 silencing.<sup>36,37</sup>

Active recombinant peroxidasin 1 (both full length hsPxd01 and C4-active) were demonstrated to promote the pro-angiogenic activity by activation of the extracellular signal-regulated kinases (ERK1/2), Protein kinase B (Akt), and FAK, which are known to regulate cellular events required for endothelial proliferation, migration and tube formation<sup>38–40</sup> similar to VEGF used as a positive control. In hsPxd01 knockdown cells, phosphorylation of Akt and FAK (but not ERK1/2) was reduced, suggesting that endogenous hsPxd01 is implicated in Akt and FAK, but not in ERK1/2 activation. A recent study showed that endogenous hsPxd01 acts upstream of the Akt pathway.<sup>41</sup> However, another study reported that

endogenous hsPxd01 could also regulate ERK1/2 activation in smooth muscle cells.<sup>13</sup> So far, no study has demonstrated a link between peroxidase 1 and FAK phosphorylation. The sustained activation of ERK1/2 may explain the rescue effect of exogenously added recombinant hsPxd01 in knockdown cells on tube formation, complementary to other signalling cascades that could be implicated. It has to be noted that endogenous hsPxd01 has been shown to activate Jun N-terminal kinase (JNK) and p38 mitogen-activated protein kinase (MAPK) in endothelial cells.<sup>42,43</sup>

Knockdown of hsPxd01 only affected the expression of PDGFB, HEY-1, and ID-2, which could be correlated to Akt or FAK but not ERK dysregulation in those cells. Indeed, the inhibition of Akt pathway in tumorigenic hepatic and melanoma cells, led to a decrease in both PDGFB and HEY-1 expression.<sup>44,45</sup> Furthermore, in a model of human embryonic stem cells, the inhibition of Src/FAK signalling suppresses ID-2 expression.<sup>46</sup> With respect to unaffected genes, the inhibition of the ERK1/2 significantly decreases CXCL-1 and HB-EGF expression in endometrial and airway smooth muscle cells respectively.<sup>47,48</sup> Moreover, SNAI-1 has been identified as a downstream effector of ERK signalling during tumour progression.<sup>49</sup>

In summary, our work supports a role of hsPxd01 as a pro-angiogenic secreted peroxidase capable of regulating vessel formation through its catalytic activity. Moreover, we suggest possible signal transduction cascades by which hsPxd01 may mediate its pro-angiogenic response. Thus, the extracellular hsPxd01 promotes Akt, FAK, and ERK1/2 activation. The activation of the two first kinases involves endogenous hsPxd01 as a link. We propose that the pro-angiogenic role of endogenous hsPxd01 may be mediated through its capacity to form hypohalous acids, known as intracellular angiogenic modulators during vascular formation and development.<sup>50</sup> Further investigations are required to precisely establish the mechanisms by which hsPxd01 activates pro-angiogenic signalling, using proteomic-based approaches to screen for intracellular post-translational modifications. Therefore, human peroxidase 1 could be an interesting angiogenic therapeutic molecule that would enhance wound repair and vascular regeneration after ischaemic events. However, additional works are required to investigate a possible implication of endogenous peroxidase 1 in angiogenesis through alternative signalling pathways.

## Supplementary material

Supplementary material is available at *Cardiovascular Research* online.

**Conflict of interest:** none declared.

## Funding

This work was supported by grants from the CHU Charleroi; the Fonds de la Chirurgie Cardiaque; Fonds de la Recherche Médicale en Hainaut (FRMH); a fellowship grant from the Tunisian Ministry of Higher Education and Scientific Research to H.M.; L.V. is Director of Research at the Belgian National Fund for Scientific Research; the Austrian Science Fund (project number P25538) and the doctoral program BioToP—Biomolecular Technology of Proteins (FWF W1224). The Analytical Platform is supported by the FRS-FNRS.

## References

- Ucuzian AA, Gassman AA, East AT, Greisler HP. Molecular mediators of angiogenesis. *J Burn Care Res* 2010;**31**:158–175.
- Kumar R, Yoneda J, Bucana CD, Fidler IJ. Regulation of distinct steps of angiogenesis by different angiogenic molecules. *Int J Oncol* 1998;**12**:749–757.
- De Cicco-Skinner KL, Henry GH, Cataisio C, Tabib T, Gwilliam JC, Watson NJ, Bullwinkle EM, Falkenburg L, O'Neill RC, Morin A, Wiest JS. Endothelial cell tube formation assay for the *in vitro* study of angiogenesis. *J Vis Exp* 2014;**91**:e51312.
- Grant DS, Kibbey MC, Kinsella JL, Cid MC, Kleinman HK. The role of basement membrane in angiogenesis and tumor growth. *Pathol Res Pract* 1994;**190**:854–863.
- Kim WY, Lee HY. Brain angiogenesis: mechanism and therapeutic intervention in brain tumors. *FEBS J* 2009;**276**:4653–4664.
- Liu Y, Senger DR. Matrix-specific activation of Src and Rho initiates capillary morphogenesis of endothelial cells. *FASEB J* 2004;**18**:457–468.
- Senger DR, Claffey KP, Benes JE, Perruzzi CA, Sergioui AP, Detmar M. Angiogenesis promoted by vascular endothelial growth factor: regulation through alpha1beta1 and alpha2beta1 integrins. *Proc Natl Acad Sci USA* 1997;**94**:13612–13617.
- Lo C-M, Wang H-B, Dembo M, Wang Y-L. Cell movement is guided by the rigidity of the substrate. *Biophys J* 2000;**79**:144–152.
- Hoeben A, Landuyt B, Highley MS, Wildiers H, Van Oosterom AT, De Bruijn EA. Vascular endothelial growth factor and angiogenesis. *Pharmacol Rev* 2004;**56**:549–580.
- Carmeliet P. Angiogenesis in life, disease and medicine. *Nature* 2005;**438**:932–936.
- Cheng G, Li H, Cao Z, Qiu X, McCormick S, Thannickal VJ, Nauseef WM. Vascular Peroxidase-1 is rapidly secreted circulates in plasma, and supports dityrosine cross-linking reactions. *Free Radic Biol Med* 2011;**51**:1445–1453.
- Zhang YS, He L, Liu B, Li NS, Luo XJ, Hu CP, Ma QL, Zhang GG, Li YJ, Peng J. A novel pathway of NADPH oxidase/vascular peroxidase 1 in mediating oxidative injury following ischemia–reperfusion. *Basic Res Cardiol* 2012;**107**:266.
- Shi R, Hu C, Yuan Q, Yang T, Peng J, Li Y, Bai Y, Cao Z, Cheng G, Zhang G. Involvement of vascular peroxidase 1 in angiotensin II-induced vascular smooth muscle cell proliferation. *Cardiovasc Res* 2011;**91**:27–36.
- Péterfi Z, Donkó A, Orient A, Sum A, Prókai A, Molnár B, Veréb Z, Rajnavölgyi E, Kovács KJ, Müller V, Szabó AJ, Geiszt M. Peroxidase 1 is secreted and incorporated into the extracellular matrix of myofibroblasts and fibrotic kidney. *Am J Pathol* 2009;**175**:725–735.
- Lázár E, Péterfi Z, Sirokmány G, Kovács HA, Klement E, Medzihradzky KF, Geiszt M. Structure-function analysis of peroxidase provides insight into the mechanism of collagen IV crosslinking. *Free Radic Biol Med* 2015;**83**:273–282.
- Soudi M, Zámocký M, Jakopitsch C, Furtmüller PG, Obinger C. Molecular evolution, structure, and function of peroxidases. *Chem Biodivers* 2012;**9**:1776–1793.
- Soudi M, Paumann-Page M, Delporte C, Pirker KF, Bellei M, Edenhofer E, Stadlmayr G, Battistuzzi G, Boudjeltia KZ, Furtmüller PG, Van Antwerpen P, Obinger C. Multidomain human peroxidase 1 is a highly glycosylated and stable homotrimeric high spin ferric peroxidase. *J Biol Chem* 2015;**290**:10876–10890.
- Cheng G, Salerno JC, Cao Z, Pagano PJ, Lambeth JD. Identification and characterization of VPO1, a new animal heme containing Peroxidase. *Free Radic Biol Med* 2008;**45**:1682–1694.
- Nelson RE, Fessler LI, Takagi Y, Blumberg B, Keene DR, Olson PF, Parker CG, Fessler JH. Peroxidase: a novel enzyme-matrix protein of *Drosophila* development. *EMBO J* 1994;**13**:3438–3447.
- Bhave G, Cummings CF, Vanacore RM, Kumagai-Cresse C, Ero-Tolliver IA, Rafi M, Kang JS, Pedchenko V, Fessler LI, Fessler JH, Hudson BG. Peroxidase forms sulfilimine chemical bonds using hypohalous acids in tissue genesis. *Nat Chem Biol* 2012;**8**:784–790.
- Ero-Tolliver IA, Hudson BG, Bhave G. The ancient immunoglobulin domains of peroxidase are required to form sulfilimine cross-links in collagen IV. *J Biol Chem* 2015;**290**:21741–21748.
- Khan K, Rudkin A, Parry DA, Burdon KP, McKibbin M, Logan CV, Abdelhamed ZI, Muecke JS, Fernandez-Fuentes N, Laurie KJ, Shires M, Fogarty R, Carr IM, Poulter JA, Morgan JE, Mohamed MD, Jafri H, Raashid Y, Meng N, Piseth H, Toomes C, Casson RJ, Taylor GR, Hammerton M, Sheridan E, Johnson CA, Inglehearn CF, Craig JE, Ali M. Homozygous mutations in *PXDN* cause congenital cataract, corneal opacity, and developmental glaucoma. *Am J Hum Genet* 2011;**89**:464–473.
- Liu Y, Carson-Walter EB, Cooper A, Winans BN, Johnson MD, Walter KA. Vascular gene expression patterns are conserved in primary and metastatic brain tumors. *J Neurooncol* 2010;**99**:13–24.
- Castronovo V, Waltregny D, Kischel P, Roesli C, Elia G, Rybak JN, Neri D. A chemical proteomics approach for the identification of accessible antigens expressed in human kidney cancer. *Mol Cell Proteomics* 2006;**5**:2083–2091.
- Van Hinsbergh VW, Koolwijk P. Endothelial sprouting and angiogenesis: matrix metalloproteinases in the lead. *Cardiovasc Res* 2008;**78**:203–212.
- Neve A, Cantatore FP, Maruotti N, Corrado A, Ribatti D. Extracellular matrix modulates angiogenesis in physiological and pathological conditions. *BioMed Res Int* 2014;**2014**:1.
- Herbert SP, Stainier DY. Molecular control of endothelial cell behaviour during blood vessel morphogenesis. *Nat Rev Mol Cell Biol* 2011;**12**:551–564.
- Davis GE, Koh W, Stratman AN. Mechanisms controlling human endothelial lumen formation and tube assembly in three-dimensional extracellular matrices. *Birth Defects Res C Embryo Today* 2007;**81**:270–285.
- Panagopoulos V, Zinonos I, Leach DA, Hay SJ, Liapis V, Zysk A, Ingman WV, DeNichilo MO, Evdokiou A. Uncovering a new role for peroxidase enzymes as drivers of angiogenesis. *Int J Biochem Cell Biol* 2015;**68**:128–138.
- Zámocký M, Jakopitsch C, Furtmüller PG, Dunand C, Obinger C. The peroxidase-cyclooxygenase superfamily: reconstructed evolution of critical enzymes of the innate immune system. *Proteins* 2008;**72**:589–605.

31. Zámocký M, Hofbauer S, Schaffner I, Gasselhuber B, Nicolussi A, Soudi M, Pirker KF, Furtmüller PG, Obinger C. Independent evolution of four heme peroxidase superfamilies. *Arch Biochem Biophys* 2015;**574**:108–119.
32. Longo PA, Kavran JM, Kim M-S, Leahy DJ. Transient mammalian cell transfection with polyethylenimine (PEI). *Methods Enzymol* 2013;**529**:227–240.
33. Zudaire E, Gambardella L, Kurcz C, Vermeren S. A computational tool for quantitative analysis of vascular networks. *PLoS One* 2011;**6**:e27385.
34. Paumann-Page M, Katz RS, Bellei M, Schwartz I, Edenhofer E, Sevcnikar B, Soudi M, Hofbauer S, Battistuzzi G, Furtmüller PG, Obinger C. Pre-steady-state kinetics reveal the substrate specificity and mechanism of halide oxidation of truncated human peroxidasin 1. *J Biol Chem* 2017;**292**:4583–4592.
35. Colon S, Bhawe G. Proprotein convertase processing enhances peroxidasin activity to reinforce collagen IV. *J Biol Chem* 2016;**291**:24009–24016.
36. Jayachandran A, Prithviraj P, Lo P-H, Walkiewicz M, Anaka M, Woods BL, Tan B, Behren A, Cebon J, McKeown SJ. Identifying and targeting determinants of melanoma cellular invasion. *Oncotarget* 2016;**7**:41186–41202.
37. Tauber S, Jais A, Jeitler M, Haider S, Husa J, Lindroos J, Knöfler M, Mayerhofer M, Pehamberger H, Wagner O, Bilban M. Transcriptome analysis of human cancer reveals a functional role of heme oxygenase-1 in tumor cell adhesion. *Mol Cancer* 2010;**9**:200.
38. Srinivasan R, Zabuawala T, Huang H, Zhang J, Gulati P, Fernandez S, Karlo JC, Landreth GE, Leone G, Ostrowski MC. *Erk1* and *Erk2* regulate endothelial cell proliferation and migration during mouse embryonic angiogenesis. *PLoS One* 2009;**4**:e8283.
39. Tavora B, Batista S, Reynolds LE, Jadeja S, Robinson S, Kostourou V, Hart I, Fruttiger M, Parsons M, Hodivala-Dilke KM. Endothelial FAK is required for tumour angiogenesis. *EMBO Mol Med* 2010;**2**:516–528.
40. Jiang BH, Liu LZ. AKT signaling in regulating angiogenesis. *Curr Cancer Drug Targets* 2008;**8**:19–26.
41. Tang Y, Xu Q, Peng H, Liu Z, Yang T, Yu Z, Cheng G, Li X, Zhang G, Shi R. The role of vascular peroxidase 1 in ox-LDL-induced vascular smooth muscle cell calcification. *Atherosclerosis* 2015;**243**:357–363.
42. Li DJ, Zhao T, Xin RJ, Wang YY, Fei YB, Shen FM. Activation of  $\alpha 7$  nicotinic acetylcholine receptor protects against oxidant stress damage through reducing vascular peroxidase-1 in a JNK signaling-dependent manner in endothelial cells. *Cell Physiol Biochem* 2014;**33**:468–478.
43. Bai YP, Hu CP, Yuan Q, Peng J, Shi RZ, Yang TL, Cao ZH, Li YJ, Cheng G, Zhang GG. Role of VPO1, a newly identified heme-containing peroxidase, in ox-LDL induced endothelial cell apoptosis. *Free Radic Biol Med* 2011;**51**:1492–1500.
44. Lau CK, Yang ZF, Ho DW, Ng MN, Yeoh GC, Poon RT, Fan ST. An Akt/hypoxia-inducible factor-1  $\alpha$ /platelet-derived growth factor-BB autocrine loop mediates hypoxia-induced chemoresistance in liver cancer cells and tumorigenic hepatic progenitor cells. *Clin Cancer Res* 2009;**15**:3462–3471.
45. Bedogni B, Warneke JA, Nickoloff BJ, Giaccia AJ, Powell MB. Notch1 is an effector of Akt and hypoxia in melanoma development. *J Clin Invest* 2008;**118**:3660–3670.
46. Afrikanova I, Yebra M, Simpkinson M, Xu Y, Hayek A, Montgomery A. Inhibitors of Src and focal adhesion kinase promote endocrine specification: impact on the derivation of  $\beta$ -cells from human pluripotent stem cells. *J Biol Chem* 2011;**286**:36042–36052.
47. Baston-Büst DM, Schanz A, Böddeker SJ, Altergot-Ahmad O, Krüssel JS, Rein D, Hess AP. CXCL1 expression in human decidua in vitro is mediated via the MAPK signalling cascade. *Cytokine* 2013;**64**:79–85.
48. Kumasawa F, Hashimoto S, Mizumura K, Takeshita I, Onose A, Jibiki I, Maruoka S, Gon Y, Kobayashi T, Takahashi N. Mitogen-activated protein kinase (MAPK) regulates leukotriene D4-induced HB-EGF and ADAM12 expression in human airway smooth muscle cells. *Asian Pac J Allergy Immunol* 2013;**31**:58–66.
49. Wang S, Cheng Y, Zheng Y, He Z, Chen W, Zhou W, Duan C, Zhang C. PRKAR1A is a functional tumor suppressor inhibiting ERK/Snail/E-cadherin pathway in lung adenocarcinoma. *Sci Rep* 2016;**6**:39630.
50. Zhou Y, Yan H, Guo M, Zhu J, Xiao Q, Zhang L. Reactive oxygen species in vascular formation and development. *Oxid Med Cell Longev* 2013;**2013**:374963.

# Posttranslational modification of heme in peroxidases – Impact on structure and catalysis

Andrea Nicolussi, Markus Auer, **Benjamin Sevcnikar**, Martina Paumann-Page, Vera Pfanzagl, Marcel Zámocký, Stefan Hofbauer. Paul G. Furtmüller and Christian Obinger

Research Article

Archives of Biochemistry and Biophysics, Volume 643, Pages 14-23, 2  
April 2018,  
DOI: 10.1016/j.abb.2018.02.008



## Posttranslational modification of heme in peroxidases – Impact on structure and catalysis

Andrea Nicolussi<sup>a</sup>, Markus Auer<sup>a</sup>, Benjamin Sevcnikar<sup>a</sup>, Martina Paumann-Page<sup>a</sup>, Vera Pfanzagl<sup>a</sup>, Marcel Zámocký<sup>a,b</sup>, Stefan Hofbauer<sup>a</sup>, Paul G. Furtmüller<sup>a</sup>, Christian Obinger<sup>a,\*</sup>

<sup>a</sup> Department of Chemistry, Division of Biochemistry, Protein Biochemistry, VIBT - Vienna Institute of BioTechnology, University of Natural Resources and Life Sciences, Muthgasse 18, A-1190 Vienna, Austria

<sup>b</sup> Institute of Molecular Biology, Slovak Academy of Sciences, Dúbravská Cesta 21, SK-84551 Bratislava, Slovakia

### ARTICLE INFO

#### Keywords:

Heme peroxidase  
Posttranslational modification  
Heme-protein link  
Ester bond  
Sulfonium ion bond  
Myeloperoxidase  
Lactoperoxidase  
Peroxidasin

### ABSTRACT

Four heme peroxidase superfamilies arose independently in evolution. Only in the peroxidase-cyclooxygenase superfamily the prosthetic group is posttranslationally modified (PTM). As a consequence these peroxidases can form one, two or three covalent bonds between heme substituents and the protein. This may include ester bonds between heme 1- and 5-methyl groups and glutamate and aspartate residues as well as a sulfonium ion link between the heme 2-vinyl substituent and a methionine.

Here the phylogeny and physiological roles of representatives of this superfamily, their occurrence in all kingdoms of life, the relevant sequence motifs for definite identification and the available crystal structures are presented. We demonstrate the autocatalytic posttranslational maturation process and the impact of the covalent links on spectral and redox properties as well as on catalysis, including Compound I formation and reduction by one- and two-electron donors. Finally, we discuss the evolutionary advantage of these PTMs with respect to the proposed physiological functions of the metalloenzymes that range from antimicrobial defence in innate immunity to extracellular matrix formation and hormone biosynthesis.

### 1. Introduction

Four heme peroxidase superfamilies evolved independently during evolution, differing in overall fold, active site structure and catalyzed reactions (Table 1) [1]. The redox cofactor is heme *b* or posttranslationally modified heme that is ligated by either a histidine or cysteine. These oxidoreductases are found in all kingdoms of life and typically catalyze the one- and two-electron oxidation of a myriad of organic and inorganic substrates (Reactions (1) & (2)). Thereby one-electron donors (AH<sub>2</sub>) are oxidized to the corresponding radicals (•AH), whereas two electron donors, like halides (X<sup>−</sup>) or thiocyanate (SCN<sup>−</sup>), are oxidized to the corresponding hypohalous acids (HOX) or hypothiocyanite (HOSCN). In addition to this *peroxidatic* activity some (sub)families show pronounced catalase (Reaction (3)) or peroxygenase activities (Reaction (4)) [1].



Three peroxidase superfamilies have (unmodified) heme *b* in the active site, whereas in the peroxidase-cyclooxygenase superfamily the heme can be posttranslationally modified and linked to the protein *via* one, two or three covalent bonds. The peroxidase-cyclooxygenase superfamily counts over 11,000 representatives in various sequence databases (December 2017, Table 1) and shows the highest diversity regarding domain architectures and composition. The superfamily was first defined in 2008 by Zámocký et al. [2] based on a reconstruction of the phylogenetic relationships of the main evolutionary lines of the mammalian heme containing peroxidases [myeloperoxidase (MPO), eosinophil peroxidase (EPO), lactoperoxidase (LPO) and thyroid peroxidase (TPO)] and the presence of two main enzymatic [i.e. peroxidase

**Abbreviations:** MPO, myeloperoxidase; LPO, lactoperoxidase; EPO, eosinophil peroxidase; TPO, thyroid peroxidase; HsPxd1, human peroxidasin 1; LspPOX, peroxidase from *Lyngbya* sp. PCC8106; DdPoxA, peroxidase A from *Dictyostelium discoideum*; HRP, horseradish peroxidase; APX, ascorbate peroxidase; CCP, cytochrome *c* peroxidase; ARP, *Arthromyces ramosus* peroxidase; PTM, posttranslational modification; *E*<sup>0</sup>, standard reduction potential; Pfam, protein families database; RR, resonance Raman; EPR, electron paramagnetic resonance; 5c, five-coordinated; 6c, six coordinated; HS, high-spin; LS, low-spin

\* Corresponding author.

E-mail address: [christian.obinger@boku.ac.at](mailto:christian.obinger@boku.ac.at) (C. Obinger).

<https://doi.org/10.1016/j.ab.2018.02.008>

Received 26 January 2018; Received in revised form 12 February 2018; Accepted 13 February 2018

Available online 17 February 2018

0003-9861/ © 2018 The Authors. Published by Elsevier Inc. This is an open access article under the CC BY-NC-ND license (<http://creativecommons.org/licenses/by-nc-nd/4.0/>).

**Table 1**

Overview about sequences coding for members of the four distinct heme peroxidase superfamilies in the protein sequence database InterPro (<https://www.ebi.ac.uk/interpro/>). In many representatives of the peroxidase-cyclooxygenase superfamily (highlighted in bold) the prosthetic group is posttranslationally modified.

Superfamily Nr.	Denomination	Proteins matched	Domain architectures
IPR002016	Peroxidase - catalase	25,751	268
IPR006314	Peroxidase - chlorite dismutase	12,699	26
<b>IPR019791</b>	<b>Peroxidase - cyclooxygenase</b>	<b>11,165</b>	<b>345</b>
IPR000028	Peroxidase - peroxigenase	2744	28

and (cyclo-) oxygenase] activities. The superfamily has Pfam accession PF03098 and its members are widely distributed among all domains of life [1,2].

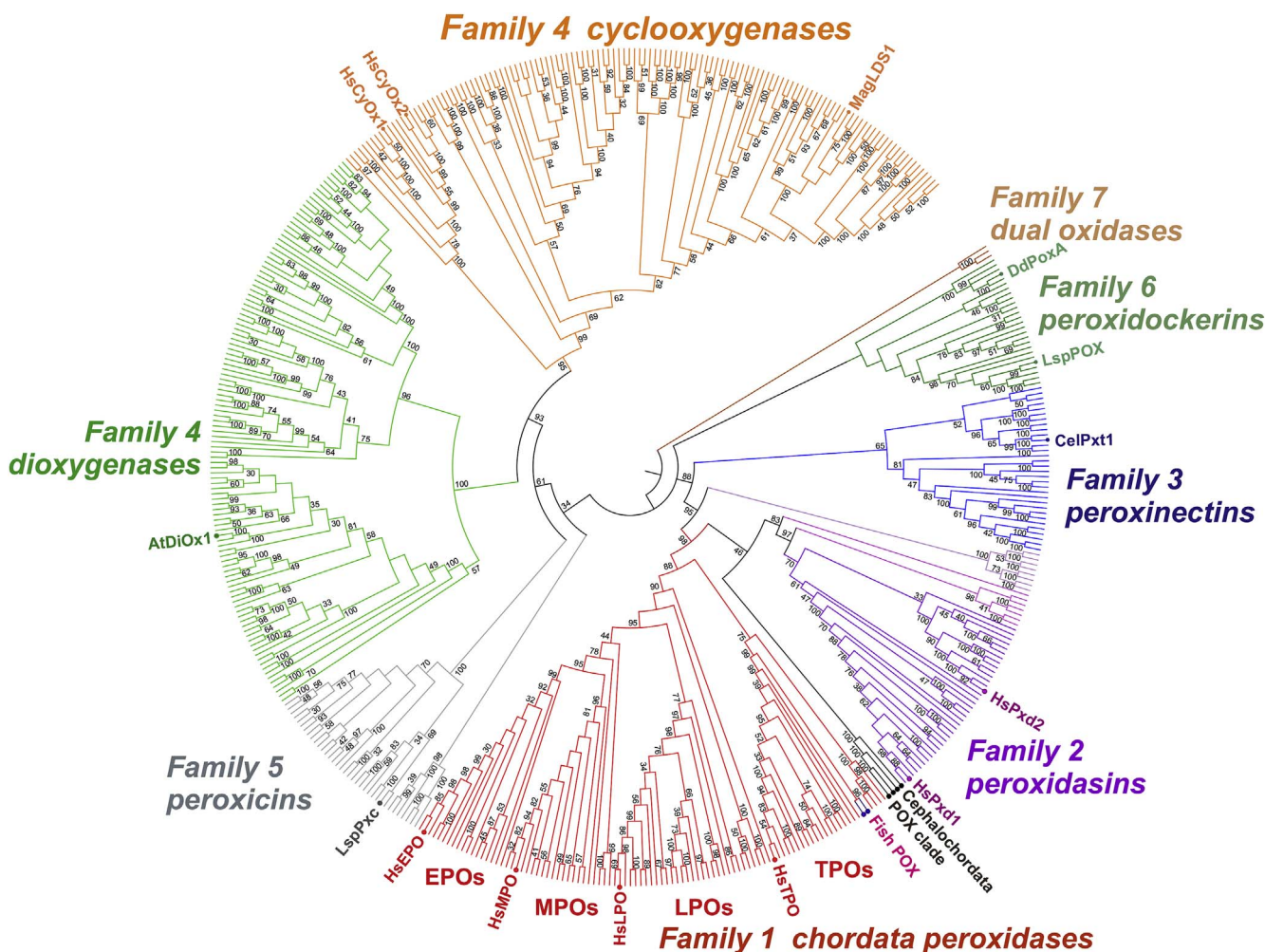
**2. Phylogeny and physiological roles of members of the peroxidase-cyclooxygenase superfamily**

Fig. 1 shows an updated reconstructed phylogenetic tree for the

peroxidase-cyclooxygenase superfamily based on the analysis of 486 full-length sequences conducted with MEGA6 [3]. In contrast to the other heme peroxidase superfamilies, many (mono-, homodi- or homotrimeric) members of the peroxidase-cyclooxygenase superfamily are multidomain proteins with one heme peroxidase domain per subunit.

The peroxidase-cyclooxygenase superfamily is divided into seven families (Fig. 1). Family 1 comprises secreted (single domain) chordata peroxidases that have been under investigation for more than 40 years [4,5]. In mammals homodimeric myeloperoxidase (MPO) as well as monomeric LPO [6] and EPO [7] have been shown to be an essential part of host defense in the innate immune system. By releasing highly reactive and oxidizing reaction products like hypohalous acids (Reaction (2)), they comprise the front line defense against invading pathogens [4–7]. Dimeric membrane-anchored thyroid peroxidase (TPO) catalyzes iodination of tyrosine residues in thyroglobulin and, finally, the synthesis of the thyroid hormones triiodothyronine (T3) and thyroxine (T4) [8].

The first Family 2 representative was detected in *Drosophila* in 1984 [9]. In this publication the name peroxidasin was coined for the first time. Family 2 members are oligomeric multidomain heme peroxidases found in invertebrates and vertebrates (Fig. 1) [10]. Recently, peroxidasins have attracted attention due to their important role in



**Fig. 1. Reconstructed phylogenetic tree for the peroxidase-cyclooxygenase superfamily.** This circular tree comprising 486 full-length members was updated from Ref. [1]. The evolutionary history was inferred by using the Maximum Likelihood method based on the Whelan and Goldman model with various substitution frequencies. The tree with the highest log likelihood (-298963.57) is shown. The percentage of trees in which the associated sequences clustered together is shown next to branches (for all values above 30%). A discrete gamma-distribution of frequencies was used to model the evolutionary rate differences among amino acid sites with four categories. This evolutionary analysis was conducted with MEGA6 [3]. Previously identified 7 families are highlighted as coloured sectors. Most important sequences of previously investigated peroxidases are labeled at their phylogenetic positions with their abbreviations used in PeroxiBase (<http://peroxibase.toulouse.inra.fr>).

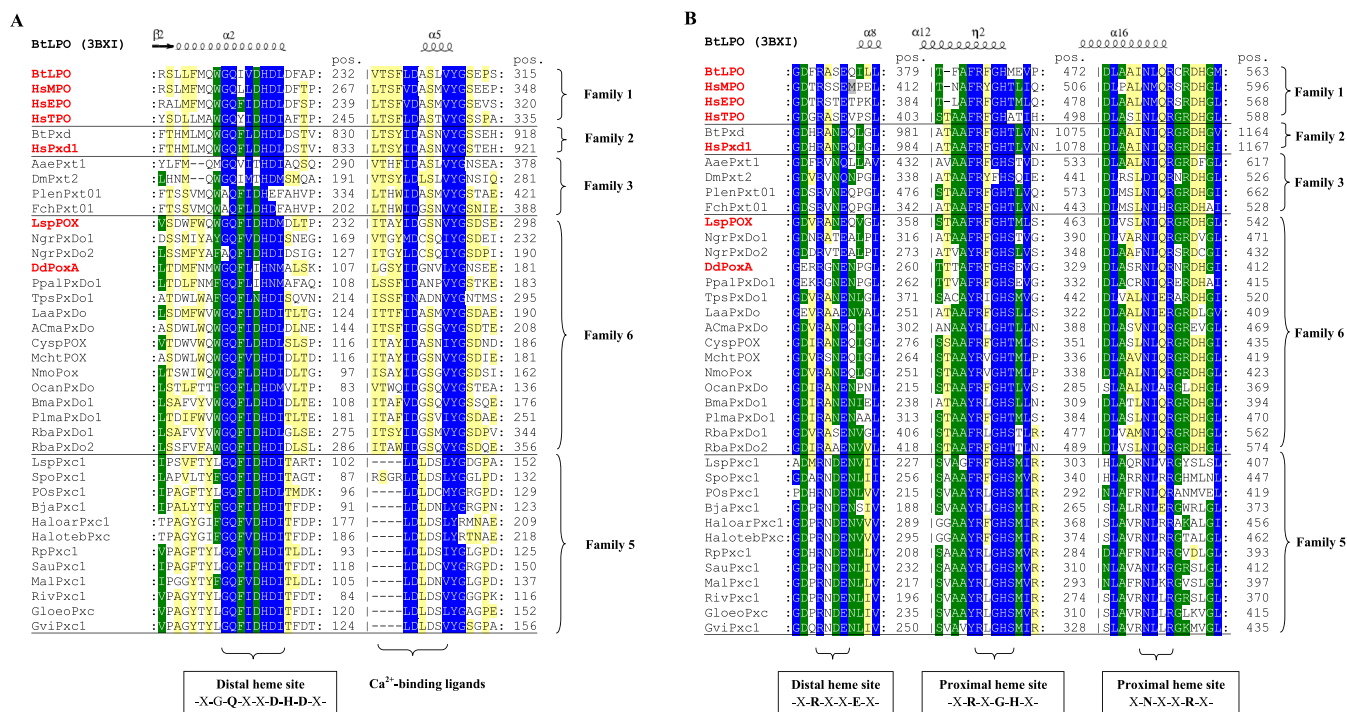


**Fig. 2.** Sequence alignment including distal and proximal residues found in representatives of the peroxidase-cyclooxygenase superfamily. (A) Distal heme site including calcium binding motif. (B) Conserved distal motif and proximal heme site. Selected members of Family 1 (LPO, MPO, EPO and TPO), Family 2 (human peroxidasin 1, HsPxd1) and Family 6 (LspPOX, DdPoxA) are shown in bold red. ESPript and MEGA 6.0 [3] software output was obtained from 38 sequence homologous of bovine LPO (3BXI). Secondary structure elements of bovine LPO are presented on the top of the alignment (helices as spirals, beta strands as arrows). Conserved residues with highest similarity are highlighted in blue (> 93% conservation), moderate similarity in green (> 70% conservation) and low similarity in pale yellow (> 33% conservation). Conserved sequence motifs are shown at the bottom and conserved residues are depicted in bold. Abbreviations of sequences are in accordance with PeroxiBase (<http://peroxidase.toulouse.inra.fr>). (For interpretation of the references to colour in this figure legend, the reader is referred to the Web version of this article.)

extracellular matrix consolidation [11–14]. These heme enzymes are secreted and comprised of leucine-rich domains, immunoglobulin domains and a C-terminal von Willebrand factor C domain in addition to the catalytic heme peroxidase domain. It has been proposed that their physiological role is providing hypobromous acid for the formation of sulfilimine crosslinks, a posttranslational modification for tissue development and architecture found within the collagen IV scaffold of basement membranes [12,15].

Family 3 contains heme peroxidases designated as peroxinectins (Fig. 1). They were shown to exhibit cell adhesion function(s) and to be involved in invertebrate immune response by production of hypohalous acids according to Reaction (2) [16]. In principle, they are also fusion proteins of a conserved heme peroxidase domain with an integrin-binding motif (i.e. KGD or RGD). Peroxinectins are widely spread mainly among the Eumetazoan phyla arthropods and nematods [1,2].

As Fig. 1 depicts, Family 5 (designated as peroxicins [2]) seems to contain the oldest representatives of the peroxidase-cyclooxygenase superfamily. The bacterial enzymes are either composed of the peroxidase domain only (short peroxicins) or can be comprised of several domains (long peroxicins) with calcium binding or hemolysin-type motifs [1]. The physiological role of Family 5 peroxidases is completely unknown. One evolutionary trend starting with Family 5 enzymes led to the stepwise evolution of Family 6 and further on to Families 3, 2 and 1, which were shortly described above.

Family 6 peroxidases (designated as peroxdockers [2]) emerged not only in eubacteria but can be also found in genomes of primitive eukaryotes like Amoebozoa. They seem to be widely distributed among the early eukaryotic world. Recently, biochemical studies on two representatives were published, namely on peroxidases from a cyanobacterium, i.e. *Lyngbya* sp. PCC 8106 (LspPOX) [17–19] and from *Dicystelium discoideum* (DdPoxA) [20]. The physiological role of bacterial Family 6 peroxidases is completely unknown. Regarding DdPoxA, it has

been demonstrated that it is upregulated and likely secreted at late multicellular development stages of the so called social amoeba *D. discoideum* when migrating slugs differentiate into fruiting bodies that contain persistent spores on top of a cellular stalk. Expression of DdPoxA is shown to restrict bacterial contamination of fruiting bodies [20]. Both LspPOX and DdPOX were shown to catalyze halide oxidation according to Reaction (2) [17–20].

In the context of the present review it is important to mention that representatives of Families 1, 2, 3, 5 and 6 have posttranslationally modified heme (see below). This is not the case for Families 4 and 7 of the peroxidase-cyclooxygenase superfamily (Fig. 1). A second evolutionary trend starting with Family 5 peroxidases led towards Family 4 including fungal and animal (cyclo-) oxygenases and plant dioxygenases (Fig. 1). Well known representatives are mammalian cyclooxygenases (COX-1 and COX-2), also known as prostaglandin-endoperoxide synthases. Finally, Family 7 was segregated from Family 6 at the level of primitive eukaryotes. These so called dual oxidases have retained an extracellular peroxidase domain of unknown function at the N-terminus followed by a transmembrane calcium-binding domain and a cytosolic flavodomain with homology to NADPH oxidase. In humans, two members (hDUOX1 and hDUOX2) are found. The function of dual oxidases is superoxide and/or hydrogen peroxide generation, however the role and interaction of the two catalytic domains (one flavo- and one heme-domain) is still under discussion. In any case, neither in representatives from Family 4 nor Family 7, the heme is covalently bound to the protein. Hence, the biochemistry of these enzymes is not examined in this review.

### 3. Conserved sequence motifs and crystal structures of peroxidases with posttranslationally modified heme

As shortly described above, in many cases members of the

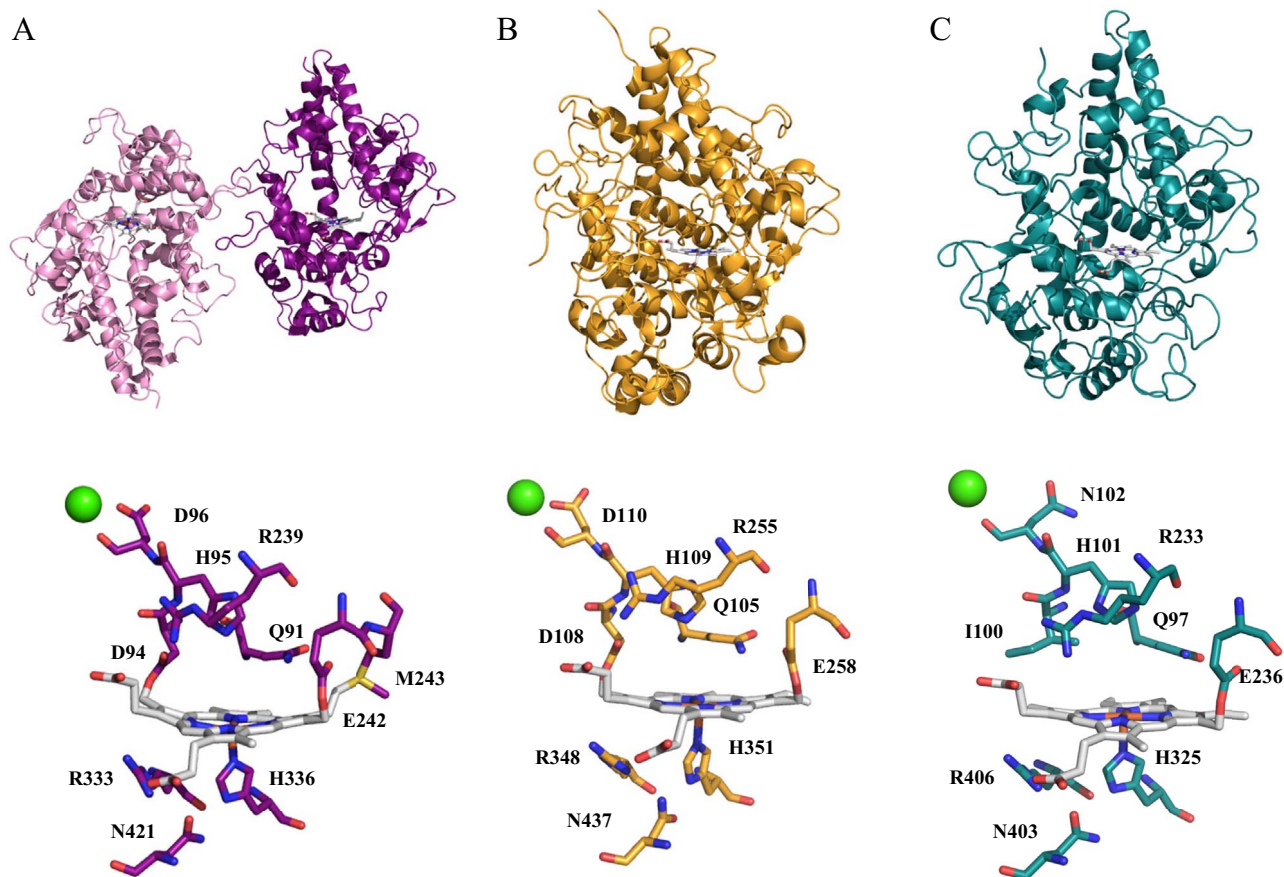


**Fig. 3.** Secondary and active site structures of myeloperoxidase (MPO), lactoperoxidase (LPO) and peroxidase from *Dictyostelium discoideum* (DdPoxA). Overall and active site structure of dimeric human MPO (A), monomeric goat LPO (B) and monomeric DdPoxA (C) revealing the mainly  $\alpha$ -helical fold. Important residues in the heme environment and distal calcium (green) are depicted in the lower panel. Figures were constructed using the coordinates deposited in the Protein Data Bank. Accession codes: 3F9P (MPO) [24], 2R5L (LPO) [25] and 6ERC (DdPoxA) [20]. (For interpretation of the references to colour in this figure legend, the reader is referred to the Web version of this article.)

peroxidase-cyclooxygenase superfamily are multidomain proteins with one heme peroxidase domain of predominantly  $\alpha$ -helical fold with a central heme-containing core of five  $\alpha$ -helices. Moreover, in five out of seven families, the prosthetic heme group is posttranslationally modified [1,2,21,22]. Fig. 2 shows the typical sequence signatures that allow the correct assignment of heme peroxidases to this superfamily. Except for Families 4 and 7 the most typical sequence is  $-X-G-Q-X-X-D-H-D-X-$  (Fig. 2A) located on  $\alpha$ -helix 2. It includes the distal catalytic histidine that is adjacent to two aspartates, the first being involved in ester bond formation with the prosthetic group and the second in  $Ca^{2+}$ -binding. The highly conserved glutamine seems to support halide binding [21,23]. Further typical distal residues include the catalytic arginine and a conserved glutamate that is also involved in the formation of the second ester bond. The typical sequence is  $-X-R-X-X-E-X-$ . Fig. 3 compares the crystal structures of human MPO (Family 1) [24], bovine LPO (Family 1) [25] and DdPoxA (Family 6) [20]. In all three representatives the fully conserved distal catalytic triad Q91-H95-R239 (MPO numbering) is at almost identical position. The mammalian enzymes have two heme to protein ester bonds between the above mentioned aspartate (D94) and glutamate (E242) residues and the 5- and 1-methyl groups of the heme. Analysis of the sequence alignment depicted in Fig. 2 suggests that - except a few peroxidases including DdPoxA (Fig. 3) [20] - all members of families 1, 2, 3, 5 and 6 have two heme to protein ester bonds. The clade of myeloperoxidases of Family 1 is unique in having a third covalent bond, i.e. a sulfonium ion linkage - between the sulfur of a methionine (M243) and the  $\beta$ -carbon of the 2-vinyl substituent of the posttranslationally modified heme [1,2,23,24,26–28]. The typical sequence motif for the Family 1 clade of

myeloperoxidases is  $-X-R-X-X-E-M-X-$ . Note that in myeloperoxidase adjacent E242 and M243 are involved in binding to the heme substituents 1-methyl and 2-vinyl resulting in a rigid conformation in this area of the active site.

Additionally to the heme to protein linkages, the distal heme cavity is stabilized by a calcium binding site with a typically pentagonal bipyramidal coordination [24,28]. Respective sequence motifs are found in families 1, 2, 3 and 6 (Fig. 2B). In all peroxidases from the peroxidase-cyclooxygenase superfamily the proximal heme iron ligand (H336) interacts with the amine side chain of a conserved asparagine (N421), whereas the carbonyl group interacts with the guanidinium group of a conserved arginine (R333) (Fig. 3). Furthermore this arginine may form a salt bridge between its guanidinium group and the 7-propionic substituent of pyrrole ring D [24,28]. This interaction requires an anionic proximal histidine, which is facilitated by lowering its  $pK_a$  by coordination of the ferric heme iron. The pronounced imidazole character of H336 might help to bridle the high reactivity of the redox intermediate Compound I (see below).

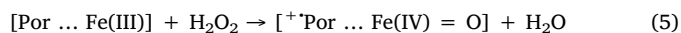
Note that except MPO, LPO and DdPoxA no crystal structures of peroxidases with posttranslationally modified heme are available. Nevertheless in human EPO and bacterial LspPOX (Family 6) proteolytic and mass spectrometric evidence has demonstrated the presence of covalent ester bonds between the heme 1- and 5-methyl and the carboxyl groups of the respective glutamate and aspartate residues [17,29]. The presence of covalent ester bonds in TPO rests on indirect evidence derived from recombinant expression of TPO in Chinese hamster ovary (CHO) cells. It has been demonstrated that incubation of cells with hydrogen peroxide significantly increased the activity of TPO

that reached the cell surface [30]. Furthermore, covalently bound heme was detected in human peroxidase 1 (hsPxd01) [14,15].

#### 4. Mechanism of posttranslational heme modification

It is well known that covalent heme binding by ester bonds is the result of an autocatalytic posttranslational maturation process. The first evidence was the finding that in recombinant LPO, produced in a baculovirus expression system, only a fraction of the protein molecules had covalently bound heme [31]. However, a higher level of covalently bound heme was obtained when a freshly isolated protein was incubated with H<sub>2</sub>O<sub>2</sub> [31,32]. Hydrolysis and analysis of the covalently bound prosthetic group in this protein confirmed that two of its original heme methyl groups now bore hydroxyl groups [31]. Similar findings were also reported for EPO [29], TPO [30], human peroxidase 1 (Family 2) [14,15] and bacterial LspPOX (Family 6) [17–19]. In this context it has to be mentioned that recent crystallographic studies on leukocyte MPO [24], the precursor promyeloperoxidase [28] and bovine lactoperoxidase [33] showed low electron density for the ester bond between the heme 1-methyl and the carboxyl groups of the respective glutamate residue, suggesting that it had high mobility and that the ester bond to this residue might have a relatively low occupancy *per se*. By contrast in DdPoxA, which cannot form an ester bond with the heme 5-methyl as the corresponding aspartate is replaced by isoleucine (Figs. 2A and 3), the occupancy of the glutamate ester bond is almost 100%.

The mechanism of formation of these posttranslational modifications has been postulated by Ortiz de Montellano [34,35]. It starts with Compound I formation and proceeds *via* a free radical mechanism. Two-electron oxidation of the heme *b* protein by hydrogen peroxide forms an oxoiron(IV) porphyrin radical Compound I and water (Reaction (5)).



Compound I oxidizes an adjacent side-chain carboxylic acid to a carboxylate radical, concomitantly reducing the heme center to the Compound II state, i.e. [Por ... Fe(IV) = O] [35]. In turn, the carboxylate radical abstracts a hydrogen atom from a methyl group, yielding a methylene radical and regenerating the carboxylic acid anion. Subsequently, intramolecular transfer of the unpaired electron from the methylene to the iron produces a methylene cation with concomitant reduction of the iron to the resting ferric state. Finally, the carboxylate anion traps the methyl cation to form the ester bond [35]. Two cycles are needed for formation of two ester bonds. In eukaryotes, this posttranslational modification most probably occurs after heme insertion in the endoplasmic reticulum [28,30]. As outlined above, ester bond formation can also be promoted by addition of H<sub>2</sub>O<sub>2</sub> to purified recombinant protein. However, typically only a small stoichiometric excess of H<sub>2</sub>O<sub>2</sub> should be added slowly in a stepwise manner, otherwise heme bleaching occurs [14,15,17–19]. This indicates that ester bond formation *in vivo* is a slow process that needs (sub)micromolar H<sub>2</sub>O<sub>2</sub>.

Support for this autocatalytic mechanism is provided by a study [36] in which a carboxyl group was introduced by site-directed mutagenesis near one of the heme methyl group of horseradish peroxidase (HRP), which is a heme *b* peroxidase from the peroxidase-catalase superfamily [1]. The variant F41E was purified with no heme covalent bonds, but upon incubation with H<sub>2</sub>O<sub>2</sub> quantitatively formed a covalent ester bond [36]. By contrast, incubation of the HRP variant S73E with H<sub>2</sub>O<sub>2</sub> oxidized the 8-methyl to 8-hydroxymethyl without forming a covalent crosslink, presumably because the carboxylic acid group could not compete with water in the final step of the reaction, in which the methylene cation is trapped. A demonstration that the hydroxyl group derives from <sup>18</sup>O-labeled water supports the proposed mechanism [35,36]. Further studies that clearly suggest autocatalytic heme-protein crosslinking were performed with ascorbate peroxidase (APX) [37–39] and cytochrome *c* peroxidase (CCP) [40], both heme *b* peroxidases from

the peroxidase-catalase superfamily [1].

The mechanism of formation of the MPO-typical M243-vinyl bond (Fig. 3) remains unclear, but it is generally assumed that it follows also an autocatalytic mechanism [34]. This is supported by H<sub>2</sub>O<sub>2</sub>-mediated bond formation between the 2-vinyl group of heme *b* and a methionine in the S160M mutant of ascorbic peroxidase [37].

The question remains whether there is a distinct sequence of posttranslational modification and, finally, bond formation. In case of MPO this was investigated by expression and characterization of D94N, D94V and E242Q mutants [41–43]. The E242Q mutant has, based on its spectroscopic properties, a normal methionine-vinyl bond [41]. This indicates that E242 is not essential for formation of the methionine-vinyl bond. This is also suggested by the crystal structure of wild-type MPO and LPO that clearly show 100% formation of the sulfonium ion linkage but less occupancy of the ester bond with E242 [24,28,33]. Both of the D94 variants yielded two proteins, one that appears to have the normal sulfonium ion linkage, and one that does not. Furthermore, it could be demonstrated that D94 is not essential for formation of either the E242-methyl link or the M243-vinyl link in MPO [42,43]. This is also supported by the fact that in DdPoxA, that lacks the respective aspartate for bond formation, the ester bond between the conserved glutamate and the heme 1-methyl is fully established. Finally, in a recent study on bacterial LspPOX (Family 6) and the mutants D109A, E238A and D109A/E238A, it was shown that both heme to protein ester bonds can form independently from each other [19].

#### 5. Impact of posttranslational modifications on spectral and redox properties

Posttranslational modification of the heme group and formation of covalent links with the protein clearly increases the overall conformational and thermal stability of the enzymes. This was demonstrated for MPO [44], proMPO [28], LPO [45] and LspPOX [17,19]. Myeloperoxidase is unique, since it forms a third covalent sulfonium ion linkage in addition to the two ester bonds. As a consequence MPO has the highest thermal and conformational stability [44] and the prosthetic group assumes a bow-shaped structure and a pronounced out-of-plane location of the ferric high-spin heme iron. The two ester bonds in LPO cause a less distorted heme (Fig. 3) [23–25,27,28,33]. As a consequence of these PTMs, peroxidases from the peroxidase-cyclooxygenase superfamily exhibit completely different spectral and redox properties compared to heme *b* peroxidases that also have a histidine as proximal ligand like HRP, APX or CCP.

Generally, the electronic absorption spectra of heme proteins are characterized by the presence of intense bands due to transitions of the  $\pi$ -electrons of the heme porphyrin group. These spectra allow the assignment of coordination and spin-states of the heme iron atom on the basis of the correlation with structurally characterized proteins and model compounds. The presence of a number of species in equilibrium, solvent effects and other factors often necessitate the use of other techniques like resonance Raman (RR) or electron paramagnetic resonance (EPR) spectroscopy.

The Soret band of ferric LPO is fairly sharp with a maximum at 412 nm, and the visible spectrum exhibits maxima at 500, 542, 590, and 630 nm [21,46]. The bandwidth and wavelength of the Soret band as well as the wavelength of the charge transfer band (CT1) at 630 nm are characteristic of a six-coordinate (6c) high-spin HS aquo ferric heme [47]. This is reflected by the crystal structures of LPO (and MPO) that contain a water molecule weakly bound to the heme iron, which is at about 2.7–2.9 Å and hydrogen bonded to the N<sub>ε</sub> of the distal histidine. Both EPO [21,48], TPO [30], human peroxidase 1 (hsPxd01) [15] and bacterial LspPOX [19] exhibit spectral features very similar to LPO suggesting similar heme cavity architectures. Table 2 and Supplemental Fig. 1 compare the absorption maxima for various representatives of the peroxidase-cyclooxygenase superfamily. Note that – compared to heme peroxidases with (unmodified) heme *b* like horseradish peroxidase

**Table 2**

Electronic absorption maxima of ferric forms of myeloperoxidase (MPO) and mutants D94V, D94N, E242Q and M243T, lactoperoxidase (LPO) and mutants E375Q and D225V, eosinophil peroxidase (EPO), human peroxidase 1 (hsPxd1), peroxidase from *Lyngbya* sp. (LspPOX) and mutants D109A, E238A and D109A/E238A, peroxidase from *Dictyostelium discoideum* (DdPoxA) and horseradish peroxidase (HRP).

	Soret region (nm)	Visible region (nm)	Reference
<b>MPO</b>	430	496, 570, 620, 690	[50,51]
D94V	430	496, 568, 620, 682	[41,55]
D94N	418, 430	496, 568, 620, 682	[41,55]
E242Q	418	510, 558, 648	[54]
M243T	413	500, 542, 590, 638	[51–53]
<b>LPO</b>	412	500, 542, 590, 630	[46]
E375Q	408	527	[56]
D225V	413	–	[56]
<b>EPO</b>	413	500, 550, 590, 638	[48]
<b>hsPxd1</b>	412	510, 547, 590, 637	[15]
<b>LspPOX</b>	413	511, 545, 584, 642	[19]
D109A	411	511, 545, 584, 642	[19]
E238A	413	511, 545, 584, 642	[19]
D109A/E238A	410	511, 545, 602, 647	[19]
<b>DdPoxA</b>	416	541, 576, 644	[20]
<b>HRP</b>	402	503, 641	[49]

(HRP) [49] (Table 2) – the Soret bands are red-shifted due to the ester bonds.

The electronic absorption maxima of ferric MPO are even more red-shifted compared to LPO and other representatives with two ester bonds (Table 2 and Supplemental Fig. 1). Its Soret maximum is at 430 nm and the spectrum shows additional bands at 496, 570, 620 and 690 nm [41,50,51]. However, upon mutation of M243 the UV-vis spectrum becomes similar to LPO (Table 2), confirming that the MPO-typical sulfonium ion linkage is responsible for these spectral properties [43,52,53]. In addition to the sulfonium ion linkage its neighbouring residue E242 contributes to the distortion from the planar conformation and the lowered symmetry [54]. The electronic absorption spectrum of the D94V MPO variant shows a splitting of the Soret absorption band into two maxima, one wild-type-like, and one similar to the M243T mutant (Table 2) [55] suggesting that exchange of D94 not only causes loss of the ester bond but also affects the sulfonium ion linkage to some extent [41,55]. Mutational studies on bovine LPO indicate that the two ester bonds in LPO are not equivalent. Loss of the glutamate linkage shows a much stronger impact on the spectral and catalytic properties than the loss of the aspartate linkage [56]. This is also supported by the spectral properties of DdPoxA (Soret band at 416 nm [20]) which lacks the aspartate ester bond (Table 2). By contrast, the Soret maximum of the LspPOX variant D109A (and the double mutant D109A/E238A, a heme *b* protein) is at 404 nm, whereas that of the variant E238A is at 411 nm [19].

The effect of the covalent bonds on the symmetry lowering of the heme group was demonstrated by RR spectroscopy in wild-type MPO and the variants M243T and D94V [53]. RR spectra of MPO are extremely rich since the three linkages significantly lower the heme group symmetry [41,53,57,58]. The richness of the RR spectra of MPO is due to the activation of almost all the porphyrin skeletal frequencies induced by the distortion imposed by the simultaneous presence of protein-porphyrin covalent bonds and the charged sulfonium group [53]. Exchange of M243 reduces the complexity of the Raman spectra. Nevertheless, in both LPO and M243 variants of MPO, the RR spectra maintain some unusual features compared to other heme proteins such as a remarkable enhancement of several out-of-plane low-frequency modes arising from a protein-induced distortion mediated by the two covalent ester bonds [22,53].

In general, the spectroscopic characteristics of ferric LPO and MPO are maintained in the ferrous forms. The electronic absorption spectrum of Fe(II) MPO is rather unique, being red-shifted with respect to other heme proteins, with a Soret maximum at 472 nm and an  $\alpha$ -band at

636 nm. Concomitantly, its vibrational spectrum is very complex [57]. Ferrous LPO has absorption maxima at 434 nm (Soret band), 561 and 593 nm [59]. This stable Fe(II) species is formed via a transient ferrous intermediate with peak maxima at 444, 561, and 593 nm. The rate of this conversion significantly increases with decreasing pH [60] and was suggested to be the result of structural changes from a relatively open, unrestricted pocket to a constrained one [61]. Interestingly, reduction of bacterial ferric LspPOX to a stable ferrous form also includes the transient formation of an unstable Fe(II) species [17]. Moreover, reduction of the MPO variant M243V gives also rise to two Fe(II) forms [53] suggesting that this is a feature common to heme peroxidases with two heme-protein ester bonds.

The low-frequency spectrum of a five-coordinated (5c) high-spin (HS) ferrous heme protein is characterized by the presence of a strong band due to the iron-imidazole stretching mode which is found in the 200–250  $\text{cm}^{-1}$  region. Its frequency correlates with the bond strength between the iron and the imidazole ring, and a shift of this band correlates with a change in the hydrogen bonding status of the proton on the proximal imidazole [62]. In both MPO and LPO the  $\nu(\text{Fe-Im})$  stretching mode is found at fairly high frequencies (248–244  $\text{cm}^{-1}$ ) [63,64] with  $\nu(\text{Fe-Im})$  of LPO being slightly higher than  $\nu(\text{Fe-Im})$  of MPO suggesting a substantial imidazolate character of the proximal histidine. This fully reflects the crystal structures of both MPO and LPO which – together with molecular dynamics simulations [24] – demonstrate the interaction of an anionic proximal histidine with the amine group of the side chain of a conserved asparagine.

Besides spectral properties, PTMs of heme have a strong impact on the redox properties of the respective heme peroxidases. Although not directly involved in the catalytic cycle, the redox behaviour of the Fe(III)/Fe(II) couple of several heme peroxidases has been analysed in a much greater detail than that of the short-living high-potential intermediates Compound I and Compound II [65], whose reduction potentials are more difficult to measure experimentally. Nevertheless, there is a general agreement that the molecular factors that determine  $E^\circ[\text{Fe(III)/Fe(II)}]$  influence also the standard reduction potential ( $E^\circ$ ) of the catalytically relevant Compound I/Fe(III) and Compound I/Compound II redox couples. Indeed, the hierarchy observed for  $E^\circ[\text{Fe(III)/Fe(II)}]$ , namely, MPO > EPO > LPO, is also reflected in  $E^\circ[\text{Compound I/Fe(III)}]$  and  $E^\circ[\text{Compound I/Compound II}]$  (Table 3) [66,67].

Typically, heme *b* peroxidases feature negative  $E^\circ[\text{Fe(III)/Fe(II)}]$  values to stabilize the ferric state for efficient reaction with  $\text{H}_2\text{O}_2$  [65], e.g. in HRP  $E^\circ[\text{Fe(III)/Fe(II)}] = -306$  mV [68]. Posttranslational modifications may increase the standard reduction potential significantly (Table 3). Myeloperoxidase is unique because the corresponding  $E^\circ$

**Table 3**

Standard reduction potentials ( $E^\circ$ ) of all relevant redox couples of myeloperoxidase (MPO wild-type) and mutants D94N, E242Q and M243V, lactoperoxidase (LPO), eosinophil peroxidase (EPO), recombinant human peroxidase 1 (HsPxd1), recombinant peroxidase from *Lyngbya* sp. PCC 8106 (LspPOX wild-type) and mutants E238A and D109A/E238A, recombinant peroxidase from *Dictyostelium discoideum* (DdPoxA) and horseradish peroxidase (HRP). Cpd I, Compound I; Cpd II, Compound II; n.d., not determined.

	Fe(III)/Fe(II) (mV)	Cpd I/Fe(III) (mV)	Cpd I/Cpd II (mV)	Cpd II/Fe(III) (mV)
<b>MPO wild-type</b>	5 [69]	1160 [76]	1350 [77]	970 [77]
D94N	–55 [67]	n.d.	n.d.	n.d.
E242Q	–94 [67]	n.d.	n.d.	n.d.
M243V	–182 [67]	n.d.	n.d.	n.d.
<b>LPO</b>	–176 [72]	1090 [75]	1140 [75]	1040 [75]
<b>EPO</b>	–126 [72]	1100 [76]	n.d.	n.d.
<b>HsPxd1</b>	–128 [15]	n.d.	n.d.	n.d.
<b>LspPOX wild-type</b>	–158 [19]	n.d.	n.d.	n.d.
E238A	–209 [19]	n.d.	n.d.	n.d.
D109A/E238A	–212 [19]	n.d.	n.d.	n.d.
<b>DdPoxA</b>	–276 [20]	n.d.	n.d.	n.d.
<b>HRP</b>	–306 [68]	883 [74]	898 [74]	869 [74]

value is +5 mV (pH 7.0) in mature dimeric leukocyte MPO or +1 mV in recombinant monomeric proMPO [69]. Variable-temperature experiments, which allow to calculate the protein and solvent derived contributions to enthalpic ( $\Delta H_{\text{rc}}^{\circ}$ ) and entropic ( $\Delta S_{\text{rc}}^{\circ}$ ) changes during reduction of Fe(III) to Fe(II), demonstrate that the sulfonium ion linkage drastically decreases the level of enthalpic stabilization of the ferric form. The positive charge of the sulfur atom electrostatically destabilizes the ferric heme. Moreover, the electron withdrawing effect of the sulfonium linkage reduces the basicity of the four pyrrole nitrogens, thereby decreasing the electron density at the heme iron. This effect might be enhanced by the pronounced distortion of the porphyrin ring. In MPO reduction  $\Delta H_{\text{rc}}^{\circ}$  and  $\Delta S_{\text{rc}}^{\circ}$  almost perfectly offset each other. Entropic changes during reduction suggests that Fe(III) reduction is accompanied by limited solvent reorganization, indicating that the hydrogen bond network of water molecules in the substrate channel leading to the distal heme site is quite rigid. This low mobility of the water molecules has been proposed to be crucial in fixing the position of the small anionic substrate chloride, and in helping the transfer and incorporation of the oxyferryl oxygen into HOCl [69]. It is important to notice that mature dimeric leukocyte MPO and recombinant monomeric, partially unprocessed proMPO share the same redox thermodynamic features suggesting almost identical heme cavity and substrate channel architectures. Recently, this could be confirmed by the crystal structure of promyeloperoxidase [28]. This is also reflected by very similar catalytic properties [70] and is the precondition that proMPO can be used in the design and testing of MPO inhibitors [71].

As outlined above, upon disruption of the sulfonium ion linkage in the M243V variant, the UV-vis and RR spectral features are considerably blue-shifted and similar to those found in LPO and EPO. In MPO M243V, the measured  $E^{\circ}$  value (−182 mV) [67] is significantly lower than in the wild-type protein and almost identical to LPO (Table 3) [72]. Redox thermodynamic studies show that protein intrinsic factors of M243V enthalpically stabilize the oxidized form more efficiently than the recombinant wild-type proMPO form. This is in agreement with the effects of disruption of the sulfonium linkage, because deletion of the (positive and electron-withdrawing) bond should stabilize the ferric form of the heme both electrostatically and electronically. Furthermore, reduction of the variant M243V is entropically favoured as a consequence of a significant reduction-induced solvent reorganization within the heme cavity not observed in wild-type MPO. This is in agreement with the proposed role of the sulfonium ion linkage in fixing the positioning of the anionic halide ions [69].

The  $E^{\circ}$  value of the MPO variant E242Q is −94 mV [67]. Disruption of the ester bond at pyrrole ring A also induces an increase in protein-based enthalpic stabilization of the ferric form, which, however, is lower than in M243V. Since in the E242Q mutant the sulfonium linkage is still present [54], the observed effect is not related to electrostatics. As suggested by RR studies [53,73] the decreased level of distortion of the heme in E242Q compared to wild-type MPO might enhance the interaction of the metal ion with the pyrrole nitrogens, thereby enthalpically stabilizing the Fe(III) form. Reduction of E242Q is entropically favoured suggesting that E242 (besides M243) is important in fixing the position of water molecules in the distal heme cavity and optimizing the position of the substrate. Indeed, the glutamate 242 ester bond is close to the bromide binding site in MPO [23], and its disruption generally decreases the halogenation activity of E242Q compared to the wild-type enzyme [54].

The standard reduction potential of the Fe(III)/Fe(II) couple of the D94V mutant is −55 mV (Table 3) [67]. Variable-temperature experiments show that elimination of this ester bond stabilizes the ferric form by protein intrinsic factors, which also reflects less distortion in D94V compared to the wild-type protein. Reduction of D94V is entropically unfavoured suggesting that this ester bond plays a minor role in stabilization of the distal H-bonding network. This is in agreement with the observation that the halide binding (and oxidation) site is close to the  $\delta$ -meso bridge and thus almost opposite to D94 (Fig. 3). The observed

negative reduction entropy [67] might be related to the destabilization of the  $\text{Ca}^{2+}$  binding site at the distal heme cavity that involves D96 in the proximity of D94 and catalytic H95 (Fig. 3). It is reasonable to assume that disruption of the ester bond at pyrrole ring C increases the mobility of the polypeptide in this region. In any case, exchange of D94 slows the chlorination and bromination reaction (see below) [55], suggesting that this ester bond contributes to the high oxidation capacity of MPO to some extent.

Heme peroxidases with two ester bonds typically have  $E^{\circ}[\text{Fe(III)/Fe(II)}]$  values between −120 mV and −180 mV, significantly more negative than MPO but more positive compared to heme *b* peroxidases, e.g. EPO (−126 mV) [72], hsPxd01 (−128 mV) [15] and LPO (−176 mV) [72] (Table 3). The reduction potential of bacterial LspPOX could only be estimated to be about −160 mV [19] since the presence of two Fe(II) forms did not allow determination of the correct value. In any case studies on the LspPOX variants D109A, E238A and D109A/E238 demonstrate that elimination of the ester bonds decreases the  $E^{\circ}$  value (Table 3) [19] underlining the impact of these PTMs on the redox properties of the heme iron. The double mutant, i.e. the heme *b* form of LspPOX, exhibits an  $E^{\circ}$  value of −227 mV. In the recently studied DdPoxA [20] that has only one (glutamate) ester linkage (Fig. 3) the standard reduction potential of the Fe(III)/Fe(II) redox couple was determined to be −276 mV. These studies clearly demonstrate the correlation between the nature and number of heme to protein linkage and  $E^{\circ}[\text{Fe(III)/Fe(II)}]$ , following the hierarchy  $E^{\circ}(\text{MPO; three linkages}) > E^{\circ}(\text{EPO, hsPxd01, LspPOX, LPO; two linkages}) > E^{\circ}(\text{DdPoxA: 1 linkage}) \sim E^{\circ}(\text{heme } b \text{ peroxidases})$ .

Studies on MPO, EPO, LPO and HRP clearly suggest that the molecular factors determining the Fe(III)/Fe(II) couple also influence the reduction potential of the catalytically relevant Compound I/Fe(III), Compound I/Compound II, and Compound II/Fe(II) couples. The lowest  $E^{\circ}$  value of the redox couples Compound I/Fe(III) and Compound I/Compound II were obtained for HRP (883 mV and 898 mV, respectively) [74]. The presence of two ester bonds significantly increases the respective  $E^{\circ}$  values as determined for LPO (1090 mV and 1140 mV, respectively) [75]. For EPO  $E^{\circ}[\text{Compound I/Fe(III)}]$  was determined to be 1100 mV [76]. As EPO exhibits structural similarities to LPO, it is reasonable to assume that the couple Compound I/Compound II has a similar  $E^{\circ}$  value to LPO. The highest standard reduction potentials of the couples Compound I/Fe(III) (1160 mV) [76] and Compound I/Compound II (1350 mV) [77] were obtained for MPO. As will be outlined below these very positive reduction potentials reflect the high oxidation capacity of MPO and its extraordinary role in substrate oxidation during bacterial killing [76,78–80].

Generally, in MPO and LPO the capacity to oxidize one-electron donors is higher for Compound I than for Compound II and this is reflected by the higher redox potential for the Compound I/Compound II couple with respect to the Compound II/Fe(III) couple. In HRP an  $E^{\circ}$  value of about 900 mV was determined for both redox intermediates (Table 3) [68], whereas differences are seen in MPO [76] and LPO [75]. Especially in MPO  $E^{\circ}[\text{Compound I/Compound II}]$  is significantly more positive compared to  $E^{\circ}[\text{Compound II/Fe(III)}]$ , which is exploited in the design of reversible MPO inhibitors [71,81]. In LPO the difference in  $E^{\circ}[\text{Compound I/Compound II}]$  and  $E^{\circ}[\text{Compound II/Fe(III)}]$  is less pronounced.

## 6. Impact of posttranslational modifications on catalysis

Peroxidases of the peroxidase-cyclooxygenase superfamily efficiently catalyze one- and two-electron oxidation reactions according to Reactions (1) and (2). In both cycles, i.e. the peroxidase cycle and the halogenation cycle, Compound I [oxoiron(IV) porphyrin radical species] is the central redox intermediate formed by reaction of the Fe(III) form with hydrogen peroxide according to Reaction (5). Here the fully conserved distal histidine-arginine couple (Fig. 3) plays a critical role in the binding, orientation and activation of  $\text{H}_2\text{O}_2$ . The histidine acts as

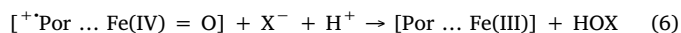
Table 4

Apparent second-order rate constants for Compound I formation and reduction as well as Compound II reduction by representatives of the peroxidase-cyclooxygenase superfamily. Myeloperoxidase (MPO) and mutants E242Q and M243V; lactoperoxidase (LPO); eosinophil peroxidase (EPO); human peroxidase 1 (hsPxd1); peroxidase from *Lyngbya* sp. PCC 8106 (LspPOX) and mutants D109A, E238A and D109A/E238A; peroxidase from *Dictyostelium discoideum* (DdPoxA) and horseradish peroxidase (HRP), -, no reaction; n.d., not determined.

Substrate	MPO	E242Q	M243V	D94N	D94V	LPO	EPO	hsPxd1	LsPOX	D109A	E238A	D109A/ E238A	DdPoxA	HRP
Reference	[79,83,85]	[54]	[43]	[55]	[55]	[46]	[48,88]	[15]	[18,19]	[19]	[19]	[19]	[20]	[49,90–92]
<b>Compound I formation</b> ( $\times 10^4 \text{ M}^{-1} \text{ s}^{-1}$ )														
H <sub>2</sub> O <sub>2</sub>	1800	78	2200	1600	870	1100	4300	1800	6000	3200	2520	1020	320	1700
<b>Compound I reduction by two-electron donors</b> ( $\times 10^4 \text{ M}^{-1} \text{ s}^{-1}$ )														
Chloride	2.5	0.0065	–	0.2	0.15	–	0.31	–	–	–	–	n. d.	–	–
Bromide	110	5.4	13	41	15	41	1900	560	126	54	2.1	n. a.	0.0015	–
Iodide	720	64	1000	1800	590	1200	9300	1680	4190	1540	2860	n. a.	10000	0.26
Thiocyanate	960	22	10000	1200	490	20000	10000	1830	2450	816	1185	n. a.	10000	–
<b>Compound I reduction by tyrosine and nitrite</b> ( $\times 10^4 \text{ M}^{-1} \text{ s}^{-1}$ )														
Tyrosine	77	0.028	n.d.	42	16	11	35	n.d.	62	n.d.	n.d.	n.d.	n.d.	5
<b>Compound II reduction by tyrosine and nitrite</b> ( $\times 10^4 \text{ M}^{-1} \text{ s}^{-1}$ )														
Tyrosine	1.57	0.018	n.d.	0.5	1.2	1	2.7	n.a.	11	n.d.	n.d.	n.d.	n.d.	1.1

proton acceptor from one oxygen and a donor to the other, while the arginine modulates the ionization of the histidine by decreasing its  $pK_a$  of the imidazole N<sub>δ</sub> and polarizes the O–O bond to promote the nucleophilic attack at the heme and subsequently heterolytic cleavage [21,82,83]. In this reaction the impact of PTM is negligible. The  $k_{app}$  values of this bimolecular reaction are within  $(0.3\text{--}4.6) \times 10^7 \text{ M}^{-1} \text{ s}^{-1}$  at pH 7.0 for posttranslationally modified heme peroxidases [15,18,19,46,48,79,83,84] (Table 4), but very similar values are found for heme *b* peroxidases [49,82]. The minor role of heme modification in Compound I formation is underlined by the fact that MPO mutants lacking D94 and M243 exhibit rates of Compound I formation very similar to wild-type MPO [43]. Since in the E242Q variant the rates of Compound I formation but also Compound I reduction (see below) as well as formation of the cyanide complex are decreased, it was hypothesized that this might be related to blocking of the substrate accessibility to the heme cavity [54]. In case of bacterial recombinant LspPOX that could be reconstituted as heme *b* protein, which was subsequently posttranslationally modified by added H<sub>2</sub>O<sub>2</sub> [19], the determined apparent rate constant for Compound I formation (and cyanide binding) significantly increases upon PTM suggesting the necessity of structural rearrangement for optimum activity of the catalytic histidine-arginine pair during heterolytic cleavage of H<sub>2</sub>O<sub>2</sub>.

In contrast to Compound I formation, the heme to protein linkages play an important role in Compound I reduction. The best studied representatives of the peroxidase-cyclooxygenase superfamily, i.e. Family 1 peroxidases like MPO, EPO, LPO and TPO, are unique in their ability to efficiently oxidize (pseudo-)halides (X<sup>−</sup>, namely Cl<sup>−</sup>, Br<sup>−</sup>, I<sup>−</sup>, SCN<sup>−</sup>) to (pseudo-)hypohalides (HOX, namely HOCl, HOBr, HOI, HOSCN) according to Reaction (6).



This redox process can be divided into two half-reactions, where the reduction of Compound I is coupled with the (pseudo-)halide oxidation, written as reduction process in Reaction (7). Standard reduction potentials for the redox couples HOX/X<sup>−</sup>, H<sub>2</sub>O at pH 7.0 are 1.28 (X<sup>−</sup> = Cl<sup>−</sup>), 1.13 (Br<sup>−</sup>), 0.78 (I<sup>−</sup>) and 0.56 (SCN<sup>−</sup>) V [66]. The reduction potential of these couples increase with decreasing pH (~30 mV per pH unit) as two electrons and one proton are involved in the corresponding half-reaction (Reaction (7)). At pH 7.0, HOCl ( $pK_a = 7.53$ ), HOBr ( $pK_a = 8.8$ ), HOI ( $pK_a = 10.0$ ) exist predominantly in the undissociated form, whereas HOSCN ( $pK_a = 5.3$ ) is dissociated [66].



Thus, the ease of oxidation of (pseudo)halide ions is the following: SCN<sup>−</sup> > I<sup>−</sup> > Br<sup>−</sup> > Cl<sup>−</sup>. Therefore, Compound I of all peroxidases, regardless whether the heme group is covalently bound or not, can

oxidize iodide and thiocyanate (Table 4). In so far studied representatives of the peroxidase-cyclooxygenase superfamilies the rates for thiocyanate oxidation are extremely high ( $\geq 9.6 \times 10^6 \text{ M}^{-1} \text{ s}^{-1}$ ), with LPO, EPO and DdPoxA being  $> 10^8 \text{ M}^{-1} \text{ s}^{-1}$ . Similarly, oxidation of iodide is very fast ( $\geq 7.2 \times 10^6 \text{ M}^{-1} \text{ s}^{-1}$ ), with EPO and DdPoxA showing the highest rates (Table 4). Except for MPO, elimination of the aspartate has no impact on thiocyanate or iodide oxidation [42], whereas disruption of the glutamate ester bond [54] significantly reduces the oxidation of both electron donors. By contrast, elimination of the sulfonium ion linkage even increases the rates of SCN<sup>−</sup> and I<sup>−</sup> oxidation [43], clearly demonstrating that this MPO-typical structural feature is not essential in oxidation of two-electron donors with  $E^{\circ}[\text{XOH}/\text{X}^-, \text{H}_2\text{O}; \text{pH } 7.0] < 0.8 \text{ V}$ . Elimination of E242 in MPO affected halide oxidation in general, most probably due to hampering proper binding and access of the electron donors [54].

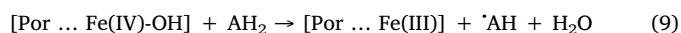
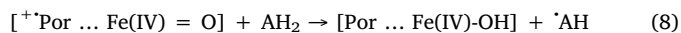
In contrast to hypothiocyanite and hypoiodous acid formation, oxidation of chloride and bromide strongly depend on the PTMs described above. Only MPO Compound I is able to react with chloride at pH 7.0 at reasonable rates (Table 4) [79,83,85], which reflects the high reduction potential of the MPO redox couple Compound I/Fe(III) discussed above [76]. At acidic pH, Compound I reduction is accelerated significantly, which is also reflected by an increase in the steady-state chlorination activity of MPO [86,87]. At pH 5, also EPO Compound I is able to oxidize chloride but at poor rates [48].

The importance of the MPO-typical sulfonium ion linkage in Compound I reduction mediated by chloride is seen in various M243 mutants that lost the chlorination activity almost completely [43,52]. This is also underlined by the LPO-like  $E^{\circ}$  values of the redox couple Fe(III)/Fe(II) of the respective M243 mutants [67]. As already outlined above, exchange of E242 also decreased the chlorination activity dramatically, whereas exchange of D94 by asparagine has almost no impact on chloride oxidation since the sulfonium ion linkage in these mutants is (partially) intact [43].

Efficient oxidation of bromide by Compound I ( $> 10^6 \text{ M}^{-1} \text{ s}^{-1}$ ) is seen in several heme peroxidases with two ester linkages following the hierarchy EPO > hsPxd01 > LspPOX > MPO at pH 7 (Table 4). These peroxidases have  $E^{\circ}$  values of the redox couple Fe(III)/Fe(II) > −160 mV and the hierarchy in  $E^{\circ}$  values reflects the apparent rate constants for Compound I reduction at pH 7.0 (compare Tables 3 and 4). The standard reduction potential of  $E^{\circ}[\text{Compound I}/\text{Fe(III)}]$  of EPO is 1100 mV. Lactoperoxidase, with  $E^{\circ}[\text{Fe(III)}/\text{Fe(II)}] = -176 \text{ mV}$  [72] and  $E^{\circ}[\text{Compound I}/\text{Fe(III)}] = 1090 \text{ mV}$  [75], shows barely detectable activity with bromide at neutral pH, suggesting that besides thermodynamics also structural features must contribute to the poor bromide oxidation capacity of LPO. The heme peroxidase from *Dictyostelium discoideum* with  $E^{\circ}[\text{Fe(III)}/\text{Fe(II)}] = -276 \text{ mV}$  [20] and only one ester linkage is unable to oxidize bromide.

Recently, the importance of PTM in the capacity to oxidize bromide was demonstrated with bacterial LspPOX [19]. In the reconstituted heme *b* form of the wild-type enzyme Compound I reacts slowly with bromide, whereas upon incubation with H<sub>2</sub>O<sub>2</sub> and establishment of the two ester bonds the rate of Compound I reduction was increased by a factor of 6300, clearly underlining that PTM – besides increasing the reduction potential of the redox couple Compound I/Fe(III) – also optimizes the heme cavity architecture for access, binding and oxidation of bromide. This study [19] also demonstrated that elimination of the glutamate ester bond in this peroxidase has almost no impact on structural rearrangement during PTM and consequently the heme *b* and PTM form of the LspPOX mutant E238A showed very similar  $E^{\circ}$  values of the Fe(III)/Fe(II) couple as well as similar kinetics of interconversion of the redox intermediates. Nevertheless, Compound I reduction by bromide was significantly slower compared to the wild-type enzyme, underlining the importance of the intact glutamate ester bond in maintenance of the halide binding network at the distal heme cavity. By contrast, the LspPOX mutant D109A showed significant structural differences in the heme cavity between the heme *b* form and the PTM version. The heme *b* form has low catalytic activity but – upon induction of PTM with hydrogen peroxide – the D109A mutant could be rescued and exhibited wild-type like activity.

Although for Family 1 and 2 enzymes the halogenation cycle (i.e. Reactions (5) & (6)) seems to be related to the physiological function, heme peroxidases of this superfamily can also follow the peroxidase cycle which includes Reactions (5), (8) and (9). In the peroxidase cycle, Compound I is reduced by two one-electron donors (AH<sub>2</sub>; e.g. tyrosine, serotonin, ascorbate, urate, nitrite etc.) via Compound II [oxoiron(IV) species] to the ferric resting state thereby releasing the corresponding radicals (AH) [21,22,66,88,89].



Typically, significant differences in rates of Reaction (8) are observed between heme *b* peroxidases [90–92] and posttranslationally modified enzymes but also within the latter group. For example MPO Compound I is a significantly better one-electron oxidant compared to LPO Compound I. By contrast, the determined rates of Compound II reduction (Reaction (9)) are similar [88,89], which is also reflected by the fact that the standard reduction potentials of the redox couple Compound II/Fe(III) enzyme for MPO and LPO are similar, with MPO (970 mV) being even 70 mV lower than LPO (1040 mV) (Table 3) [75]. Regarding Compound II reduction mediated by tyrosine [ $E^{\circ}(\text{tyrosyl radical/tyrosine}) = 0.94 \text{ V}$  at pH 7] [66] both LPO and MPO show rate constants that are similar to that of the heme *b* enzyme HRP (Table 4) [66,91–93]. Regarding Compound I reduction by tyrosine marked differences are observed, with MPO Compound I being an extremely strong oxidant of one-electron donors which is reflected by the very positive reduction potential of the Compound I/Compound II couple (Table 3). Compound I of MPO is able to oxidize substrates with a reduction potential around 1.2 V and even higher [81]. This again underlines the role of the sulfonium ion linkage in further increasing the electron deficiency of the porphyrin  $\pi$ -cation radical of Compound I. In Compound II the porphyrin radical is quenched but the heme iron is still in its low-spin form which favours a more in-plane position compared to its native high-spin state. This could partially explain the large difference of  $E^{\circ}$  of the Fe(III)/Fe(II) couple between MPO and LPO, whereas the  $E^{\circ}$  values for the Compound II/Fe(III) couple are similar. The binding and oxidation site for the (aromatic) substrates should be identical in Compound I and Compound II, namely a hydrophobic region at the entrance to the distal cavity almost centered above the pyrrole ring D 8-methyl group [21,93–95].

The marked difference in  $E^{\circ}$  value of the MPO Compound I/Compound II and Compound II/Fe(III) couple is unique among heme peroxidases and is exploited in the design of reversible inhibitors of

MPO [71,81,93–95]. These inhibitors of typically very positive reduction potential compete with the substrate chloride and are efficiently oxidized by MPO Compound I. Thereby, Compound II is formed, which is unable to oxidize both chloride and these inhibitors. As a consequence MPO is trapped in the Compound II state and the chlorination activity of MPO is dampened.

## 7. Conclusion

Contrary to former assumption, posttranslational attachment of the heme *via* ester bonds is not limited to vertebrate peroxidases but widespread within the peroxidase-cyclooxygenase superfamily. A hydrogen peroxide-driven autocatalytic radical mechanism post-translationally modifies heme peroxidases of five out of seven families of this superfamily. As a consequence enzymes with one, two, or three covalent heme-protein bonds are synthesized. During PTM significant structural rearrangements at the distal heme cavity occur that distort the prosthetic group, lower its symmetry and promote the out-of-plane location of the heme iron as well as optimize the binding of small anionic substrate like halides. As a consequence, these oxidoreductases show peculiar spectral features and typically positive reduction potentials of the redox couples Fe(III)/Fe(II), Compound I/Fe(III) and Compound I/Compound II. The capacity to oxidize two- and one-electron donors by the catalytically relevant redox intermediate Compound I is higher than in heme *b* enzymes. There is only one clade of Family I, i.e. myeloperoxidases, that have in addition to two ester linkages an electron withdrawing sulfonium ion linkage. As a consequence the prosthetic group of MPO is strongly distorted and the relevant  $E^{\circ}$  values are very positive, enabling MPO to play a prominent role in innate immunity by producing antimicrobial hypochlorous acids.

Several representatives from Families 1, 2 and 6 with two ester linkages are able to oxidize bromide to hypobromous acid, which can play a function in the innate immune system of mammals as demonstrated for EPO, but also in biosynthesis of extracellular matrix as shown for peroxidase 1. The physiological relevance of bromide oxidation by bacterial representatives like LspPOX is completely unknown. Furthermore, there are heme peroxidases with two- or one ester bonds that are unable to oxidize bromide but efficiently produce hypothiocyanite or hypiodous acid. These reaction products again can be used as either antimicrobial agents as demonstrated for LPO and DdPoxA or in biosynthesis as shown for TPO. Further studies must reveal the crystal structures of more PTM peroxidases (e.g. EPO, TPO, hsPxd01) in order to understand the relationships between structure, function and physiological roles of these oxidoreductases.

## Conflicts of interest

The authors declare no competing financial interest.

## Acknowledgements

This work was supported by the Austrian Science Fund FWF [Doctoral Program BioToP – Biomolecular Technology of Proteins (W1224)].

## Appendix A. Supplementary data

Supplementary data related to this article can be found at <http://dx.doi.org/10.1016/j.abb.2018.02.008>.

## References

- [1] M. Zamocky, S. Hofbauer, I. Schaffner, B. Gasselhuber, A. Nicolussi, M. Souidi, K.F. Pirker, P.G. Furtmüller, C. Obinger, Arch. Biochem. Biophys. 574 (2015) 108–119.
- [2] M. Zamocky, C. Jakopitsch, P.G. Furtmüller, C. Dunand, C. Obinger, Proteins 71 (2008) 589–605.

- [3] K. Tamura, G. Stecher, D. Peterson, A. Filipiski, S. Kumar, *Mol. Biol. Evol.* 30 (2013) 2725–2729.
- [4] S.J. Klebanoff, *J. Leukoc. Biol.* 77 (2005) 598–625.
- [5] M.J. Davies, C.L. Hawkins, D.I. Pattison, M.D. Rees, *Antioxid. Redox Signal* 10 (2008) 1199–1234.
- [6] R. Ihalin, V. Loimaranta, J. Tenovu, *Arch. Biochem. Biophys.* 445 (2006) 261–268.
- [7] A. Malik, J.K. Batra, *Crit. Rev. Microbiol.* 38 (2012) 168–1816.
- [8] J. Ruf, P. Carayon, *Arch. Biochem. Biophys.* 445 (2006) 269–277.
- [9] R.E. Nelson, L.I. Fessler, Y. Takagi, B. Blumberg, D.R. Keene, P.F. Olson, C.G. Parker, J.H. EMBO J. 13 (1994) 3438–3447.
- [10] M. Soudi, M. Zamocky, C. Jakopitsch, P.G. Furtmüller, C. Obinger, *Chem. Biodivers.* 9 (2012) 1776–1793.
- [11] G. Bhavé, C.F. Cummings, R.M. Vanacore, C. Kumagai-Cresse, I.A. Ero-Tolliver, M. Rafi, J.S. Kang, V. Pedchenko, L.I. Fessler, J.H. Fessler, B.G. Hudson, *Nat. Chem. Biol.* 8 (2012) 784–790.
- [12] A.S. McCall, C.F. Cummings, G. Bhavé, R. Vanacore, A. Page-McCaw, B.G. Hudson, *Cell* 157 (2014) 1380–1392.
- [13] Z. Peterfi, M. Geiszt, *Trends Biochem. Sci.* 39 (2014) 305–307.
- [14] M. Soudi, M. Paumann-Page, C. Delporte, K.F. Pirker, M. Bellei, E. Edenhofer, G. Stadlmayr, G. Battistuzzi, K. Zouaoui Boudjeltia, P.G. Furtmüller, P. Van Antwerpen, C. Obinger, *J. Biol. Chem.* 290 (2015) 10876–10890.
- [15] M. Paumann-Page, R.-S. Katz, M. Bellei, I. Schwartz, E. Edenhofer, B. Sevcnikar, M. Soudi, S. Hofbauer, G. Battistuzzi, P.G. Furtmüller, C. Obinger, *J. Biol. Chem.* 292 (2017) 4583–4592.
- [16] A. Vizzini, D. Parrinello, M.A. Sanfratello, V. Mangano, N. Parrinello, M. Cammarata, *Dev. Comp. Immunol.* 41 (2013) 59–67.
- [17] M. Auer, C. Gruber, M. Bellei, K.F. Pirker, M. Zamocky, D. Kroiss, A.S. Teufer, S. Hofbauer, M. Soudi, G. Battistuzzi, P.G. Furtmüller, C. Obinger, *J. Biol. Chem.* 288 (2013) 27181–27199.
- [18] M. Auer, A. Nicolussi, G. Schütz, P.G. Furtmüller, C. Obinger, *J. Biol. Chem.* 289 (2014) 31480–31491.
- [19] A. Nicolussi, M. Auer, J. Weissensteiner, G. Schütz, S. Katz, D. Maresch, S. Hobauer, M. Bellei, G. Battistuzzi, P.G. Furtmüller, C. Obinger, *Biochemistry* 56 (2017) 4525–4538.
- [20] A. Nicolussi, J.D. Dunn, G. Mlynek, M. Bellei, M. Zamocky, G. Battistuzzi, K. Djinović-Carugo, P.G. Furtmüller, T. Soldati, C. Obinger, *J. Biol. Chem.* 293 (2018), <http://dx.doi.org/10.1074/jbc.RA117.000463>.
- [21] P.G. Furtmüller, M. Zederbauer, W. Jantschko, J. Helm, M. Bogner, C. Jakopitsch, C. Obinger, *Arch. Biochem. Biophys.* 445 (2006) 199–213.
- [22] M. Zederbauer, P.G. Furtmüller, S. Brogioni, C. Jakopitsch, G. Smulevich, C. Obinger, *Nat. Prod. Rep.* 24 (2007) 571–584.
- [23] T.J. Fiedler, C.A. Davey, R.E. Fenna, *J. Biol. Chem.* 275 (2000) 11964–11971.
- [24] X. Carpena, P. Vidossich, K. Schroettner, B.M. Calisto, S. Banerjee, J. Stampfer, M. Soudi, P.G. Furtmüller, C. Rovira, I. Fita, C. Obinger, *J. Biol. Chem.* 284 (2009) 25929–25937.
- [25] A.K. Singh, N. Singh, S. Sharma, S.B. Singh, P. Kaur, A. Bhushan, A. Srinivasan, T.P. Singh, *J. Mol. Biol.* 376 (2008) 1060–1075.
- [26] I.M. Kooter, B.P. Koehler, N. Moguilevsky, A. Bollen, R. Wever, M.K. Johnson, *J. Biol. Inorg. Chem.* 4 (1993) 684–691.
- [27] R. Fenna, J. Zeng, C. Davey, *Arch. Biochem. Biophys.* 316 (1995) 653–656.
- [28] I. Grishkovskaya, M. Paumann-Page, R. Tscheliensnig, J. Stampfer, S. Hofbauer, M. Soudi, B. Sevcnikar, C. Oostenbrink, P.G. Furtmüller, K. Djinović-Carugo, W.M. Nauseef, C. Obinger, *J. Biol. Chem.* 292 (2017) 8244–8261.
- [29] C. Oxvig, A.R. Thomsen, M.T. Overgaard, E.S. Sorensen, P. Højrup, M.J. Bjerrum, G.J. Gleich, L. Sottrup-Jensen, *J. Biol. Chem.* 274 (1999) 16953–16958.
- [30] L. Fayadat, P. Niccoli-Sire, J. Lanet, J.-L. Franc, *J. Biol. Chem.* 274 (1999) 10533–10538.
- [31] G.D. DePillis, S. Ozaki, J.M. Kuo, D.A. Maltby, R.R. Ortiz de Montellano, *J. Biol. Chem.* 272 (1997) 8857–8860.
- [32] C. Colas, J.M. Kuo, P.R. Ortiz de Montellano, *J. Biol. Chem.* 277 (2002) 7191–7200.
- [33] P.K. Singh, H.V. Sirohi, N. Iqbal, P. Tiwari, P. Kaur, S. Sharma, T.P. Singh, *Biochim. Biophys. Acta* 1865 (2017) 329–335.
- [34] C. Colas, P.R. Ortiz de Montellano, *Chem. Rev.* 103 (2003) 2305–2332.
- [35] P.R. Ortiz de Montellano, E. Raven, B. Dunford (Eds.), *Heme Peroxidases*, Royal Society of Chemistry, Cambridge, U.K., 2016, pp. 3–30 (Chapter 1).
- [36] C. Colas, P.R. Ortiz de Montellano, *J. Biol. Chem.* 279 (2004) 24131–24140.
- [37] C.L. Metcalfe, M. Ott, N. Patel, K. Singh, S.C. Mistry, H.M. Goff, E.L. Raven, *J. Am. Chem. Soc.* 126 (2004) 16242–16248.
- [38] Z. Pipirou, A.R. Bottril, C.M. Metcalfe, S.C. Mistry, S.K. Badyal, B.J. Rawlings, E.L. Raven, *Biochemistry* 46 (2007) 13269–13278.
- [39] C.L. Metcalfe, O. Daltrop, S.J. Ferguson, E.L. Raven, *Biochem. J.* 15 (2007) 355–361.
- [40] B. Bhaskar, C.E. Immoos, H. Shimizu, F. Sulc, P.J. Farmer, T.L. Poulos, *J. Mol. Biol.* 328 (2003) 157–166.
- [41] I.M. Kooter, N. Moguilevsky, A. Bollen, N.M. Sijtsma, C. Otto, H.L. Dekker, R. Wever, *Eur. J. Biochem.* 264 (1999) 211–217.
- [42] M. Zederbauer, P.G. Furtmüller, M. Bellei, J. Stampfer, C. Jakopitsch, G. Battistuzzi, N. Moguilevsky, C. Obinger, *J. Biol. Chem.* 282 (2007) 17041–17052.
- [43] M. Zederbauer, P.G. Furtmüller, B. Ganster, N. Moguilevsky, C. Obinger, *Biochem. Biophys. Res. Commun.* 356 (2007) 450–456.
- [44] S. Banerjee, J. Stampfer, P.G. Furtmüller, C. Obinger, *Biochim. Biophys. Acta* 1814 (2011) 375–387.
- [45] S. Banerjee, P.G. Furtmüller, C. Obinger, *Biotechnol. J.* 6 (2011) 231–243.
- [46] P.G. Furtmüller, W. Jantschko, G. Regelsberger, C. Jakopitsch, J. Arnhold, C. Obinger, *Biochemistry* 41 (2002) 11895–11900.
- [47] G. Smulevich, F. Neri, O. Willemsen, K. Choudhury, M.P. Marzocchi, T.L. Poulos, *Biochemistry* 34 (1995) 13485–13490.
- [48] P.G. Furtmüller, U. Burner, G. Regelsberger, C. Obinger, *Biochemistry* 39 (2000) 15578–15584.
- [49] H.B. Dunford, H.B. Dunford (Ed.), *Heme Peroxidases*, WILEY-VCH, New York, 1999, pp. 58–91 (Chapter 4).
- [50] P.C. Andrews, N.I. Krinsky, *J. Biol. Chem.* 256 (1981) 4211–4218.
- [51] R. Wever, H. Plat, *Biochim. Biophys. Acta* 661 (1981) 235–239.
- [52] I.M. Kooter, N. Moguilevsky, A. Bollen, L.A. van der Veen, C. Otto, H.L. Dekker, R. Wever, *J. Biol. Chem.* 274 (1999) 26794–267802.
- [53] S. Brogioni, A. Feis, M.P. Marzocchi, M. Zederbauer, P.G. Furtmüller, C. Obinger, G. Smulevich, *J. Raman Spectrosc.* 37 (2006) 263–276.
- [54] M. Zederbauer, W. Jantschko, K. Neuschwandtner, C. Jakopitsch, N. Moguilevsky, C. Obinger, P.G. Furtmüller, *Biochemistry* 44 (2005) 6482–6491.
- [55] M. Zederbauer, P.G. Furtmüller, M. Bellei, J. Stampfer, C. Jakopitsch, G. Battistuzzi, N. Moguilevsky, C. Obinger, *J. Biol. Chem.* 282 (2007) 17041–17052.
- [56] G. Suriano, S. Watanabe, E. Ghibaudi, A. Bollen, R.P. Ferrari, N. Moguilevsky, *Bioorg. Med. Chem. Lett* 11 (2001) 2827–2831.
- [57] R. Floris, N. Moguilevsky, G. Puppels, A. Jacquet, R. Renirie, A. Bollen, R.J. Wever, *Am. Chem. Soc.* 117 (1995) 3907–3912.
- [58] I.M. Kooter, B.P. Koehler, N. Moguilevsky, A. Bollen, R. Wever, M.K. Johnson, *J. Biol. Inorg. Chem.* 4 (1999) 684–691.
- [59] W. Jantschko, P.G. Furtmüller, M. Zederbauer, K. Neuschwandtner, C. Jakopitsch, C. Obinger, *Arch. Biochem. Biophys.* 434 (2005) 51–59.
- [60] P.I. Ohlsson, *Eur. J. Biochem.* 142 (1984) 233–238.
- [61] H.M. Abu-Soud, S.L. Hazen, *Biochemistry* 40 (2001) 10747–10755.
- [62] G. Smulevich, A. Feis, B.D. Howes, *Acc. Chem. Res.* 38 (2005) 433–440.
- [63] T. Kitagawa, S. Hashimoto, J. Teraoka, S. Nakamura, H. Yajima, T. Hosoya, *Biochemistry* 22 (1983) 2788–2792.
- [64] K. Kitagawa, K. Nagai, M. Tsubaki, *FEBS Lett.* 104 (1979) 376–378.
- [65] G. Battistuzzi, M. Bellei, C.A. Bortolotti, M. Sola, *Arch. Biochem. Biophys.* 500 (2010) 21–36.
- [66] J. Arnhold, E. Monzani, P.G. Furtmüller, M. Zederbauer, L. Casella, C. Obinger, *Eur. J. Inorg. Chem.* 19 (2006) 3801–3811.
- [67] G. Battistuzzi, J. Stampfer, M. Bellei, J. Vlasits, M. Soudi, P.G. Furtmüller, C. Obinger, *Biochemistry* 50 (2011) 7987–7994.
- [68] G. Battistuzzi, M. Borsari, J. Ranieri, M. Sola, *J. Am. Chem. Soc.* 124 (2001) 26–27.
- [69] G. Battistuzzi, M. Bellei, M. Zederbauer, P.G. Furtmüller, M. Sola, C. Obinger, *Biochemistry* 45 (2006) 12750–12755.
- [70] P.G. Furtmüller, W. Jantschko, G. Regelsberger, C. Jakopitsch, N. Moguilevsky, C. Obinger, *FEBS Lett.* 503 (2001) 147–150.
- [71] E. Malle, P.G. Furtmüller, W. Sattler, C. Obinger, *Br. J. Pharmacol.* 152 (2007) 838–854.
- [72] G. Battistuzzi, M. Bellei, J. Vlasits, S. Banerjee, P.G. Furtmüller, M. Sola, C. Obinger, *Arch. Biochem. Biophys.* 494 (2010) 72–77.
- [73] S. Brogioni, J. Stampfer, P.G. Furtmüller, A. Feis, C. Obinger, G. Smulevich, *Biochim. Biophys. Acta* 1784 (2008) 843–849.
- [74] Z.S. Farhangrazi, M.E. Fossett, L.S. Powers, W.R. Ellis, *Biochemistry* 34 (1995) 2866–2871.
- [75] P.G. Furtmüller, J. Arnhold, W. Jantschko, M. Zederbauer, C. Jakopitsch, C. Obinger, *J. Inorg. Biochem.* 99 (2005) 1220–1229.
- [76] J. Arnhold, P.G. Furtmüller, G. Regelsberger, C. Obinger, *Eur. J. Biochem.* 268 (2001) 5142–5148.
- [77] P.G. Furtmüller, J. Arnhold, W. Jantschko, H. Pichler, C. Obinger, *Biochem. Biophys. Res. Commun.* 301 (2003) 551–557.
- [78] J. Arnhold, P.G. Furtmüller, C. Obinger, *Redox Rep.* 8 (2003) 179–186.
- [79] P.G. Furtmüller, U. Burner, C. Obinger, *Biochemistry* 37 (1998) 17923–17930.
- [80] W. Jantschko, P.G. Furtmüller, M. Allegra, M.A. Livrea, C. Jakopitsch, G. Regelsberger, C. Obinger, *Arch. Biochem. Biophys.* 398 (2002) 12–22.
- [81] W. Jantschko, P.G. Furtmüller, M. Zederbauer, K. Neuschwandtner, I. Lehner, C. Jakopitsch, J. Arnhold, C. Obinger, *Biochem. Pharmacol.* 69 (2005) 1149–1157.
- [82] T.L. Poulos, J. Kraut, *J. Biol. Chem.* 255 (1980) 8199–8205.
- [83] L.A. Marquez, J.T. Huang, H.B. Dunford, *Biochemistry* 33 (1994) 1447–1454.
- [84] P.G. Furtmüller, U. Burner, G. Regelsberger, C. Obinger, *Biochemistry* 39 (2000) 15578–15584.
- [85] P.G. Furtmüller, C. Obinger, Y. Hsuanyu, H.B. Dunford, *Eur. J. Biochem.* 267 (2000) 5858–5864.
- [86] H.C. Lee, K.S. Booth, W.S. Caughey, M. Ikeda-Saito, *Biochim. Biophys. Acta* 1076 (1991) 317–320.
- [87] D.R. Ramos, M.V. García, M.V. Canle, A. Santaballa, P.G. Furtmüller, C. Obinger, *Arch. Biochem. Biophys.* 466 (2007) 221–233.
- [88] P.G. Furtmüller, W. Jantschko, G. Regelsberger, C. Obinger, *Biochim. Biophys. Acta* 1548 (2001) 121–128.
- [89] L.A. Marquez, H.B. Dunford, *J. Biol. Chem.* 270 (1995) 30434–30440.
- [90] T. Arasio, H.B. Dunford, *Biochem. Biophys. Res. Commun.* 94 (1972) 1171–1182.
- [91] R. Roman, H.B. Dunford, *Biochemistry* 11 (1972) 2017–2079.
- [92] I. Ralston, H.B. Dunford, *Can. J. Biochem.* 56 (1978) 1115–1119.
- [93] J. Soubhye, M. Prevost, P. Van Antwerpen, K.M. Boudjeltia, A. Rousseau, P.G. Furtmüller, C. Obinger, M. Vanhaeverbeek, J. Ducobu, J. Neve, M. Gelbcke, F. Dufresne, *J. Med. Chem.* 53 (2010) 8747–8759.
- [94] I. Aldib, J. Soubhye, K. Zouaoui Boudjeltia, M. Vanhaeverbeek, A. Rousseau, P.G. Furtmüller, C. Obinger, F. Dufresne, J. Nève, P. Van Antwerpen, M. Prevost, *J. Med. Chem.* 55 (2012) 7208–7218.
- [95] J. Soubhye, I. Aldiba, B. Elfving, G. Wegener, M. Gelbcke, P.G. Furtmüller, M. Podrecca, R. Conotte, J.-M. Colet, A. Rousseau, F. Reye, A. Sarakbi, M. Vanhaeverbeek, J.M. Kauffmann, C. Obinger, J. Nève, M. Prevost, K. Zouaoui Boudjeltia, F. Dufresne, P. Pierre Van Antwerpen, *J. Med. Chem.* 56 (2013) 3944–3958.

# Structure of human promyeloperoxidase (proMPO) and the role of the propeptide in processing and maturation

Irina Grishkovskaya, Martina Paumann-Page, Rupert Tscheliessnig, Johanna Stampler, Stefan Hofbauer, Monika Soudi, **Benjamin Sevcnikar**, Chris Oostenbrink, Paul G. Furtmüller, Kristina Djinović-Carugo, William M. Nauseef and Christian Obinger

Research Article

The Journal of Biological Chemistry Vol. 292, No. 20, pp. 8244-826,  
March 27, 2017

DOI: 10.1074/jbc.M117.775031



# Structure of human promyeloperoxidase (proMPO) and the role of the propeptide in processing and maturation

Received for publication, January 3, 2017, and in revised form, March 9, 2017. Published, Papers in Press, March 27, 2017, DOI 10.1074/jbc.M117.775031

✉ Irina Grishkovskaya<sup>‡</sup>, Martina Paumann-Page<sup>§</sup>, Rupert Tscheliessnig<sup>¶</sup>, Johanna Stampler<sup>§</sup>, ✉ Stefan Hofbauer<sup>‡</sup>, Monika Soudi<sup>§</sup>, Benjamin Sevcnikar<sup>§</sup>, ✉ Chris Oostenbrink<sup>||</sup>, ✉ Paul G. Furtmüller<sup>§</sup>, ✉ Kristina Djinović-Carugo<sup>‡\*\*</sup>, ✉ William M. Nauseef<sup>††1,2</sup>, and Christian Obinger<sup>§1,3</sup>

From the <sup>‡</sup>Department of Structural and Computational Biology, Max F. Perutz Laboratories, University of Vienna, A-1030 Vienna, Austria, the <sup>§</sup>Department of Chemistry, Division of Biochemistry, BOKU-University of Natural Resources and Life Sciences, Muthgasse 18, A-1190 Vienna, Austria, the <sup>¶</sup>Austrian Centre of Industrial Biotechnology (ACIB), Muthgasse 11, A-1190 Vienna, Austria, the <sup>||</sup>Department of Material Sciences and Process Engineering, Institute of Molecular Modeling and Simulation, BOKU-University of Natural Resources and Life Sciences, A-1190 Vienna, Austria, the <sup>††</sup>Inflammation Program and Department of Medicine, Roy J. and Lucille A. Carver College of Medicine, University of Iowa, Iowa City, Iowa 52242, and the <sup>\*\*</sup>Department of Biochemistry, Faculty of Chemistry and Chemical Technology, University of Ljubljana, Večna pot 113, 1000 Ljubljana, Slovenia

Edited by Norma Allewell

Myeloperoxidase (MPO) is synthesized by neutrophil and monocyte precursor cells and contributes to host defense by mediating microbial killing. Although several steps in MPO biosynthesis and processing have been elucidated, many questions remained, such as the structure-function relationship of monomeric unprocessed proMPO *versus* the mature dimeric MPO and the functional role of the propeptide. Here we have presented the first and high resolution (at 1.25 Å) crystal structure of proMPO and its solution structure obtained by small-angle X-ray scattering. Promyeloperoxidase hosts five occupied glycosylation sites and six intrachain cystine bridges with Cys-158 of the very flexible N-terminal propeptide being covalently linked to Cys-319 and thereby hindering homodimerization. Furthermore, the structure revealed (i) the binding site of proMPO-processing proconvertase, (ii) the structural motif for subsequent cleavage to the heavy and light chains of mature MPO protomers, and (iii) three covalent bonds between heme and the protein. Studies of the mutants C158A, C319A, and C158A/C319A demonstrated significant differences from the wild-type protein, including diminished enzymatic activity and prevention of export to the Golgi due to prolonged association with the chaperone calnexin. These structural and functional findings provide novel insights into MPO biosynthesis and processing.

Neutrophils figure prominently in human host defense against infection, and optimal antimicrobial action in neutrophils relies on the action of hypochlorous acid (HOCl), the product of the myeloperoxidase (MPO)<sup>4</sup>-H<sub>2</sub>O<sub>2</sub>-chloride system (1). Production and targeting of MPO to azurophilic granules occur in promyelocytic myeloid precursors in normal human bone marrow (2), and only neutrophils and monocytes express MPO. However, MPO shares many structural features with other members of the peroxidase-cyclooxygenase superfamily (3, 4), most notably the presence of covalent bonds between the heme group and the peptide backbone (5, 6). In MPO, the prosthetic group is covalently linked to the protein via autocatalytic formation of two ester bonds with highly conserved aspartate and glutamate residues and a sulfonium ion linkage between the 2-vinyl group and a conserved methionine (5, 7–9). The existence of these three covalent heme-to-protein bonds correlates with the peculiar spectroscopic, redox, and catalytic properties of this metalloprotein (6, 10–12) and its capacity to catalyze hypochlorous acid production in phagosomes of stimulated human neutrophils (13).

Among members of the peroxidase-cyclooxygenase superfamily, mature MPO alone is a functional dimer, composed of two identical glycosylated protomers that contain covalently bound heme, an N-terminal 14.5-kDa light polypeptide (L-chain), and a 59-kDa heavy polypeptide (H-chain) (5, 7, 8), with the two H-chains linked covalently by a single Cys-319–Cys-319 bridge. Each heavy-/light-chain subunit-containing protomer (*i.e.* hemi-MPO) exhibits the same specific peroxidase activity as does the holoenzyme (14), suggesting that dimerization contributes little to the overall enzymatic activity of mature MPO and leaving the structural or functional advantages of dimerization unknown.

MPO biosynthesis encompasses a series of critical proteolytic processing steps during synthesis and intracellular traffick-

This work was supported by the Austrian Science Fund, FWF (Doctoral Program BioToP-Molecular Technology of Proteins (W1224) and P20664). This work also was supported by National Institutes of Health Grants A1116546 and A1044642 and a Merit Review Award from the U. S. Department of Veterans Affairs (to W. M. N.). The authors declare that they have no conflicts of interest with the contents of this article. The content is solely the responsibility of the authors and does not necessarily represent the official views of the National Institutes of Health.

✂ Author's Choice—Final version free via Creative Commons CC-BY license.

The atomic coordinates and structure factors (code 5MFA) have been deposited in the Protein Data Bank (<http://wwpdb.org/>).

<sup>1</sup> Both authors contributed equally to this work.

<sup>2</sup> To whom correspondence may be addressed. Tel.: 319-335-4278; Fax: 319-335-4194; E-mail: william-nauseef@uiowa.edu.

<sup>3</sup> To whom correspondence may be addressed. Tel.: 43-1-47654-77273; Fax: 43-1-47654-77059; E-mail: christian.obinger@boku.ac.at.

<sup>4</sup> The abbreviations used are: MPO, myeloperoxidase; proMPO, promyeloperoxidase; CRT, calreticulin; aa, amino acid; CLN, calnexin; ER, endoplasmic reticulum; PDB, Protein Data Bank; SAXS, small-angle X-ray scattering; DSC, differential scanning calorimetry; Bicine, *N,N*-bis(2-hydroxyethyl)glycine.

ing. Fig. 1 depicts schematically the overall structure of monomeric proMPO (90 kDa) and homodimeric MPO ( $2 \times 74$  kDa) and also provides the corresponding amino acid sequence of the primary translation product (15). In MPO biosynthesis the primary translational product (80 kDa, 745 aa) is converted into 90-kDa apoproMPO (700 aa) after cotranslational cleavage of the signal peptide and *en bloc* N-linked glycosylation followed by limited deglycosylation (16). ApoproMPO acquires heme in the endoplasmic reticulum (ER) thereby becoming enzymatically active 90-kDa promyeloperoxidase or proMPO (Fig. 1) (2, 17). Its export from the ER and subsequent processing require heme acquisition (17–19). ProMPO contains a 116-amino acid N-terminal pro-region that is required for its stability, as its deletion results in retention of proMPO in the ER and failure to undergo proteolytic processing to generate mature MPO (20), but its precise function and fate during MPO biosynthesis are unknown. A proconvertase eliminates the pro-region in a post-ER compartment producing a 74-kDa intermediate species that is subsequently further processed by cysteine proteases to the L-chain and H-chain (21) followed by dimerization. Most of the proMPO synthesized in the ER follows this proteolytic processing and targeting to azurophilic granules, but a substantial fraction is also constitutively secreted by normal bone marrow granulocyte precursors (2) and human myeloid cell lines (16, 22) as well as by heterologous MPO-expressing K562 cells (23), human embryonic kidney 293 (HEK) cells (24), or Chinese hamster ovary (CHO) cells (25).

Although several steps in MPO biosynthesis and processing have been elucidated, many unanswered questions remain, especially with respect to (i) the structure-function relationships of monomeric unprocessed proMPO *versus* mature dimeric MPO purified from azurophilic granules and (ii) the functional role of the propeptide. Here we explored the structure of proMPO, the importance of Cys-319 and Cys-319–Cys-319 bridge formation for stability, and the consequences of disrupting the dimerization of MPO. We present the high-resolution crystal structure of proMPO recombinantly produced by CHO cells and demonstrate how the flexible propeptide blocks dimerization by the formation of a disulfide bridge between Cys-158 from the propeptide and Cys-319. We show that the architecture of the heme cavity and the substrate access channel is already fully established at the proMPO stage and that the presence of the Cys-158–Cys-319 disulfide bond is essential for allowing proMPO to exit the ER and enter the Golgi apparatus for subsequent proteolytic processing. In the absence of the Cys-158–Cys-319 bridge, proMPO remains arrested in the ER, associated with the chaperones calnexin and calreticulin, and fails to undergo proteolytic processing to mature MPO.

## Results

### Biochemical properties and structural heterogeneities of proMPO and MPO

Fig. 2A compares the electronic absorption spectra of the ferric forms of monomeric proMPO (*green line*) recombinantly produced in CHO cells with dimeric MPO (*gray line*) purified from neutrophils. The almost identical spectral features (Soret maximum at 428 nm and additional bands at 570, 620, and 690

nm) of proMPO and MPO clearly suggest the presence of a six-coordinated high-spin heme embedded in a very similar heme cavity (12). It is important to note that proMPO heterologously expressed in HEK293 cells exhibits almost identical biochemical properties (8).

The structural component of the present study utilized proMPO produced in CHO cells. The purity number ( $A_{428}/A_{280}$ ) of the recombinant protein varied between 0.54 and 0.58, suggesting heme occupancy of  $>85\%$ . Despite identical spectral features, proMPO and MPO exhibited significant differences in thermal stability and overall composition (see also Fig. 1). Monomeric 90-kDa proMPO showed one prominent endotherm upon unfolding with a  $T_m$  value at 83 °C (Fig. 2B). The endotherm with  $T_m$  at 53 °C can be assigned to unfolding of the fraction of heme-free protein, in agreement with the purity numbers ( $\sim 15\%$  apoprotein), suggesting that the heme stabilizes proMPO. By comparison, homodimeric (mature) MPO comprises two 74-kDa protomers, each being composed of an L-chain (14.5 kDa) and an H-chain (59 kDa) (Fig. 2C). The thermal stability of the mature MPO ( $T_m = 90$  °C) was higher compared with that of proMPO (Fig. 2B), indicating that proteolytic processing and subsequent dimerization further stabilize the enzyme. It has to be mentioned that with both proMPO and MPO, deconvolution of the main endotherm suggests the presence of non-two-state transitions (*i.e.* the presence of at least one unfolding intermediate) but with close  $T_m$  values (see corresponding fits in Fig. 2B).

Before undertaking X-ray structure determination, we analyzed the two purified MPO forms by mass spectrometry in order to probe the heterogeneity of the N termini of the respective polypeptide chains. Additionally, the N terminus of proMPO was tested by both Edman degradation and mass spectrometry. Upon using Edman degradation the N-terminal sequence A49-A-P-A-V-L-G-E-V-D-T was found and confirmed by mass spectrometry. Upon peptide mass mapping and analysis the peptide with the sequence A49-A-P-A-V-L-G-E-V-D-T-S-L-V-L-S-S-M-E-E-A-K was identified.

Interestingly, mass spectrometry revealed also that proteolytic maturation of MPO did not result in defined N termini of both the L- and the H-chain. In MPO purified from leukocytes, three different N termini for the L-chain were found, namely Gly-164 (identified peptide:  $^{164}\text{GVTCPEQDKYR}^{174}$ ), Val-165 ( $^{165}\text{VTCPEQDKYR}^{174}$ ), and Thr-166 ( $^{166}\text{TCPEQDKYR}^{174}$ ), respectively, resulting from the proteolytic elimination of the propeptide during maturation (compare with Fig. 1A). Another maturation step in MPO biosynthesis is the elimination of the hexapeptide  $^{273}\text{ASFVTG}^{278}$  resulting in the formation of the L- and H-chain (Fig. 1A). However, upon tryptic digestion of MPO and peptide analysis, it could be demonstrated also that the N terminus of the H-chain showed some heterogeneity, because three peptides ( $^{277}\text{TGVNCTSCVQQPPCFPLK}^{295}$ ,  $^{278}\text{GVNCTSCVQQPPCFPLK}^{295}$ , and  $^{279}\text{VNCETSCVQQPPCFPLK}^{295}$ ) were identified by mass spectrometric analysis of leukocyte MPO (compare with Fig. 1B). The amino acids  $^{273}\text{ASFV}^{276}$  could not be detected by MS analysis. This demonstrates that leukocyte MPO protomers were cleaved into the L- and H-chains by the elimination of tetra- ( $^{273}\text{ASFV}^{276}$ ), penta- ( $^{273}\text{ASFVT}^{277}$ ), or hexapeptides ( $^{273}\text{ASFVTG}^{278}$ ).

## Structure of proMPO and its impact on maturation

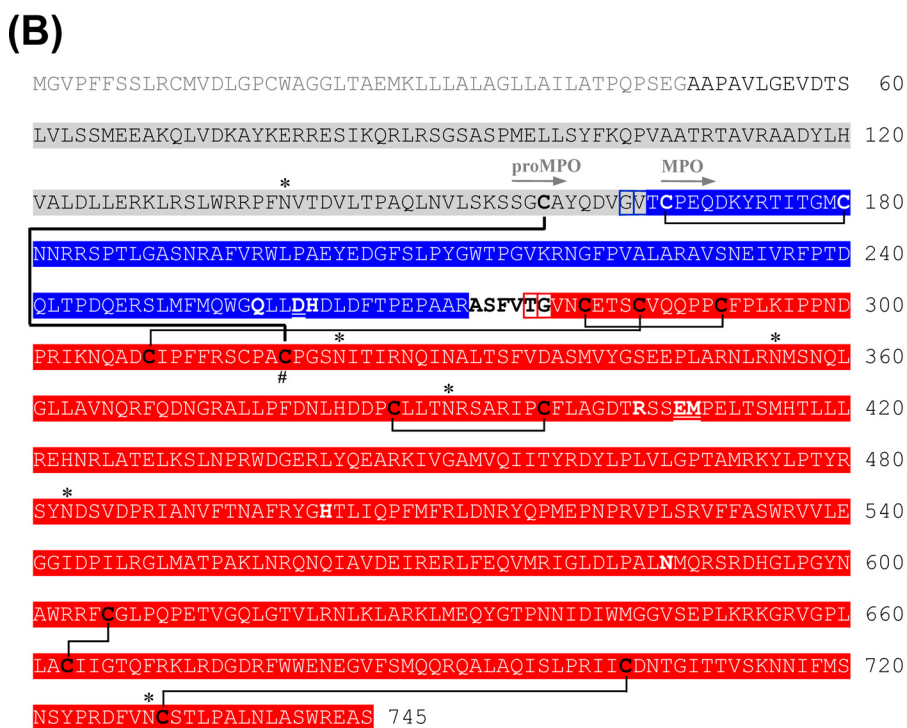
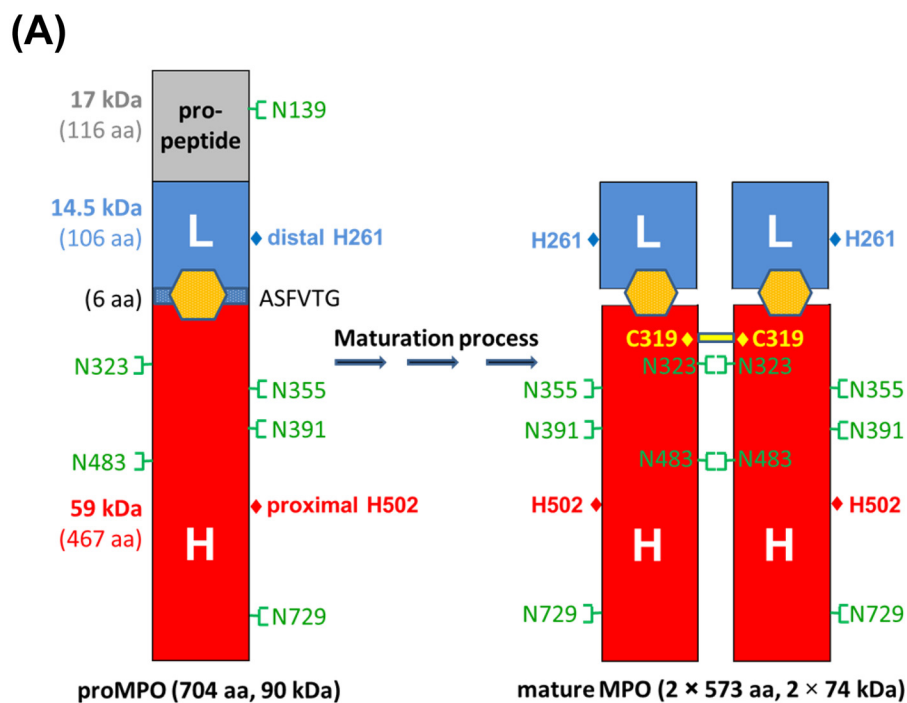


**Figure 1. Structure and sequence of proMPO and mature MPO.** *A*, schematic presentation of the structure of monomeric unprocessed proMPO and dimeric mature MPO, including the locations of the distal and proximal catalytic histidines (His-261 and His-502) and the *N*-glycosylation sites. The propeptide of proMPO and the L- and H-chain of mature MPO are depicted in gray, blue, and red, respectively, together with the respective molar masses and number of amino acids. *B*, sequence of the primary translation product of human myeloperoxidase. Mature MPO is a homodimer with each monomer composed of a light (blue) and heavy chain (red). The signal peptide (light gray), the propeptide (gray), and a small peptide (depicted in bold black letters) are excised co- and posttranslationally. Boxed in blue and red are the alternative N termini of the light and heavy chains, respectively. Cysteine residues are depicted in bold black or white, and cysteine residue 319, which is responsible for dimer formation in mature MPO, is marked by the # symbol. Disulfides of MPO are shown by black lines. The cystine bridge in proMPO between Cys-158 and Cys-319 is shown as a bold black line. The *N*-glycosylation sites of both MPO forms are marked by an asterisk (\*). ProMPO is a single peptide chain (Ala-49–Ser-745). The first resolved amino acid residues of the crystal structures of proMPO and MPO are depicted with gray arrows. Important catalytic residues are depicted in bold, and amino acid residues involved in the covalent heme to protein links are underlined and bold.

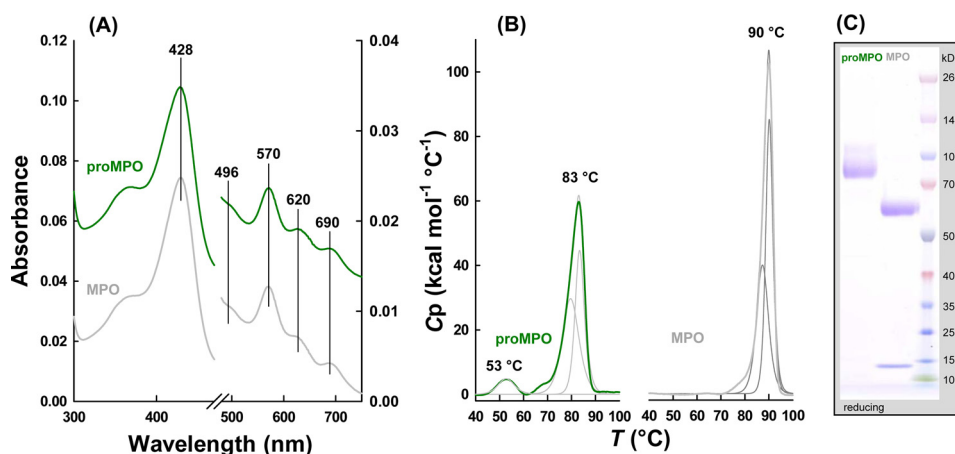


**Figure 2. Biochemical properties of monomeric proMPO and dimeric MPO.** *A*, UV-visible spectra of 8  $\mu\text{M}$  (per heme) of proMPO (green) and MPO (gray) recorded in PBS. Spectra were shifted along the y axis for better visualization. *B*, thermal stability of proMPO and MPO evaluated by DSC. Thermal transitions of proMPO (green) and MPO (gray) were fitted to non-two-state equilibrium-unfolding models by the Levenberg-Marquardt nonlinear least squares method, and fits are depicted in dark green for proMPO and dark gray for MPO. *C*, SDS-PAGE of 2  $\mu\text{g}$  of proMPO and MPO was resolved under reducing conditions on a 4–12% gradient gel.

### Crystal structure of proMPO

Monoclinic proMPO crystals (space group C2) were grown with one proMPO molecule per asymmetric unit (Table 1). The structure was solved at 1.25-Å resolution by molecular replacement using the atomic coordinates of human leukocyte myeloperoxidase (PDB accession code 1MHL) as a search model. Interestingly, continuous electron density could only be seen for residues Gly-157 to Ala-744, with Gly-157–Val-165 belonging to the propeptide, whereas residues Ala-49–Ser-156 could not be modeled (compare with Fig. 1*B*). Analysis of the crystal packing boundaries showed a symmetry-related molecule in close contact with the propeptide region Gly-157–Val-165. If the propeptide were fully folded and in the position observed in the small-angle X-ray scattering (SAXS)-derived model (see below), the propeptide would clash with a symmetry-related molecule (Fig. 3*B*). However, solvent channels along crystallographic axis *b* are wide enough ( $38 \times 36$  Å) to accommodate the propeptide, which is about 29 Å wide in the folded state. Because an SDS-PAGE of the crystals demonstrated the presence of the full-length protein (Fig. 3*A*), this clearly suggests that the propeptide exhibits a high flexibility compared with the core of the protein (Thr-166–Ala-744). Analysis of the solvent content and Matthews coefficient ( $V_M$ ) for one molecule of proMPO per asymmetric unit yields 2.28 Å<sup>3</sup>/Da, well within the commonly observed range of  $1.62 < V_M < 3.53$  Å<sup>3</sup>/Da).

The greater flexibility of the propeptide compared with that of the core of proMPO is also reflected in the observed differences in thermal stability between proMPO and MPO (see above). Regarding the core structure of proMPO, the averaged root mean square deviation for the C $\alpha$  atoms with respect to the 1MHL protomer structure of mature MPO revealed high similarity with a root mean square deviation of 0.49 Å over 576 superposed C $\alpha$  atoms.

The segment of the propeptide visible in the electron density of proMPO (Fig. 4*B*) is anchored to the core protein via a cystine bridge (Cys-158–Cys-319) together with polar and hydrophobic interactions, resulting in a buried surface area of 399 Å<sup>2</sup>. In particular, the guanidinium group of Arg-193 is engaged in two hydrogen bonds with the main chain carbonyl groups of

**Table 1**

### Data collection and refinement statistics

DATA COLLECTION	
Source	ID29, ESRF
Wavelength (Å)	0.98
Resolution (Å)	44.7 – 1.25 (1.27–1.25) <sup>a</sup>
Space group	C2
Unit cell (Å, °)	a=106.15, b=109.15 c = 83.97; $\alpha = \gamma = 90$ ; $\beta = 122.6$
Molecules / a.u.	1
Unique reflections	211866 (7053)
Completeness (%)	95.7 (64.6)
R <sub>merge</sub> <sup>b</sup>	0.110 (0.814)
R <sub>meas</sub> <sup>c</sup>	0.121 (0.986)
R <sub>pim</sub> <sup>d</sup>	0.049 (0.541)
CC <sub>1/2</sub>	0.993 (0.521)
Multiplicity	5.6 (3.0)
I/sig(I)	8.2 (1.3)
B <sub>Wilson</sub> (Å <sup>2</sup> )	12.4
REFINEMENT	
R <sub>cryst</sub> <sup>e</sup> / R <sub>free</sub> <sup>f</sup>	12.0 / 13.6
R.m.s.d. bonds (Å)	0.008
R.m.s.d. angles (°)	1.14

<sup>a</sup> Values in parentheses are for the highest resolution shell.

$${}^b R_{\text{merge}} = \frac{\sum_{hkl} \sum_{i=1}^N |I_{i(hkl)} - \bar{I}(hkl)|}{\sum_{hkl} \sum_{i=1}^N I_{i(hkl)}}$$

$${}^c R_{\text{meas}} = \frac{\sum_{hkl} \sqrt{N/(N-1)} \sum_{i=1}^N |I_{i(hkl)} - \bar{I}(hkl)|}{\sum_{hkl} \sum_{i=1}^N I_{i(hkl)}}$$

$${}^d R_{\text{pim}} = \frac{\sum_{hkl} \sqrt{1/(N-1)} \sum_{i=1}^N |I_{i(hkl)} - \bar{I}(hkl)|}{\sum_{hkl} \sum_{i=1}^N I_{i(hkl)}}$$

Where  $\bar{I}(hkl)$  is the mean intensity of multiple  $I_{i(hkl)}$  observations of the symmetry-related reflections, *N* is the redundancy

$${}^e R_{\text{cryst}} = \frac{\sum \|F_{\text{obs}} - |F_{\text{calc}}|\|}{\sum \|F_{\text{obs}}\|}$$

<sup>f</sup> R<sub>free</sub> is the cross-validation R<sub>factor</sub> computed for the test set of reflections (5 %) which are omitted in the refinement process.

Ala-159 and Gln-161, which stabilizes the main-chain conformation of the propeptide, whereas the side chain of Val-165 makes hydrophobic interactions with Met-179.

## Structure of proMPO and its impact on maturation

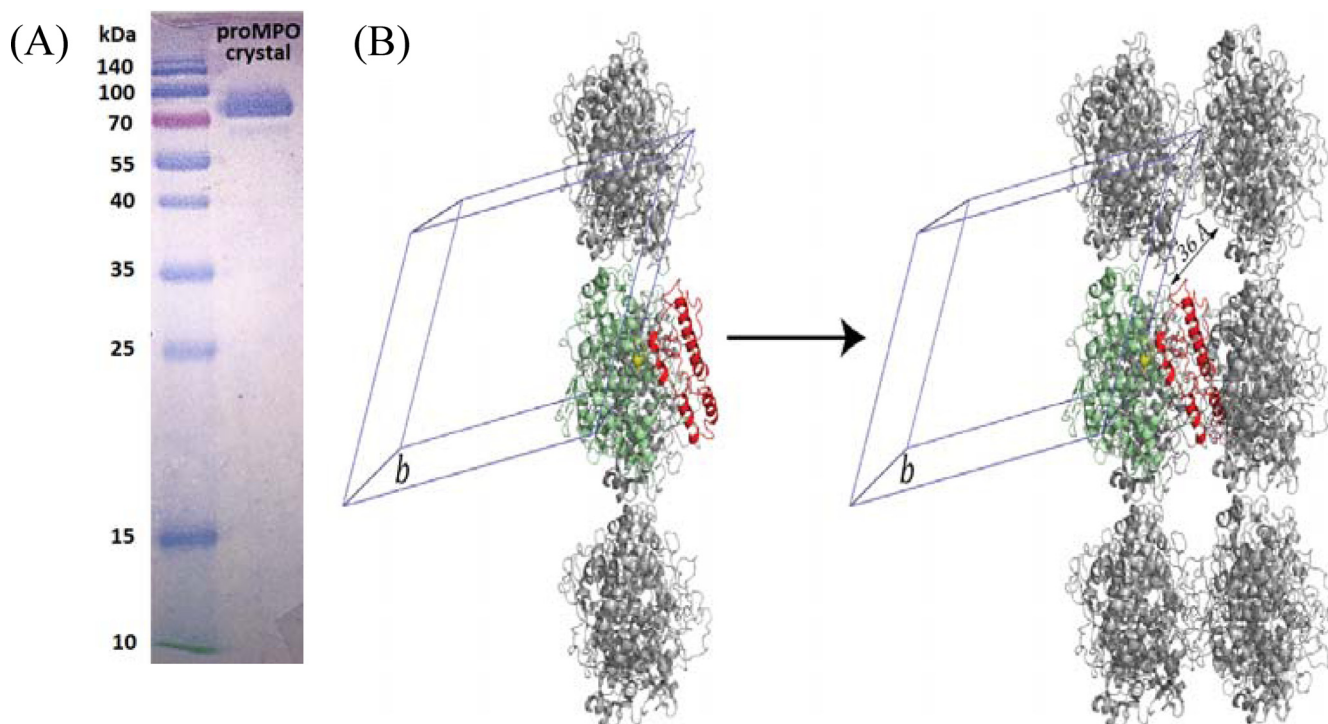


**Figure 3. Crystal packing.** *A*, SDS-PAGE of proMPO crystals. *B*, crystal packing. The core protein of proMPO of the asymmetric unit is presented in green, and the propeptide derived from modeling is shown in red. Symmetry-related molecules are presented in gray. The crystallographic axis *b* is indicated to help identify the solvent channels parallel to it. Additionally, one solvent-channel-width dimension is given.

The structure of proMPO appeared to be highly glycosylated, showing five occupied *N*-glycosylation sites at Asn-323, Asn-355, Asn-391, Asn-483, and Asn-729, respectively (compare Fig. 4A with Fig. 1A), which confirms a recent comparative study on the *N*-glycan composition of MPO and proMPO (26). Clear electron density could be observed in all of them for the first *N*-linked GlcNac, with the exception of Asn-729 where electron density was poor due to either high flexibility or low occupancy of this site. The electron density indicates the presence of an additional sugar monomer in Asn-355, Asn-483, and Asn-391. Weak electron density could be observed for the branched GlcNac2-Man3 structure at Asn-355. Generally, the B-factors for the sugar atoms were relatively high, with an average value of 45.5 Å<sup>2</sup> (average B-factor for the protein atoms is 17.5 Å<sup>2</sup>), which is consistent with the mobility and flexibility of glycan structures.

In mature MPO the glycan at Asn-323 (and to some extent sugar residues at Asn-483) contributes mainly to the interface between the two protomers (schematically shown in Fig. 1A) and thus stabilizes the homodimeric structure (5, 7, 8). The hybrid model (see below) suggested that Asn-323 was embedded in the interface between the propeptide and the core protein. The putative *N*-glycosylation site at the propeptide (Asn-139) could not be verified here because of the lack of electron density. However, recent mass spectrometric analysis showed that Asn-139 of the recombinant form is glycosylated (26). Moreover, the hybrid model and the SAXS data (see below) suggest that Asn-139 is in proximity to Asn-323, which might indicate that the respective glycan chains interact. By contrast, in proMPO the glycan at Asn-483 did not participate to the interface between the propeptide and the core protein.

Furthermore, the crystal structure of proMPO displayed the presence of six disulfide intrachain bridges, namely Cys-167–Cys-180, Cys-281–Cys-291, Cys-285–Cys-309, Cys-387–Cys-398, Cys-606–Cys-663, and Cys-704–Cys-730, respectively (Fig. 4A; compare with Fig. 1B). The same disulfide bridges are found in mature MPO, with Cys-167–Cys-180 located in the L-chain and the remaining disulfide bridges belong to the H-chain of leukocyte MPO. However, most interestingly, Cys-319 of proMPO, which is known to form an interchain disulfide bridge between the H-chains of the symmetry-related halves (74 kDa) in dimeric MPO (compare with Fig. 1A) (5, 7, 8), formed a disulfide bridge with Cys-158 of the propeptide. Fig. 4B depicts a close-up of the C-terminal stretch of the propeptide (Gly-157–Val-165) and the neighboring core-protein region including the Cys-158–Cys-309 intrachain bridge in comparison with the interface between the two protomers in mature MPO, which are linked by the Cys-319–Cys-319 interchain bridge.

As outlined above, one proteolytic maturation step of proMPO includes the excision of a tetra-, penta-, or hexapeptide resulting in the creation of the L- and H-chain. It has been proposed that the hydrolytic cleavage is mediated by a cysteine protease located in the Golgi network (21). The crystal structure of proMPO shows that the stretch <sup>273</sup>ASFVTG<sup>278</sup> was part of a surface-exposed  $\alpha$ -helix loop segment (Fig. 4C) with all six amino acids surface exposed (accessible surface areas follow the hierarchy Phe-275 > Gly-278 > Val-276 > Ala-273 > Ser-274 > Thr-277) (Fig. 4C). Interestingly, the hybrid model (see below) indicates that Lys-129 and Ser-132 of the helix formed by the residues Leu-125–Ser-132 of the propeptide interact with this region of the core protein (Fig. 4C). Note that

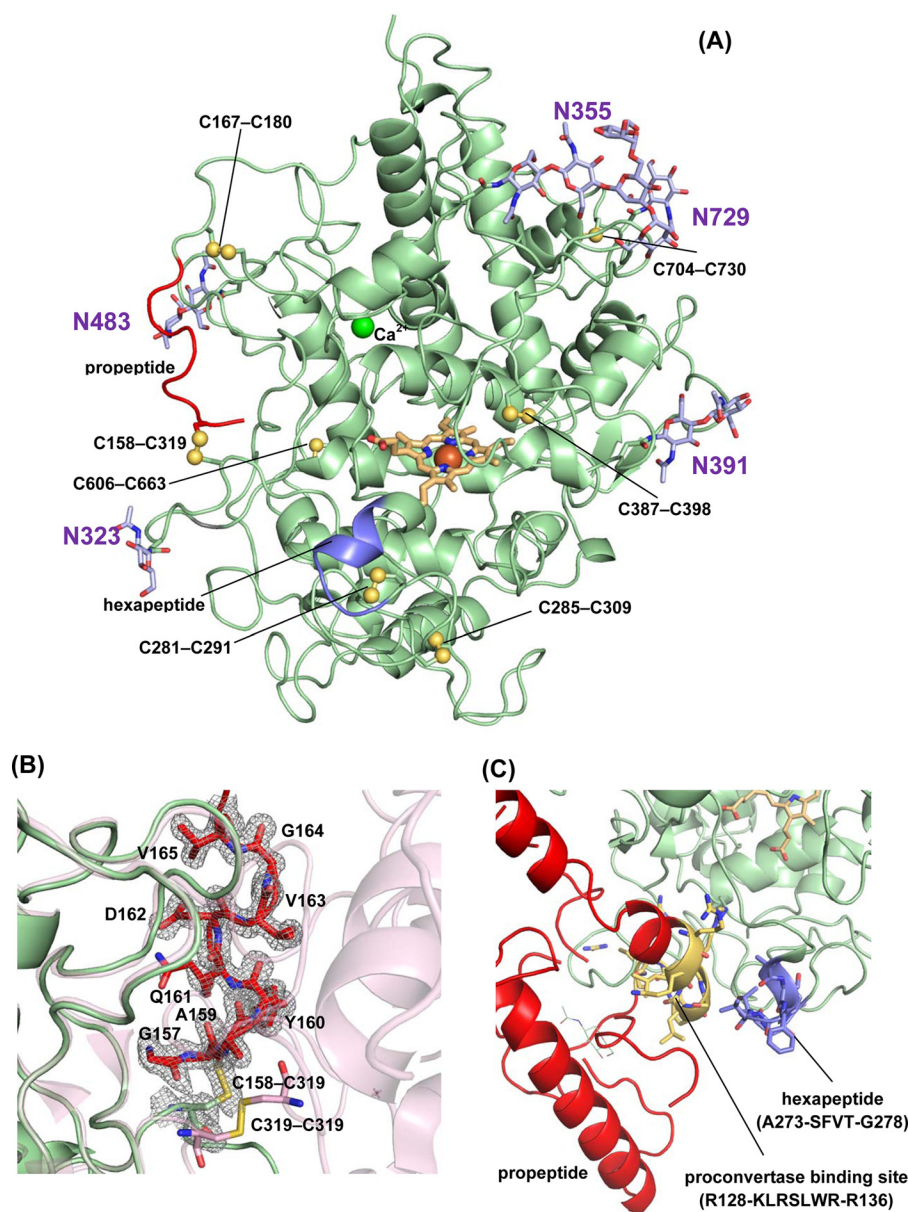


**Figure 4. Overall structure of proMPO.** A, crystal structure of recombinant proMPO. The disulfide bridges are depicted in yellow. In addition the N-glycosylation sites are shown in light violet. The segment of the propeptide visible in the electron density is shown in red, and the hexapeptide is shown in blue. B, close-up view of the C-terminal stretch of the propeptide (Gly-157–Val-165, shown in red) and the surrounding core-protein region, including the Cys-158–Cys-309 bridge, together with the  $2F_o - F_c$  electron density map contoured at the  $1\sigma$  level. The second protomer in dimeric MPO, including the Cys-319–Cys-319 disulfide bridge, is depicted in light pink for comparison. C, close-up view of the area around the hexapeptide  $^{273}\text{ASFVTG}^{278}$  (blue) and neighboring proposed proconvertase-binding site ( $^{128}\text{RKLRS}^{132}$ ) (highlighted in yellow). The rest of the propeptide is depicted in red.

$^{128}\text{RKLRS}^{132}$  is part of the proposed proconvertase-binding site (see below). This suggests that the propeptide not only hinders dimerization by blocking Cys-319 and embedding the glycan at Asn-323 in the propeptide-core protein interface but also hinders access of the cysteine protease to the surface-exposed  $^{273}\text{ASFVTG}^{278}$  region.

Importantly, the propeptide of proMPO did not interfere with substrate accessibility to the heme cavity. Fig. 5A schematically presents and compares the main access channels in the two protomers of MPO and proMPO. The length of the channels in MPO and proMPO (20.3 and 20.7 Å), the bottleneck radius (0.97 and 1.03 Å), and the curvature (length over distance, 1.29 and 1.34), respectively, were almost identical. More-

over, the architecture of the heme cavity was almost superimposable. In both MPO and proMPO the heme group is posttranslationally modified and covalently linked with the protein. The ester bond between Asp-260 and a hydroxymethyl group on pyrrole ring C was present, as was the sulfonium ion linkage between the  $\beta$ -carbon of the vinyl group on pyrrole ring A and the sulfur atom of Met-409 (Fig. 5B). Similar to leukocyte MPO (8), the side chain of Glu-408 had a low electron density, indicating high mobility and suggesting that the ester bond was present only in a fraction of the population of protein molecules (Fig. 5B). Similar to MPO, the electron density at the methyl substituent of pyrrole ring A in proMPO suggested hydroxylation. As a consequence of these modifications, pyrrole ring A

## Structure of proMPO and its impact on maturation

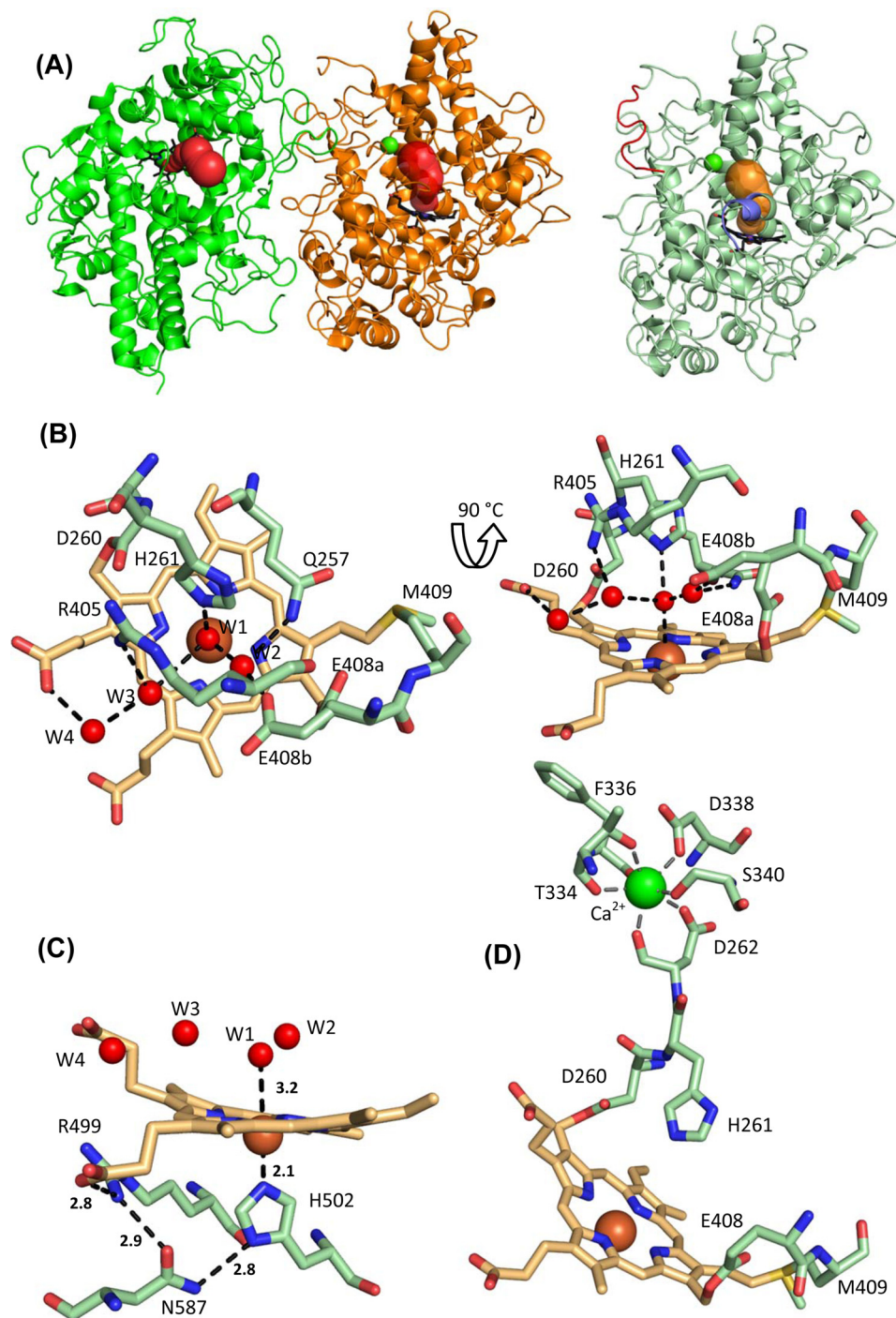


**Figure 5. Heme cavity architecture of proMPO.** *A*, substrate-access channels in mature MPO (*left panel*) and proMPO (*right panel*). The segment of the propeptide visible in the electron density map is shown in *red*. The channels were calculated using the tool CAVER 3.0 (57). For better orientation, the prosthetic group is highlighted in *bold black*. *B*, distal heme cavity and H-bonding network of proMPO. The catalytic residues His-261, Arg-405, and Gln-257 including W1–W4 and H-bondings are shown. The residues Asp-260, Glu-408, and Met-409 are involved in heme-to-protein linkages. The split conformation of Glu-408 is designated *E408a* and *E408b*. *C*, prosthetic group and proximal ligand His-502 together with the interaction network His-502–Asn-587–Arg-499 and the propionate of pyrrole ring D (distances are given in Å). *D*, calcium-binding site in proMPO.

and, to a lesser extent, ring C were tilted toward the distal side, resulting in a bow-shaped heme structure.

The prominent catalytic distal residues in proMPO are His-261 and Arg-405, which are important in heterolytic cleavage of hydrogen peroxide during compound I formation, and Gln-257, which is involved in halide binding. The distal heme cavity contained four water molecules (W1–

W4), which formed hydrogen bonds with His-261, Arg-405, and Gln-257, and to the heme pyrrole ring C propionate as well as between themselves. The distal His-261 was hydrogen-bonded to W1, which is positioned approximately midway between the histidine nitrogen and the iron (Fig. 5*B*). Overall, this H-bonding network was almost identical to that in mature MPO.

The proximal heme-iron ligand, His-502, interacted with the amine group of the side chain of Asn-587, whereas the carbonyl group of Asn-587 interacted with the guanidinium group of Arg-499. Furthermore, Arg-499 formed a salt bridge with the heme propionic group at pyrrole ring D (Fig. 5B). This interaction, identical to that in leukocyte MPO (8), requires an anionic His-502, which was facilitated by lowering the  $pK_a$  in His-502 as a result of its coordination with the heme iron. The respective distances in proMPO and MPO were almost identical (Fig. 5C). The structural similarities between proMPO and dimeric MPO apply also to the distal  $Ca^{2+}$ -binding site with its typical pentagonal bipyramidal coordination provided by residues Asp-262, Thr-334, Phe-336, Asp-338, and Ser-340 (Fig. 5D).

### Hybrid model of proMPO

Because the structure of a significant portion (Ala-49–Ser-156) of the N-terminal propeptide in proMPO could not be resolved in electron density maps, SAXS analysis was performed in addition (see below). For the propeptide domain an  $\alpha$ -helical structural model was calculated using the PHYRE2 Protein Fold Recognition Server (Structural Bioinformatics Group, Imperial College, London). The confidence level of the predicted structure was at most 76%, covering the main helical regions (Leu-54–Ile-84 and Ser-90–Val-121) and suggesting that alternative conformations are not unlikely.

The residues Gly-157–Val-163 of this model structure were superposed with the corresponding resolved N terminus in the X-ray structure, thus maintaining the Cys-158–Cys-319 disulfide bridge. Finally, this hybrid model was energy-minimized with MOE (molecular operating environment) (27) and the Amber99 (28) force field and used to fit the experimental SAXS data of proMPO. Eight of the 697 residues in the resulting model are outside the allowed regions in the Ramachandran plot (7 of the 107 modeled propeptide residues), further suggesting that alternative conformations of the propeptide are not unlikely.

Fig. 6 compares the interface between the two protomers in mature MPO (basis is the X-ray structure with PDB accession code 1MHL) with that between the propeptide and the core protein in proMPO (basis: hybrid model). The residues involved in noncovalent interactions in the interface between the two protomers of mature MPO (Arg-184–Glu-202, Ser-18–Ala-201, Thr-187–Gly-204, Arg-193–Asn-323, Arg-193–Ile-324, Ala-201–Ser-185, Glu-202–Arg-184, Gly-204–Thr-187, Lys-218–Glu-169, Cys-319–Cys-319, Asn-323–Arg-193, and Ile-324–Arg-193) (Fig. 5A) are completely different from the residues involved in noncovalent interactions between the propeptide and the core of the protein in proMPO (Glu-127–Cys-316, Arg-131–Arg-314, Arg-135–Gly-321, Lys-15–Thr-325, Ser-155–Cys-319, Cys-158–Cys-319, Ala-159–Arg-191, Gln-161–Arg-191, and Val-165–Met-179, with the latter three interactions also seen in the crystal structure) (Fig. 6B). A comparison of Fig. 6, A and B, clearly demonstrates that the interface in mature MPO exhibits significantly more noncovalent interactions that contribute to its higher thermal stability compared with proMPO. This effect results in a  $1332\text{-}\text{\AA}^2$  buried surface area upon MPO dimer formation compared with  $399\text{-}\text{\AA}^2$  between the propeptide and the core protein in proMPO.

Moreover, the two interfaces are not topologically equivalent, as illustrated in Fig. 6C, which shows a surface representation of the overlay of mature MPO and the propeptide of proMPO.

The most important proteolytic maturation step in MPO biosynthesis concerns the cleavage of the propeptide. It has been demonstrated that an inhibitor of subtilisin-like proteases blocks cleavage of the propeptide in a post-ER compartment; by mutational studies the positively charged proconvertase target sequence  $^{128}\text{RKLRLSLWRR}^{136}$  was identified (21). The hybrid-model structure suggests that Arg-128, Lys-129, Leu-133, Trp-134, and Arg-136 have a highly accessible surface area for interaction with the proconvertase (Fig. 6D).

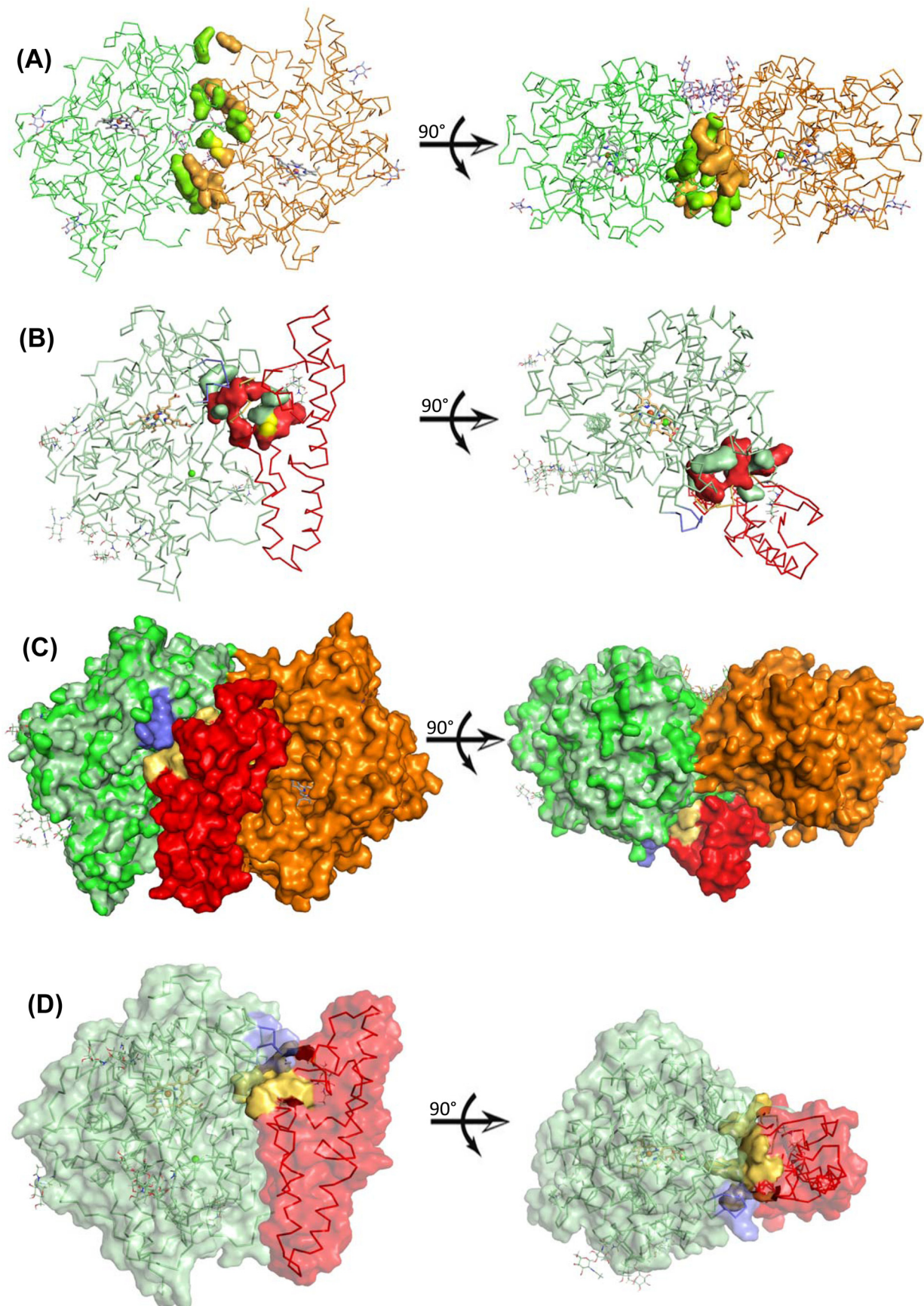
### Solution structures of proMPO and MPO

Next we performed a SAXS analysis of proMPO and MPO in solution (50 mM PBS, pH 7.4). Fig. 7A shows the scattering intensity (I) for proMPO plotted versus the scattering vector (Q), with *gray circles* representing experimental data and the *blue line* the corresponding fit. The *inset* (Fig. 7A) shows the pair-density distribution  $p(\zeta)$  computed for the crystal structure of proMPO (*dotted gray line 1*), for the hybrid model (*gray line 2*), and for the background-corrected scattering data (*blue line 3*). The pair-density distribution computed for the hybrid structure showed only small deviations from  $p(\zeta)$  as deduced from the background-corrected scattering data, thus increasing confidence in the propeptide model (the agreement between the computed and experimental  $p(\zeta)$  is as good for the dimeric MPO structure; see below). Differences were seen at distances  $>4$  nm with a more pronounced tailing of  $p(\zeta)$  computed for the experimental data.

In addition Fig. 7A depicts the corresponding calculated surface models. The pair-density distribution computed for the hybrid-model structure (Fig. 7A, *gray model 2*) was refined, leading to volume *models 3* and *5* with *blue* surfaces representing the (rigid) regions of the protein that contribute to the scattering signal with weights  $>1$ ; The *light blue* surface comprises residues that potentially contribute to the interface between the propeptide and the compact rest of the protein. *Model 4* (Fig. 7A) depicts the secondary structural elements of the hybrid structure of proMPO for orientation. Upon inspection of these data it is evident that the scattering contrast in the propeptide and the interface region was low, suggesting less compactness of the propeptide and a loose interaction with the rest of the protein, which may also explain the absence of defined electron density in the majority of the propeptide in the X-ray structure of proMPO.

For comparison, leukocyte MPO was analyzed under identical conditions (50 mM PBS, pH 7.4). The *inset* in Fig. 7B shows the pair-density distribution  $p(\zeta)$  computed for the background-corrected scattering data (*blue line 3*) and the crystal structure of MPO (*gray line 1*) (PDB accession code 3F9P). Both  $p(\zeta)$  values are scale-invariant although differing slightly in corugation. The corresponding surface models (Fig. 7B) are shown in *gray (model 1)* and *blue (model 3)*, with the *light blue* surface comprising residues that potentially contribute to the interface of the dimer. *Model 2* (Fig. 7B) depicts the secondary structural elements of the crystal structure of the two protomers of MPO for orientation. It is evident that the interaction

## Structure of proMPO and its impact on maturation



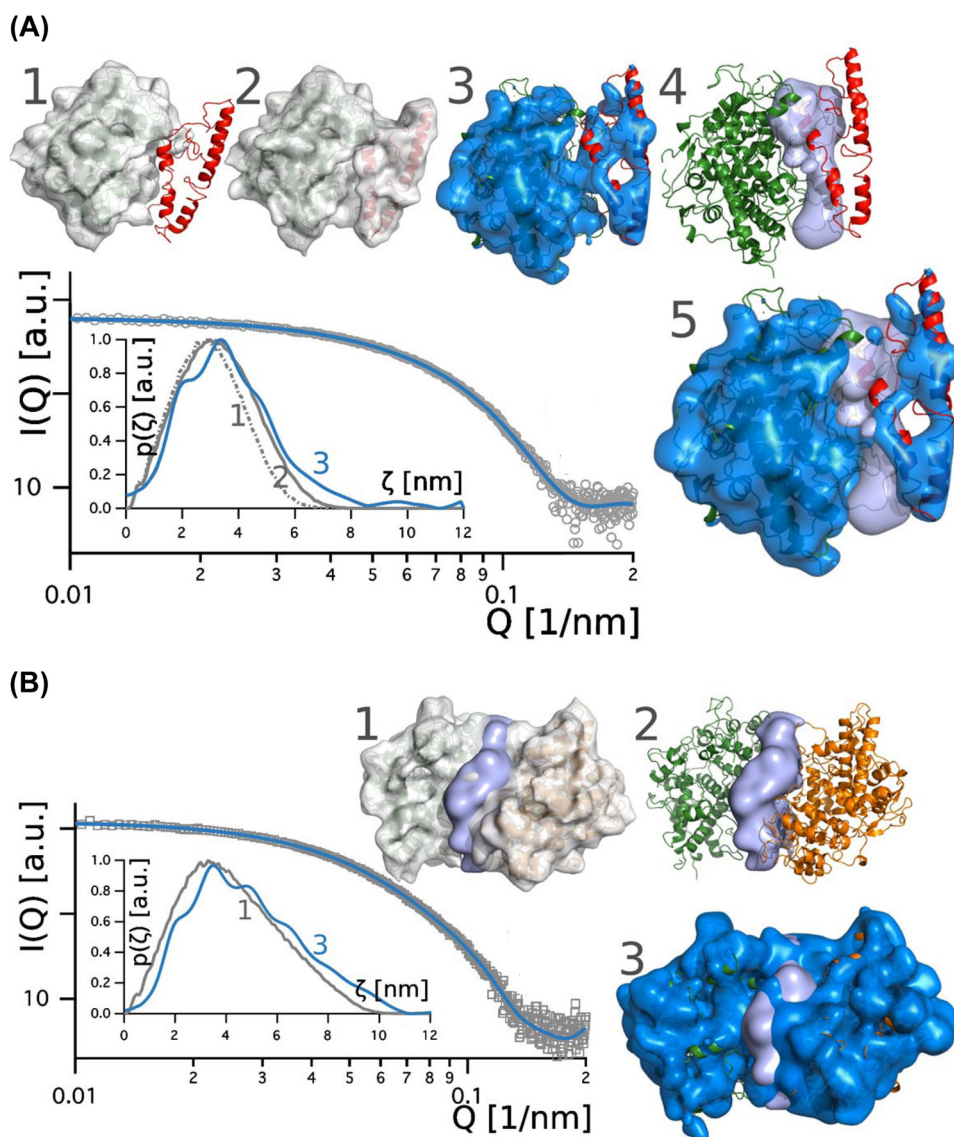


**Figure 7. Solution structures of proMPO and dimeric leukocyte MPO obtained by SAXS.** *A*, promyeloperoxidase: plot of scattering intensity  $I(Q)$  (gray circles) and fit (blue line) versus scattering vector. The inset shows pair-density distributions  $p(\zeta)$  computed for: the proMPO crystal structure (dotted gray line 1); the hybrid model, which contains the propeptide (gray line 2); and  $p(\zeta)$  computed from the scattering intensity (solid blue line 3). The corresponding surface models (depicted in gray) are superimposed onto the schematic representation of the crystal structure (model 1) and the hybrid model structure (model 2) of proMPO. The blue surfaces in models 3 and 5 comprise scattering sites that contribute to  $I(Q)$ ;  $\chi^2$  of the model is 0.91. The light blue surface comprises residues that potentially contribute to the interface between the propeptide and the compact rest of the protein. In model 4 the secondary structural elements of the core protein (green) and the propeptide (red) are shown. *B*, mature dimeric leukocyte MPO: plot of scattering intensity  $I(Q)$  (gray circles) versus scattering vector including fit (blue line). In the inset we compared the pair-density distribution  $p(\zeta)$  computed for the background-corrected data (blue line) and the MPO crystal structure (gray line). The corresponding surface models are depicted in gray (model 1) and blue (model 3);  $\chi^2$  of the model is 0.90. The light blue surface comprises residues that potentially contribute to the interface of the dimer. In model 2 the secondary structural elements of the two protomers of MPO are depicted in green and orange. *a. u.*, arbitrary units.

between the two protomers in MPO was significantly tighter than between the propeptide and the rest of the protein in proMPO.

Fig. 8 compares the Guinier plots for four different times of data acquisition (0.5, 1, 3, and 4 s), demonstrating that up to 2 s of beam-exposure scattering data is free of radiation damage.

**Figure 6. Hybrid-model structure of proMPO.** *A*, interface between the two identical protomers (chain A depicted as a green ribbon and chain B as an orange ribbon) of mature MPO (PDB accession code 3F9P). Residues involved in noncovalent interactions are presented as space-filling models (Arg-184–Glu-202, Ser-185–Ala-201, Thr-187–Gly-204, Arg-193–Asn-323, Arg-193–Ile-324, Ala-201–Ser-185, Glu-202–Arg-184, Gly-204–Thr-187, Lys-218–Glu-169, Cys-319–Cys-319, Asn-323–Arg-193, and Ile-324–Arg-193). *B*, interface between the propeptide (red) and the core protein of proMPO (pale green). Residues involved in noncovalent interactions are presented as space-filling amino acids (Glu-127–Cys-316, Arg-131–Arg-314, Arg-135–Gly-321, Lys-154–Thr-325, Ser-155–Cys-319, and Cys-158–Cys-319). Sulfur atoms in Cys-158–Cys-319 are shown in yellow. Residues belonging to the propeptide are shown in red. *C*, surface representation of the overlay of mature MPO and propeptide of proMPO in the colors described above. The hexapeptide is depicted in blue. *A–C* are represented from identical angles. *D*, proposed binding site ( $^{128}\text{RRKLRSLWR}^{136}$ ) of proconvertase in proMPO (yellow surface). The propeptide is depicted in red and the core protein of proMPO in pale green.

## Structure of proMPO and its impact on maturation

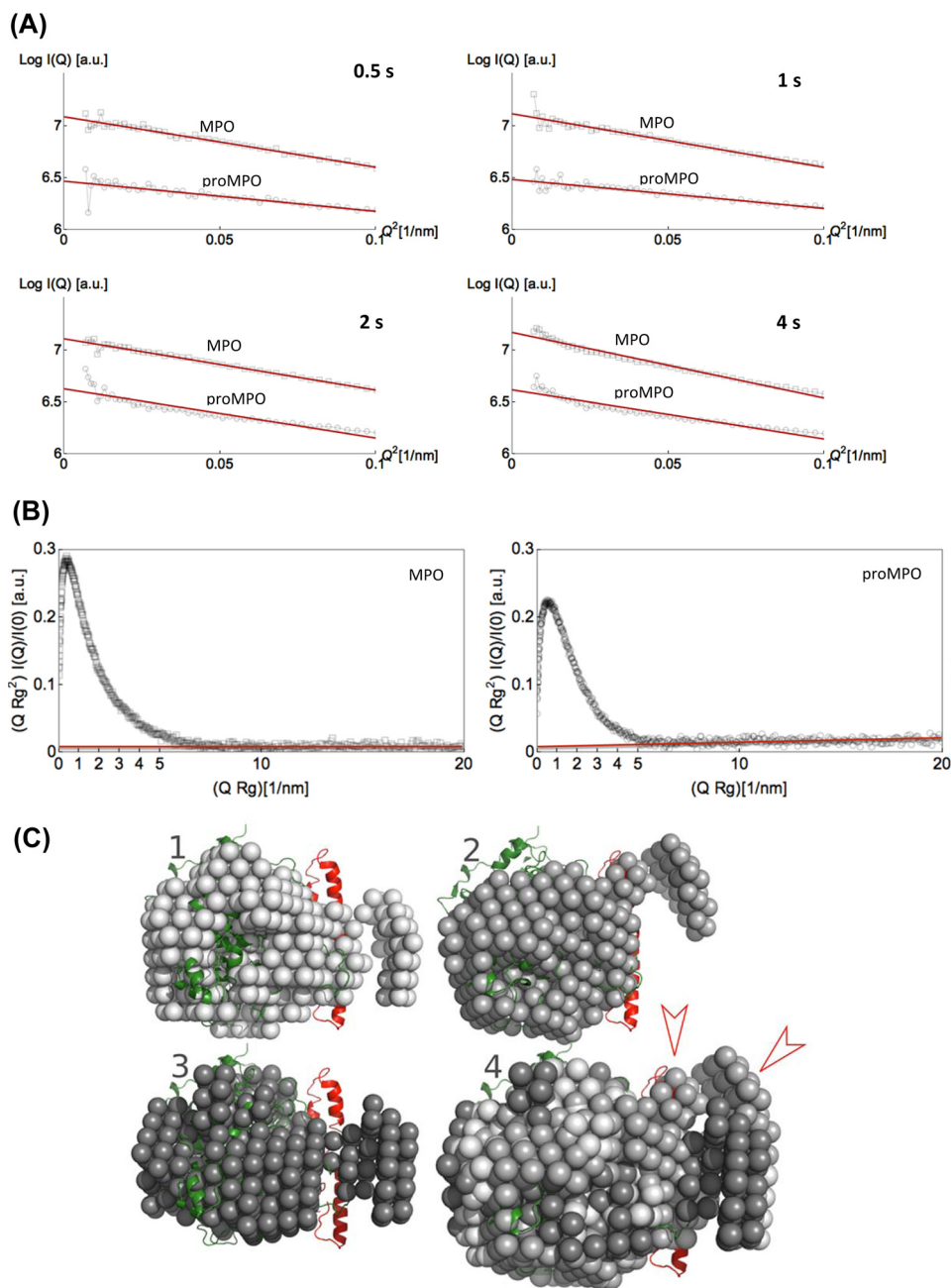


**Figure 8. Guinier and normalized Kratky plots of dimeric MPO and proMPO and bead models of proMPO.** *A*, Guinier plots. The logarithm of scattering intensity ( $\ln I(Q)$ ) of dimeric mature MPO (gray squares) and proMPO (gray circles) are given as a function of  $Q^2$ . Four different times of data acquisition (0.5, 1, 2, and 4 s) are compared. For leukocyte MPO, nonlinearity is seen after 4 s, whereas for proMPO, nonlinearity is seen already after 2 s of beam exposure. Nonlinearity is taken as an indication of the onset of radiation damage. *B*, normalized Kratky plot given as a function of the radii of gyration  $R_g$  and extrapolated scattering intensity  $I(Q)$  for dimeric mature MPO (gray squares) and proMPO (gray circles). Note the difference in slope of the baseline (red line). Although the baseline for leukocyte MPO is constant, the baseline for proMPO shows a positive slope, which is an indication of the soft binding of the propeptide to the core of proMPO. *a. u.*, arbitrary units. *C*, bead models of proMPO derived from data analysis using the software ATSAS 2.7.2. We computed three different models using the program package ATSAS 2.7.2. For computation of the bead models, we used the pair-density distributions depicted in Fig. 6A. These bead models were aligned by PyMOL and superimposed in model 4.

From the Guinier plots, the radii of gyration for dimeric MPO (3.8 nm) and monomeric proMPO (2.9 nm) were obtained, again demonstrating that the latter is less compact. Additionally, we computed normalized Kratky plots (Fig. 8B). Both proteins exhibited shapes characteristic of folded proteins. However, although the baseline for MPO is constant, the slope is positive for proMPO, which indicates increased flexibility in the latter.

Moreover, we computed a set of bead models for proMPO accessed by the program ATSAS (Fig. 8C) (29). We changed the maximum particle diameter between 10 and 10.5 nm and constructed therefrom three different bead models (Fig. 8C, models 1–3). In model 4 we aligned the bead models using PyMOL, and finally, we manually superimposed the hybrid model in a schematic representation (Fig. 8C). The propeptide appears partially structured but flexible, and the two clusters of beads (Fig.

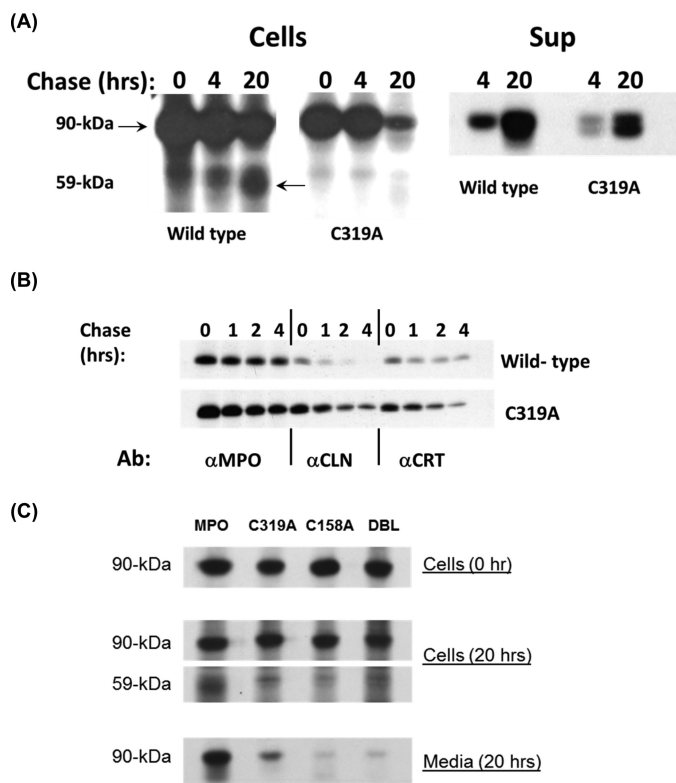


**Figure 9. Biosynthesis of mutants C319A and C158A and double mutant C158A/C319A.** A, transfectants expressing wild-type MPO or C319A were radiolabeled biosynthetically and chased for 0–20 h. Cell lysates (Cells) and supernatants (Sup) were immunoprecipitated for MPO-related proteins, including the 90-kDa precursors (apo- and proMPO) and the 59-kDa heavy subunit of mature MPO. B, stable transfectants expressing wild-type MPO or C319A were radiolabeled biosynthetically and chased for 0–4 h. Lysates were immunoprecipitated for MPO ( $\alpha$ MPO) or sequentially immunoprecipitated with  $\alpha$ CLN  $\rightarrow$   $\alpha$ MPO to recover CLN-associated MPO ( $\alpha$ CLN) or with  $\alpha$ CRT  $\rightarrow$   $\alpha$ MPO to recover CRT-associated MPO ( $\alpha$ CRT). A representative of three to five independent experiments is shown. C, transfectants expressing wild-type MPO, C319A, C158A, or C319A/C158A (DBL) were radiolabeled biosynthetically and chased for 0–20 h. Cell lysates (Cells) and supernatants (Media) were immunoprecipitated for MPO-related proteins, including the 90-kDa precursors (apo- and proMPO) and the 59-kDa heavy subunit of mature MPO. A representative of four to six independent experiments is shown.

8C, red arrowheads) indicate a compact and less compact configuration. This is in line with findings of the normalized Kratky plot. In summary, the SAXS analysis clearly suggests that the propeptide is structured (as suggested by the hybrid model) but flexible, thus leading to incoherent scattering and missing electron density in the crystal structure.

#### Biosynthesis and enzymatic activity of the mutant proteins C319A, C158A, and C158A/C319A

In mature MPO the interchain disulfide bond bridges the two heavy-chain subunits (5, 7, 8). Our structural data demonstrated that in proMPO, Cys-319 existed in an intrachain disulfide linkage with Cys-158 of the propeptide region. To analyze the importance of dimerization to biosynthesis and the activity of mature MPO, we generated stable HEK transfectants expressing the mutant C319A. The mutant protein did not undergo significant proteolytic processing to form mature dimeric MPO even after prolonged chase (Fig. 9A). However, a fraction of the mutant precursor entered the secretory pathway and appeared in culture media, as occurred with transfectants

**Table 2**  
Processing of wild-type and mutant proMPO

Stably transfected HEK cells expressing wild-type or mutant MPO were radiolabeled biosynthetically, and MPO-related proteins were immunoprecipitated immediately after labeling (at 0 h) and 20 h after chase. Immunoprecipitates were separated by SDS-PAGE. The amount of immunoprecipitated 90- and 59-kDa MPO-related protein at 20 h of chase and the amount of MPO-related protein secreted was quantitated using a phosphorimaging device.

Source	90 kDa:59 kDa ( <i>n</i> ) <sup>a</sup>	% Secreted <sup>b</sup>
Wild-type MPO	0.72 ± 0.08 (13)	100
C319A	1.96 ± 0.27 (5)	28.8 ± 7.9
C158A	1.62 ± 0.24 (6)	5.1 ± 2.0
C158A/C319A	1.64 ± 0.30 (4)	11.9 ± 1.3

<sup>a</sup> The ratio of precursor to mature MPO (90 kDa:59 kDa) is shown as mean ± S.E. for *n* number of experiments. The *p* values for the differences of 90 kDa:59 kDa for C319A, C158A, and C158A/C319A versus that of wild-type MPO are .0001, .0003, and .0009, respectively.

<sup>b</sup> The percent MPO-related protein normalized to that secreted by HEK-MPO cells is shown as the mean ± S.E. for four separate experiments.

expressing wild-type MPO (Fig. 9A). Fractionation of biosynthetically radiolabeled transfectants on sucrose-density gradients demonstrated a difference in the distribution of precursors in cells expressing wild-type or mutant protein. After a 4-h chase, wild-type MPO species were distributed in two peaks (fractions 8–9 and fraction 16), whereas MPO-related immunoreactivity for C319A was found only in fractions 8–9 (not shown), fractions that we had shown previously to be enriched for ER (30). These data suggested that the mutant C319A was retained in the ER and did not gain access to the cellular compartments where proteolytic processing of proMPO normally occurs (17, 22).

Early in its biosynthesis, MPO precursors apoMPO and proMPO associate transiently with molecular chaperones calreticulin (CRT) and calnexin (CLN) (23, 31). To determine how the mutant C319A interacts with ER chaperones, we immunoprecipitated CRT- and CLN-associated MPO precursors from transfectants expressing wild-type or mutant MPO. The association of CLN with C319A was especially prolonged in comparison with that seen for wild-type MPO (Fig. 9B). At 4 h of chase, 2.5% of the wild-type proMPO remained associated with CLN, whereas 34.5% of the mutant protein was in a complex.

Additionally, we created HEK cell lines expressing targeted mutations at Cys-158 as well as both Cys-158 and Cys-319. The biosynthesis of the respective mutant proteins was compromised in a similar fashion in both cell lines, with dramatic effects both on proteolytic processing to mature MPO subunits and on the secretion of proMPO into the culture medium (Fig. 9C). For example, the ratio of the 90-kDa MPO precursor to the 59-kDa heavy-chain subunit of mature MPO, a calculation that correlates with efficient processing of proMPO (21), was increased in C319A, C158A, and C158/C319A relative to that in cells expressing wild-type MPO (Table 2). In addition, cells expressing the mutant forms of MPO secreted significantly less proMPO than did transfectants expressing normal MPO. Like the C319A proMPO, the precursors of C158A and C319A/C158A exhibited prolonged associations with CLN (data not shown). Taken together, the failure to form a disulfide bond between Cys-158 and Cys-319 in the MPO precursor in the ER disrupted both normal proteolytic processing and the secretion of mutant proMPO.

During the processing of normal MPO, apoproMPO acquires heme in the ER, and the resultant proMPO exits the

## Structure of proMPO and its impact on maturation

**Table 3**  
Peroxidase activity of wild-type and mutant cell-associated MPO and secreted proMPO species

Cell lysates and conditioned culture media from stably transfected HEK cells expressing wild-type or mutant MPO were assayed for peroxidase activity. Lysates of  $5 \times 10^5$  cultured cells and  $10 \mu\text{g}$  of column-enriched culture media were used in the assays, except for spent media from transfectants expressing normal MPO (\*), where  $1 \mu\text{g}$  was used. Under the assay conditions, the  $\Delta A_{650}$  value for 2 pmol of purified MPO was  $0.190 \pm 0.007$  ( $n = 9$ ).

Source	Cell-associated MPO (n) <sup>a</sup>	Secreted proMPO (n) <sup>a</sup>
HEK cells	$0.043 \pm 0.001$ (9)	$0.046 \pm 0.001$ (3)
Wild-type MPO	$0.346 \pm 0.009$ (9)	$1.264 \pm 0.173^*$ (3)
C319A	$0.097 \pm 0.004$ (6)	$0.648 \pm 0.038$ (3)
C158A	$0.043 \pm 0.001$ (6)	$0.058 \pm 0.005$ (3)
C158/C319A	$0.048 \pm 0.001$ (3)	$0.517 \pm 0.089$ (3)

<sup>a</sup> The results are given as mean  $\pm$  S.E.  $n = 3-9$  for studies of cell-associated activity and  $n = 3$  for studies of secreted proMPO. The peroxidase activity of lysates from C158A and C158/C319A was not significantly different from that of untransfected HEK cells. The activity of C319A differed from that of the untransfected cells ( $p = .007$ ).

ER, undergoes proteolytic processing, and after a prolonged period (32, 33) forms homodimeric MPO (reviewed in Ref. 15). Previous studies have linked heme acquisition by MPO precursors to the egress of proMPO from ER and subsequent maturation. Pharmacologic inhibition of heme synthesis by succinyl acetone results in a maturation arrest in MPO biosynthesis, with accumulation of enzymatically inactive apoproMPO (17, 18). Consequently, we reasoned that the formation of the Cys-158–Cys-319 disulfide bond might influence efficient heme incorporation into apoproMPO and the generation of proMPO. To assess heme acquisition by mutant precursors, we measured the enzymatic activity of lysates of HEK cells and HEK transfectants expressing wild-type MPO and the three mutants. Given that both peroxidase activity and chlorinating activity each depends on the functional integrity of the heme center and that the inability to support peroxidation would preclude the capacity to chlorinate, we elected to compare the peroxidase activity of the mutants with that of wild-type MPO. Compared with the activity of HEK transfectants expressing wild-type MPO, the activities of the mutant cell lines were significantly reduced. Whereas the activities of C158A and C158A/C319A were not significantly higher than that of wild-type HEK cells, which lack an endogenous peroxidase, lysates of C319A possessed peroxidase activity, albeit significantly less than that of transfectants expressing normal MPO (Table 3).

During MPO biosynthesis in myeloid precursors from bone marrow, myeloid cell lines, or transfectants expressing heterologous MPO, a fraction of the newly made proMPO is constitutively released into the culture medium (2, 16, 20, 32, 34–37). Secreted proMPO exhibits the same specific activity as intracellular proMPO or mature MPO (38), thus providing an additional insight into the functional status of the respective proforms of the mutants. Secreted proMPO was isolated from spent media using cation chromatography as done previously (21), and peroxidase activity was measured (Table 3). Overall, the activity of supernatants from all mutants was less than that of normal proMPO. Because this method recovers all cationic proteins in spent media and provides material enriched for proMPO, we performed immunoblots of samples eluted from the beads to assess the fraction of MPO-related proteins in supernatant. Compared with the amount of proMPO secreted by transfectants expressing normal MPO, all mutants were

reduced; C319A, C158A, and C158A/C319A secreted  $8.4 \pm 0.8$ ,  $7.5 \pm 0.2$ , and  $5.9 \pm 0.6\%$  ( $n = 4$  for each), respectively, of the amount of normal proMPO. Even when corrected for the relative amount of MPO-related protein, the peroxidase activity of secreted proMPO from all three mutants was depressed compared with normal proMPO, with C158A being the most profoundly decreased (Table 3).

## Discussion

The structural and functional studies presented here elucidate several previously unknown features of MPO biosynthesis. Myeloperoxidase gene transcription is limited to early myeloid precursors in the bone marrow, when MPO is synthesized and stored in azurophilic granules for subsequent release from stimulated neutrophils. With the help of the atypically long 45-aa N-terminal signal peptide, the primary translation product channels into the ER, where it undergoes cotranslational cleavage of the signal peptide and *en bloc* N-linked glycosylation with two N-acetylglucosamine residues at the base of the six-glycan chains to yield apoproMPO. ApoproMPO has a very long half-life in the ER. The added oligosaccharides contribute to interactions with the ER molecular chaperones CRT, CLN, and ERp57 (23, 31), which generally promote proper folding and quality control in glycoprotein biosynthesis (39). In addition to the presence of N-linked oligosaccharides, the overall conformation of the apoproMPO influences its interaction with the ER chaperones, as demonstrated by the impact of disruption of the Cys-158–Cys-319 disulfide bridge on association with CLN (Fig. 9B). The compactness and noncovalent interactions at the interface between the propeptide and the core protein in proMPO is less pronounced compared with the interface in mature homodimeric MPO, and elimination of the Cys-158–Cys-319 disulfide bridge in proMPO will even boost this difference and promote (partial) unfolding. The same holds true for apoproMPO.

Heme insertion into apoproMPO occurs in the ER, as disruption of the Golgi by treating promyelocytes with brefeldin A arrests MPO biosynthesis in the proMPO stage but has no impact on correct heme incorporation (17). In both wild-type proMPO and mature MPO the posttranslationally modified heme group significantly contributes to the overall stability through covalently linking the N- and C-terminal regions of the two chains as observed by Banerjee *et al.* (40). In the absence of the Cys-158–Cys-319 disulfide bridge, heme occupancy was diminished, was reflected by the significantly reduced enzymatic activity of the respective mutants. Typically, the apof orm of heme proteins (and also apoproMPO) acquires the prosthetic group via the main substrate access channel (41). As our studies have demonstrated, this access channel was structurally apart from the interface between the propeptide, the core protein, and the bridging disulfide bond (Fig. 5A). This finding supports the hypothesis that disruption of the Cys-158–Cys-319 disulfide bridge destabilizes the fold integrity of apoproMPO, thus compromising stable heme incorporation.

Wild-type proMPO is catalytically fully active. In recent studies it has been demonstrated that recombinant monomeric proMPO shares almost identical spectral and enzymatic features with the mature dimeric leukocyte enzyme (12, 38, 42, 43),

and this similarity extends to the redox thermodynamics of the Fe(III)/Fe(II) couple (11). Furthermore, intracellular MPO and secreted proMPO from HEK cell cultures show almost identical enzymatic activities. The structure of proMPO that we reported here fully supports these findings, because it demonstrates that its core structure, including the substrate access channel and heme cavity architecture, was almost identical to that of the protomer of mature MPO. Moreover, the crystal structure clearly demonstrates that the posttranslational autocatalytic modifications of the prosthetic group (9) were already established in proMPO, suggesting that the formation of these covalent bonds must occur in the ER. The reaction requires  $H_2O_2$  to generate compound I in order to oxidize the nearby carboxylate groups of Asp-260 and Glu-408 and most probably involves the formation of a carbocation followed by hydrogen abstraction from the heme methyl groups (9). A comparable mechanism has been proposed for the autocatalytic formation of the sulfonium-ion linkage that occurs in MPO but not in related peroxidases (9).

Additionally, our proMPO structure demonstrates that the formation of two covalent bonds at pyrrole ring A of proMPO by neighboring Glu-408 and Met-409 destabilized the ester but not the sulfonium bond, a phenomenon already seen in mature leukocyte MPO (8). Catalysis of chloride oxidation to antimicrobial hypochlorous acid needs the presence of an intact electron-withdrawing sulfonium-ion linkage (44–46), whereas the impact of the ester bond with Glu-408 on activity seems to be less important. Furthermore, the almost identical heme-cavity architecture of proMPO and MPO was evident by inspection of (i) the close proximal His-502–Asn-587–Arg-499 interaction and the resulting anionic character of His-502, (ii) the distal catalytic residues, and (iii) the geometry of the distal  $Ca^{2+}$ -binding site. This clearly suggests that the active site is preassembled in proMPO.

After heme insertion the enzymatically active proMPO undergoes a series of proteolytic events. The present study suggests that the first and most important step is the elimination of the propeptide by proteolytic cleavage, a process that earlier studies suggest is mediated by a proconvertase in the Golgi (21). The overall structure of proMPO must be preserved for successful transport from the ER to the trans-Golgi, as disruption of the Cys-158–Cys-319 bond kept proMPO associated with CLN in the ER. To eliminate the propeptide, a protease needs access to the target sequence in the C-terminal region of the propeptide. The flexible nature of the propeptide, reflected by the absence of electron density for residues Ala-49–Ser-156 in the crystal structure, and its loose interaction with the core protein should facilitate access of the subtilisin-like proconvertase to its arginine-rich binding site in the propeptide. The solvent-accessible volume at the interface between the propeptide and the core protein in proMPO was significantly bigger than that between the two protomers in MPO (Fig. 7). Mutation of the target sequence in the propeptide blocks processing of proMPO and results in unstable intracellular forms (21). Our hybrid model of proMPO suggests that at least three basic amino acids of this target sequence are surface-exposed and can interact with the protease.

Simultaneously with the proteolytic event, the Cys-158–Cys-319 bridge is most likely cleaved, and a 74-kDa intermediate species is formed, thereby enabling dimerization, because both Cys-319 and the glycans at Asn-323 and Asn-483 would be accessible in the resulting 74-kDa protomers. Moreover, the elimination of the propeptide additionally exposes the hexapeptide loop for proteolytic cleavage (Figs. 1 and 4C). From a structural point of view, the latter proteolytic event could take place in either the monomeric or the homodimeric state. In any case, it cleaves the protomer into the L- and H-chain. The purpose of this step is unclear because the structure in mature MPO shows an almost continuous electron density between the resulting C terminus of the L-chain and the N terminus of the H-chain (8), suggesting a direct interaction between the two polypeptides. Thus the impact of this maturation step on the conformational stability and on catalytic properties should be negligible. Finally, after transport from the ER and through the complex Golgi network, the resulting mature MPO reaches its final intracellular destination in azurophilic granules.

Altogether, we solved the first crystal and solution structure of proMPO, thereby providing new insights into myeloperoxidase processing and targeting. The most interesting finding concerns the Cys-158–Cys-319 disulfide bridge between the structured but very flexible propeptide and the core protein of proMPO, which supports the proper folding of apoproMPO and heme incorporation in the ER. Heme incorporation into the pre-formed cavity is followed by autocatalytic processing and the formation of three covalent bonds between the prosthetic group and the protein. The propeptide hinders dimerization and formation of the Cys-319–Cys-319 disulfide bridge in mature homodimeric MPO. After transport to the trans-Golgi, the loose interaction between the flexible and solvent-exposed propeptide and the core protein in proMPO enables the access of a subtilisin-like proconvertase to its arginine-rich binding site in the C-terminal region of the propeptide. Finally, cleavage of the propeptide enables access of another protease to eliminate a hexapeptide loop in the resulting 74-kDa intermediate, thereby forming the L- and H-chain of the mature protomer of leukocyte MPO.

## Experimental procedures

### Materials

Highly purified dimeric leukocyte myeloperoxidase with a purity index ( $A_{428}/A_{280}$ ) of at least 0.85 was purchased as lyophilized powder from Planta Natural Products (Vienna, Austria). Heterologous expression, purification of recombinant monomeric proMPO in CHO cells, and characterization have been described (25, 38). The purity index ( $A_{428}/A_{280}$ ) of recombinant proMPO varied between 0.61 and 0.65. The concentration of both MPO forms was determined spectrophotometrically using  $\epsilon_{428} = 91,000 \text{ M}^{-1} \text{ cm}^{-1}$ .

Human erythroleukemia cell K562 (CCL-243) and HEK293 cells (CRL-1573) were obtained from American Type Culture Collection (Manassas, VA). The vectors pREP10 and pcDNA3.1 and the antibiotics hygromycin and G-418 sulfate were obtained from Invitrogen. [ $^{35}\text{S}$ ]Methionine/cysteine (Easy Tag Expre $^{35}\text{S}^{35}\text{S}$  protein labeling mix, 37.0 TBq/mmol, 11 mCi/

## Structure of proMPO and its impact on maturation

ml) was obtained from PerkinElmer Life Sciences. All tissue-culture reagents were obtained from the hybridoma facility at the University of Iowa. Antibody against calnexin was obtained from Stressgen Bioreagents (Ann Arbor, MI). The monospecific rabbit antibody against human MPO was generated in our laboratory as described previously (47), as was the rabbit antibody against human calreticulin (23), which is also available commercially from Thermo Fisher Scientific (antibody PA3-9000).

Unless specified otherwise, all other reagents were purchased from Sigma-Aldrich.

### Stably transfected cell lines

Clones of stably transfected cell lines were created and maintained, using pREP10 in K562 cells and pcDNA3.1 in HEK cells as described previously (23, 24, 30, 31, 48). PCR was used to create specific mutations in wild-type MPO cDNA for stable heterologous expression in K562 or HEK cells, which are devoid of endogenous MPO. The cDNA was sequenced prior to transfection to confirm the presence of the desired mutation and the absence of unintended mutations. Once the sequence was confirmed, stable transfectants were selected and cloned by limiting dilution.

### MPO biosynthesis by transfectants

Stably transfected cells were used to examine the biosynthesis of wild-type and mutant forms of MPO as done previously (23, 24, 30, 31, 48). In summary, cells were grown at low density in medium supplemented with 2  $\mu\text{g}/\text{ml}$  hemin for 24 h prior to biosynthetic radiolabeling and then placed in methionine-free medium supplemented with hemin, dialyzed fetal bovine serum, and antibiotics for 1 h prior to pulse labeling with [ $^{35}\text{S}$ ]methionine/cysteine. After the indicated period of biosynthetic radiolabeling, the cells were recovered or chased by the addition of cold methionine (1000-fold excess) before solubilization for subsequent analysis. Radiolabeled cells were solubilized and used in immunoprecipitations as described previously (24, 30, 48).

Biosynthetically radiolabeled MPO-related proteins were recovered from cell lysates or culture medium by immunoprecipitation with monospecific polyclonal rabbit anti-human MPO as described previously (16, 17, 22–24, 30, 31, 48). To recover MPO-related proteins associated with CRT or CLN, we performed sequential immunoprecipitation as described previously (23, 30, 31). Cell lysates were immunoprecipitated first with antibodies against CRT or CLN under nondenaturing conditions. The CRT- or CLN-associated proteins in the recovered complex were released by heating in the presence of 2% SDS, and the solution was cooled and diluted 10-fold before proceeding with an immunoprecipitation with MPO antiserum. Radiolabeled MPO-related proteins were separated by SDS-PAGE followed by autoradiography and quantitated by direct measurement of radioactivity using a PhosphorImager (Typhoon 9410, GE Healthcare).

### Secreted proMPO

Secreted proMPO was isolated and analyzed as described previously (21). For analysis of secreted proMPO, the spent

culture medium was collected from HEK cells, both wild-type and transfectants, after cells had reached  $\sim 80\%$  confluence in T162 culture flasks. The spent medium was clarified by centrifugation, diluted 1:1 with 10 mM Tris-HCl, pH 7.4, and incubated with SP Sepharose Fast Flow beads (GE Healthcare) that had been washed in 10 mM Tris-HCl, pH 7.4. After tumbling in diluted medium, the beads were pelleted, resuspended in Tris-buffered saline (TBS) pH 7.4, and washed three times in TBS. Bound proMPO species were eluted from beads in 1.5 M NaCl in Tris-HCl, pH 7.4, at 4  $^{\circ}\text{C}$ . The eluted supernatant was dialyzed against PBS and concentrated  $\sim 3$ -fold using an Amicon Ultracel (30K). The protein concentration was determined using the Pierce BCA protein assay. The amount of MPO-related protein recovered as secreted proMPO was determined by immunoblotting. Samples were subjected to SDS-PAGE and blotting as described previously, with blots incubated with MPO antibody (1:20,000 dilution) followed by donkey anti-rabbit antibody conjugated with horseradish peroxidase (1:50,000) and processed with Pierce West Femto chemiluminescence reagent. The chemiluminescent signal was quantitated directly using a Typhoon 9410 PhosphorImager.

### Peroxidase activity

The peroxidase activity of the cell lysates as well as proMPO recovered from spent culture medium was quantitated spectrophotometrically using a modified version of a published technique (49). Cell pellets were solubilized in 0.2% (v/v) Triton X-100/PBS at a density of  $1 \times 10^6$  cells/ $20 \mu\text{l}$  and stored on ice. Peroxidase assay was performed in a water bath held at 37  $^{\circ}\text{C}$ . The reaction mixture contained 20  $\mu\text{l}$  of cell lysate, 380  $\mu\text{l}$  of assay buffer (1.4 mM tetramethylbenzidine, 8.8% (v/v) dimethylformamide, and 50 mM sodium acetate, pH 5.4), and 300  $\mu\text{M}$   $\text{H}_2\text{O}_2$  (verified spectrophotometrically using  $\epsilon_{240 \text{ nm}} = 43.6 \text{ M}^{-1} \text{ cm}^{-1}$ ). The reaction was stopped after the addition of 1.7 ml of ice-cold 0.2 M acetic acid. Absorbance at 655 nm was measured spectrophotometrically. Assays of cell lysates used  $5 \times 10^5$  cell equivalents, whereas 10  $\mu\text{g}$  of protein was used to assess the peroxidase activity of secreted mutant proMPO and 1  $\mu\text{g}$  of secreted wild-type MPO.

### Differential scanning calorimetry

Differential scanning calorimetric (DSC) measurements were performed using a VP capillary DSC microcalorimeter from MicroCal with a cell volume of 137  $\mu\text{l}$ . The measurements were controlled by the VP viewer program, and the instrument was equipped with an autosampler for 96-well plates. Samples were analyzed using a programmed heating scan rate of 60  $^{\circ}\text{C h}^{-1}$  over a temperature range from 20 to 100  $^{\circ}\text{C}$ , and cell pressure was  $\sim 60$  psi (4.136 bar). DSC thermograms were corrected for buffer baseline and protein concentration. The conditions were: 14.3  $\mu\text{M}$  recombinant proMPO or 8.1  $\mu\text{M}$  mature leukocyte MPO in PBS buffer, pH 7.4. For data analysis and conversion, MicroCal Origin software was used. Heat capacity ( $C_p$ ) was expressed in  $\text{kcal mol}^{-1} \text{ K}^{-1}$ . Data points were fitted to non-two-state equilibrium-unfolding models by the Levenberg-Marquardt nonlinear least squares method.

### Crystallization, data collection, structure determination, and refinement

Crystals of recombinant proMPO were obtained initially in the Morpheus crystallization screen (Molecular Dimensions Limited Ltd., Suffolk, United Kingdom) using the sitting-drop vapor-diffusion technique and a nanodrop-dispensing robot (Phoenix RE, Rigaku Europe, Kent, United Kingdom) and optimized to 10% (w/v) PEG 20,000, 20% PEG 550 monomethyl ether, 0.1 mM Tris-Bicine, pH 8.5, and 0.05 mM CaCl<sub>2</sub> using the hanging-drop vapor-diffusion technique at 22 °C. The crystals were flash-cooled directly from the mother liquor in liquid nitrogen prior to data collection.

The data set was collected at the ESRF Synchrotron (Grenoble, France) at beamline ID29 at 100 K using a wavelength of 0.98 Å. The data frames were processed using the XDS package (50) and converted to MTZ format using AIMLESS (51). The structure was solved by molecular replacement with the program PHASER (51, 52) using atomic coordinates of human MPO (PDB accession code 1MHL) as a search model. The structure was refined using the programs REFMAC (51, 53) and Phenix Refine (54) and rebuilding was done using the program Coot (55). Coordinates were deposited in the Protein Data Bank (PDB code 5MFA). The data collection and refinement statistics are reported in Table 1. The stereochemistry and structure quality were checked using the program MolProbity (56).

Analysis of the substrate access channel in MPO and proMPO were performed using the tool CAVER 3.0 (57). Figs. 4–6 were produced using the program PyMOL (58).

### Small-angle X-ray scattering

Dimeric, mature MPO and recombinant proMPO were concentrated to 1 mg/liter and stored at 4 °C. For both systems the scattering data were collected at SIBYLS beam line 12.3.1 at the Advanced Light Source at Lawrence Berkeley National Laboratory following standard procedures (59). Both proteins were spun at 3000 rpm for 10 min and kept at 10 °C before data collection. Finally, samples were loaded into a SAXS cuvette and kept at 20 °C for 15 s. For each sample, four data sets were accumulated, namely for 0.5, 1, 2, and 4 s of radiation exposure. Data sets were background-corrected and analyzed for radiation damage. No radiation damage was observed, and background-corrected data sets accumulated after 0.5 s were chosen for further evaluation. From the scattering data we computed the pair-density distribution for MPO and proMPO.

Because we had crystal structures of proMPO and MPO in hand, we did not follow the usual approach that computes SAXS models by a reverse Monte Carlo method and tempered annealing procedures followed by matching the sphere model and the crystallographic models. We computed a centroid for each amino acid (*i.e.* potential scattering site) and attributed a particular weight to each. Next, we analytically computed the pair-density distribution for the 3D model and adapted the weight of each site until this pair-density contribution fitted to the pair-density contribution calculated from the experimental data. Initially, each site was weighted as 1. In the case of proMPO, the weights of the scattering sites of the core domain

### Structure of proMPO and its impact on maturation

were kept constant, whereas those of the propeptide model were varied to compensate for the differences in the pair-density distributions.

Calculation of  $\chi^2$ , Guinier, and normalized Kratky plots were performed as described in the literature (60–62). Additionally, bead model structures for proMPO were calculated by using the software ATSAS 2.7.2 (EMBL, Hamburg, Germany).

### Mass spectrometry

The relevant protein bands were S-alkylated with iodoacetamide and digested in-gel with trypsin (Promega). Alternatively, the same procedure was also performed in solution. The digested samples were loaded on a BioBasic C18 column (150 × 0.32 mm, 5  $\mu$ m, Thermo Fisher Scientific) using 65 mM ammonium formate buffer as the aqueous solvent. A gradient from 5% B (B: 100% acetonitrile) to 32% B in 35 min was applied followed by a 15-min gradient from 32% B to 75% B to facilitate the elution of large peptides. The flow rate was 6  $\mu$ l/min. Detection was performed with QTOF MS (Bruker maXis 4G) equipped with the standard ESI source in positive-ion DDA mode (switching to MS/MS mode for eluting peaks). MS scans were recorded (range, 150–2200 Da), and the six highest peaks were selected for fragmentation. Instrument calibration was performed using an ESI calibration mixture (Agilent Technologies). Using data analysis software from Bruker, the files were converted to mgf files, which are suitable for performing a MS/MS ion search with GPM (global proteome machine). Additionally, manual searches were made. N-terminal sequencing of proMPO by Edman degradation was performed by Dr. Bettina Sarg from the Division of Clinical Biochemistry at the Medical University in Innsbruck, Austria.

---

*Author contributions*—C. O., W. M. N., and K. D. conceived and coordinated the study and wrote the paper. I. G. performed proMPO crystallization, data collection, structure determination, and refinement. M. P., J. S., S. H., M. S., B. S., and P. G. F. produced and characterized MPO and proMPO. R. T. was responsible for SAXS data collection and structure determination, and C. O. created the hybrid model of proMPO.

---

*Acknowledgments*—The Austrian Centre of Industrial Biotechnology was supported by the Federal Ministry of Economy, Family, and Youth (BMWFJ), the Federal Ministry of Traffic, Innovation, and Technology (BMVIT), the Styrian Business Promotion Agency (SFG), and the Standortagentur Tirol and ZIT-Technology Agency of the City of Vienna through the COMET-Funding Program managed by the Austrian Research Promotion Agency (FFG). The Nauseef laboratory had the use of facilities at the Iowa City Dept. of Veterans Affairs Medical Center, Iowa City, IA.

---

*Note added in proof*—During the preparation of the galley proofs for publication, we became aware of our unintentional oversight of a publication describing the importance of Cys-319 in production of MPO expressed in two malignant cell lines. The mechanism responsible for the faulty synthesis of MPO with mutated Cys-319 was not identified, but the phenomenon was demonstrated in the following paper: Laura, R. P., Dong, D., Reynolds, W. F., and Maki, R. A. (2016) T47D cells expressing myeloperoxidase are able to process, traffic and store the mature protein in lysosomes: Studies in T47D cells

## Structure of proMPO and its impact on maturation

reveal a role for Cys319 in MPO biosynthesis that precedes its known role in inter-molecular disulfide bond formation. *PLoS One* **11**, 0149391.

### References

1. Nauseef, W. M. (2014) Myeloperoxidase in human neutrophil host defence. *Cell. Microbiol.* **16**, 1146–1155
2. Olsson, I., Persson, A. M., and Strömberg, K. (1984) Biosynthesis, transport and processing of myeloperoxidase in the human leukaemic promyelocytic cell line HL-60 and normal marrow cells. *Biochem. J.* **223**, 911–920
3. Zamocky, M., Jakopitsch, C., Furtmüller, P. G., Dunand, C., and Obinger, C. (2008) The peroxidase-cyclooxygenase superfamily: reconstructed evolution of critical enzymes of the innate immune system. *Proteins* **72**, 589–605
4. Zámocký, M., Hofbauer, S., Schaffner, I., Gasselhuber, B., Nicolussi, A., Souidi, M., Pirker, K. F., Furtmüller, P. G., and Obinger, C. (2015) Independent evolution of four heme peroxidase superfamilies. *Arch. Biochem. Biophys.* **574**, 108–119
5. Fiedler, T. J., Davey, C. A., and Fenna, R. E. (2000) X-ray crystal structure and characterization of halide binding sites of human myeloperoxidase at 1.8 Å resolution. *J. Biol. Chem.* **275**, 11964–11971
6. Battistuzzi, G., Stampfer, J., Bellei, M., Vlasits, J., Souidi, M., Furtmüller, P. G., and Obinger, C. (2011) Influence of the covalent heme to protein bonds on the redox thermodynamics of human myeloperoxidase. *Biochemistry* **50**, 7987–7994
7. Blair-Johnson, M., Fiedler, T., and Fenna, R. (2001) Human myeloperoxidase: structure of a cyanide complex and its interaction with bromide and thiocyanate substrates at 1.9 Å resolution. *Biochemistry* **40**, 13990–13997
8. Carpena, X., Vidossich, P., Schroettner, K., Calisto, B. M., Banerjee, S., Stampfer, J., Souidi, M., Furtmüller, P. G., Rovira, C., Fita, I., and Obinger, C. (2009) Essential role of proximal histidine-asparagine interaction in mammalian peroxidases. *J. Biol. Chem.* **284**, 25929–25937
9. Ortiz de Montellano, P. R. (2016) Self-processing of peroxidases, in *Heme Peroxidases* (Raven, E., and Dunford, B., eds) pp 3–30, Royal Society of Chemistry, Cambridge, United Kingdom
10. Arnhold, J., Monzani, E., Furtmüller, P. G., Zederbauer, M., Casella, L., and Obinger, C. (2006) Kinetics and thermodynamics of halide and nitrite oxidation by heme peroxidases. *Eur. J. Inorg. Chem.* **380**, 3801–3811
11. Battistuzzi, G., Bellei, M., Zederbauer, M., Furtmüller, P. G., Sola, M., and Obinger, C. (2006) Redox thermodynamics of the Fe(III)/Fe(II) couple of human myeloperoxidase in its high-spin and low-spin forms. *Biochemistry* **45**, 12750–12755
12. Zederbauer, M., Furtmüller, P. G., Brogioni, S., Jakopitsch, C., Smulevich, G., and Obinger, C. (2007) Heme to protein linkages in mammalian peroxidases: impact on spectroscopic, redox and catalytic properties. *Nat. Prod. Rep.* **24**, 571–584
13. Kettle, A. J., and Winterbourne, C. C. (2016) Myeloperoxidase: structure and function of the green heme peroxidase of neutrophils, in *Heme Peroxidases* (Raven, E., and Dunford, B., eds) pp 272–308, Royal Society of Chemistry, Cambridge, United Kingdom
14. Andrews, P. C., Parnes, C., and Krinsky, N. I. (1984) Comparison of myeloperoxidase and hemimyeloperoxidase with respect to catalysis, regulation, and bactericidal activity. *Arch. Biochem. Biophys.* **228**, 439–442
15. Hansson, M., Olsson, I., and Nauseef, W. M. (2006) Biosynthesis, processing, and sorting of human myeloperoxidase. *Arch. Biochem. Biophys.* **445**, 214–224
16. Nauseef, W. M. (1987) Posttranslational processing of a human myeloid lysosomal protein, myeloperoxidase. *Blood* **70**, 1143–1150
17. Nauseef, W. M., McCormick, S., and Yi, H. (1992) Roles of heme insertion and the mannose-6-phosphate receptor in processing of the human myeloid lysosomal enzyme myeloperoxidase. *Blood* **80**, 2622–2633
18. Castañeda, V. L., Parmley, R. T., Pinnix, I. B., Raju, S. G., Guzman, G. S., and Kinkade, J. M., Jr. (1992) Ultrastructural, immunochemical, and cytochemical study of myeloperoxidase in myeloid leukemia HL-60 cells following treatment with succinylacetone, an inhibitor of heme biosynthesis. *Exp. Hematol.* **20**, 916–924
19. Pinnix, I. B., Guzman, G. S., Bonkovsky, H. L., Zaki, S. R., and Kinkade, J. M., Jr. (1994) The post-translational processing of myeloperoxidase is regulated by the availability of heme. *Arch. Biochem. Biophys.* **312**, 447–458
20. Andersson, E., Hellman, L., Gullberg, U., and Olsson, I. (1998) The role of the propeptide for processing and sorting of human myeloperoxidase. *J. Biol. Chem.* **273**, 4747–4753
21. McCormick, S., Nelson, A., and Nauseef, W. M. (2012) Proconvertase proteolytic processing of an enzymatically active myeloperoxidase precursor. *Arch. Biochem. Biophys.* **527**, 31–36
22. Nauseef, W. M., and Clark, R. A. (1986) Separation and analysis of subcellular organelles in a human promyelocyte leukemia cell line, HL-60: application to the study of myeloid lysosomal enzyme synthesis and processing. *Blood* **68**, 442–449
23. Nauseef, W. M., McCormick, S. J., and Clark, R. A. (1995) Calreticulin functions as a molecular chaperon in the biosynthesis of myeloperoxidase. *J. Biol. Chem.* **270**, 4741–4747
24. Goedken, M., McCormick, S., Leidal, K. G., Suzuki, K., Kameoka, Y., Astern, J. M., Huang, M., Cherkasov, A., and Nauseef, W. M. (2007) Impact of two novel mutations on the structure and function of human myeloperoxidase. *J. Biol. Chem.* **282**, 27994–28003
25. Moguilevsky, N., Garcia-Quintana, L., Jacquet, A., Tournay, C., Fabry, L., Piérard, L., and Bollen, A. (1991) Structural and biological properties of human recombinant myeloperoxidase produced by Chinese hamster ovary cell lines. *Eur. J. Biochem.* **197**, 605–614
26. Van Antwerpen, P., Slomianny, M. C., Boudjeltia, K. Z., Delporte, C., Faid, V., Calay, D., Rousseau, A., Moguilevsky, N., Raes, M., Vanhamme, L., Furtmüller, P. G., Obinger, C., Vanhaeverbeek, M., Nève, J., and Michalski, J. C. (2010) Glycosylation pattern of mature dimeric leucocyte and recombinant monomeric myeloperoxidase: glycosylation is required for optimal enzymatic activity. *J. Biol. Chem.* **285**, 16351–16359
27. Chemical Computing Group (2016) *MOE: Molecular Operating Environment 2013.08*, Chemical Computing Group Inc., Montreal
28. Wang, J. M., Cieplak, P., and Kollman, P. A. (2000) How well does a restrained electrostatic potential (RESP) model perform in calculating conformational energies of organic and biological molecules? *J. Comput. Chem.* **21**, 1049–1074
29. Petoukhov, M. V., Franke, D., Shkumatov, A. V., Tria, G., Kikhney, A. G., Gajda, M., Gorba, C., Mertens, H. D., Konarev, P. V., and Svergun, D. I. (2012) New developments in the ATSAS program package for small-angle scattering data analysis. *J. Appl. Crystallogr.* **45**, 342–350
30. DeLeo, F. R., Goedken, M., McCormick, S. J., and Nauseef, W. M. (1998) A novel form of hereditary myeloperoxidase deficiency linked to endoplasmic reticulum/proteasome degradation. *J. Clin. Invest.* **101**, 2900–2909
31. Nauseef, W. M., McCormick, S. J., and Goedken, M. (1998) Coordinated participation of calreticulin and calnexin in the biosynthesis of myeloperoxidase. *J. Biol. Chem.* **273**, 7107–7111
32. Akin, D. T., and Kinkade J. M., Jr. (1986) Processing of a newly identified intermediate of human myeloperoxidase in isolated granules occurs at neutral pH. *J. Biol. Chem.* **261**, 8370–8375
33. Taylor, K. L., Guzman, G. S., Burgess, C. A., and Kinkade J. M., Jr. (1990) Assembly of dimeric myeloperoxidase during posttranslational maturation in human leukemic HL-60 cells. *Biochemistry* **29**, 1533–1539
34. Nauseef, W. M., Olsson, I., and Arnljots, K. (1988) Biosynthesis and processing of myeloperoxidase: a marker for myeloperoxidase differentiation. *Eur. J. Haematol.* **40**, 97–110
35. Yamada, M., Hur, S. J., and Toda, H. (1990) Isolation and characterization of extracellular myeloperoxidase precursor in HL-60 cell cultures. *Biochem. Biophys. Res. Commun.* **166**, 852–859
36. Hasilik, A., Pohlmann, R., Olsen, R. L., and von Figura, K. (1984) Myeloperoxidase is synthesized as larger phosphorylated precursor. *EMBO J.* **3**, 2671–2676
37. Yamada, M. (1982) Myeloperoxidase precursors in human myeloid leukemia HL-60 cells. *J. Biol. Chem.* **257**, 5980–5982
38. Furtmüller, P. G., Jantschko, W., Regelsberger, G., Jakopitsch, C., Moguilevsky, N., and Obinger, C. (2001) A transient kinetic study on the reactivity of recombinant unprocessed monomeric myeloperoxidase. *FEBS Lett.* **503**, 147–150

39. Helenius, A., Trombetta, E. S., Hebert, D. N., and Simons, J. F. (1997) Calnexin, calreticulin and the folding of glycoproteins. *Trends Cell Biol.* **7**, 193–200
40. Banerjee, S., Stampler, J., Furtmüller, P. G., and Obinger, C. (2011) Conformational and thermal stability of mature dimeric human myeloperoxidase and a recombinant form from CHO cells. *Biochim. Biophys. Acta* **1814**, 375–387
41. Hofbauer, S., Dalla Sega, M., Scheiblbrandner, S., Jandova, Z., Schaffner, I., Mlynek, G., Djinović-Carugo, K., Battistuzzi, G., Furtmüller, P. G., Oostenbrink, C., and Obinger, C. (2016) Chemistry and molecular dynamics simulations of heme *b*-HemQ and coproheme-HemQ. *Biochemistry* **55**, 5398–5412
42. Brogioni, S., Feis, A., Marzocchi, M. P., Zederbauer, M., Furtmüller, P. G., Obinger, C., and Smulevich, G. (2006) Resonance assignment of myeloperoxidase and the selected mutants Asp94Val, and Met242Thr: effect of heme distortion. *J. Raman Spectrosc.* **37**, 263–276
43. Brogioni, S., Stampler, J., Furtmüller, P. G., Feis, A., Obinger, C., and Smulevich, G. (2008) The role of the sulfonium ion linkage in the stabilization of the heme architecture of the ferrous form of myeloperoxidase: a comparison with lactoperoxidase. *Biochim. Biophys. Acta* **1784**, 843–849
44. Zederbauer, M., Jantschko, W., Neugschwandtner, K., Jakopitsch, C., Moguilevsky, N., Obinger, C., and Furtmüller, P. G. (2005) The role of the covalent Glu242-heme linkage in the formation and reactivity of redox intermediates of human myeloperoxidase. *Biochemistry* **44**, 6482–6491
45. Zederbauer, M., Furtmüller, P. G., Bellei, M., Stampler, J., Jakopitsch, C., Battistuzzi, G., Moguilevsky, N., and Obinger, C. (2007b) Disruption of the aspartate to heme ester linkage in human myeloperoxidase: impact on ligand binding, redox chemistry, and interconversion of redox intermediates. *J. Biol. Chem.* **282**, 17041–17052
46. Zederbauer, M., Furtmüller, P. G., Ganster, B., Moguilevsky, N., and Obinger, C. (2007) Manipulating the vinyl-sulfonium bond in human myeloperoxidase: impact on compound I formation and reduction by halides and thiocyanate. *Biochem. Biophys. Res. Commun.* **356**, 450–456
47. Nauseef, W. M., Root, R. K., and Malech, H. L. (1983) Biochemical and immunologic analysis of hereditary myeloperoxidase deficiency. *J. Clin. Invest.* **71**, 1297–1307
48. Nauseef, W. M., Cogley, M., and McCormick, S. (1996) Effect of the R569W missense mutation on the biosynthesis of myeloperoxidase. *J. Biol. Chem.* **271**, 9546–9549
49. Suzuki, K., Ota, H., Sasagawa, S., Sakatani, T., and Fujikura, T. (1983) Assay method for myeloperoxidase in human polymorphonuclear leukocytes. *Anal. Biochem.* **132**, 345–352
50. Kabsch, W. (2010) XDS. *Acta Crystallogr. D Biol. Crystallogr.* **66**, 125–132
51. Winn, M. D., Ballard, C. C., Cowtan, K. D., Dodson, E. J., Emsley, P., Evans, P. R., Keegan, R. M., Krissinel, E. B., Leslie, A. G., McCoy, A., McNicholas, S. J., Murshudov, G. N., Pannu, N. S., Pottterton, E. A., Powell, H. R., *et al.* (2011) Overview of the CCP4 suite and current developments. *Acta Crystallogr. D Biol. Crystallogr.* **67**, 235–242
52. McCoy, A. J. (2007) Solving structures of protein complexes by molecular replacement with Phaser. *Acta Crystallogr. D Biol. Crystallogr.* **63**, 32–41
53. Murshudov, G. N., Vagin, A. A., and Dodson, E. J. (1997) Refinement of macromolecular structures by the maximum-likelihood method. *Acta Crystallogr. D Biol. Crystallogr.* **53**, 240–255
54. Adams, P. D., Afonine, P. V., Bunkóczi, G., Chen, V. B., Davis, I. W., Echols, N., Headd, J. J., Hung, L. W., Kapral, G. J., Grosse-Kunstleve, R. W., McCoy, A. J., Moriarty, N. W., Oeffner, R., Read, R. J., Richardson, D. C., *et al.* (2010) PHENIX: a comprehensive Python-based system for macromolecular structure solution. *Acta Crystallogr. D Biol. Crystallogr.* **66**, 213–221
55. Emsley, P., and Cowtan, K. (2004) Coot: model-building tools for molecular graphics. *Acta Crystallogr. D Biol. Crystallogr.* **60**, 2126–2132
56. Chen, V. B., Arendall, W. B., 3rd, Headd, J. J., Keedy, D. A., Immormino, R. M., Kapral, G. J., Murray, L. W., Richardson, J. S., and Richardson, D. C. (2010) MolProbity: all-atom structure validation for macromolecular crystallography. *Acta Crystallogr. D Biol. Crystallogr.* **66**, 12–21
57. Chovancova, E., Pavelka, A., Benes, P., Strnad, O., Brezovsky, J., Kozlikova, B., Gora, A., Sustr, V., Klvana, M., Medek, P., Biedermannova, L., Sochor, J., and Damborsky, J. (2012) CAVER 3.0: a tool for the analysis of transport pathways in dynamic protein structures. *PLoS Comput. Biol.* **8**, e1002708
58. DeLano, W. L. (2002) *The PyMol Molecular Graphics System*, DeLano Scientific LLC, San Carlos, CA
59. Hura, G. L., Menon, A. L., Hammel, M., Rambo, R. P., Poole, F. L., 2nd, Tsutakawa, S. E., Jenney, F. E., Jr., Classen, S., Frankel, K. A., Hopkins, R. C., Yang, S. J., Scott, J. W., Dillard, B. D., Adams, M. W., and Tainer, J. A. (2009) Robust, high-throughput solution structural analyses by small angle X-ray scattering (SAXS). *Nat. Methods* **6**, 606–612
60. Franke, D., Jeffries, C. M., and Svergun, D. I. (2015) Correlation Map, a goodness-of-fit test for one-dimensional X-ray scattering spectra. *Nat. Methods* **12**, 419–422
61. Song, C., Havlin, S., and Makse, H. A. (2005) Self-similarity of complex networks. *Nature* **433**, 392–395
62. Putnam, C. D., Hammel, M., Hura, G. L., and Tainer, J. A. (2007) X-ray solution scattering (SAXS) combined with crystallography and computation: defining accurate macromolecular structures, conformations and assemblies in solution. *Q Rev. Biophys.* **40**, 191–285

**Structure of human promyeloxygenase (proMPO) and the role of the propeptide in processing and maturation**

Irina Grishkovskaya, Martina Paumann-Page, Rupert Tscheliessnig, Johanna Stampler, Stefan Hofbauer, Monika Soudi, Benjamin Sevcnikar, Chris Oostenbrink, Paul G. Furtmüller, Kristina Djinovic-Carugo, William M. Nauseef and Christian Obinger

*J. Biol. Chem.* 2017, 292:8244-8261.

doi: 10.1074/jbc.M117.775031 originally published online March 27, 2017

---

Access the most updated version of this article at doi: [10.1074/jbc.M117.775031](https://doi.org/10.1074/jbc.M117.775031)

Alerts:

- [When this article is cited](#)
- [When a correction for this article is posted](#)

[Click here](#) to choose from all of JBC's e-mail alerts

This article cites 58 references, 15 of which can be accessed free at <http://www.jbc.org/content/292/20/8244.full.html#ref-list-1>

## Curriculum Vitae

# DIPL-ING. BENJAMIN SEVCNIKAR



### PERSONAL INFORMATION

---

Address Bloch-Bauer-Promenade 20/34  
1100 Vienna  
Mobile phone +43 699 15 66 28 68  
E-Mail benjamin.sevcnikar@gmail.com  
Citizenship Austria  
Date of birth 20. September 1990

### EDUCATION

---

- As of 2015 **University of Natural Resources and Life Sciences, Vienna**  
PhD Program „BioTop“ Biomolecular Technology of Proteins  
Thesis title: „*Biochemistry of invertebrate peroxidases*“ under supervision of Prof. Christian Obinger
- Jan. 2019 – Apr. 2019 **University of Copenhagen, DEN, Visiting Scientist**  
Mass spectrometric analysis of oxidative damage to basement membrane proteins under supervision of Prof. Michael Jonathan Davies
- May 2018 – Aug. 2018 **University of Copenhagen, DEN, Visiting Scientist**  
Identification of a peroxidase binding partner under supervision of Prof. Michael Jonathan Davies
- Oct. 2013 – Jun. 2015 **University of Natural Resources and Life Sciences, Vienna**  
Master of Science in Biotechnology  
Thesis title: „*Plant extract 1201 affects the aging process of human dermal fibroblasts*“ under supervision of Assoc. Prof. Johannes Grillari
- Oct. 2010 – Sep. 2013 **University of Natural Resources and Life Sciences, Vienna**  
Bachelor of Science in Food- and Biotechnology  
Thesis title: „*Production, purification and characterization of various pyranose dehydrogenase mutants in Pichia pastoris*“ under supervision of Prof. Dietmar Haltrich
- Jun. 2009 **Bundesrealgymnasium Gröhrmühlgasse Wiener Neustadt**  
Higher school certificate with focus on natural sciences

## PROFESSIONAL EXPERIENCE

---

- Oct.2019 – Sep.2020 **Traineeship at Octapharma Pharmazeutika Produktionsgesellschaft m.b.H. (Corporate Project Management Office)**  
Time, scope, budget and risk management, creation of business cases, managing suppliers, development of agile project management methods and tools
- Jul. 2014 – Aug. 2014 **Internship at Boehringer Ingelheim RCV GmbH**  
Internship in the division Process Science – Analytics  
Analysis of samples from Up- and Downstream development using HPLC and SDS-PAGE.
- Jul. 2013 – Sep. 2013 **Internship at Boehringer Ingelheim RCV GmbH**  
Internship in the division Process Science – Analytics  
Analysis of recombinant proteins and pDNA using HPLC and spectrophotometry.
- Oct. 2012 – Sep.2019 **Study assistant and Lector at the University of Natural Resources and Life Sciences, Vienna**  
Supervision of students in analytical and instrumental chemistry as well as biochemical practical courses.
- Aug. 2012 **Internship at Givaudan Austria GmbH**  
Internship in the division of snack product development
- Oct. 2011 – Oct. 2013 **Salesman at XXXLutz Wiener Neustadt**  
Planning, advising and selling of dining room furniture
- Jul. 2011 – Aug. 2011 **Paramedic at Red Cross Wiener Neustadt**  
Handling of ambulance and emergency service

## OTHER ACTIVITIES

---

- Oct. 2010 – May. 2016 **Volunteer at Red Cross Wiener Neustadt**  
Voluntary day and night shifts performing ambulance and emergency service

## CIVILIAN SERVICE

---

- Jan. 2010 – Sep. 2010 **Paramedic at Red Cross Wiener Neustadt**  
Handling of ambulance and emergency service

## HONORS AND AWARDS

---

- 2018/17/15/14/13/12 Merit-based scholarship – University of Natural Resources and Life Sciences, Vienna
- 2017 Young Investigator Award – 10th Human Peroxidase Meeting
- 2012 Michael von Zoller scholarship

## SELECTED SCI PUBLICATIONS

---

- May 2020 **Sevcnikar, B.**, Schaffner, I., Chuang, C. Y., Gamon, L., Paumann-Page, M., Hofbauer, S., Davies, M. J., Furtmüller, P. G., and Obinger, C. (2020) The leucine-rich repeat domain of human peroxidase 1 promotes binding to laminin in basement membranes. Arch. Biochem. Biophys. 689, 108443
- Jan. 2020 **Sevcnikar, B.**, Paumann-Page, M., Hofbauer, S., Pfanzagl, V., Furtmüller, P. G., and Obinger, C. (2020) Reaction of human peroxidase 1 compound I and compound II with one-electron donors. Arch. Biochem. Biophys. 681, 108267

## CONFERENCE CONTRIBUTIONS

---

- Posters **Sevcnikar, B.**, Paumann-Page, M., Katz, R.S., Soudi, M., Furtmüller, P.G., Obinger, C. (2018) Substrate Specificity and Solution Structure of Truncated Human Peroxidase 1 (Poster) [International Conference on Porphyrins and Phthalocyanines ICPP-10, Munich Germany July 1-6, 2018]
- Sevcnikar, B.**, Soudi, M., Paumann-Page, M., Furtmüller, P., Obinger, C. (2016) Human Peroxidase 1: A multidomain heme peroxidase (Poster) [13th European Biological Inorganic Chemistry, Budapest, Hungary, 28 August - 01 September, 2016]
- Talks **Sevcnikar, B.**, Chuang, C.Y., Gamon, L., Paumann-Page, M., Davies, M.J., Furtmüller, P.G., Obinger, C. (2019) Laminin – A potential binding partner for peroxidase in the extracellular matrix (Talk) [11th International Peroxidase Meeting, Brno, Czech Republic, September 04-07, 2019]
- Sevcnikar, B.**, Paumann-Page, M., Tscheliessnig, R., Katz, R.S., Soudi, M., Furtmüller, P.G., Obinger, C. (2017) Substrate specificity and SAXS-derived structural data of human peroxidase (Talk) [10th International Peroxidase Meeting, Breckenridge, Colorado, USA, August 28 -31, 2017]